DEVELOPMENT AND POTENTIAL BEHAVIORAL SIGNIFICANCE OF PRECISE TONOTOPY IN AN INHIBITORY CIRCUIT OF THE AUDITORY BRAINSTEM

by

Amanda Clause

BS, Bucknell University, 2005

Submitted to the Graduate Faculty of

the School of Medicine in partial fulfillment

of the requirements for the degree of

Doctor of Philosophy

University of Pittsburgh

2011

UNIVERSITY OF PITTSBURGH

School of Medicine

This dissertation was presented

by

Amanda Clause

It was defended on

February 10, 2011

and approved by

Elias Aizenman, PhD, Dept. Neurobiology

Alison Barth, PhD, Carnegie Mellon University Dept. Biological Sciences

Erika Fanselow, PhD, Dept. Neurobiology

Edda Thiels, PhD, Dept. Neurobiology

Thanos Tzounopoulos, PhD, Dept. Otolaryngology

Dan Sanes, PhD, New York University Center for Neural Science

Dissertation Advisor: Karl Kandler, PhD, Dept. Otolaryngology

DEVELOPMENT AND POTENTIAL BEHAVIORAL SIGNIFICANCE OF PRECISE TONOTOPY IN AN INHIBITORY CIRCUIT OF THE AUDITORY BRAINSTEM

Amanda Clause, B.S.

University of Pittsburgh, 2011

Precise neuronal connections are crucial for normal brain function. Often this is accomplished during development, as initially imprecise connections are refined in a manner that depends on neural activity, both spontaneous and sensory-evoked. In the auditory system, many connections are topographically organized according to frequency, or tonotopically, an organizational scheme important for processing information about sound.

In this thesis, I investigated the development of precise tonotopy in the inhibitory connections between the medial nucleus of the trapezoid body (MNTB) and the lateral superior olive (LSO), a pathway in the auditory brainstem involved in sound localization. Although MNTB-LSO connections exhibit tonotopy from the outset, tonotopic precision increases during development through a process of silencing imprecise inputs and strengthening maintained connections before hearing onset, followed by anatomical pruning after hearing. I teased apart the relationship between functional and anatomical refinement, as well as the degree to which spontaneous and sound-evoked activity play a role in each. Finally, I attempted to link the tonotopic specificity of this circuit to a specific aspect of auditory perception, frequency discrimination.

In Chapter 2, I mapped the tonotopic precision of individual MNTB axons in the LSO over the first three weeks of postnatal development and showed that pruning does not take place before hearing onset, indicating that functional and anatomical refinement take place during distinct developmental periods. In Chapter 3, I showed that anatomical refinement after hearing

onset depends on efferent cholinergic transmission in the cochlea, most likely due to its role in patterning pre-hearing spontaneous activity and the functional refinement of connections. In Chapter 4, I showed that eliminating the normal spectrotemporal structure of sound-evoked activity by rearing animals in pulsed white noise does not disrupt pruning. Finally, in Chapter 5, I showed that the loss of tonotopic precision that results from the elimination of cochlear cholinergic transmission is also accompanied by impaired frequency discrimination, providing a link between tonotopic refinement, the efferent system, and auditory perception. I discuss the results in the context of a model of tonotopic refinement and a new role of the efferent system during development.

TABLE OF CONTENTS

LIST OF FIGURES

PREFACE

I would like to thank J. Cook, R. Kelly, J.P. Mayo, and D. Simons for help with Matlab and LabView programming. Without their help I would likely still be hampered by the vast limitations of Excel. I would also like to thank T. Nguyen for writing the startle and PPI software and for help choosing the necessary hardware. Many thanks to current and past members of the Kandler lab, as well as new colleagues from the Tzounopoulos and Rubio labs, for their experience, advice, and helpful discussion. Thanks also to the members of my committee, who graciously took time out of their busy schedules to offer thoughtful insight and suggestions, which always made my work better. Special thanks to E. Aizenman, whose loan of a physiology rig kept my work going for a few months when it otherwise would have ground to a halt. Special thanks also to D. Sanes, whose own work is not only part of the foundation of my work, but who generously donated his time during his sabbatical to offer his expert opinion. Extra special thanks to my mentor, K. Kandler, for inspiring me to join his lab by his proseminar presentation and for supporting and encouraging me throughout my years there. I also appreciate the support of the CNUP and CNBC communities, both scientifically and socially, as well as the work of P. Argenzio and J. Blaney, whose administrative excellence keeps everyone on track. Special thanks to the CNBC IGERT program for providing the funds necessary to develop the behavioral techniques. Thanks to my parents, family, and friends who remind me of the world

outside of my little microcosm of research, and for the understanding of those family and friends who know firsthand how easy it is to be consumed by your little microcosm of research. Finally, I would like to dedicate this thesis to Patrick, the best part of my graduate school experience and who I value far more than a degree.

1.0 GENERAL INTRODUCTION

1.1 ACTIVITY-DEPENDENT REFINEMENT OF NEURONAL CONNECTIONS

In order to function, the nervous system relies on the organization of precise circuits, carved out of the synaptic contacts between hundreds of thousands of neurons. Initial assembly of these circuits is directed by genetic programs and molecular interactions (Goodman and Shatz, 1993; Tessier-Lavigne and Goodman, 1996). Although these initial connection patterns can be very precise, early development involves large amounts of synapse addition, elimination, and reorganization that refine the initial connections to achieve adult-like patterns of connectivity (Cohen-Cory, 2002). Often, neural activity plays an important role in the process of refinement by providing a signal whereby desirable connections can be maintained and strengthened while undesirable ones can be eliminated.

A key mechanism by which neural activity is known to regulate refinement is through activity-dependent competition, where different axons "compete" for innervation of a shared target (Lohof et al., 1996). In the neuromuscular junction, for example, muscle fibers at birth are innervated by the axons of multiple motor neurons. But over the next three weeks, all of the initial inputs save one are eliminated, creating the mono-innervation pattern important for mature functioning of the motor unit (Colman and Lichtman, 1993; Wyatt and Balice-Gordon, 2003). Changes in the strength of inputs precedes the withdrawal of axon branches: the strength of the

fibers that will eventually withdraw become progressively weaker, while the axon that is maintained becomes stronger (Colman et al., 1997). If synchronous activity is artificially imposed on the inputs to a single muscle fiber, the progression to mono-innervation is impaired (Busetto et al., 2000), indicating that the relative pattern of activity plays a key role in the competition.

This sort of winner-take-all competition takes place in other developing circuits as well. In the cerebellum, for example, Purkinje cells are initially innervated by the axons of multiple climbing fibers (CFs). Over the first three weeks of postnatal development, however, surplus CF inputs are eliminated, producing a mono-innervation pattern like that of the neuromuscular junction (Kano and Hashimoto, 2009). During this process, one CF is selectively strengthened (Hashimoto and Kano, 2003, 2005), likely through the differential expression of activity-dependent plasticity. Repeated pairing of CF stimulation and postsynaptic spikes induces long-term potentiation at the strongest CF input, but the same protocol induces long-term depression at weaker CF inputs that will presumably be eliminated (Bosman et al., 2008).

In a similar way, activity can refine circuits that do not result in a winner-take-all outcome. In the lateral geniculate nucleus (LGN), for example, axons of retinal ganglion cells (RGCs) from the two eyes are initially intermingled, but then segregate to form eye-specific layers (Katz and Shatz, 1996). Segregation occurs as synapses and axon terminals are elaborated in the same-eye territory, and eliminated in opposite-eye territory (Sretavan and Shatz, 1984). This process takes place before eye-opening, but still depends on activity. Before the onset of vision, spontaneous bursts of action potentials in RGCs travel across the retina in waves (Meister et al., 1991). Waves initiate at random locations but propagate over spatially-restricted domains, such that the activity of a RGC is correlated with its neighbors, but not with more distant RGCs,

or with RGCs at a similar spatial location in the opposite eye (Wong, 1999). The high frequency correlated bursting of neighboring RGCs is a key factor in the development of eye-specific retinogeniculate projections, as RGC axons segregate through competitive interactions involving the relative levels of spiking between the two eyes (Penn et al., 1998; Stellwagen and Shatz, 2002; Torborg et al., 2005). The eye-specific and retinotopic information contained in retinal waves also shapes other visual pathways, including the refinement of retinotopic maps in the superior colliculus and LGN, and the development and maintenance of ocular dominance columns in primary visual cortex (Huberman et al., 2008; Wong, 1999).

Taken together, these studies have shown that activity-dependent refinement is a central mechanism by which precise neuronal connections are established during development. Differential patterns of activity between inputs activate plasticity mechanisms that lead to some inputs being maintained and strengthened while others are eliminated. For excitatory systems such as those described above, classic Hebbian rules apply: inputs that contribute to the firing of action potentials by the postsynaptic neuron are elaborated, while inputs whose activity does not cause postsynaptic spikes are eliminated (Hata and Stryker, 1994; Lowel and Singer, 1992). At inhibitory synapses, however, the desired role of the input is to inhibit firing in the postsynaptic cell, adding an additional layer of complexity to a process of inhibitory circuit refinement. Although evidence from multiple systems indicates activity can regulate the strength (Kilman et al., 2002; Morales et al., 2002), number (Micheva and Beaulieu, 1995), and organization (Kapfer et al., 2002) of inhibitory synapses, much less is known about the development and refinement of inhibitory circuits, even though inhibition plays an essential role in many aspects of brain function (McBain and Fisahn, 2001). This is largely because in many areas of the brain, inhibition is comprised of intricate local networks of phenotypically diverse interneurons that

lack clear spatial organization and are difficult to access experimentally, making it difficult to study synaptic reorganization.

Here I circumvent those issues and investigate inhibitory circuit refinement in the auditory brainstem, where the axons of a homogeneous population of inhibitory neurons in the medial nucleus of the trapezoid body form a long-range, topographically organized pathway with their postsynaptic target, the lateral superior olive.

1.2 THE MNTB-LSO CIRCUIT

The MNTB-LSO circuit is part of a primary sound localization pathway in the auditory brainstem. Unlike other sensory systems where the spatial location of a stimulus is directly encoded by the site of stimulation on the receptor sheet, such as the skin or retina, the cochlea provides no information about the direction of incoming sound. Thus instead of topographically mapping space in the external world, the cochlea contains a topographic representation of sound frequency. Auditory space must therefore be computed completely *de novo* by the central nervous system. Small differences in the intensity of sound between the two ears provide a primary cue for the horizontal direction of incoming sound. These interaural sound level (intensity) differences (ILDs) are first encoded in the auditory brainstem by neurons in the lateral superior olive (LSO; Boudreau and Tsuchitani, 1968).

LSO neurons receive binaural input; excitation from the ipsilateral ear via a glutamatergic projection from the anteroventral cochlear nucleus (AVCN; Cant and Casseday, 1986), and inhibitory input from the contralateral ear via the GABA/glycinergic principal cells of the medial nucleus of the trapezoid body (MNTB; Fig. 1-1; Friauf and Ostwald, 1988; Spangler et al., 1985;

Zook and DiCaprio, 1988). Both the excitatory projection from the AVCN and inhibitory projection from the MNTB are organized tonotopically, with high frequencies represented medially and low frequencies represented laterally (Friauf, 1992; Kandler and Friauf, 1993; Kil et al., 1995; Tsuchitani, 1977). Because ILDs are calculated in a frequency-specific manner, the function of LSO neurons is dependent on the precise alignment of excitatory and inhibitory inputs along the frequency axis. Accordingly, the tonotopic maps of ipsilateral and contralateral inputs are matched, such that LSO neurons receive excitation and inhibition corresponding to the same frequency (Sanes and Rubel, 1988). Due to this pattern of inputs, LSO neurons tend to respond more vigorously when sounds are located closer to the ipsilateral ear, since excitation from the CN then dominates (Fig. 1-2). Although the role of the LSO in sound localization is well-established - discrimination of horizontal sound source locations is impaired in animals in which LSO neurons or their input pathways are lesioned (Kavanagh and Kelly, 1992; Masterton et al., 1967), and the best-threshold ILDs of single LSO neurons are comparable to behavioral performance (Tollin et al., 2008) - the frequency-specific input the LSO provides to the inferior colliculus is likely also important for other forms of auditory perception.

Thus compared to the heterogeneous and complex local networks of inhibition generally found in brain circuits, the inhibitory projection from the MNTB to the LSO is well-defined, highly organized, and has a known function. Because MNTB-LSO connections become more tonotopically precise during early postnatal development, the circuit provides an advantageous system to study how inhibitory circuits are refined.

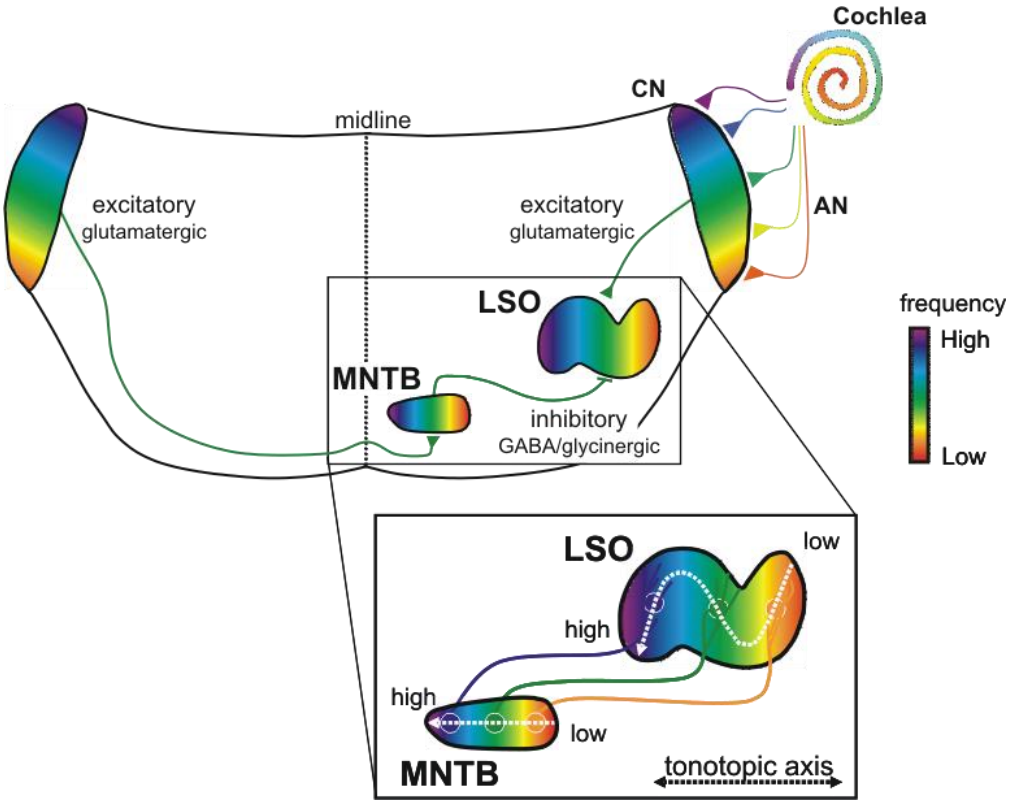

Figure 1-1. Schematic illustration of the MNTB-LSO circuit.

LSO neurons receive binaural input, excitation from the ipsilateral ear via the CN, and inhibition from the contralateral ear via the ipsilateral MNTB. Both pathways are arranged tonotopically such that LSO neurons receive frequency-matched excitation and inhibition used to compute interaural sound level differences for the localization of sounds in horizontal space. AN, auditory nerve; CN, cochlear nucleus; MNTB, medial nucleus of the trapezoid body; LSO, lateral superior olive.

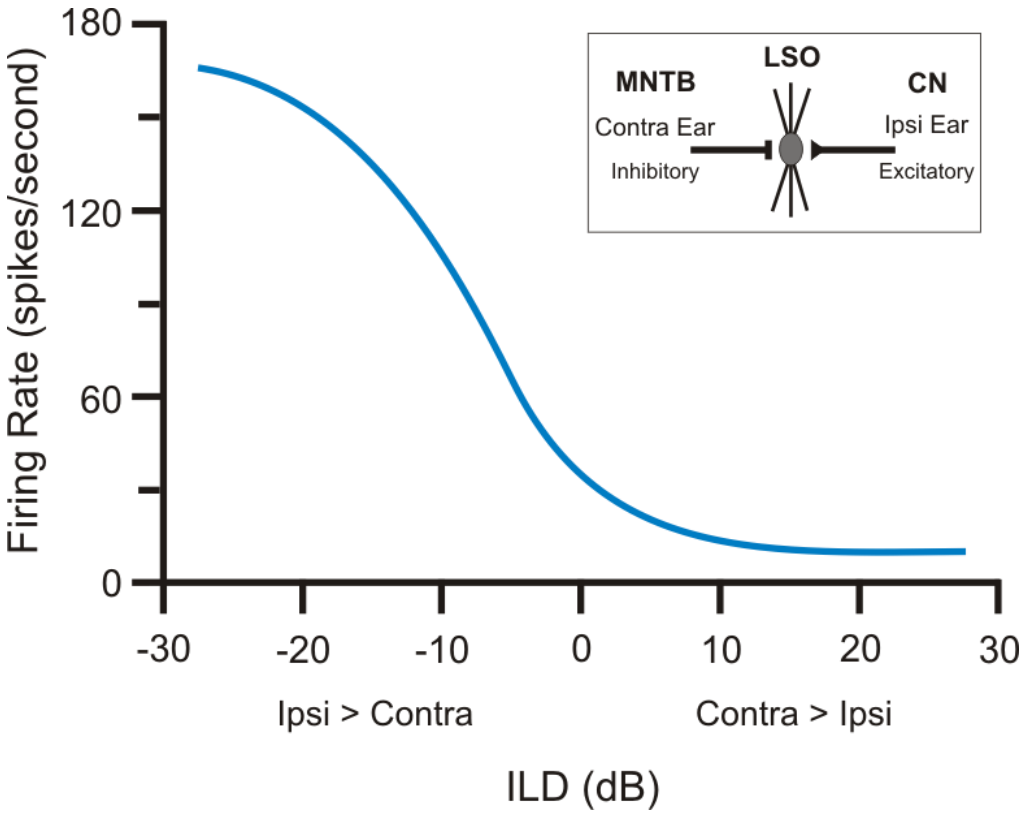

Figure 1-2. ILD coding by LSO neurons.

Hypothetical data representing the ILD tuning of LSO neurons. When sound is louder in the ipsilateral ear (corresponding to a negative ILD), the neuronal response is greater than if the sound is louder in the contralateral ear (positive ILD) since input from the contralateral ear is inhibitory via the MNTB and input from the ipsilateral ear is excitatory via the CN. The majority of LSO ILD tuning curves are sigmoidal as shown. Ipsi, ipsilateral; contra, contralateral; ILD, interaural level difference; dB, decibels; MNTB, medial nucleus of the trapezoid body; LSO, lateral superior olive; CN, cochlear nucleus. Data adapted from Tollin et al., 2008.

1.3 TONOTOPIC REFINEMENT OF DEVELOPING MNTB-LSO CONNECTIONS

Both glutamatergic and glycinergic synapses in the LSO are functional before birth (Kandler and Friauf, 1995), with topography in the MNTB-LSO pathway present soon after (Kandler and Friauf, 1993). Analysis of the termination patterns of individual MNTB axons in the LSO of gerbils first revealed that additional tonotopic sharpening occurs during early development. Following the onset of hearing around postnatal day (P) 12-13, axonal pruning and synapse elimination result in a reduction of the number of boutons per MNTB axon in the LSO. Because the elimination is specific and reduces the spread of boutons along the LSO frequency axis, these anatomical changes increase the tonotopic specificity of the projection during the first week of auditory experience (Sanes and Siverls, 1991). Complementary changes take place in the dendrites of LSO neurons as well. The dendritic field is wide in young animals, but by ~P21, dendritic branches are confined to a narrower region of the LSO frequency axis (Rietzel and Friauf, 1998; Sanes and Chokshi, 1992).

Consistent with numerous lines of evidence that activity plays an important role in circuit refinement (Huberman et al., 2008; Kano and Hashimoto, 2009; Zhang and Poo, 2001), sharpening of MNTB-LSO anatomical connections is severely impaired if cochlear-generated activity is blocked. When the contralateral cochlea is ablated at P8, before the onset of hearing, pruning of MNTB axons in the LSO is severely disrupted (Sanes and Takacs, 1993). Dendritic refinement in LSO neurons is also impaired by cochlear ablation at P7, as well as being impaired in animals in which glycine receptors are pharmacologically blocked by systemic administration of strychnine during development (Sanes and Chokshi, 1992; Sanes et al., 1992a). Each of these

studies point to the importance of active glycinergic transmission for anatomical refinement. Furthermore, because the anatomical changes were not observed until after the onset of hearing, they suggested that sound-evoked activity from the cochlea was the source of the activity needed for refinement.

However, mapping the synaptic connections of the MNTB-LSO pathway via focal photolysis of caged glutamate demonstrated that functional connectivity is tonotopically refined during the first postnatal week, days before the onset of hearing and well before anatomical refinement (Kim, 2004; Kim and Kandler, 2003; Noh et al., 2010). During functional refinement, the region of the MNTB that provides synaptic input to a single LSO neuron is reduced to ~25 % of its original size, indicating that LSO neurons become functionally disconnected from the majority of their initial presynaptic partners. This silencing is also tonotopically specific, narrowing the input region along the frequency axis by ~50 %.

Before the onset of hearing around P12-13 in rodents (Geal-Dor et al., 1993), the structure of the inner and outer ear is immature, and the thresholds of auditory nerve fibers so high that the auditory system is insensitive to airborne sounds at environmentally relevant levels. Functional refinement therefore takes place before sound-evoked activity is present. However, it is still thought to depend on activity. Before the onset of hearing, spontaneous bursts of activity are generated in the pre-hearing cochlea by the spontaneous release of ATP by supporting cells, which causes the depolarization of nearby inner hair cells (IHCs). Groups of depolarized IHCs then synchronously release glutamate and trigger coordinated bursts of action potentials in the auditory nerve (Tritsch and Bergles, 2010; Tritsch et al., 2007). Due to the pattern of ATP release from support cells, the activity of neighboring, tonotopically similar inner hair cells is correlated. Downstream connections of the auditory nerve are already functional days before

birth (Kandler and Friauf, 1995; Kotak and Sanes, 1995; Wu and Oertel, 1987), and rhythmic bursts of action potentials have been recorded in many types of central auditory neurons before the onset of hearing (Jones et al., 2001; Jones et al., 2007; Lippe, 1994; Sonntag et al., 2009). The spontaneous firing patterns of neurons in central nuclei like the MNTB and inferior colliculus are similar to those of spiral ganglion neurons, indicating that patterned spontaneous activity transmitted from the cochlea along the ascending auditory pathway shapes the firing of central auditory neurons even before they respond to sound (Tritsch et al., 2010).

Pre-hearing spontaneous activity patterns consist of discrete bursts, each of which is made up of distinct mini-bursts separated by ~100-300 ms. Each mini-burst is comprised of small groups of action potentials spaced ~10 ms apart (Tritsch et al., 2010). Because the spontaneous activity patterns generated during the pre-hearing period are similar to stimulation patterns used to induce plasticity such as long-term potentiation (Larson et al., 1986), it is generally believed that these bursts of activity play a critical role in the topographic refinement of auditory connections before hearing onset, in a manner similar to what takes place in the developing visual system where the spatiotemporal structure of spontaneous retinal waves shapes the refinement of retinotopic and eye-specific pathways (Huberman, 2007; Penn et al., 1998; Stellwagen and Shatz, 2002; Weliky, 2000).

Evidence for this hypothesis can be seen in α9 KO mice, whose hair cells are functionally de-enervated of their cholinergic input due to a null mutation for the α9 subunit of the acetylcholine receptor, which is necessary for cholinergic transmission in the cochlea (Fig. 1-3 B; Vetter et al., 1999). Cholinergic transmission in the cochlea originates from medial olivocochlear (MOC) neurons in the brainstem (Fig. 1-3 A). MOC neurons receive afferent

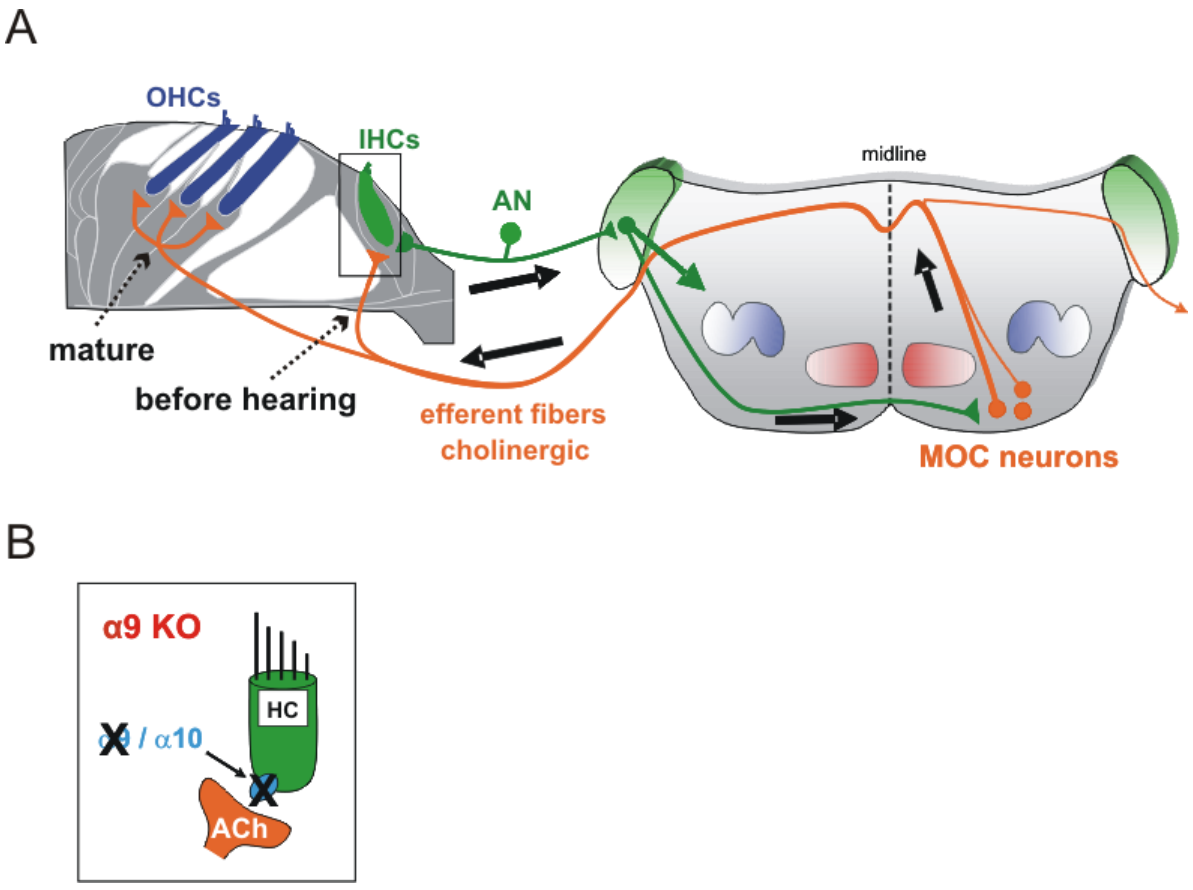

Figure 1-3. Schematic illustration of the MOC efferent feedback system disrupted in α9 KO mice.

(A) Cholinergic efferent fibers from MOC neurons in the brainstem innervate OHCs at maturity, but transiently innervate IHCs before the onset of hearing, where they are thought to influence the pattern of spontaneous activity. The majority of MOC neurons project to the contralateral cochlea, the same cochlea from which they receive afferent input, but ~1/3 project to the ipsilateral cochlea, forming an intercochlear effector pathway. Afferent pathways depicted in green, efferent pathways in orange. Black arrows depict flow of activity. Box represents portion of diagram expanded in (B). (B) ACh receptors on HCs contain α9 and α10 subunits. If the α9 subunit is deleted, as in the α9 KO mouse, then HCs lose their ability to respond to ACh. OHCs, outer hair cells; IHCs, inner hair cells; HC, hair cell; ACh, acetylcholine; AN, auditory nerve; MOC, medial olivocochlear.

input from the CN and project back to the cochlea, providing a feedback loop whereby incoming sound can modulate cochlear sensitivity to subsequent sounds (Warr, 1992). Before the onset of hearing, MOC fibers make transient synapses with α9-containing acetylcholine receptors on IHCs (Bruce et al., 2000; Luo et al., 1998; Simmons and Morley, 1998). Because acetylcholine released by efferent fibers can inhibit the spontaneous firing of IHCs (Glowatzki and Fuchs, 2000), and their transection abolishes the normal bursting pattern of immature cochlear nucleus neurons (Walsh and McGee, 1988), it has been proposed that this innervation helps shape or impose rhythmicity on the bursting pattern of spontaneous activity.

Although efferent input does not seem to be required to initiate rhythmic activity in spiral ganglion neurons (Tritsch et al., 2010), spontaneous activity recorded in MNTB neurons in α9 KO mice before the onset of hearing is missing the fine temporal structure normally observed (Fig. 1-4). Specifically, α9 KO mice have a higher percentage of interspike intervals (ISIs) between 50-750 ms, resulting in a smoother ISI distribution and a less temporally structured pattern (Fig. 1-4 C). Importantly, the overall level of activity, as measured by the spontaneous rate, remains unchanged (Fig. 1-4 D). Thus only the pattern of activity is altered in α9 KO mice. Synaptic silencing is severely impaired in α9 KO mice, with each LSO neuron receiving twice as many MNTB inputs around hearing onset as LSO neurons in control mice (Kim, 2004). The silencing is also less frequency-specific; the region of the MNTB that provides functional input to a single LSO neuron covers significantly more of the MNTB frequency axis in α9 KO mice (Fig. 1-5). Because the specific manner in which spontaneous activity patterns are altered is known in α9 KO mice, impaired silencing and refinement in α9 KO mice provides strong evidence that functional refinement depends on the precise temporal structure of pre-hearing spontaneous activity.

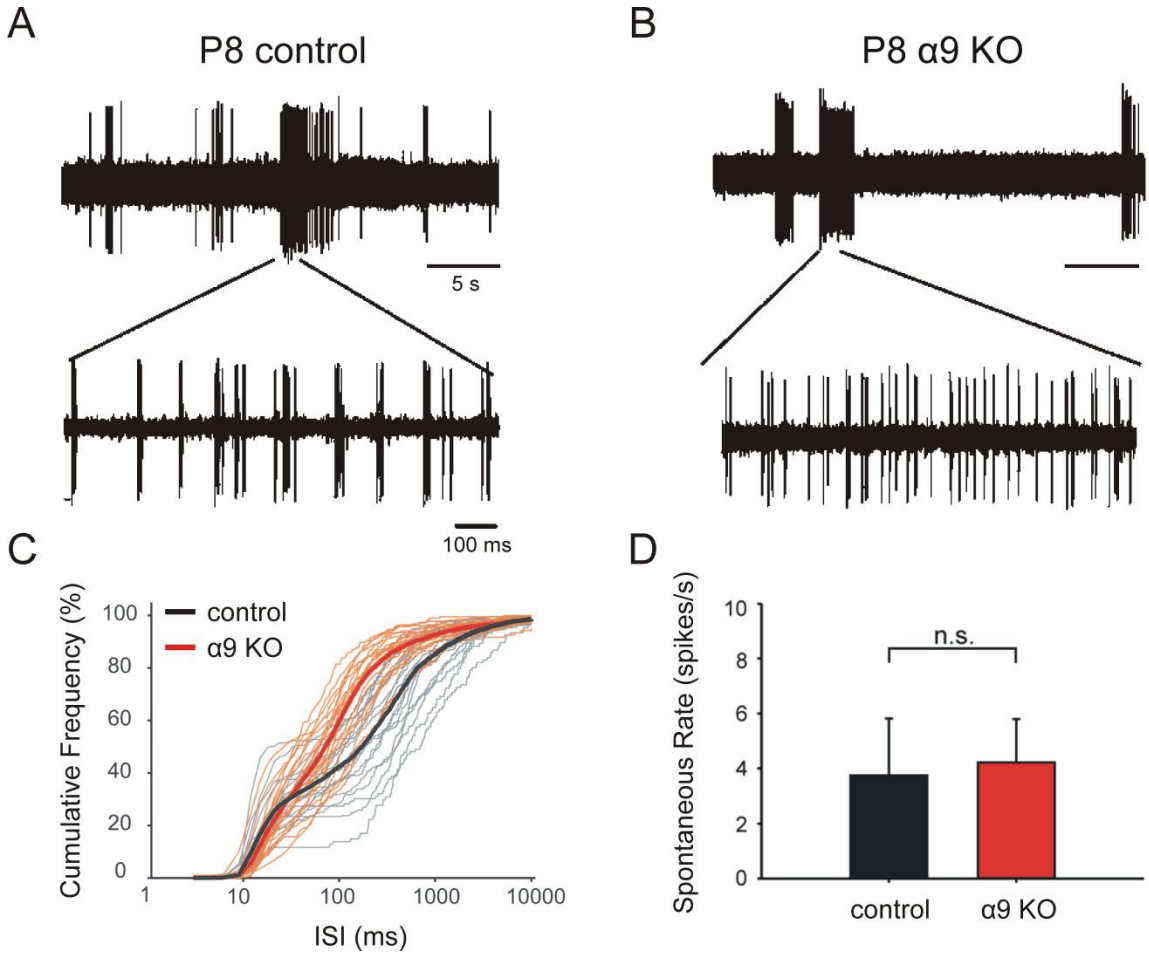

Figure 1-4. Loss of fine temporal structure in pre-hearing spontaneous activity in α9 KO mice.

(A) Example single-unit recording of spontaneous activity in a P8 control MNTB neuron. (B) Example single-unit recording of spontaneous activity in a P8 α9 KO MNTB neuron. (C) Cumulative frequency distribution of ISIs for the population of control (black; n = 21) and α9 KO (red; n = 21) units. (D) Rate of spontaneous firing. Bars represent mean ± s.e.m. ISI, interspike interval; n.s., not significant. Unpublished data provided by M. Sonntag and R. Rubsamen.

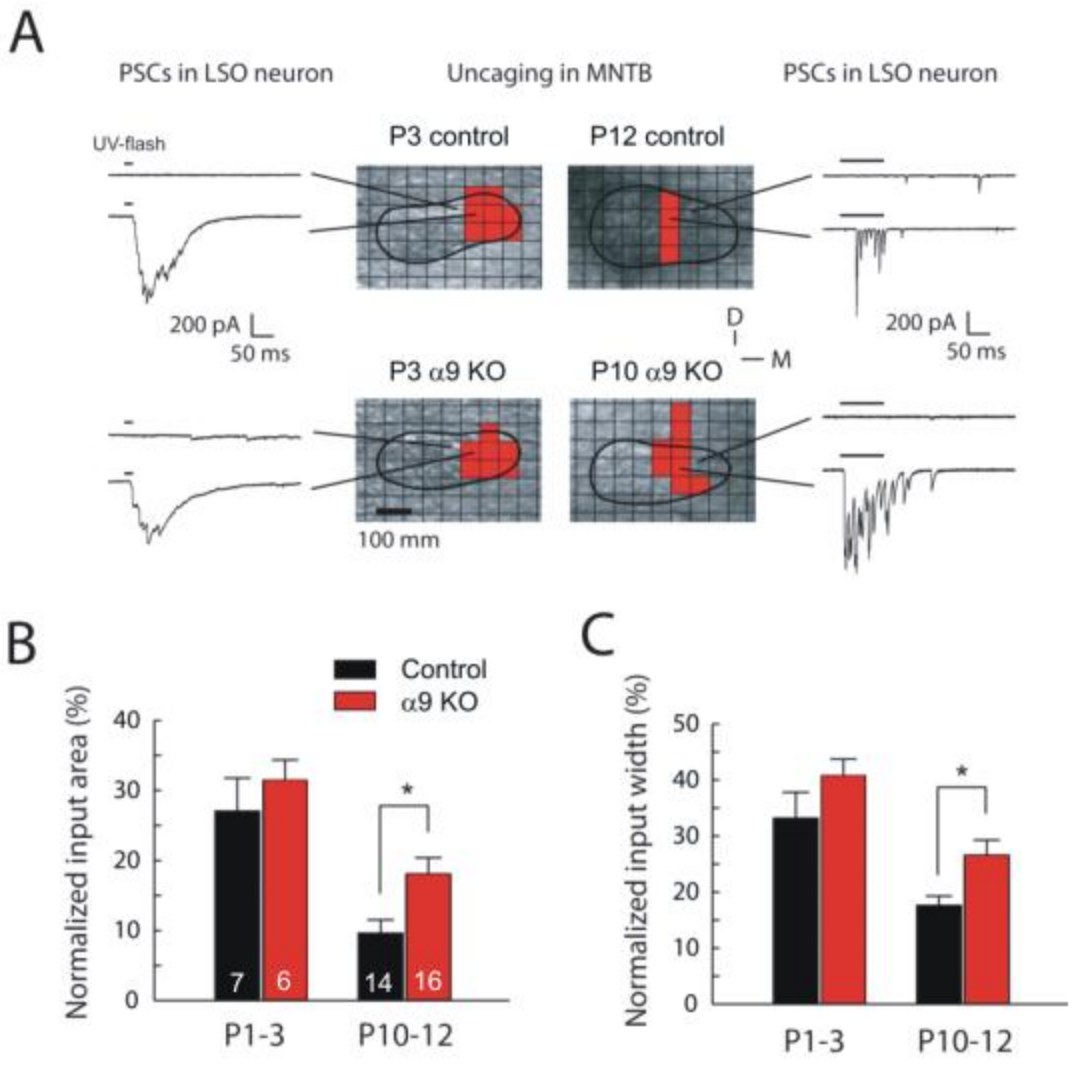

Figure 1-5. Tonotopic sharpening of functional MNTB-LSO connections is impaired in α9 KO mice.

(A) Examples of input maps obtained from P3 and P12 control mice (upper row) and P3 and P10 α9 KO mice. Example traces show synaptic responses elicited by uncaging glutamate at corresponding MNTB sites. MNTB is outlined in black. Stimulation locations are depicted as squares and locations from which responses could be elicited are shown filled in red. Dorsal is to the top, medial to the right. (B) Population data of input areas normalized to the corresponding MNTB area from control and α9 KO mice obtained at P1-3 and P10-12. (C) Normalized mediolateral length (input widths along the tonotopic axis) of maps shown in (B). Asterisk, p = 0.01, Student's t-test. PSC, post-synaptic current. Unpublished data provided by G. Kim.

1.3.1 Two phase model of tonotopic refinement of the developing MNTB-LSO pathway

As a whole, functional and anatomical studies seem to indicate that tonotopic refinement of the inhibitory MNTB-LSO pathway takes place in discrete phases, each characterized by the presence of a different type of activity within the system (Fig. 1-6). In the first phase, silencing of synapses increases the tonotopic precision of functional connections before the onset of hearing, in a manner dependent on the fine temporal pattern of spontaneous activity. In the second phase, pruning of MNTB axons increases the tonotopic precision of anatomical connectivity after hearing onset, during the first week of sound-evoked activity. Connections that are deemed functional through electrophysiological methods imply the presence of anatomical connections, yet methods of assessing anatomical connectivity, such as the reconstruction of dye-filled axons, provide no information about functionality - whether active neurotransmission is taking place. Often anatomical connections are assumed to reflect functional connectivity, yet in the MNTB-LSO system this does not seem to be the case. For this reason, I use the term functional refinement to refer to the silencing of connections as assessed electrophysiologically, and the term anatomical refinement to refer to the elimination of boutons and axonal reorganization assessed through the reconstruction of axon branches. Furthermore, although phases of refinement have also been identified in other systems (Kano and Hashimoto, 2009), a distinction between functional and anatomical remodeling has not generally been made.

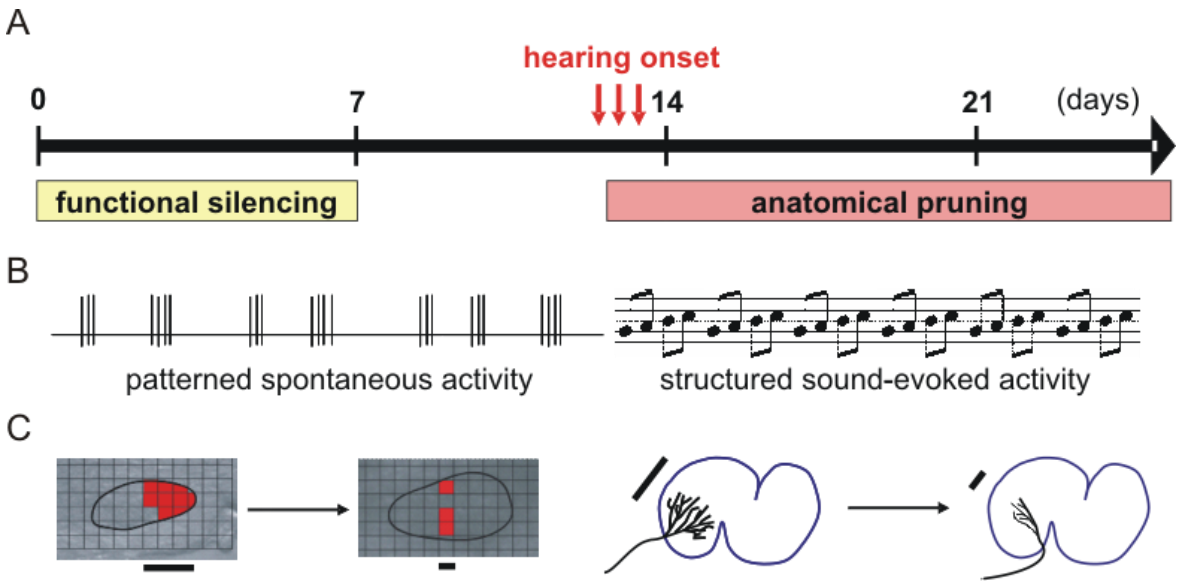

Figure 1-6. Two-phase model of the tonotopic refinement of developing MNTB-LSO connections.

(A) Timeline of tonotopic refinement relative to mouse hearing development. Before the onset of hearing at the end of the second postnatal week, functional silencing of synapses takes place and is largely complete by P7. After the onset of hearing, anatomical pruning takes place. (B) Type of activity present through development. Before hearing onset, patterned spontaneous activity generated in the cochlea propagates through ascending auditory connections. After hearing onset, activity is generated based on the structure of airborne sound. (C) Cartoon data illustrating refinement. During pre-hearing development, the region of the MNTB that provides synaptic input to a single LSO neuron (shown in red within the black outline of the MNTB) becomes spread across a smaller proportion of the frequency axis (denoted by the black bar). During early post-hearing development, the spread of individual MNTB axons along the LSO frequency axis (again denoted by the black bar) becomes narrower.

However, the nature of the relationship between functional and anatomical refinement remains unclearly defined. Pre-hearing functional refinement of the MNTB-LSO pathway has been shown to take place in both rats (Kim and Kandler, 2003) and several strains of mice (Kim, 2004; Noh et al., 2010), indicating that it is a general feature of the development of this circuit. Anatomical refinement of MNTB axons, however, has only been shown in gerbils, with quantitative analysis of boutons restricted to post-hearing development only (Sanes and Siverls, 1991). Thus it remains unclear whether functional and anatomical refinement take place during completely distinct periods of development, or whether they occur during overlapping time periods, in a manner more typical of excitatory systems. The degree to which functional and anatomical processes of refinement are independent, or whether pruning depends on synaptic silencing is also unknown. Similarly, because previous studies were not designed to distinguish between pre-hearing spontaneous activity and activity evoked by sound, attempts to determine the activity-dependence of refinement often manipulated both forms. As a result, the contribution of each of these types of activity to anatomical refinement remains unclear as well.

In this thesis I attempt to tease apart the relationship between functional and anatomical refinement of MNTB-LSO connections during early development, and determine the degree to which spontaneous and sound-evoked activity play a role in each of these processes. Finally, I attempt to link the tonotopic precision of this circuit to a specific aspect of auditory perception, frequency discrimination.

To do so, I first mapped the tonotopic precision of individual MNTB axons in the LSO over the first three weeks of postnatal development in a mouse strain in which functional silencing has already been characterized in order to clearly determine whether functional silencing and anatomical pruning take place during distinct developmental periods. I next

examined whether the pattern of pre-hearing spontaneous activity and resulting functional refinement influence anatomical refinement using α9 KO mice. Third, I investigated the role of structured sound-evoked activity in anatomical refinement by rearing animals in pulsed white noise, which eliminates the spatiotemporal structure of sound present in normal auditory environments. Finally, I developed and used an acoustic startle-based method of assessing frequency discrimination in α9 KO mice to test whether discrimination is affected by the loss of cholinergic efferent innervation of the cochlea and tonotopic specificity.

2.0 DEVELOPMENT OF TONOTOPIC SPECIFICITY IN INDIVIDUAL MNTB AXONS IN THE LSO

2.1 INTRODUCTION

Determining the location of a sound source in space is a major task of the auditory system because, unlike the visual or somatosensory systems, stimulus location is not directly encoded by the site of stimulation on the receptor sheet. The cochlea provides no information about the direction of incoming sound, which must be computed completely *de novo* by the central nervous system. A major cue by which mammals localize sound in horizontal space is small differences in the level of sound between the two ears, which are called interaural intensity differences. These cues are first processed in the central nervous system by binaural neurons in the lateral superior olive (LSO; Boudreau and Tsuchitani, 1968). LSO neurons receive excitatory inputs from the ipsilateral ear via a glutamatergic projection from the cochlear nucleus, and inhibitory inputs from the contralateral ear via a primarily glycinergic projection from the medial nucleus of the trapezoid body (Banks and Smith, 1992; Cant and Casseday, 1986; Sommer et al., 1993). Each projection is tonotopically organized and are aligned so that LSO neurons receive excitatory and inhibitory inputs tuned to the same sound frequency (Sanes and Rubel, 1988; Tollin, 2003).

These pathways are initially formed prenatally, as both glutamatergic and glycinergic synapses in the LSO are functional before birth (Kandler and Friauf, 1995, 1993). Tonotopic precision, however, emerges gradually through both anatomical and synaptic changes during early postnatal development (Kandler et al., 2009; Sanes and Friauf, 2000). Before rats and mice become capable of hearing airborne sound around the end of the second postnatal week (Geal-Dor et al., 1993), the majority of the connections between the MNTB and LSO are silenced, while the connections that are maintained are strengthened (Kim and Kandler, 2003, 2010; Noh et al., 2010). In mice, the silencing of inputs sharpens the tonotopic precision of the connections by ~30-45 % (Fig. 1-5; Noh et al., 2010). After the onset of hearing, pruning and synapse elimination result in fewer boutons per MNTB axon in the LSO and a reduction in the spread of boutons along the LSO frequency axis by ~20 % (Sanes and Siverls, 1991).

Functional weakening of synapses often precedes elimination, but these processes generally occur in rapid succession, and for a given circuit simultaneously (Antonini and Stryker, 1993; Colman et al., 1997). In the inhibitory MNTB-LSO circuit however, synaptic silencing is largely complete by the end of the first postnatal week (Kim and Kandler, 2003), which is days before hearing onset, yet, based on results in gerbils (Sanes and Siverls, 1991), the anatomical elimination of boutons does not take place until the first week of auditory experience. Refinement of tonotopic MNTB-LSO connections thus seems to take place in discrete phases, each confined to a temporally distinct developmental period. However, because mapping of functional connections was performed in rats and mice, while anatomical connections were investigated only in post-hearing gerbils, it remains unclear whether functional and anatomical refinement are truly temporally separated.

To resolve this issue, I dissected these phases of refinement by comprehensively mapping the tonotopic precision of individual MNTB axons in the LSO over the first three weeks of postnatal development, both before and after the onset of hearing. By using a mouse strain in which functional silencing has already been characterized (Fig. 1-5; Kim and Kandler, 2010), I could clearly determine whether pruning and anatomical reorganization of MNTB axons accompanies synaptic silencing before the onset of hearing, or whether functional silencing and anatomical pruning are two distinct phases in the tonotopic refinement of MNTB-LSO connections.

2.2 MATERIALS AND METHODS

2.2.1 Experimental Animals

All experiments were performed using 129S6/SvEv mice (gift of D. Vetter, Tufts University). All experimental procedures were in accordance with NIH guidelines and were approved by the Institutional Animal Care and Use Committee at the University of Pittsburgh.

2.2.2 Acute Slice Preparation

Mice were anesthetized with isoflurane (Piramal Healthcare, Eagle, ID) at postnatal days (P) 2-4, 12-14, or 19-21, decapitated, and the brain removed and bathed in ice-cold artificial cerebrospinal fluid (ACSF; composition in mM: 124 NaCl, 26 $NaHCO_3$, 10 glucose, 5 KCl, 1.25 KH_2PO_4, 1.3 $MgSO_4$, 2 $CaCl_2$, pH 7.4 when aerated with 95% O_2/5% CO_2). ACSF for slice

preparation also included 1 mM kynurenic acid to prevent excitotoxicity. Three hundred fifty μm thick coronal brain slices were then prepared with a vibratome (Leica VT 1200). Slices containing the MNTB and LSO were transferred to an interface chamber with aerated aCSF, and incubated for one hour at room temperature. Slices from P19-21 animals were incubated at 32°C. After incubation, slices were maintained at room temperature until used.

2.2.3 Electrophysiology & Intracellular Fills

Slices were transferred to a submerged-type recording chamber continuously perfused with aerated aCSF. Individual neurons primarily within the medial, high frequency portion of the MNTB were held in whole-cell configuration for approximately 30 minutes with 8-15 MΩ pipettes filled with an internal solution containing (in mM) 100 K-gluconate, 11 EGTA, 10 KCl, 1 $MgCl_2$, 1 $CaCl_2$-H_2O, 10 Hepes, 0.3 Na-GTP, 2 Mg-ATP, 0.1 Alexa Fluor 568 hydrazide (Invitrogen, Carlsbad, CA), and 0.5 % biocytin (pH 7.2, 280 mOsm/L). Alexa 568 was included in the pipette for immediate identification of axons that were cut during slicing. Pipettes were pulled from borosilicate glass capillary tubes (outer diameter 1.5 mm, inner diameter 1.10 mm, 10 cm length; Sutter Instrument Co., Novato, CA) using a Sutter model P-97 puller. Voltage responses to current steps were recorded and used to electrophysiologically confirm MNTB cell identity based on the presence of sag when hyperpolarized (indicative of I_H), and the firing of a single spike in response to suprathreshold depolarization (Banks and Smith, 1992). Cell viability was monitored by eliciting a spike in response to depolarizing current injection. After the 30-minute holding period, slices were then incubated in the interface chamber for approximately one hour at room temperature before being fixed in 4 % paraformaldehyde in 0.01 M phosphate-buffered saline (PBS) for 1-7 days and transferred to 30 % sucrose in PBS for cryoprotection.

The location of all MNTB neurons used for axon reconstruction and quantitative analysis can be found in Appendix A.

2.2.4 Histology

P12-14 and P19-21 slices were cryo-sectioned approximately in half using a sliding, freezing microtome (Microm HM 430). Slices from animals at P2-4 were not re-sectioned. All sections were sequentially frozen on dry ice and thawed three times before being treated with 10 % methanol and 3 % H_2O_2 in PBS for 30 minutes. Sections were washed in PBS and then incubated in blocker (2 % normal goat serum and 0.2 % Triton X-100 in PBS) for four hours before being reacted with an avidin-biotin reagent (ABC Elite Kit, Vector Laboratories, Burlingame, CA) in blocker for two hours at room temperature and then overnight at 4ºC. Sections were then washed in PBS and reacted with 0.05 % diaminobenzidine-tetracholoride (DAB; Sigma, St. Louis, MO) in a solution containing 1 % $CoCl_2$, 1 % $Ni(NH_4)_2SO_4$, and 0.3 % H_2O_2 in PBS. Sections were washed in PBS, mounted on gelatinized glass slides, dehydrated in an ethanol/xylene series, and coverslipped with Permount (Fisher Scientific, Fair Lawn, NJ).

2.2.5 Axon Reconstruction

Complete axonal arbors within the LSO were reconstructed using a Neurolucida system (MBF Bioscience, Williston, VT). The reconstructed axons of all cells used for quantitative analysis can be found in Appendix A. Putative synaptic boutons were identified and marked based on their characteristic round shape and diameter greater than 2x the width of the parent axon. While the complete axon was usually reconstructed, only the portions within the LSO were analyzed.

To ensure analyzed arbors were complete, cells with axon branches within the LSO that were cut during slicing (identified by a large bulbous axonal ending at the slice surface) were discarded from analysis. For analysis, 3-dimensional reconstructions were flattened rostro-caudally into a 2-dimensional, mediolaterally- and dorsoventrally-defined Cartesian coordinate system.

2.2.6 Quantitative Analysis of Reconstructed Axons

Neurolucida Explorer (MBF Bioscience, Williston, VT) was used for basic analysis of reconstructions, including the calculation of cross-sectional nucleus area and the number of boutons within the LSO. The tonotopic specificity of MNTB-LSO connections was determined based on the spread of boutons along the LSO frequency axis, "bouton spread," and the area covered by boutons in the LSO, "bouton area." These measures were quantified using an ellipse-fitting method that captured the elongated shape of termination regions in the LSO. All data are reported as mean ± s.e.m.

2.2.6.1 Ellipse-fitting

An ellipsoid was fit to the coordinates of LSO boutons that maximized the density of boutons within the confines of the ellipse. Because the shape, orientation, and size of the ellipse were objectively determined to maximize density, boutons located outside the main termination region were not always included. As a result, this method is less likely to be influenced by the presence of single or small numbers of boutons located far outside the main region of termination.

Custom-written LabView (National Instruments, TX) programs were used to extract the Cartesian coordinates of boutons located with the LSO from Neurolucida ASC files. A minimum volume enclosing ellipsoid was then fit to these coordinates using custom-written

MATLAB (Mathworks, Natick, MA) scripts based on the Khachiyan Algorithm. The ellipse axis that was most closely oriented mediolaterally was defined as the LSO frequency axis. The diameter of the ellipse along the frequency axis was then used as a measure of bouton spread, or tonotopic specificity, and the area of the ellipse as a measure of bouton area. The statistical significance of group differences was assessed using a two-tailed Student's t-test based on the number of cells.

2.2.6.2 Density Heat Maps

Within Neurolucida, the boutons of each reconstructed axon were overlaid with a 2-dimensional grid comprised of 56.8 μm^2 (at P2-4) or 100 μm^2 (at P12-14 and P19-21) bins. The bin size was chosen to encompass a constant proportion of LSO area (~0.08 %) across all ages. The grid covered the total area of the LSO and was positioned consistently in relation to the bouton centroid of each axon, defined as the center of mass of the boutons of that axon located in the LSO. As a result, the data from each axon were aligned at the bouton centroid, to account for differences in the location of terminations within the LSO and along its frequency axis. Neurolucida Explorer was used to compute the number of boutons per bin.

Custom LabView programs were then used to sort the number of boutons per bin into vector and matrix formats that maintained the geographical position of the boutons in mediolaterally- and dorsoventrally-defined space. The vector data for all of the axons in each group were averaged and the means converted into matrix form. The mean matrix data was then plotted as a heat map of average bouton density using MATLAB. To better illustrate developmental differences in the distribution of boutons between age groups, the difference between the averages was also plotted.

For presentation purposes, the average and difference maps were positioned medially within a representative outline of the LSO, to reflect the position of the majority of termination regions, though the actual location of individual axon terminations within the LSO varied.

2.2.6.3 Density of Boutons along the LSO Frequency Axis

Histograms of bouton density along the LSO frequency axis were generated in MATLAB. First, the Cartesian coordinates of each axon's boutons were rotated around the centroid by an angle theta, which was defined by the orientation of its fitted ellipse. As a result, the horizontal axis of the coordinate system now corresponded to the putative LSO frequency axis, rather than mediolateral space, with an origin at the bouton centroid. The frequency axis was then divided into bins that corresponded to 1 % of the mediolateral length of the LSO. For each axon, counts of the number of boutons per bin were computed and then normalized to the total number of boutons per axon found in the LSO and expressed as a percentage of the total number of boutons per axon. The absolute and relative (normalized) histogram data for all of the axons in each age group were then averaged.

For the presentation of histograms, the mean population data were smoothed with a 3 bin-wide moving average, and then fit with the Gaussian function $f(x) = a1*\exp(-((x-b1)/c1)^2)$, where a1 = the maximum height and b1 = the x-coordinate at maximum height. c1 is related to width such that full width at half the maximum height (FWHM) = 2*c1*sqrt(log(2)). The tonotopic spread of the distributions was quantified by determining the percentage of LSO length present between the medial- and lateral-most bins in which bouton density of the smoothed data sets was ≥ 1 bouton per MNTB axon for absolute histograms, and 0.75 % of the total number of boutons per axon for relative histograms.

To gauge statistical significance, each axon's histogram data was also smoothed and fit with a Gaussian. The descriptive characteristics a1, b1, c1, and tonotopic spread of the individual Gaussians were then averaged for all of the axons of each age group and the statistical significance of age group differences assessed using a two-tailed Student's t-test based on the number of cells.

For plots of developmental change in bouton density relative to initial bouton density along the LSO frequency axis, change was determined using the same method employed when plotting developmental change heat maps. For pre-hearing addition, the mean number of boutons per 1 % LSO length at P12-14, smoothed by the 3 bin-wide moving average, was subtracted from the mean number of boutons per bin at P2-4. For post-hearing elimination, the mean number of boutons per bin at P12-14, smoothed by the 3 bin-wide moving average, was subtracted from the mean number of boutons per bin at P19-21. The change was then plotted against the initial density of boutons along the LSO frequency axis at the earlier developmental age, for pre-hearing addition, relative to density at P2-4, for post-hearing elimination, relative to density at P12-14. ANOVA was used to determine whether the initial density had a significant effect ($p < 0.05$) on the developmental change in bouton number. Pearson correlation was used to determine the strength of the relationship between initial density and developmental change.

2.3 RESULTS

Consistent with previous anatomical studies (Banks and Smith, 1992; Sanes and Siverls, 1991), the axons of individual MNTB neurons terminated in a confined region of the LSO according to the tonotopic location of the soma within the MNTB, even soon after birth at P2-4. At all ages

termination regions tended to be elongated perpendicularly to the largely mediolaterally oriented LSO frequency axis.

At P2-4, the cross-sectional area of the LSO and the termination regions of MNTB axons within it were noticeably smaller than at later ages. Over the first two postnatal weeks, both MNTB axons and the LSO grew (Fig. 2-1 A, B). The average number of boutons per axon within the LSO increased almost 2.5-fold (Fig. 2-1 C), from 127 ± 13 at P2-4 (n = 9 axons) to 302 ± 29 at P12-14 (n = 10 axons; $p < 0.001$, Student's t-test). The spread of boutons along the LSO frequency axis also increased significantly during pre-hearing development, by almost 2-fold (from 96 ± 9 µm at P2-4, to 133 ± 4 µm at P12-14; $p < 0.01$, Student's t-test). Similarly, the cross-sectional area of the LSO covered by boutons increased approximately 1.4-fold (from 13.3 x 10^3 ± 1.6 x 10^3 µm^2 at P2-4, to 24.0 x 10^3 ± 1.5 x 10^3 µm^2 at P12-14; $p < 0.01$; Student's t-test). However, axonal growth and the addition of boutons was matched by expansion of the LSO nucleus itself, such that relative bouton spread or area did not change when normalized to LSO length and area, respectively ($p = 0.29$ for relative spread, Fig. 2-1 D; $p = 0.99$ for relative area, Fig. 2-1 E, Student's t-test). Therefore, while functional MNTB-LSO connections become more tonotopically precise before hearing onset through the silencing of inputs (Kim and Kandler, 2003, 2010; Noh et al., 2010), the number of boutons per individual MNTB axon increases over the same time period, with no change in tonotopic specificity.

However, the developmental addition of boutons to MNTB axons in the LSO before hearing was spatially specific. At P2-4, the boutons of individual axons were distributed relatively evenly across the region of termination, with only a slight increase in density near the center of the termination regions, around the bouton centroid (Fig. 2-2 A). The region of peak density, like the termination region itself, was elongated orthogonal to the frequency axis. At

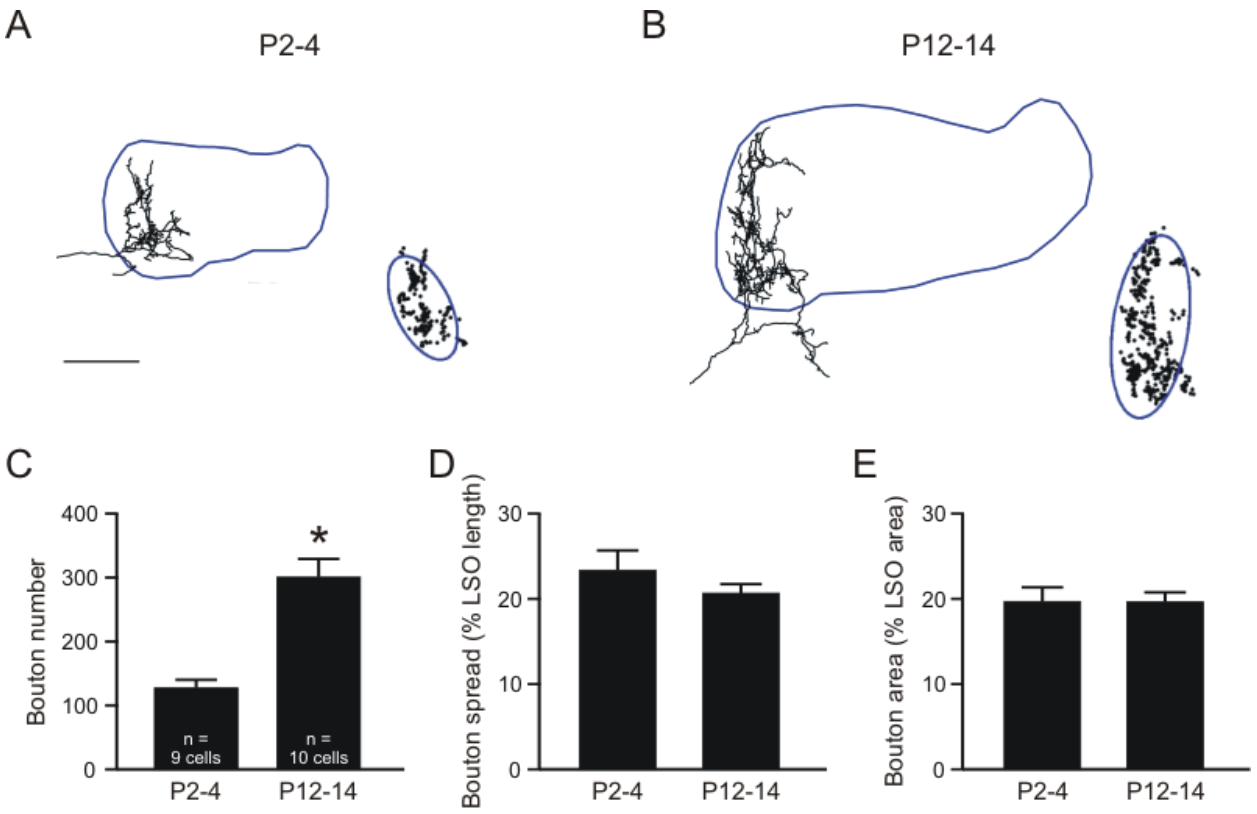

Figure 2-1. Pre-hearing growth of MNTB axons in the LSO.

(A) Example reconstruction of an MNTB axon and its boutons in the LSO at P4. Upper left portion shows the reconstructed axon in black and the outline of the LSO in blue. Lower right portion shows the boutons of that axon located within the LSO in black, and the ellipse fit to those boutons in blue. Dorsal is to the top, medial to the left. Scale bar, 100 µm. (B) Example reconstruction of an MNTB axon and its boutons in the LSO at P13. Scale and conventions same as in (A). (C) Number of boutons per MNTB axon found in the LSO at P2-4 and P12-14. Data show mean ± s.e.m.; n = 9 axons from 6 animals at P2-4, n = 10 axons from 8 animals at P12-14. (D) Spread of boutons along the LSO frequency axis at P2-4 and P12-14. (E) Cross-sectional area of the LSO covered by the boutons of individual MNTB axons at P2-4 and P12-14. Asterisk, $p < 0.05$, Student's t-test.

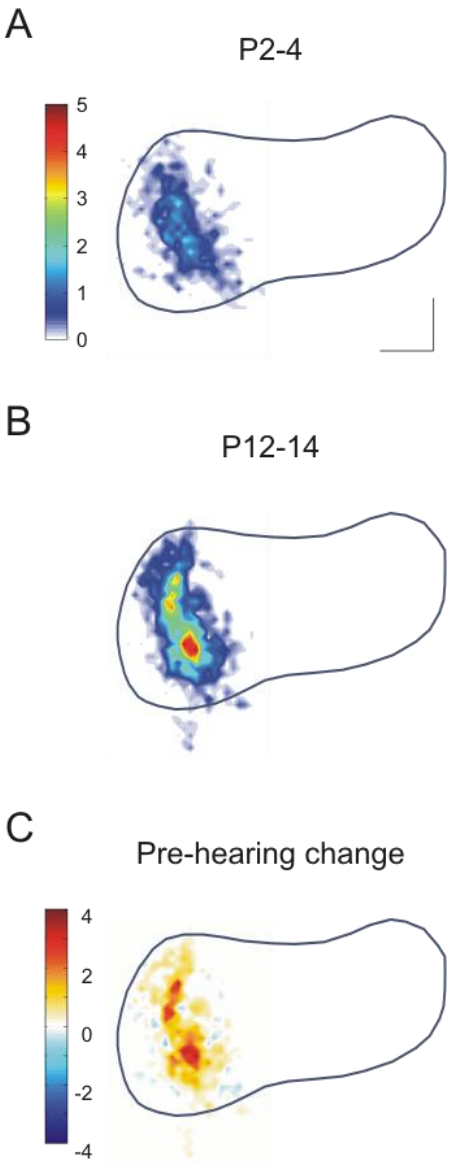

Figure 2-2. Spatial distribution of the boutons of MNTB axons in the LSO over pre-hearing development.

(A) Average density of the boutons of individual MNTB axons within the LSO at P2-4. Dorsal is to the top, medial to the left. Color bar, average number of boutons per axon per 0.17% LSO area; scale bars, 20% mediolateral LSO length and 40% dorsoventral LSO height. (B) Average density of the boutons of individual MNTB axons within the LSO at P12-14. Scale and conventions same as in (A). (C) Change in the average density of the boutons of individual MNTB axons within the LSO over pre-hearing development. Change shows the difference between P2-4 and P12-14. Warm colors indicate an increase in density with development; cool colors indicate a decrease with development. Color bar, average change in bouton number per axon per 0.17% LSO area; scale and orientation same as in (A).

P12-14, bouton density was at a similarly low level at the most peripheral portions of the termination, but density in the center was much greater than it was at P2-4, and declined much more steeply with distance from the center (Fig. 2-2 B). Thus during pre-hearing development, boutons were selectively added to the center of termination regions rather than around the periphery (Fig. 2-2 C). As a result, at P12-14 there was a steep peak in the density of boutons along an isofrequency contour-like band near the center of the termination region, although the boutons remain spread over a constant proportion of the LSO.

In contrast to the axonal growth and addition of boutons that took place before the onset of hearing, during the first week after hearing onset MNTB axons were pruned and boutons eliminated (Fig. 2-4). The number of boutons in the LSO was reduced by more than half, from 302 ± 29 boutons per MNTB axon at P12-14 (n = 10 axons) to 137 ± 21 boutons at P19-21 (n = 9 axons; $p < 0.001$, Student's t-test; Fig. 2-4 C). Furthermore, the elimination of boutons increased the tonotopic specificity of the projection by 1.5-fold, with a 35 % reduction in the spread of boutons along the frequency axis (from 21 ± 1 % LSO length at P12-14 to 14 ± 2 % LSO length at P19-21; $p = 0.002$, Student's t-test; Fig. 2-4 D) and a 50 % reduction in bouton area (from 20 ± 1 % LSO area at P12-14 to 10 ± 2 % LSO area at P19-21; $p < 0.001$, Student's t-test; Fig. 2-4 E). Significant reductions in bouton spread and area took place in the absence of any change in the size of the LSO, indicating that true pruning was taking place, rather than growth of the nucleus around a static axon and bouton area.

Tonotopic sharpening did not occur through the selective elimination of boutons from the extreme medial and lateral edges of the terminations (Fig. 2-5). Instead, boutons were lost across the entire termination region. In fact, the greatest elimination took place near the center of the termination, where density was highest at P12-14, not at the terminations' periphery.

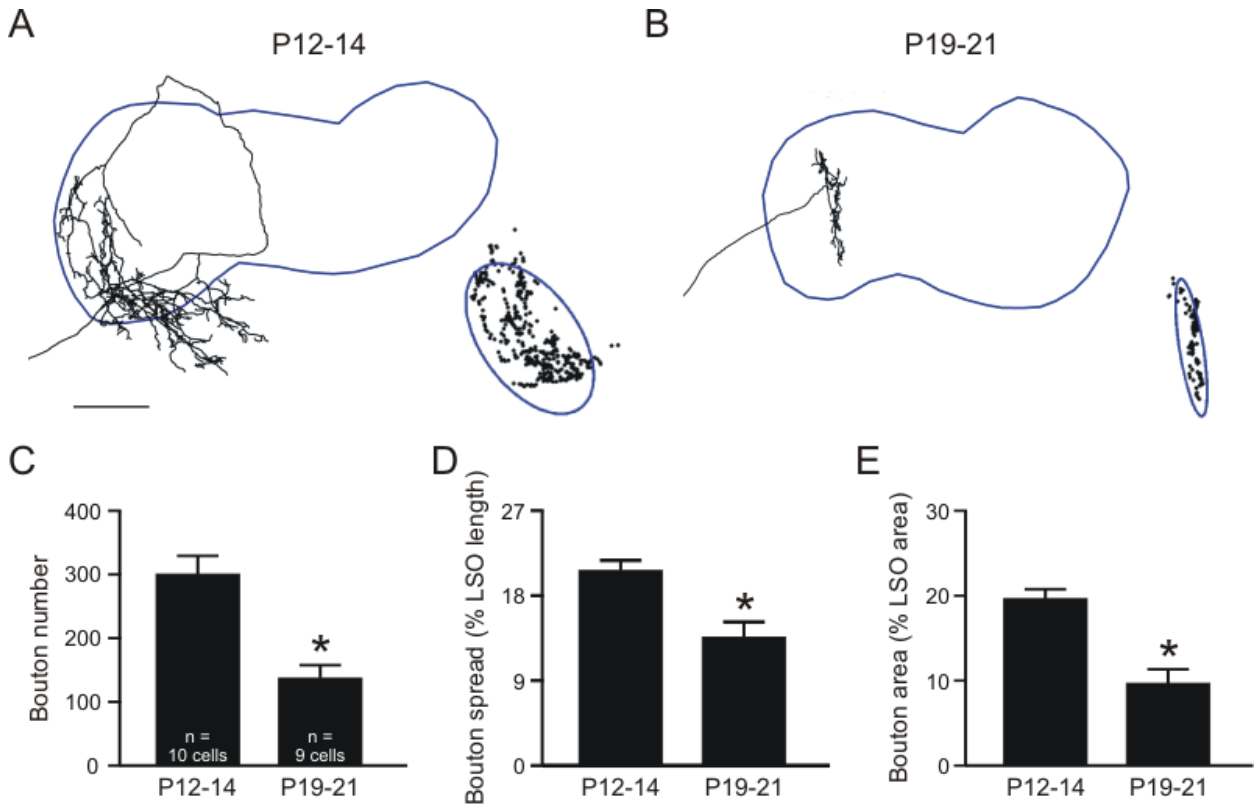

Figure 2-3. Post-hearing refinement of MNTB axons in the LSO.

(A) Example reconstruction of an MNTB axon and its boutons in the LSO at P12. Upper left portion shows the reconstructed axon in black and the outline of the LSO in blue. Lower right portion shows the boutons of that axon located within the LSO in black, and the ellipse fit to those boutons in blue. Dorsal is to the top, medial to the left. Scale bar, 100 µm. (B) Example reconstruction of an MNTB axon and its boutons in the LSO at P20. Scale and conventions same as in (A). (C) Number of boutons per MNTB axon found in the LSO at P12-14 and P19-21. Data show mean ± s.e.m.; n = 10 axons from 8 animals at P12-14; n = 9 axons from 8 animals at P19-21. (D) Spread of boutons along the LSO frequency axis at P12-14 and P19-21. (E) Cross-sectional area of the LSO covered by the boutons of individual MNTB axons at P12-14 and P19-21. Asterisk, $p < 0.05$, Student's t-test.

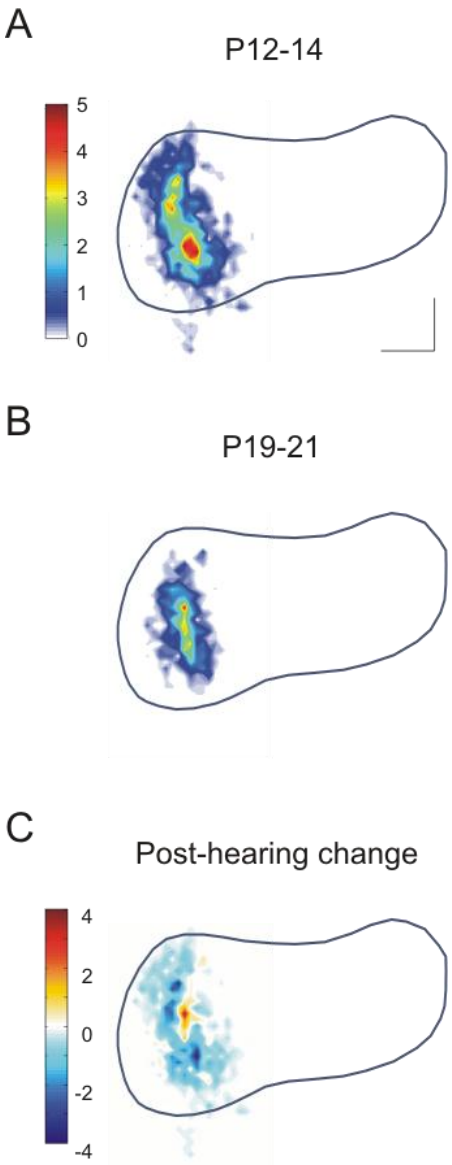

Figure 2-4. Spatial distribution of the boutons of MNTB axons in the LSO over post-hearing development.

(A) Average density of the boutons of individual MNTB axons within the LSO at P12-14. Dorsal is to the top, medial to the left. Color bar, average number of boutons per axon per 0.17% LSO area; scale bars, 20% mediolateral LSO length and 40% dorsoventral LSO height. (B) Average density of the boutons of individual MNTB axons within the LSO at P19-21. Scale and conventions same as in (A). (C) Change in the average density of the boutons of individual MNTB axons within the LSO over post-hearing development. Change shows the difference between P12-14 and P19-21. Warm colors indicate an increase in density with development; cool colors indicate a decrease with development. Color bar, average change in bouton number per axon per 0.17% LSO area; scale and orientation same as in (A).

Consistent with the significant loss of boutons, the only place density was higher at P19-21 than at P12-14 resulted from a slight dorsal shift in the location of peak density. The elongated region of peak density was also lower at P19-21 than at P12-14, and appeared to occupy a narrower region along the frequency axis.

I found that the orientation of the elongated termination regions of MNTB axons in the LSO could vary by as much as 47° (compare Fig. 2-4 A and B for an example), presumably due to the curvature of the LSO frequency axis in following the "S" shape of the nucleus. If the termination regions of some axons were tilted more mediolaterally than others due to their position along the frequency axis, the spatial distribution of boutons in mediolaterally- and dorsoventrally-defined coordinate space may not completely accurately describe the distribution along the tonotopic axis. In addition, density maps are largely descriptive and not easily compared statistically. Therefore, to more quantitatively compare the distribution of boutons along the LSO frequency axis over development, I aligned the boutons of each axon along the frequency axis, as defined by the orientation of the fitted ellipse, instead of in mediolateral-dorsoventral space. I eliminated the spatial dimension perpendicular to the frequency axis and created histograms that described the density of boutons along the LSO frequency axis relative to the bouton centroid, both in terms of the absolute number of boutons per axon and the relative percentage of the total number of boutons per axon.

Overall, the histograms were well fit by Gaussian functions (R^2 = 0.93 ± 0.02 for P2-4, 0.93 ± 0.01 for P12-14, and 0.96 ± 0.01 for P19-21 for both absolute and relative distributions), corresponding with the appearance of density maps. For the average number of boutons per axon, the Gaussian was shallow at P2-4, with boutons distributed relatively evenly along the frequency axis, with a slight peak near the bouton centroid (Fig. 2-5 A). At P12-14, the peak

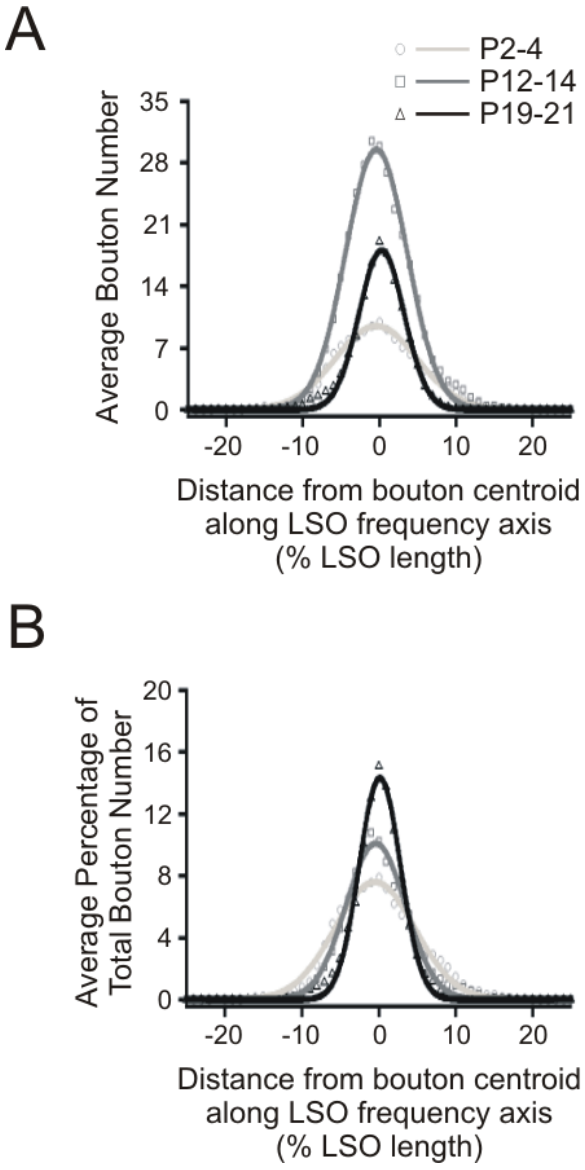

Figure 2-5. Developmental change in the distribution of boutons along the LSO frequency axis.

(A) Histograms of the average absolute distribution of boutons per MNTB axon along the frequency axis at P2-4 (lt. grey, circles), P12-14 (dk. grey, squares) and P19-21 (black, triangles). Symbols represent population means smoothed by a 3-bin moving average, lines show the Gaussian fit to the smoothed data. Negative distances, medial; positive distances, lateral. (B) Histograms of the average relative distribution of boutons per MNTB axon along the frequency axis. Conventions same as in (A).

near the centroid was three times greater than at P2-4 ($p < 0.001$, Student's t-test), consistent with the selective addition of boutons primarily to the center of termination bands before hearing onset. The width of the distribution at the base, which most closely corresponds to tonotopic specificity, did not change between P2-4 and P12-14 ($p = 0.80$, Student's t-test).

Between P12-14 and P19-21, the maximum density of boutons was significantly reduced ($p = 0.002$, Student's t-test), and the width at the base of the distribution was reduced as well ($p < 0.001$, Student's t-test). Again, both the reduction of the peak and narrowing of the base seemed to result from the elimination of boutons across the whole termination. As indicated by the distance between the P19-21 Gaussian and P12-14 Gaussian, more boutons were lost from the center regions of highest density, rather than at the periphery. As a result of the density-dependent elimination of boutons, the distribution at P19-21 looked like the distribution at P12-14 that has been shifted downward, causing the reduction in spread. These results are all consistent with estimates of bouton spread generated with ellipse fitting that showed tonotopic sharpening after, but not before, hearing onset.

I also normalized the distributions to the total number of boutons per axon (Fig. 2-5 B). Displayed this way, the curves show the average relative distribution of each axon's boutons along the frequency axis, with an equal area under each age group's Gaussian. In this case, each axon contributes equally to the mean distribution, regardless of its total number of boutons. Similar to the absolute distributions, the relative peak density of boutons also became greater over pre-hearing development, from 7.7 ± 0.6 % of the total number of boutons per axon at P2-4 to 10.6 ± 0.6 % of the total number of boutons per axon at P12-14 ($p = 0.005$, Student's t-test), without a significant change in the tonotopic width of the distribution at the base ($p = 0.35$, Student's t-test). Over post-hearing development, because the width of the base of the

distribution became narrower ($p < 0.001$, Student's t-test), the relative peak density continued to increase, reaching a level approximately twice what it was at P2-4. Observing the same developmental changes in the relative distribution of boutons indicates that the distributions of absolute bouton number were not skewed or dominated by axons with a higher number of boutons, and are likely to be characteristic of the population of axons as a whole.

Both the density heat maps and histograms indicated that the change in bouton density at a specific location in the termination was related to the initial number of boutons present at that location. Therefore, I investigated how the change in bouton number over development was related to bouton density along the LSO frequency axis. As expected, the density of boutons along the frequency axis at P2-4 significantly affected the number of boutons added during pre-hearing development (Fig. 2-6 A; $F = 3184$, $p < 0.001$, One-way ANOVA). There was a strong positive correlation between the initial density and change in density ($R^2 = 0.87$, $p < 0.001$, Pearson correlation), indicating that for every additional bouton present per percent LSO length at P2-4, the number of boutons added during pre-hearing development increased by ~1.75. However, even though the linear regression was significant, the relationship was better described by a quadratic polynomial ($R^2 = 0.97$), suggesting that the rate of change between density at P2-4 and boutons added during pre-hearing development increased with increasing density.

Similarly, the density of boutons along the frequency axis at P12-14 had a significant effect on the number of boutons eliminated during post-hearing development (Fig. 2-6 B; $F = 18271$, $p < 0.001$, One-way ANOVA), consistent with the density-dependent elimination indicated by the heat maps and histograms. Again, there was a strong positive correlation between the initial density and change in density ($R^2 = 0.87$, $p < 0.001$, Pearson correlation). The relationship between initial density and bouton elimination was also better described by a

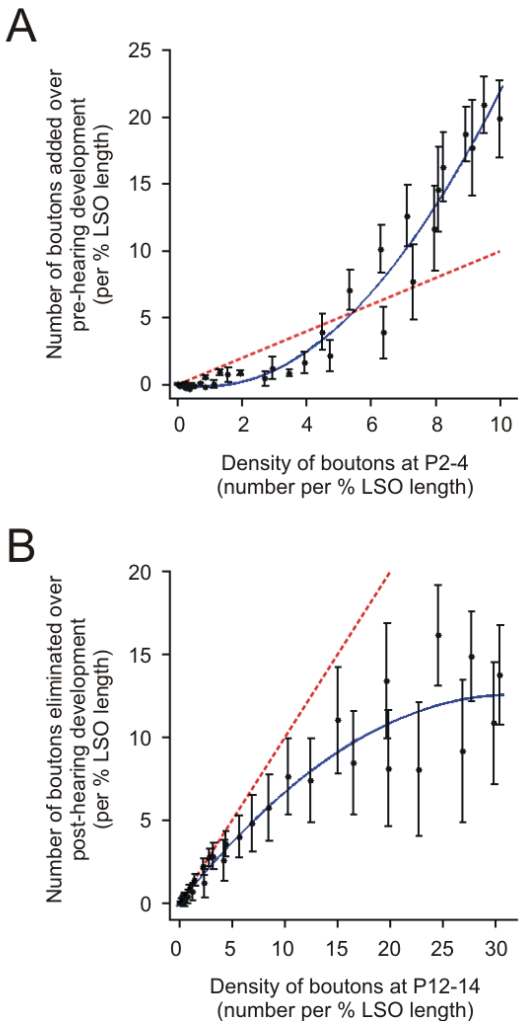

Figure 2-6. The addition and elimination of boutons during development is density-dependent.

(A) The addition of boutons before hearing is density-dependent. The number of boutons added to a specific location along the LSO frequency axis over pre-hearing development (between P2-4 and P12-14) was strongly correlated with the density of boutons at that location at P2-4. $p < 0.001$, Pearson correlation. (B) The elimination of boutons after hearing is density-dependent. The number of boutons eliminated from a specific location along the LSO frequency axis over post-hearing development (between P12-14 and P19-21) was strongly correlated with the density of boutons at that location at P12-4. $p < 0.001$, Pearson correlation. Symbols represent mean ± s.e.m.; blue line, quadratic polynomial fit, $f(x) = p1*x\text{^}2 + p2*x + p3$, $R^2 = 0.97$ in (A), 0.92 in (B); red dashed line, unity line.

quadratic polynomial ($R^2 = 0.92$), although the gain in goodness-of-fit was small. In contrast to the density-dependence of pre-hearing addition, the rate of change between density at P12-14 and boutons eliminated during post-hearing development decreased with increasing density, indicating that fewer boutons were eliminated from locations with the highest density than would be expected if the relationship was completely linear.

2.4 DISCUSSION

2.4.1 Two phases of refinement

Analyzing the termination patterns of single MNTB axons in the LSO of mice confirmed that no tonotopic sharpening of anatomical connections takes place before hearing onset. Between P2-4 and P12-14, axons in the LSO grew, significantly increasing in absolute bouton area and spread. But because this growth was matched by growth of the LSO nucleus, the relative proportion of the LSO covered by the boutons of individual MNTB axons remained constant. Between P12-14 and P19-21, elimination of boutons resulted in anatomical connections that were ~1.5 times more tonotopically precise. Because no anatomical refinement took place before hearing onset, when synaptic silencing increases the tonotopic specificity of functional MNTB-LSO connections, the current results support the two phase model of refinement, with functional refinement taking place before hearing, and anatomical refinement restricted to post-hearing development. The lack of pre-hearing anatomical refinement also indicates that the mechanisms underlying frequency-specific synaptic silencing are not reflected in the number and distribution of the boutons of individual MNTB axons.

In the gerbil (Sanes and Siverls, 1991), MNTB axonal branches initially cover ~6 % of the cross-sectional area of the LSO at P2-3. Although I examined bouton area instead of axonal branches and used a different method of quantification, this is comparable to the 10 ± 1 % covered by boutons in P2-4 mice. Just before hearing onset, at P10-13, relative axonal area had not changed and remained ~6 %, consistent with the lack of refinement of relative bouton area I found between P2-4 and P12-14. Also at P10-13 in gerbils, 244 ± 16 boutons were spread across 121 ± 11 µm of the LSO frequency axis, which is again comparable with the 301 ± 21 boutons per axon spread across 133 ± 4 µm in P12-14 mice, although the relative proportion of the frequency axis is likely to differ due to differences in the size and shape of the LSO between mice and gerbils. After hearing onset, between P10-13 and P18-25, the number of boutons was reduced by ~35 %, to 158 ± 13, and the spread along the frequency by ~23 %, to 93 ± 11 µm, although the relative axonal area was only reduced very slightly, by ~1 %. Between P12-14 and P19-21 in the mouse, bouton number was reduced by ~54 %, to 137 ± 21, and spread reduced by ~42 %, to 77 ± 7 µm. In absolute terms then, there may be slightly more post-hearing anatomical refinement of MNTB axons in the LSO in mice than in gerbils. The lack of a significant reduction in axonal area after hearing onset in gerbils despite the reduction in bouton spread suggests that axonal area may not accurately reflect tonotopic precision. Thus it is difficult to determine whether the maintenance of a constant relative axonal area before hearing onset in gerbils reflects a lack of tonotopic refinement, as I found in the mouse. Overall, however, the mouse data are consistent with the gerbil data in that the number and spread of the boutons of individual MNTB axons in the LSO was significantly reduced during early post-hearing development.

2.4.2 The relationship between functional and anatomical refinement

No tonotopic refinement took place before hearing onset (Fig. 2-1), despite the ~45 % sharpening of functional connections over the same period (Fig. 1-5). However, the distribution of boutons in the LSO and along its frequency axis did change during pre-hearing development. Specifically, the addition of boutons was selective to the center of the termination regions of MNTB axons. The spatially-selective addition of boutons may play a role in the strengthening of functionally maintained connections that takes place during the same period (Kim, 2004; Kim and Kandler, 2010).

Between P1-3 and P10-12, the mean amplitude of LSO post-synaptic currents elicited by stimulation of single MNTB axonal fibers increased from 30 ± 4 to 470 + 93 pA in 129S6/SvEv mice, the same mice used in the current study of anatomical refinement. Single fiber strengthening results primarily from the addition of new release sites (~7 per fiber) between individual MNTB axons and single LSO neurons (Kim and Kandler, 2010). Unfortunately there is no way of knowing how the boutons of individual MNTB axons are distributed among multiple LSO neurons based on the data from single biocytin-filled neurons and I cannot directly relate anatomically-defined boutons to functional release sites in the MNTB-LSO circuit without additional ultrastructural analysis. Still, it is likely that the addition of boutons to biocytin-filled MNTB axons reflects the addition of release sites, since boutons identified in HRP-labeled axons at the level of light microscopy have been shown to display the ultrastructural features of synaptic release sites, including vesicles, active zones, and close apposition to postsynaptic sites (Pierce and Mendell, 1993). It is thus likely that the location of boutons on MNTB axons is closely correlated with sites of synaptic transmission. Accordingly, the spatially-selective addition of boutons to individual MNTB axons is likely reflective of the addition of release sites

to specific post-synaptic LSO neurons, contributing to the strengthening of maintained single fiber inputs.

It is tempting to assume that synapses that were functionally silenced before hearing onset correspond to boutons that were anatomically eliminated after hearing onset, especially because synapse weakening does often precede elimination (Antonini and Stryker, 1993; Colman et al., 1997). Based on comparisons of the tonotopic specificity in functional and anatomical maps before and at hearing onset, this is likely to be at least partly the case, although one cannot be fully sure until it becomes possible to follow an identified functionally silent synapse during the week-long delay that takes place before anatomical elimination. Between P1 and P14, functional maps become narrower in both absolute and normalized measurements (Kim and Kandler, 2003). Over the same period, the absolute spread of boutons increases, but the relative spread remains constant (Fig. 2-1), suggesting that boutons on the peripheral edges of the spread are non-functional. Since boutons at the outermost edges of the spread are eliminated after hearing onset, it is likely at least some of the boutons eliminated after hearing onset correspond to functionally-silenced synapses. However, because boutons were also eliminated from other portions of the termination region, like the large number from the center, it is also likely that functional, non-silent synapses were eliminated as well.

2.4.3 Sinking the iceberg: a model of tonotopic refinement of MNTB axons in the LSO

Developmental refinement of neuronal connectivity is often described as the elimination of initially exuberant inputs from imprecise or "incorrect" targets, accompanied by the maintenance and strengthening of "correct" connections. Such descriptions suggest that certain connections can be identified as incorrect, often through activity-dependent mechanisms, and selectively

eliminated. Based on this reasoning, in the case of tonotopic anatomical connections between the MNTB and LSO, the correct connections would most likely be those in the center of the termination, where the density of boutons was highest from the start. If the addition of boutons is related to the strengthening of maintained inputs, than the selective addition to the center also suggests that the connections formed there are tonotopically correct in that they correspond to those inputs that were not eliminated during functional silencing. Conversely, boutons located furthest from the centroid along the frequency axis would then be in an incorrect tonotopic location, and therefore slated for elimination.

However, after hearing onset, tonotopic sharpening of MNTB axons in the LSO did not take place through the elimination of boutons only from the outermost edges of the termination region. Boutons were lost across the whole termination area, effectively "sinking the iceberg" (Fig. 2-7). In fact, fewer boutons were eliminated from the periphery than from the center, since, like addition, the loss of boutons after hearing onset was strongly correlated with the density of boutons along the LSO frequency axis at P12-14. Although boutons lost from the periphery likely correspond to silent synapses (see above), the large number of boutons lost from the center suggests that tonotopically correct connections were also affected by anatomical elimination. If pruning resulted in the elimination of all of the boutons between the MNTB axon and a single LSO neuron, this could mean the elimination of a functional input. If only some of the boutons connecting the pair were eliminated, the connection would likely be weaker.

Although the non-spatially selective elimination of boutons suggests that sharpening of MNTB-LSO tonotopy after hearing does not proceed through the sole elimination of tonotopically incorrect connections, it is also possible that boutons eliminated from the tonotopically correct center of the termination were connected to less tonotopically precise LSO

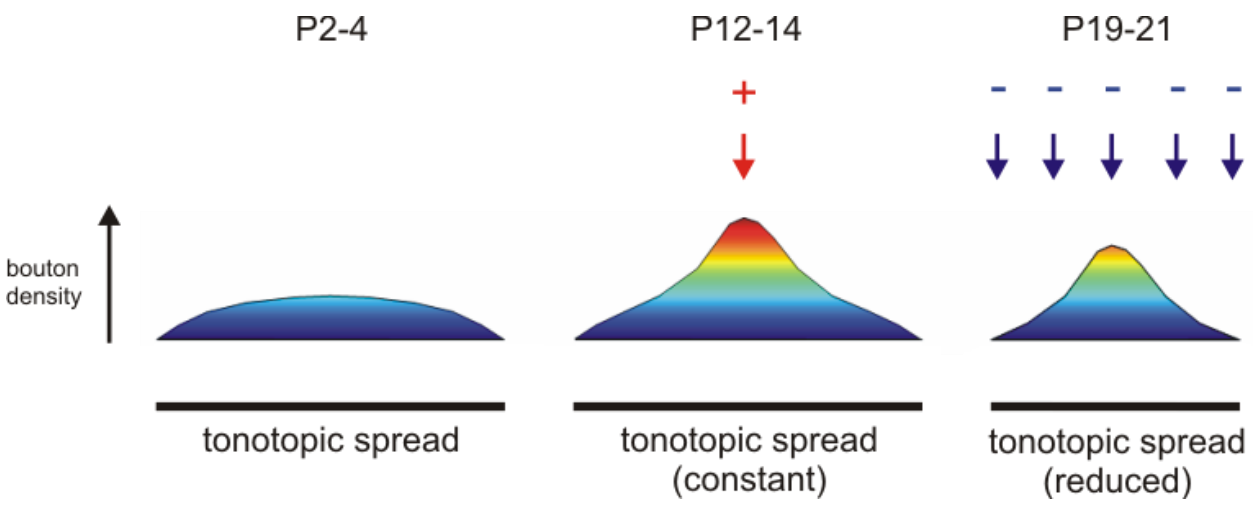

Figure 2-7. An iceberg model of tonotopic refinement of MNTB axons in the LSO.

Soon after birth, at P2-4, boutons are evenly distributed across the frequency axis, with only a slight peak in density near the center. Over pre-hearing development, boutons are selectively added to center of the isofrequency band, such that around hearing onset, at P12-14, the peak density near the center is greater, but there is no change in the tonotopic spread of the distribution. During post-hearing development, elimination of boutons is not spatially selective to the outer edges of the termination region. Instead, boutons are lost across the entire region of innervation, such that the reduction in tonotopic spread at P19-21 results from 'sinking the iceberg.'

neurons through more distal dendrites. If so, boutons lost from the center could contribute to tonotopic sharpening as much as boutons lost from the periphery. There is evidence that MNTB inputs are mostly found on LSO somata and proximal dendrites in adult animals (Spangler et al., 1985), consistent with a loss of input to distal dendrites. Similarly, glycine receptors on LSO neurons become concentrated to the soma during the third postnatal week (Friauf et al., 1997), indicating that synapses with MTNB axons are less likely to be found on distal dendrites at later developmental stages. In the gerbil, LSO dendrites extend ~90 μm along the frequency axis at P13-14 (Sanes et al., 1992b), so somata located on the edges of bouton termination regions could easily extend distal dendrites into the central regions of bouton termination regions that are 133 ± 4 μm in diameter. This type of synaptic reorganization would be consistent with the refinement of inhibitory input in the gerbil medial superior olive (MSO), where glycinergic synapses and MNTB axonal endsegments are reorganized between P10 and adulthood to become more concentrated on MSO somata rather than distal dendrites (Kapfer et al., 2002; Werthat et al., 2008).

Examining functional connections after hearing onset would provide insight into whether all anatomically eliminated boutons corresponded to silenced inputs. If single fiber strength was reduced between hearing onset and P19-21, it would suggest that some of the boutons eliminated were lost from tonotopically correct connections that were functionally maintained and strengthened before hearing, and thus were not silent. Similarly, if the width of input maps continued to decrease, it would provide strong evidence that not all boutons eliminated after hearing onset corresponded to synapses that had been functionally silenced.

Importantly, the elimination of boutons from all frequency regions of the distribution still caused the tonotopic precision of termination regions to increase, because although boutons at

the periphery were not the only ones lost, some of them were eliminated as well. According to the iceberg analogy, sinking the iceberg makes it appear smaller, since the outermost edges that were previously visible are now below the waterline. In the MNTB-LSO circuit, this type of density-dependent bouton elimination has the added function of reducing the number of boutons while still maintaining the relationship between density and distance from the centroid along the frequency axis, in a manner reminiscent of the homeostatic scaling of synaptic strength (Turrigiano and Nelson, 2004).

However, homeostatic scaling is generally thought to adjust the firing rate of a neuron by adjusting the strength of its inputs through modulation of the physiological characteristics or numbers of postsynaptic receptors (Turrigiano, 2008), which is an intracellular process. But in the MNTB-LSO circuit, a homeostatic mechanism that involved the elimination of boutons from the presynaptic MNTB axon would presumably act to regulate the firing rate of the postsynaptic LSO neuron, not the firing rate of the MNTB neuron itself. Therefore, such a mechanism would require a retrograde messenger from the LSO neuron to convey a signal to reduce connection strength via bouton elimination. Endocannabinoids are a likely candidate, since retrograde endocannabinoid signaling mediates long-term plasticity in many subcortical auditory circuits, including the dorsal cochlear nucleus (Tzounopoulos et al., 2007; Zhao et al., 2009), auditory midbrain (Penzo and Pena, 2009), and the calyx of Held (Kushmerick et al., 2004). CB1 receptors are also heavily expressed in the LSO after hearing onset, in a pattern consistent with localization to MNTB terminals (Chi and Kandler, unpublished observations). Such a retrograde signal could either act locally in a synapse-dependent manner, or generate more global effects across the entire axon.

If bouton elimination is homeostatic, then one possibility is that it serves to regulate either the number or density of boutons per axon. In the neuromuscular junction, for example, axon branches from motor neurons with more extensive overall axonal arbors are at a disadvantage in the competition to innervate individual muscle fibers, suggesting that each axon has a limited amount of resources to devote to transmission with its postsynaptic partners (Kasthuri and Lichtman, 2003). It could be that doubling the number of boutons before hearing onset exceeds the resources of the axon, causing the need for bouton elimination afterwards. Resource availability may also be related to the level or pattern of activity, such that fewer synapses can be supported once the system is activated by sound.

Alternatively, bouton elimination could function to homeostatically regulate the strength of the output of the axon to its postsynaptic LSO partners, perhaps to regulate the strength of inhibition relative to the strength of excitation from the CN. Since it is likely that bouton density is proportional to input strength, bouton elimination might be triggered when density exceeds some threshold. If so, elimination would depend on the steep increase in density near the center of termination regions, and thus the spatially-selective addition of boutons before hearing onset. It remains to be seen, however, what factors are important for the selective addition of boutons to the center of termination regions, and whether it depends on the pattern of pre-hearing functional refinement or spontaneous activity.

2.4.4 Tonotopic refinement of developing axons elsewhere in the auditory brainstem

Here I examined the terminations of individual MNTB axons in the LSO during the first three weeks of postnatal development, both before and after the onset of hearing. I found that tonotopic refinement takes place only after hearing onset, through the elimination of boutons and

a reduction in the spread of boutons along the LSO frequency axis. This elimination of boutons and reduction in spread are consistent with the refinement of inhibitory input in the gerbil MSO, where the spread of MNTB axonal endsegments along the MSO frequency axis is also reduced (Werthat et al., 2008), although whether these changes in the MSO are also preceded by synaptic silencing before hearing onset is unknown.

Nevertheless, the time scale and mechanisms of the tonotopic refinement of MNTB axons in the LSO also differ significantly from the tonotopic refinement of axons elsewhere in the auditory brainstem. Another well-studied example is the development of tonotopy in the projection of spiral ganglion (SG) neurons to the three subdivisions of the cochlear nucleus (CN; Leake et al., 2002; Snyder and Leake, 1997; Snyder et al., 1997). Like MNTB-LSO connections, tonotopy is already present during initial circuit formation, and is likely set up through molecular guidance mechanisms (Cramer, 2005; Farinas et al., 2001; Huffman and Cramer, 2007). In addition, similar to MNTB axons in the LSO, the tonotopic specificity of SG axons in the CN increases over development. In the MNTB-LSO circuit, tonotopic sharpening of MNTB axons takes place through true pruning; at P19-21, the absolute area and spread of boutons in the LSO are significantly smaller than they were at P12-14. In contrast, tonotopic sharpening of SG axons in the CN occurs through disproportionate growth of the axons and their target region. When small groups of neighboring SG neurons were labeled by focal injection of neurobiotin into the cochlea, the absolute size of the termination region in the CN increased by ~25 % over development. However, the target nucleus grew ~45 % over the same time period (Leake et al., 2002; Rubel and Cramer, 2002). As a result, the projection, even though it was larger, occupied a smaller proportion of frequency space and was more tonotopically precise. In contrast to the

MNTB-LSO projection, sharpening therefore occurred not through pruning, but through growth of the target.

In the CN, sharpening of SG axons also took place earlier in development than refinement of MNTB axons in the LSO. The spread of SG termination regions in the CN were as tonotopically precise at P6 as they were in the adult (Snyder and Leake, 1997). Since cats begin to hear around P3-4, all sharpening therefore took place before hearing onset, rather than after. Similarly, refinement of endbulb synapses between SG axons and nucleus magnocellularis neurons (the avian homolog of the ventral CN) takes place between embryonic day (E) 12 and E17 (Jackson and Parks, 1982; Jhaveri and Morest, 1982; Lu and Trussell, 2007). Since responsiveness to sound does not emerge until ~E15 in chick SG neurons (Jones et al., 2006), the majority of endbulb refinement takes place before hearing onset as well. In contrast, refinement of MNTB axons in the LSO did not take place until after hearing onset.

Differences in the time scale of refinement may reflect the importance of certain factors, such as activity, and of differing underlying mechanisms, which may also be related to the characteristics of the circuit itself. The projection from the MNTB to the LSO, for example, is inhibitory and part of a binaural circuit, while the SG-CN projection is excitatory and monaural. The relationship between circuit properties and refinement will be further explored in the General Discussion.

3.0 ROLE OF PRE-HEARING SPONTANEOUS ACTIVITY AND FUNCTIONAL REFINEMENT IN THE TONOTOPIC SHARPENING OF MNTB AXONS IN THE LSO

3.1 INTRODUCTION

In Chapter 2, I showed that tonotopic refinement of MNTB axons in the LSO does not take place before the onset of hearing, despite the fact that functional connections become almost twice as precise over the same period. The delay between pre-hearing synaptic silencing and post-hearing axonal pruning indicates that tonotopic refinement of the MNTB-LSO pathway takes place in two stages. Before the onset of hearing, synapses are silenced, and LSO neurons are functionally disconnected from ~2/3 of their initial presynaptic partners in the MNTB (Kim and Kandler, 2010). The silencing of synapses is frequency-specific and reduces the tonotopic width of the region of the MNTB that provides input to a given LSO neuron (Fig. 1-5). However, the sharpening of functional connectivity is not accompanied by corresponding changes in the individual MNTB axons; before hearing onset, axonal growth is matched by expansion of the LSO such that the tonotopic specificity of the boutons of individual MNTB axons in the LSO remains constant. Only after hearing onset does bouton elimination reduce the spread of boutons along the frequency axis.

Although functional silencing and anatomical pruning take place during distinct developmental periods, it is unknown whether they are completely independent processes.

Despite the temporal delay between them, the silencing of synapses during functional refinement may be a necessary first step in the sequence of events that lead to bouton elimination and anatomical refinement. Here I investigate whether the anatomical refinement of MNTB axons in the LSO is influenced by disrupted functional refinement before hearing onset. To do so I utilize α9 KO mice, which are functionally de-efferented due to loss of the α9 subunit of the acetylcholine receptor (Vetter et al., 1999). As a result, cochlear hair cells in α9 KO mice lack cholinergic input from efferent fibers, which in early development influence the pattern of pre-hearing spontaneous activity. Consequently, functional connections are significantly less tonotopically precise in α9 KO mice as they are in controls around the time of hearing onset (Fig. 1-5). Half as many MNTB inputs to a given LSO neuron are silenced, and maintained inputs are strengthened less than half as much (Kim, 2004). But because the α9 subunit is only expressed in the cochlea within the auditory system (Elgoyhen et al., 1994), and α9 KO mice do not exhibit hearing deficits (May et al., 2002), sound-evoked activity after hearing onset is unaffected by the knockout. Thus in α9 KO mice I can test the hypothesis that pre-hearing synaptic silencing produces a functional template that influences anatomical pruning after hearing.

3.2 MATERIALS AND METHODS

3.2.1 Experimental Animals

Experiments were carried out on α9 KO mice (gift of D. Vetter, Tufts University), which are homozygous for a null deletion of the α9 nAChR gene (Vetter et al., 1999). Mice were used at P2-4, P12-14, and P19-21. All experimental procedures were in accordance with NIH guidelines

and were approved by the Institutional Animal Care and Use Committee at the University of Pittsburgh.

3.2.2 Slice preparation, electrophysiology, histology, axon reconstruction, and quantitative analysis

Slice preparation, electrophysiology, histology, axon reconstruction, and quantitative analysis followed the same methods described in Chapter 2. α9 KO data were compared with control data from Chapter 2.

3.3 RESULTS

Anatomical connectivity in neonatal α9 KO mice looked very similar to age-matched controls (Fig. 3-1 A, B left). Accordingly, axons from α9 KO mice at P2-4 showed no significant differences from control in either the number of boutons per MNTB axon in the LSO (control: 127 ± 13, n = 9; α9 KO: 112 ± 12, n = 9; p = 0.39, Student's t-test; Fig. 3-1 C), the spread of boutons along the frequency axis (control: 23 ± 2 % LSO length, n = 9; α9 KO: 20 ± 2 % LSO length, n = 8; p = 0.35, Student's t-test; Fig. 3-1 D), or the area covered by boutons in the LSO (control: 20 ± 2 % LSO area, n = 9; α9 KO: 16 ± 2 % LSO area, n = 8; p = 0.22, Student's t-test; Fig. 3-1 E), indicating that initial anatomical MNTB-LSO connections, like functional connections, form normally in α9 KO mice and thus do not depend on cholinergic transmission in the cochlea.

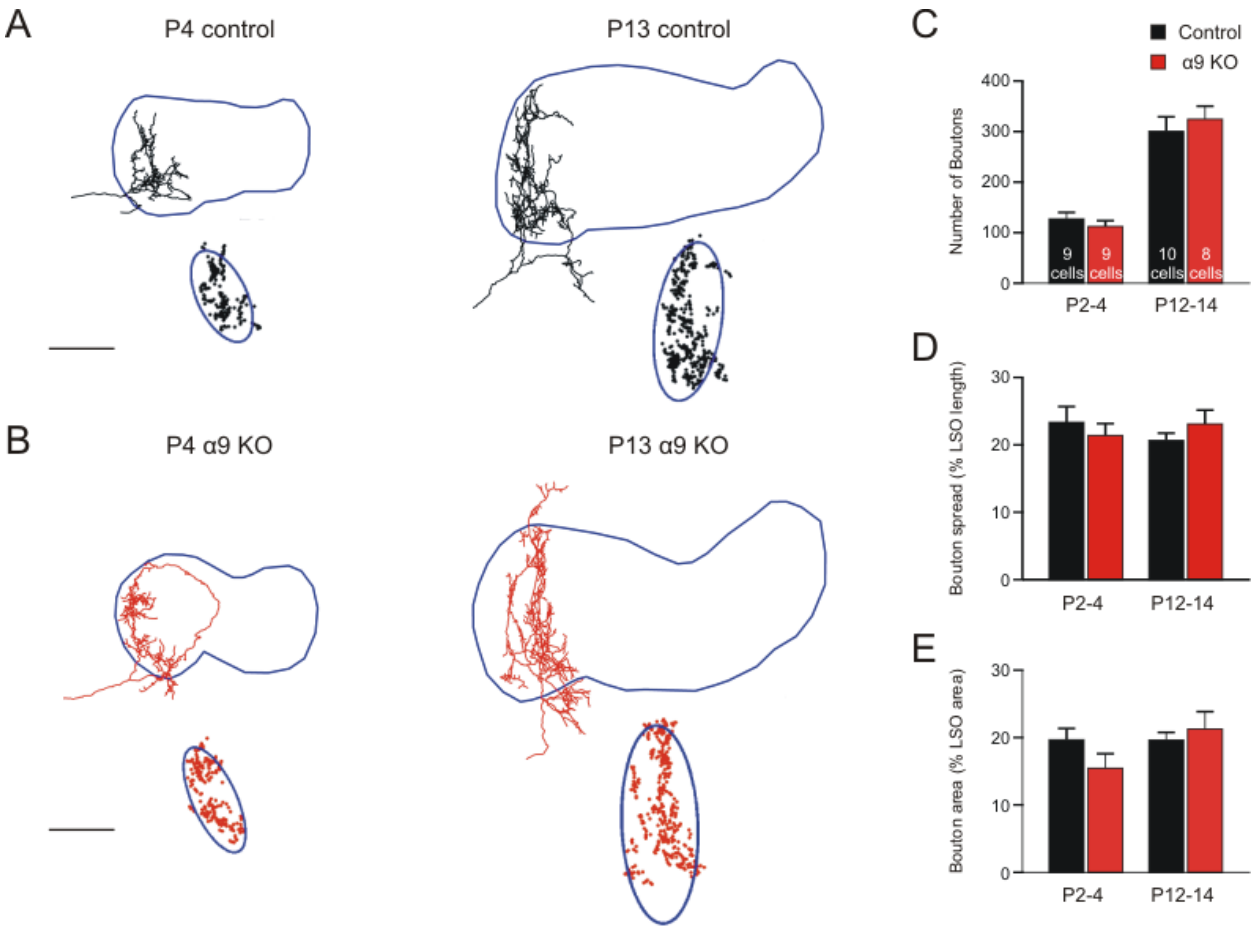

Figure 3-1. Pre-hearing growth of MNTB axons in the LSO of α9 KO mice.

(A) Example reconstructions of a control MNTB axon and its boutons in the LSO at P4 (left) and P13 (right). Upper portion shows the reconstructed axon in black and the outline of the LSO in blue. Lower right portion shows the boutons of that axon located within the LSO in black, and the ellipse fit to those boutons in blue. Dorsal is to the top, medial to the left. Scale bar, 100 µm. (B) Example reconstructions of an α9 KO MNTB axon and its boutons in the LSO at P4 (left) and P13 (right). Scale and conventions same as in (A), except that KO axons and boutons are depicted in red. (C) Number of boutons per MNTB axon found in the LSO in controls (black) and α9 KOs (red) at P2-4 and P12-14. Data show mean ± s.e.m.; at P2-4, n = 9 axons from 6 animals in control and n = 9 axons from 8 animals in α9 KO; at P12-14, n = 10 axons from 8 animals in control and n = 8 axons from 6 animals in α9 KO. (D) Spread of boutons along the LSO frequency axis in controls and α9 KOs at P2-4 and P12-14. (E) Cross-sectional area of the LSO covered by the boutons of individual MNTB axons in controls and α9 KOs at P2-4 and P12-14.

Over the next 10 days, axonal growth and bouton addition took place to the same extent in α9 KO mice as it had in controls (Fig. 3-1), with no significant differences in bouton number (control: 302 ± 29 LSO boutons/MNTB axon, n = 10; α9 KO: 325 ± 26 LSO boutons/MNTB axon, n = 8; p = 0.56, Student's t-test; Fig. 3-1 C), spread (control: 21 ± 1 % LSO length, n = 10; α9 KO: 23 ± 2 % LSO length, n = 8; p = 0.28, Student's t-test; Fig. 3-1 D), or area (control: 20 ± 1 % LSO area, n = 10; α9 KO: 21 ± 3 % LSO area, n = 8; p = 0.54, Student's t-test; Fig. 3-1 E) around the time of hearing onset (P12-14). Interestingly then, the tonotopic specificity of anatomical connections did not differ between control and α9 KO mice at hearing onset, despite the fact that functional connectivity was ~1.5 times as broad in KO mice, with twice as many maintained inputs. The mismatch between functional and anatomical measures of connectivity again indicates that functional refinement is not evident in the distribution of the boutons of MNTB axons in the LSO. Nevertheless, the addition of the same number of boutons over the same area of the LSO over pre-hearing development indicates that these processes are not dependent on cholinergic transmission in the cochlea, or the concurrent functional changes.

At P2-4 the spatial distribution of the boutons of individual MNTB axons in the LSO also appeared not to differ between control and α9 KO mice (Fig. 3-2 A, C left). In both cases, the boutons were distributed relatively evenly across the region of termination, with only a slight increase in density near the center of the termination regions. In control animals, the addition of boutons to MNTB axons between P2 and P14 is spatially-specific, causing a steep peak in the density of boutons along an isofrequency contour-like band near the center of the termination region, in the absence of any change in the proportion of the LSO covered by the boutons (Fig. 3-2 A,B). In α9 KO mice, more boutons were also added to the center than to the outer edges of the termination, causing an increase in peak density, although the magnitude of the peak

appeared slightly less than what it was in controls (Fig. 3-2 C, D). As a result, the control and α9 KO distributions at P12-14, like the distributions at P2-4, were similar. However, plotting the change in density over pre-hearing development suggested that the addition of boutons was not as spatially-specific in α9 KO mice, as indicated by the fact that the yellow area of addition is stretched out over a larger portion of the frequency axis in α9 KOs than in controls. The dark red regions of greatest increase are also not as dark in α9 KO mice as in controls, indicating that the density change at the peak was not as great in α9 KOs. A less spatially-selective addition of boutons in α9 KO mice over pre-hearing development is consistent with the slightly lower peak density at P12-14, since the same number of boutons are added over the same area in both control and α9 KO mice. However, the distribution of boutons at P2-4 also influences the developmental change, so a slightly broader and flatter peak at P2-4 in α9 KO mice could also contribute to the appearance of less spatially-specific bouton addition. Therefore it is unclear from the density heat maps whether the loss of cochlear cholinergic transmission and impaired functional refinement results in the less spatially-specific addition of boutons before hearing onset.

I next investigated whether post-hearing anatomical pruning was affected by the loss of cochlear cholinergic transmission and impaired functional refinement in α9 KO mice. Following one week of auditory experience, MNTB axons in α9 KOs had significantly more boutons in the LSO than controls (P19-21 α9 KO: 278 ± 28, n = 9; P19-21 control: 137 ± 21 LSO boutons/MNTB axon, n = 9; p = 0.001, Student's t-test; Fig. 3-3 A-C), and those boutons covered almost twice as much of the LSO frequency axis (P19-21 α9 KO: 27 ± 3 % LSO length, n = 9; P19-21 control: 14 ± 2 % LSO length, n = 9; p = 0.002, Student's t-test; Fig. 3-3 D).

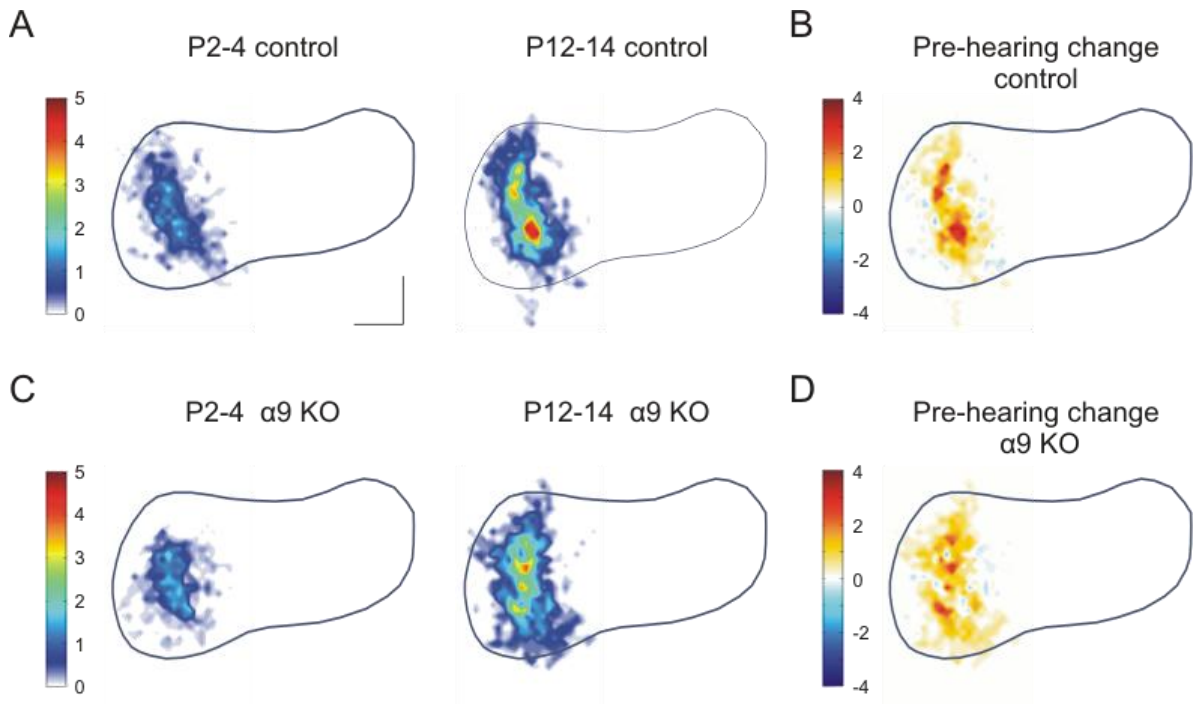

Figure 3-2. Spatial distribution of the boutons of MNTB axons in the LSO over pre-hearing development in α9 KO mice.

(A) Average density of the boutons of individual control MNTB axons in the LSO at P2-4 (left) and P12-14 (right). Dorsal is to the top, medial to the left. Color bar, average number of boutons per axon per 0.17% LSO area; scale bars, 20% mediolateral LSO length and 40% dorsoventral LSO height. (B) Change in the average density of the boutons of individual control MNTB axons in the LSO over pre-hearing development. Change shows the difference between P2-4 and P12-14. Warm colors indicate an increase in density with development; cool colors indicate a decrease with development. Color bar, average change in bouton number per axon per 0.17% LSO area; scale and orientation same as in (A). (C) Average density of the boutons of individual α9 KO MNTB axons in the LSO at P2-4 (left) and P12-14 (right). Scale and conventions same as in (A). (D) Change in the average density of the boutons of individual α9 KO MNTB axons in the LSO over pre-hearing development. Color bar, scale, and conventions same as in (B).

Thus, while the tonotopic specificity of MNTB axons increased significantly by ~1.5-fold in control mice during the first week after hearing onset, in α9 KO mice no tonotopic sharpening occurred ($p = 0.34$, Student's t-test), despite the lack of hearing deficits. These results demonstrate that anatomical refinement, even though it does not take place until after hearing onset, depends on cholinergic transmission in the cochlea and the pattern of functional connections created by synapse silencing and strengthening before hearing onset.

Consistent with the non-significant change in the number of boutons per MNTB axon during post-hearing development in α9 KO mice, the spatial distribution of boutons in the LSO at P19-21 was very similar to the distribution at P12-14 (Fig. 3-4 C), and covered the same proportion of the LSO. However, like the density-dependent pattern of bouton elimination in control mice, among the small number of boutons eliminated, more seemed to be lost from the terminations' center, the region of highest density, rather than selectively from the terminations' periphery (Fig. 3-4 D). Accordingly, the peak density seemed slightly smaller at P19-21 than at P12-14 in α9 KO mice, although the reduction was much less than that observed in control mice. The lack of bouton elimination in α9 KO mice after hearing onset indicates that pruning depends on functional refinement before hearing onset. However, although many fewer boutons were eliminated in α9 KO mice, the spatial pattern of elimination, in taking place across the whole of the termination region in a density-dependent manner, seemed to be largely maintained. Thus even though the amount of post-hearing pruning is strongly dependent on pre-hearing synaptic silencing, the manner in which pruning proceeds, as indicated by the spatial pattern of bouton elimination, may not depend on cholinergic transmission or functional refinement.

I next aligned the boutons of each axon along the frequency axis in order to account for variation in the orientation of the LSO frequency axis in dorsoventral, mediolateral space due to

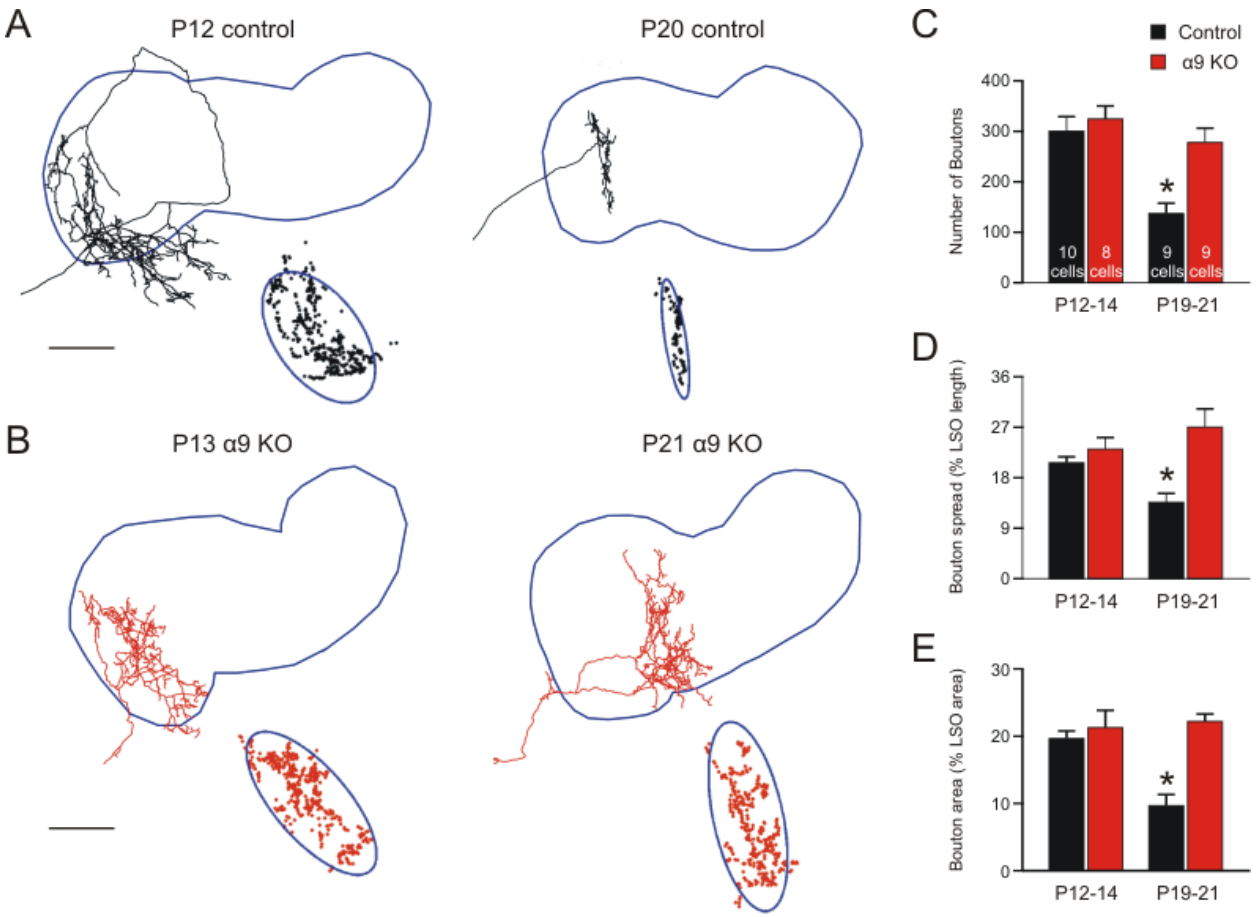

Figure 3-3. Post-hearing refinement of MNTB axons in the LSO of α9 KO mice.

A) Example reconstructions of a control MNTB axon and its boutons in the LSO at P12 (left) and P20 (right). Upper portion shows the reconstructed axon in black and the outline of the LSO in blue. Lower right portion shows the boutons of that axon located within the LSO in black, and the ellipse fit to those boutons in blue. Dorsal is to the top, medial to the left. Scale bar, 100 µm. (B) Example reconstructions of an α9 KO MNTB axon and its boutons in the LSO at P13 (left) and P21 (right). Scale and conventions same as in (A), except that KO axons and boutons are depicted in red. (C) Number of boutons per MNTB axon found in the LSO in controls (black) and α9 KOs (red) at P12-14 and P19-21. Data show mean ± s.e.m.; at P12-14, n = 10 axons from 8 animals in control and n = 8 axons from 6 animals in α9 KO; at P19-21, n = 9 axons from 8 animals in control and n = 9 axons from 8 animals in α9 KO. Asterisk indicates a significant difference between controls and α9 KOs for that age group; $p < 0.05$, Student's t-test. (D) Spread of boutons along the LSO frequency axis in controls and α9 KOs at P12-14 and P19-21. (E) Cross-sectional area of the LSO covered by the boutons of individual MNTB axons in controls and α9 KOs at P12-14 and P19-21.

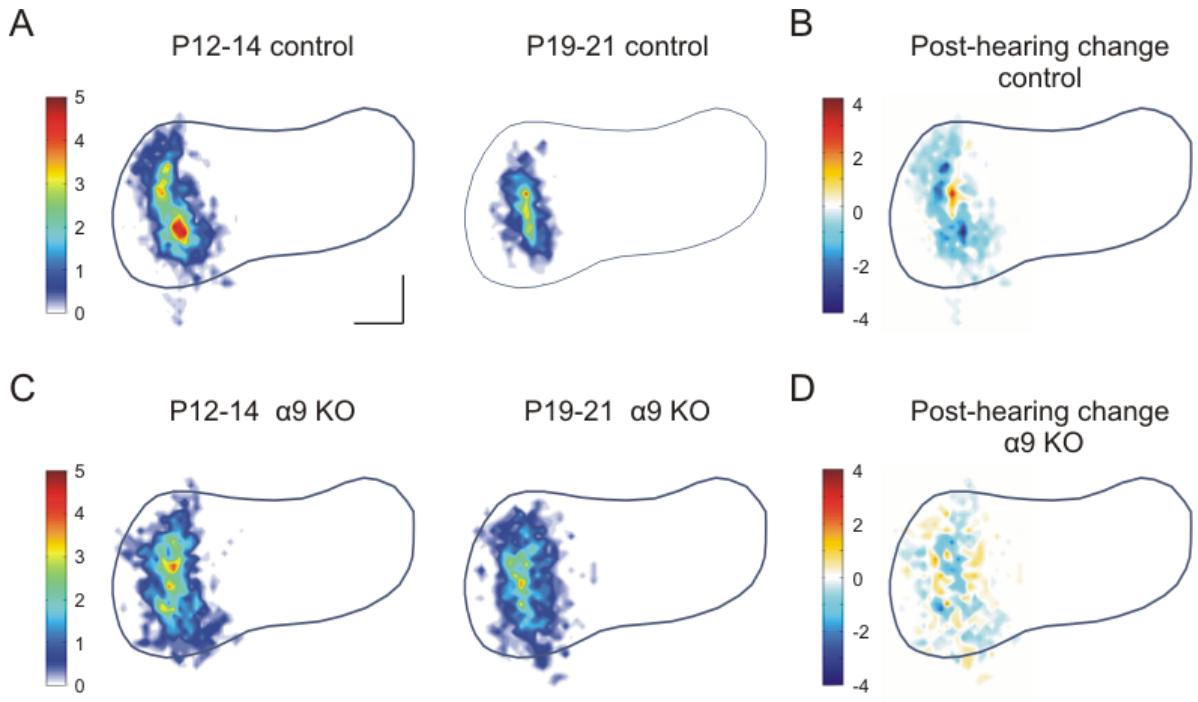

Figure 3-4. Spatial distribution of the boutons of MNTB axons in the LSO over post-hearing development in α9 KO mice.

(A) Average density of the boutons of individual control MNTB axons in the LSO at P12-14 (left) and P19-21 (right). Dorsal is to the top, medial to the left. Color bar, average number of boutons per axon per 0.17% LSO area; scale bars, 20% mediolateral LSO length and 40% dorsoventral LSO height. (B) Change in the average density of the boutons of individual control MNTB axons in the LSO over post-hearing development. Change shows the difference between P12-14 and P19-21. Warm colors indicate an increase in density with development; cool colors indicate a decrease with development. Color bar, average change in bouton number per axon per 0.17% LSO area; scale and orientation same as in (A). (C) Average density of the boutons of individual α9 KO MNTB axons in the LSO at P12-14 (left) and P19-21 (right). Scale and conventions same as in (A). (D) Change in the average density of the boutons of individual α9 KO MNTB axons in the LSO over post-hearing development. Color bar, scale, and conventions same as in (B).

its S-shape, and to more quantitatively compare the distribution of boutons along the LSO frequency axis between control and α9 KO mice over development. I eliminated the dorsoventral dimension orthogonal to the frequency axis and created histograms that described the density of boutons along the LSO frequency axis relative to the bouton centroid.

The distribution of boutons along the frequency axis closely matched the developmental sequence of events responsible for tonotopic sharpening indicated by the spatial density maps. At P2-4, Gaussian functions fit to the histograms were shallow in both control and α9 KO mice (Fig. 3-5) and did not differ significantly in maximum height ($p = 0.81$, Student's t-test) the width of the distribution at the base ($p = 0.61$, Student's t-test), or the full width at half the maximum height (FWHM; $p = 0.93$, Student's t-test), supporting the conclusion that initial MNTB-LSO connections form normally in α9 KO mice. There was also no significant difference between the goodness-of-fit of the Gaussians between control and α9 KO mice at any age ($p > 0.05$, Student's t-test).

In control mice, the maximum height near the centroid became three times greater at P12-14 than at P2-4 ($p < 0.001$, Student's t-test), without an accompanying change in the width of the distribution at the base ($p = 0.80$, Student's t-test). As a result, the FWHM was reduced (from 12.6 ± 1.0 at P2-4 to 9.4 ± 0.6 at P12-14; $p = 0.01$, Student's t-test). In α9 KO mice, the maximum height also increased three times from birth to hearing onset ($p = 0.002$, Student's t-test), again with no change in the width at the base ($p = 0.31$, Student's t-test). Thus the peak density of boutons along the frequency axis at P12-14 did not differ between control and α9 KO mice (control: 31 ± 2 boutons per percent LSO length; α9 KO: 30 ± 3 boutons per percent LSO length; $p = 0.73$, Student's t-test).

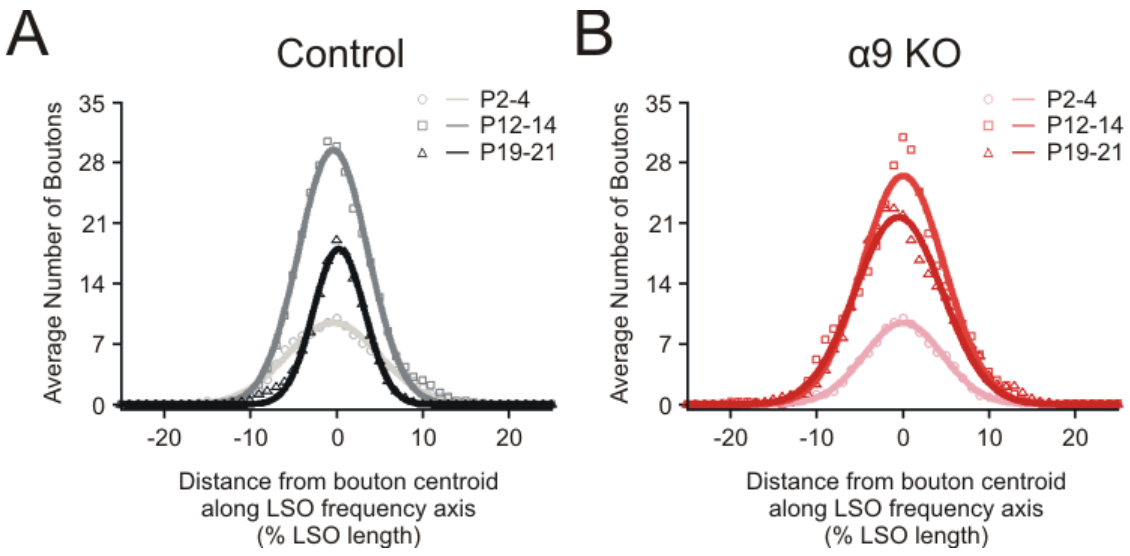

Figure 3-5. Developmental change in the distribution of boutons along the LSO frequency axis in α9 KO mice.

(A) Histograms showing the average absolute distribution of boutons per control MNTB axon along the frequency axis at P2-4 (lt. grey, circles), P12-14 (dk. grey, squares) and P19-21 (black, triangles). Symbols represent population means smoothed by a 3-bin moving average, lines show the Gaussian fit to the smoothed data. Negative distances, medial; positive distances, lateral. (B) Histograms showing the average absolute distribution of boutons per α9 KO MNTB axon along the frequency axis at P2-4 (lt. pink, circles), P12-14 (dk. pink, squares) and P19-21 (dk. red, triangles). Rest of the conventions same as in (A).

The α9 KO distribution at P12-14 again appeared slightly broader than the control distribution. Since there was no difference in the distribution of boutons along the frequency axis at P2-4 between α9 KOs and controls, a broader distribution at P12-14 in α9 KOs would be consistent with a slightly less spatially-selective addition of boutons. And although the difference between the FWHM of the P12-14 control and α9 KO Gaussians did not reach statistical significance (FWHM at P12-14: 9.4 ± 0.6 % LSO length in control, 11.0 ± 1.5 % LSO length in α9 KO; $p = 0.19$, Student's t-test), the FWHM in α9 KOs did not decrease significantly between P2-4 and P12-14 ($p = 0.64$, Student's t-test), compared to the significant (~22 %) reduction that took place in controls.

Between P12-14 and P19-21, elimination of boutons in control mice caused a significant reduction in the maximum density of boutons by 1/3 ($p = 0.002$, Student's t-test), and in the width of the distribution at its base by a similar amount ($p < 0.001$, Student's t-test). Again, both the reduction of the peak and narrowing of the base seemed to result from the elimination of boutons across the whole termination, with more boutons lost from the center regions of highest density, rather than from the periphery. In contrast, there was no change in the distribution of α9 KO mice over post-hearing development. Neither the maximum height ($p = 0.44$, Student's t-test), width at the base ($p = 0.34$, Student's t-test), or FWHM ($p = 0.80$, Student's t-test) changed significantly, again indicating that pruning was severely impaired by the loss of cholinergic transmission in the cochlea and impaired functional refinement.

In control animals, the developmental change in bouton density at a specific location in the termination region is related to the initial number of boutons present at that location. Since density is highest at the center and lowest at the periphery from the outset, this density-dependence reflects the spatial pattern of bouton addition and elimination during development.

In α9 KO mice, however, the addition of boutons to termination regions before hearing onset seemed to be less spatially-specific. Therefore, I looked at whether the relationship between initial bouton density at P2-4, tonotopic location, and the developmental addition of boutons differed between control and α9 KO mice (Fig. 3-6).

In both control and α9 KO mice, the density of boutons at P2-4 had a significant effect on the percentage of boutons added over pre-hearing development (control: $R^2 = 0.87$, $p < 0.001$); α9 KO: $R^2 = 0.94$, $p < 0.001$; Pearson correlation). However, there was a significant interaction between genotype and bouton density at P2-4 ($p = 0.02$, ANOCOVA), indicating that the slope of the linear regression differed significantly between genotypes (slope = 1.03 in control, 0.87 in α9 KO). A shallower slope indicates that the percentage of boutons added during pre-hearing development does not increase as quickly with increasing density at P2-4 in α9 KO mice as it does in control mice. Since regions with high density are closer to the center of the termination and regions with low density are closer to the peripheral edges, a shallower slope is consistent with the addition of boutons being more spread out along the termination region in α9 KO mice. Specifically, a greater percentage of boutons were added at tonotopic locations of intermediate density (~1 - 4 boutons per % LSO length) in α9 KO mice than were added in control mice over pre-hearing development. At P2-4, a density of ~1 – 4 boutons per % LSO length corresponded to a tonotopic location between ~6 and 10 % LSO length from the bouton centroid (Fig. 3-6 B). Thus a greater percentage of bouton addition at those intermediate tonotopic locations is also consistent with the broader Gaussian at P12-14 and a less spatially-specific addition of boutons over pre-hearing development in α9 KO mice.

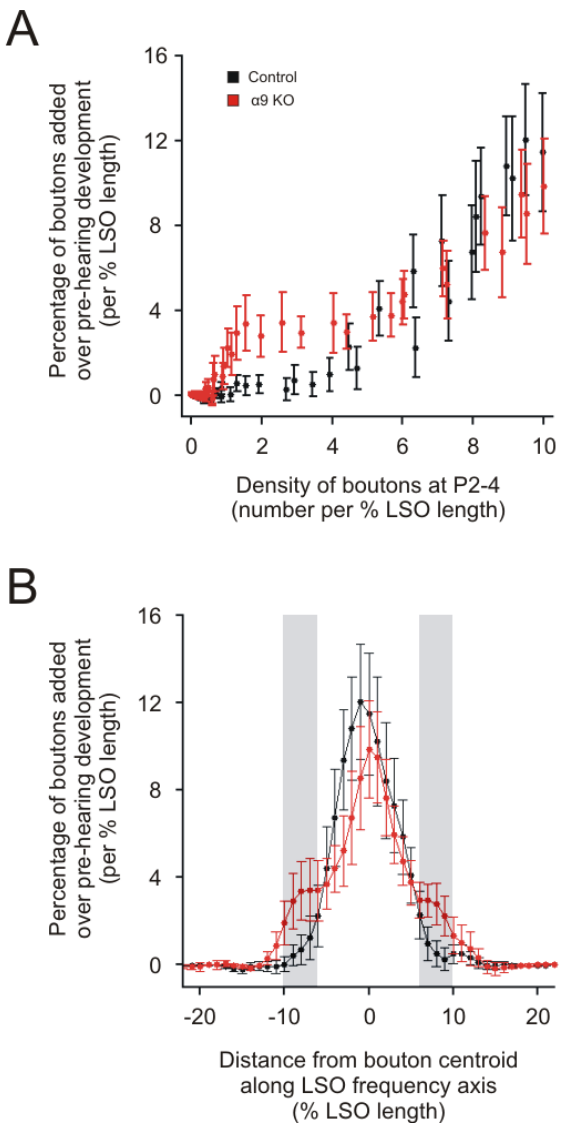

Figure 3-6. The relationship between initial bouton density, tonotopic location, and the percentage of boutons added over pre-hearing development in control and α9 KO mice.

(A) In both control and α9 KO mice, the density of boutons at P2-4 had a significant effect on the percentage of boutons added over pre-hearing development (control: $R^2 = 0.87$, $p < 0.001$); α9 KO: $R^2 = 0.94$, $p < 0.001$; Pearson correlation), although a greater percentage of boutons seemed to be added to tonotopic locations of intermediate density (~1-4 boutons per % LSO length) in α9 KO mice than were added in control mice. (B) At P2-4, a density of ~1 – 4 boutons per % LSO length corresponds to a tonotopic location between ~6 and 10 % LSO length from the bouton centroid (highlighted in grey), consistent with a less spatially-specific addition of boutons over pre-hearing development in α9 KO mice. Symbols represent mean ± s.e.m.

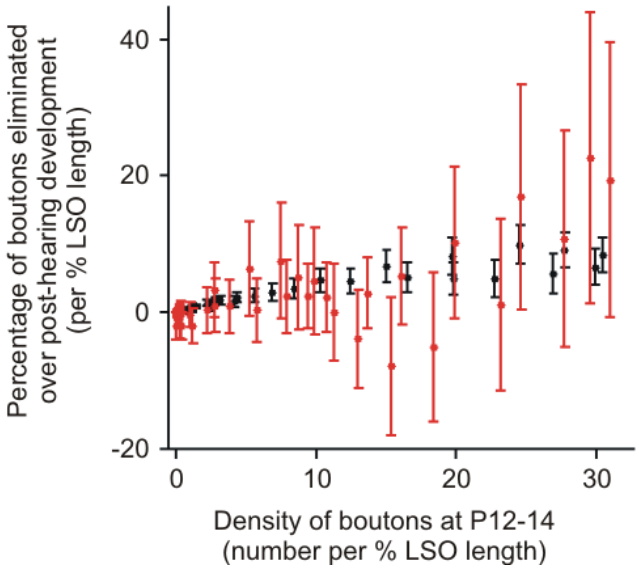

Figure 3-7. The relationship between initial bouton density and percentage of boutons eliminated over post-hearing development in control and α9 KO mice.

In both control (black) and α9 KO (red) mice, the density of boutons at P12-14 had a significant effect on the percentage of boutons eliminated over post-hearing development (control: $R^2 = 0.90$, $p < 0.001$); α9 KO: $R^2 = 0.47$, $p < 0.001$; Pearson correlation). Although the error in α9 KO mice is an order of magnitude larger than in controls due to the elimination of so few boutons, there does not appear to be a systematic difference in the density-dependence of bouton elimination over post-hearing development between control and α9 KO mice. Symbols represent mean ± s.e.m.

In contrast, there did not seem to be a significant difference in the density-dependence of bouton elimination after hearing onset (Fig. 3-7) between control and α9 KO mice, suggesting that although the number of boutons eliminated between P12-14 and P19-21 was significantly less in α9 KO mice, the pattern in which they were eliminated was unchanged.

3.4 DISCUSSION

3.4.1 The functional map as a template for anatomical pruning

Post-hearing pruning of MNTB axons in the LSO, like pre-hearing synaptic silencing and strengthening, was severely impaired in α9 KO mice, indicating that cholinergic transmission in the cochlea plays a key role in anatomical as well as functional refinement. Although activity blockade studies suggest that pruning is activity-dependent (Sanes and Takacs, 1993), loss of cholinergic transmission should not affect activity after hearing onset, since α9 KO mice have normal cochlear sensitivity and hearing (May et al., 2002; Vetter et al., 1999), and should therefore have normal sound-evoked responses. Thus, deficits in tonotopic refinement after hearing onset seem to stem from deficits in the refinement of functional connections before the onset of hearing, indicating that the pre-hearing phase of tonotopic refinement plays a key role in the post-hearing phase.

In control mice, pruning proceeds through the density-dependent elimination of boutons across the entire region of termination, increasing tonotopic precision in a manner analogous to sinking an iceberg. But in α9 KO mice, no pruning occurred after hearing onset, suggesting that the trigger for elimination was never reached due to the impaired functional refinement.

Functional refinement, however, consists of both the frequency-specific silencing of connections and the strengthening of maintained connections, and the relative contribution of each of these aspects of functional refinement to pruning is unknown.

In Chapter 2, I speculated that pruning could be the result of homeostatic regulation, possibly of the number of boutons per axon, or of input strength. Axons in α9 KO mice at P19-21 contained twice as many boutons as control axons, suggesting that pruning does not function strictly to regulate the number of boutons per axon. Similarly, the number of boutons per axon at P12-14 did not differ between controls and α9 KOs, indicating that overall bouton number does not serve as a trigger for pruning. However, even though there were approximately twice as many boutons per axon in α9 KO mice at P19-21, they were also spread out over an area that was approximately twice as large. Thus it remains possible that pruning could serve to regulate the average density of boutons in the axonal termination region. Consistent with this idea, the average bouton density (number of boutons per axon/μm of bouton area) did not differ between control and α9 KO mice at P19-21 (control: 0.014 ± 0.001 boutons; α9 KO: 0.011 ± 0.001 boutons; $p = 0.16$, Student's t-test). The average bouton density also did not change significantly over pre-hearing or post-hearing development in either control or α9 KO mice ($p > 0.05$, Student's t-test).

Input strength could provide another trigger for pruning. Around hearing onset, LSO neurons in α9 KO mice remain synaptically connected to twice as many MNTB neurons as LSO neurons in control animals (Kim, 2004). However, these maintained fibers are less than half as strong in α9 KOs as they are in controls. If the strength of the input to a single LSO neuron produces a retrograde signal to regulate input strength via bouton elimination, then it is possible that the weaker single fibers in α9 KO mice are not strong enough to elicit the signal, resulting in

a lack of pruning. Similarly, pruning could serve to regulate input strength to balance excitation and inhibition originating from the CN and MNTB inputs to LSO neurons. Since hearing seems to be normal in α9 KO mice, a narrow-band sound stimulus after hearing onset would likely activate the same number of MNTB neurons as in control mice (assuming that the tonotopic specificity of upstream connections is unchanged, a point that will be addressed later in the Discussion). However, because the strength of each activated fiber is less, the inhibition received by an LSO neuron in α9 KO mice is likely less than that received by an LSO neuron in controls. Thus a lack of pruning in α9 KO mice could also reflect the homeostatic regulation of overall inhibitory drive.

Because the addition of presynaptic release sites is a large component of strengthening, impaired strengthening in α9 KO mice was likely reflected in the less spatially-specific addition of boutons to MNTB axons over pre-hearing development. Although the same number of boutons were added in α9 KO mice as were added in controls, the maintenance of a higher number of weaker MNTB inputs per LSO neuron in α9 KO mice indicates they were distributed over a larger number of postsynaptic LSO neurons. Functional input maps were also broader in α9 KOs, indicating that maintained connections were less tonotopically precise, which is consistent with a greater addition of boutons to tonotopic locations further from the center of the termination in α9 KO mice.

The fact that largely normal hearing could not rescue tonotopic refinement in α9 KO mice suggests that the pre-hearing phase of refinement plays a critical role in determining the tonotopic precision of MNTB-LSO connections. However, it remains unclear whether sound-evoked activity also plays a necessary role, by either enabling or directing the transition from

functionally- to anatomically-defined mature tonotopy. This topic will be further addressed in Chapter 4.

3.4.2 Tonotopic refinement of MNTB-LSO connections depends on pre-hearing spontaneous activity.

If post-hearing anatomical pruning is impaired in α9 KO mice due to impaired functional refinement before hearing onset, then what is the cause of disrupted functional refinement? In α9 KO mice, loss of cholinergic transmission in the cochlea disrupts the pattern of spontaneous activity in MNTB neurons before hearing onset (Fig. 1-4). The importance of spontaneous activity patterns in driving development of topographic connections has been well-established in the visual system, where the spatio-temporal structure of spontaneous retinal waves shapes the refinement of retinotopic and eye-specific pathways even before eye-opening (Huberman, 2007; Penn et al., 1998; Stellwagen and Shatz, 2002; Weliky, 2000). In the auditory system, the spontaneous activity of IHCs before hearing onset is believed to play a similar role in the refinement of central tonotopic maps, so it is likely that the disruptions in tonotopic refinement in α9 KO mice result from the altered activity pattern inherited from the cochlea due to the loss of cholinergic transmission. Although it is possible that deletion of α9 has other effects that could negatively influence refinement, these possibilities are unlikely to explain the deficits observed here.

First, within the auditory system, the α9 subunit of the acetylcholine receptor is expressed only in the cochlea (Elgoyhen et al., 1994). Thus cholinergic transmission elsewhere in the brain is spared in α9 KO mice; only the effects of acetylcholine release from medial olivocochlear

(MOC) efferents in the cochlea is blocked. Therefore it is unlikely that non-specific effects of the knockout would influence tonotopic refinement in an auditory circuit.

Nonetheless, loss of cholinergic transmission in the cochlea would also eliminate any possible trophic effects it might have during development, which could lead to hair cell and neuronal death. Similarly, if the loss of cholinergic transmission in α9 KOs reduced the firing rate of inner hair cells, reduced afferent activity could lead to loss of protein synthesis and the death of cochlear nucleus (CN) neurons (Born and Rubel, 1988). While substantial cell loss could affect tonotopic maps and their refinement, we did not observe any quantitative differences in the size of the MNTB or LSO in α9 KO mice, or any qualitative differences in the size of the CN, as would be expected if substantial cell loss had occurred. α9 KO mice also exhibit normal cochlear sensitivity and auditory function except for the specific loss of MOC effects (He et al., 2004; May et al., 2002; Vetter et al., 1999), further arguing against cell death or general cochlear malfunction. Normal rates of spontaneous spike activity in the MNTB of α9 KO mice indicates that overall activity levels before hearing onset were unchanged as well, which should protect against activity-dependent cell loss.

Finally, it is possible that less tonotopically precise anatomical connections in α9 KO mice do not stem directly from the altered spontaneous activity pattern and less precise functional template, but instead are inherited from disordered topography upstream. For example, less precise tonotopy in the projection from the MNTB to the LSO could be inherited from less precise connections between the CN and the MNTB, or between spiral ganglion (SG) cell processes and CN neurons. In the MNTB, this is unlikely to be the case since maturation of the calyx of Held, the synapse between globular bushy cells in the CN and MNTB neurons, seems to be largely activity-independent, taking place without the need for spontaneous activity

in the auditory nerve (Youssoufian et al., 2005). One of its most defining characteristics, the innervation of the majority of MNTB neurons by a single calyx, is present as soon as calyces form (Hoffpauir et al., 2009), and does not seem to involve the activity-dependent elimination of initial supernumerary inputs such as that occurring in the neuromuscular junction (Wyatt and Balice-Gordon, 2003) and at the climbing fiber-Purkinje cell synapse in the cerebellum (Hashimoto and Kano, 2005).

In the CN, the initial formation of tonotopic SG projections seems to be activity-independent, as tonotopy is already present at the time hair cells begin to differentiate (Koundakjian et al., 2007). In the cat, tonotopic precision is increased during late embryonic/early postnatal development and before hearing. However, specificity is increased through the disproportionate expansion of the CN relative to axonal growth, rather than pruning (Leake et al., 2002). In animals deafened at birth, tonotopy is somewhat degraded, as the labeled fibers from a similarly-sized injection cover a greater proportion of the CN than they do in normal-hearing controls. The absolute size of the termination area did not differ between control and deaf animals however, indicating that the loss of specificity was not due to a change in the axons, but as a result of the profound loss of CN cross-sectional area (Leao et al., 2006). Therefore, abolishing activity via deafening most likely leads to a loss of tonotopic precision due to cell death related to activity-deprivation, rather than by impairing an active refinement mechanism. Since overall spontaneous activity levels were unchanged in α9 KO mice (Fig. 1-4) and there was no evidence of cell death or a change in CN size, it seems unlikely that the tonotopic precision of the SG-CN projection is affected by the knockout.

Finally, to further address the possibility of upstream deficits in tonotopic specificity, we also bulk-labeled SG processes in the auditory nerve, and the axons of globular bushy cells as

they crossed the midline into the MNTB. We saw no qualitative difference in the appearance of labeled fibers in control and α9 KO mice, or in the innervation pattern of endbulbs in the CN or calyces in the MNTB (data not shown). Although we did not quantitatively map tonotopic precision, the absence of any double calyces or other gross abnormalities provides further support that alterations in upstream connections were not responsible for impaired refinement in α9 KO mice.

Although excitatory tuning in LSO neurons seems to develop in parallel to inhibitory tuning (Sanes and Rubel, 1988), little is known about whether tonotopic CN-LSO inputs undergo a similar process of developmental refinement as MNTB-LSO connections do. If they do, it remains an open possibility that the tonotopic precision of CN-LSO connections may also be affected in α9 KO mice. If the refinement of MNTB-LSO connections depends on the tonotopic specificity of CN-LSO connections, loss of tonotopic precision in the CN-LSO pathway could also contribute to the impaired refinement of the MNTB-LSO pathway in α9 KO mice.

3.4.3 The activity pattern is key in shaping connections

Impaired tonotopic refinement in α9 KO mice provides the first experimental evidence of the importance of the specific pattern of pre-hearing spontaneous activity in sharpening central auditory connections during development. In α9 KO mice, the overall level of spontaneous activity was unchanged, and activity even continued to take place in bursts. Only the finest temporal structure of the pattern was missing. The specific loss of only certain aspects of the activity pattern points to the key properties necessary for refinement and may provide insight into the underlying mechanisms.

In normal MNTB neurons, spontaneous activity before hearing onset consists of discrete bursts, each of which is comprised of clusters of mini-bursts. Each mini-burst is then made up of small numbers of action potentials spaced ~10 ms apart (Tritsch et al., 2010). In α9 KO mice, the spontaneous firing of MNTB neurons before hearing has a higher percentage of interspike intervals between ~50-750 ms, resulting in a smoother ISI distribution (Fig. 3). Since ~100-300 ms is the interval between mini-bursts, loss of structure in the spontaneous activity of MNTB neurons in α9 KO mice seems to result in spikes that are less organized into mini-bursts. Because activity-dependent synaptic plasticity is often highly dependent on the frequency and pattern of stimulation (Larson and Lynch, 1986; Larson et al., 1986), such a change could easily affect the accessibility of plasticity mechanisms such as long-term depression and long-term potentiation and impair refinement. Unlike its importance for refinement, normal tonotopic specificity of functional and anatomical connections in α9 KO mice at P1-4 suggests that the fine temporal structure of spontaneous activity is not involved in the initial formation of topographic MNTB-LSO connections. This is in contrast to developing motor axons, where the frequency of spontaneous rhythmic activity can influence axonal pathfinding decisions (Hanson and Landmesser, 2006; Hanson et al., 2008).

Interestingly, an abnormal pattern of spontaneous activity is more disruptive for refinement mechanisms than a complete lack of activity seems to be. Genetic deletion of otoferlin, the proposed calcium sensor and vesicle-binding protein in hair cells (Ramakrishnan et al., 2009; Roux et al., 2006), prevents the release of glutamate from inner hair cells, thereby eliminating all forms of cochlear-generated activity. And yet, in otoferlin KO mice, functional refinement of MNTB-LSO connections seems to proceed normally (Noh et al., 2010). One potential explanation for this is that, in the absence of cochlear-generated activity, secondary

mechanisms of generating patterned activity are activated, possibly through intrinsic cellular properties or circuits.

In the visual system, for example, spontaneous activity generated in the retina before eye opening is transmitted through ascending connections and influences the development of retinotopic and eye-specific connections in the lateral geniculate nucleus (LGN) and tectum, as well as ocular dominance columns in primary visual cortex (Huberman, 2007; Torborg and Feller, 2005). Transection of the optic nerve before eye opening initially abolishes all spontaneous activity in the LGN. In the cortex, however, a slightly different pattern of activity is unmasked by the absence of LGN input. Over a period of a few hours, spontaneous firing in the LGN returns, but has been entrained by descending cortico-thalamic connections to match the intrinsic pattern of the cortex (Chiu and Weliky, 2001; Katz et al., 1998). The prime importance of precisely patterned activity for the refinement of circuits during development may thus have resulted in the development of reserve mechanisms to protect the system from the failure of the initial pattern generator. The auditory system is also rich with descending connections (Coomes and Schofield, 2004; Schofield and Cant, 1999; Schofield and Coomes, 2006), so it is likely that a similar process could account for the preservation of refinement in otoferlin knockout mice.

It is possible that the fine temporal structure is not the only characteristic of the spontaneous activity pattern that is disrupted in α9 KO mice. MOC efferents form a tonotopically-organized feedback loop (Fig. 1-3). Thus it is possible that efferent feedback also contributes to the spatial pattern of spontaneous activity, where the activity of neighboring hair cells, which are tonotopically similar, are activated together. In the absence of tonotopically-organized efferent feedback, it is possible that the spatial correlation of spontaneous activity is also disrupted in α9 KO mice. A loss of spatial (frequency-specific) structure would also likely

contribute to impaired tonotopic refinement. Similarly, because there is a bilateral component to the MOC efferent pathway, it provides a mechanism for introducing binaural structure into the spontaneous activity pattern. If this is the case and tonotopic matching of CN- and MNTB inputs to the LSO is an important component of refinement, then the loss of binaurally-coordinated spontaneous activity in α9 KO mice would likely also contribute to impaired refinement.

Finally, it is possible that refinement of MNTB-LSO connections is only delayed in α9 KO mice and could eventually reach a normal degree of tonotopic specificity. Based on the hypothesis that synaptic silencing, synaptic strengthening, and anatomical pruning are restricted to distinct developmental critical periods according to the availability of the underlying mechanisms, I believe this is unlikely to be the case. In Chapter 5 I present some behavioral data that is consistent with the idea that impaired tonotopic precision in α9 KO mice persists beyond the end of the third postnatal week.

4.0 ROLE OF STRUCTURED SOUND-EVOKED ACTIVITY IN TONOTOPIC REFINEMENT OF MNTB AXONS IN THE LSO

4.1 INTRODUCTION

Before the onset of hearing, functional connections between the MNTB and LSO are tonotopically sharpened (Kim and Kandler, 2003; Noh et al., 2010). During the first two postnatal weeks, the region of the MNTB that provides synaptic input to a single LSO neuron is reduced to ~25% of its original size. The synaptic silencing is tonotopically specific, narrowing the maps along the frequency axis and producing an adult-like degree of tonotopic precision. Evidence from α9 KO mice suggests that this functional refinement depends on the precise temporal pattern of spontaneous activity that is generated in the cochlea before the onset of hearing and which propagates through ascending auditory connections (Fig. 1-4, 1-5; Tritsch et al., 2010; Tritsch et al., 2007).

The tonotopic sharpening of functional connections is not accompanied by congruent sharpening of anatomical connections however. Before hearing onset, MNTB axons grow and add boutons to their termination regions in the LSO, but the relative proportion of the LSO frequency axis covered by boutons remains constant during the first two postnatal weeks, indicating a lack of tonotopic sharpening (Chapter 2). After the onset of hearing, pruning of

axon branches and boutons results in a reduction of the number of boutons per MNTB axon and in their spread along the LSO frequency axis (Chapter 2; Sanes and Siverls, 1991).

The coincidence of pruning with the first week of auditory experience, together with impaired refinement in unilaterally cochlear-ablated animals (Sanes and Takacs, 1993), suggests that sound-evoked auditory activity plays an important role in driving tonotopic sharpening the MNTB-LSO pathway. This idea is supported by evidence from other auditory areas that the quality and characteristics of early sound exposure influence the maturation of auditory circuits and neuronal response properties, including frequency-tuning (Chang and Merzenich, 2003; Sanes and Constantine-Paton, 1983, 1985b; Zhang et al., 2001; Zhou and Merzenich, 2008). Thus it seemed likely that sound-evoked activity during the third postnatal week played an instructive role in sharpening the tonotopic specificity of anatomical MNTB-LSO connections.

Contrary to this hypothesis, however, pruning can be severely impaired even when hearing and early auditory experience appear quite normal, as is the case with α9 KO mice (Chapter 3). These mice lack the α9 subunit of the nicotinic acetylcholine receptor necessary for cholinergic transmission in the cochlea (Vetter et al., 1999). As a result, α9 KO mice exhibit no obvious hearing deficits, as indicated by normal thresholds, tone detection, and intensity discrimination (May et al., 2002), but have significantly less precise functional connections around the time of hearing onset due to reduced synaptic silencing during the first two postnatal weeks (Fig. 1-5). The role of sound-evoked activity in pruning is thus unclear because data from α9 KO mice suggest that pre-hearing functional refinement plays a more important role in determining the precision of anatomical connections following early auditory experience than the quality of the auditory experience itself.

Previous cochlear ablations were performed well before hearing onset (Sanes and Takacs, 1993), thereby eliminating pre-hearing spontaneous activity in addition to preventing sound-evoked activity after the onset of hearing. Thus it is possible that the effects of pre-hearing cochlear ablation on anatomical refinement were due to the elimination of the pre-hearing spontaneous activity required for functional refinement, not the elimination of later sound-evoked activity. To further dissect the role of spontaneous vs. sound evoked activity in tonotopic sharpening and to specifically delineate the role of hearing experience in refinement of anatomical MNTB-LSO connections, I tested whether pruning of MNTB axons depends on normally patterned sound-evoked activity. I approached this by raising mice in an altered acoustic environment dominated by pulsed white noise, an acoustic manipulation that is known to disrupt the maturation of tonotopicity in brainstem (Sanes et al., 1989), midbrain (Sanes and Constantine-Paton, 1985b), and cortical (Zhang et al., 2002; Zhou and Merzenich, 2008) auditory circuits. Under these conditions, firing of auditory nerve fibers will be largely synchronous across all frequencies, eliminating the spectrotemporal activity patterns normally evoked by environmental sound. I predicted that if pruning depends on the normal spectrotemporal patterns of sound-evoked activity, then animals reared in pulsed white noise should show impaired tonotopic sharpening of anatomical MNTB-LSO connections during the third postnatal week.

4.2 MATERIALS AND METHODS

4.2.1 Experimental Animals

All experiments were performed using 129S6/SvEv mice (gift of D. Vetter, Tufts University). All experimental procedures were in accordance with NIH guidelines and were approved by the Institutional Animal Care and Use Committee at the University of Pittsburgh.

4.2.2 Noise-rearing Protocol

Noise-reared (NR) mice were reared from P8 until P19-21 in pulsed white noise. Litters were culled to six pups, then home cages containing the pups and their mother were placed in a sound-attenuating chamber (Coulbourn Instruments, PA) lined with anechoic foam with a 12 hour light/dark cycle. White noise pulses at 70 decibels sound pressure level (dB SPL) were generated (Coulbourn tone/noise generator A69-20, Coulbourn Instruments, PA) and delivered to the chamber by an isodynamic tweeter (RT2H-A, HiVi Research, CA) mounted 30 cm above the cage floor. The loudspeaker had a relatively flat frequency response over much of the normal hearing range of the mouse (~2-50 kHz; Fig. 4-1 C). In order to minimize adaptation effects, white noise pulses were pseudorandomly presented through the use of three triggers generated by a pulse stimulator (Master-8, A.M.P.I., Israel). The triggers looped simultaneously at 3, 3.5, and 6 second intervals. Interaction of the triggers resulted in pulses ~700-1400 ms in duration, at a rate of ~36 per minute (Fig. 4-1 A, B). Acoustic stimuli were calibrated with a ¼" diameter microphone (4939, Brüel & Kjær, Denmark) placed at the level of the animals within the housing. Microphone signals were sent to a signal conditioning amplifier (Nexus 2690-A-OS1,

Brüel & Kjær, Denmark) and analyzed using commercial software (SoundCheck, Listen, MA). Food and water were provided *ad libitum*. Behavior and weight of the mice were monitored to ensure that the animals were not experiencing noticeable stress due to noise exposure. NR pups were similar in weight to control pups at the time of sacrifice, indicating normal maternal care. Control mice were reared within the normal acoustic environment of the animal facility.

4.2.3 Slice preparation, electrophysiology, histology, axon reconstruction, and quantitative analysis

Slice preparation, electrophysiology, histology, axon reconstruction, and quantitative analysis followed the same methods described in Chapter 2 for animals aged P19-21. NR data was compared with control data from Chapter 2.

For cumulative distribution plots, the histogram data of average bouton density were collapsed in the mediolateral dimension and plotted as the cumulative likelihood that a bouton, on average, would be located some distance from the centroid along the LSO frequency axis. Again, distances were expressed as a percentage of the mediolateral length of the LSO. Statistical significance of group differences was assessed using the Komolgorov-Smirnoff test.

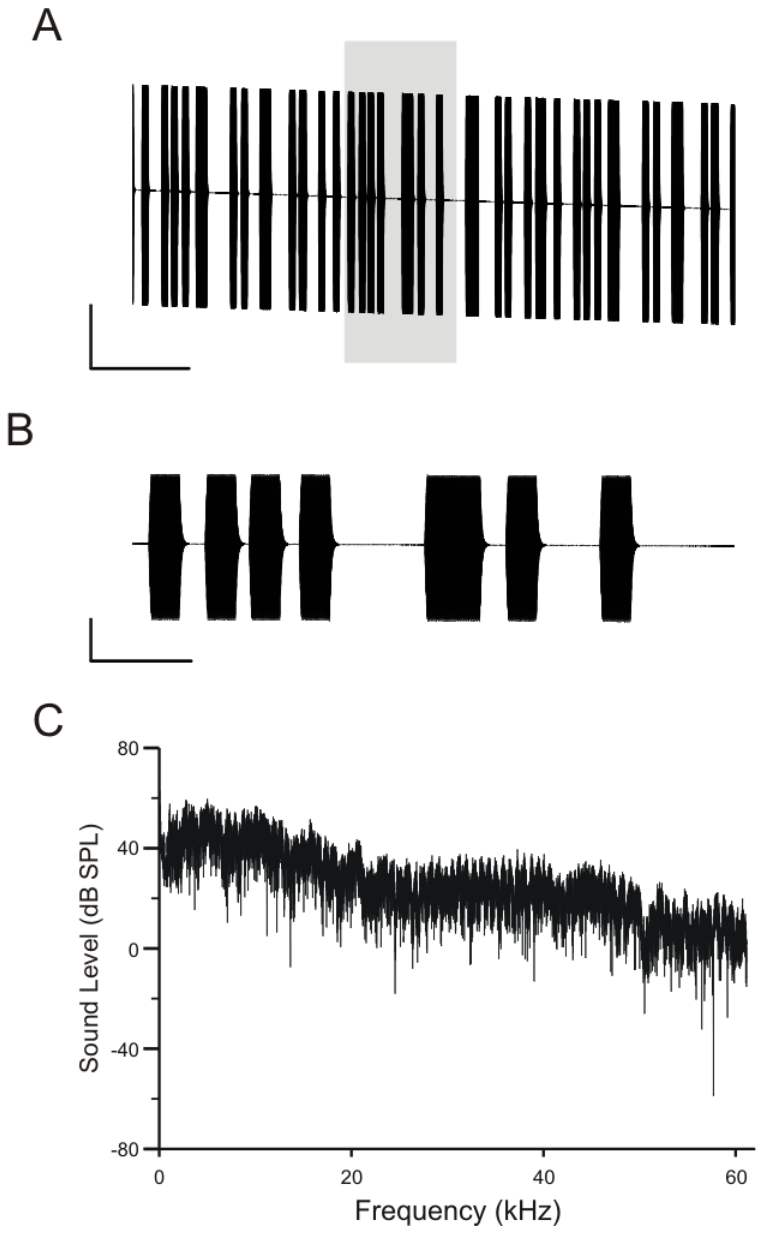

Figure 4-1. Acoustic stimulus used for noise-rearing.

(A) Signal sent to the loudspeaker by the noise generator during a representative one minute segment of the pulsed noise stimulus. Grey rectangle denotes portion of signal expanded in (B). Scale bar, 0.4 amperes, 10 seconds. (B) Expansion of the portion of the signal shaded in grey in (A). Scale bar, 0.4 amperes, 2 seconds. (C) Frequency spectrum of white noise used for noise-rearing recorded at the level of the animals' ears within the chamber.

4.3 RESULTS

By holding MNTB neurons in whole-cell configuration and allowing biocytin to diffuse from the pipette into the cell, we were able to visualize the neurons' complete axonal arbor present in the slice, including fine branches and the round swellings we identified as putative synaptic boutons. The appearance of DAB-stained MNTB axons was qualitatively identical between control and pulsed noise-reared (NR) animals. The location of MNTB neuronal soma relative to the medial edge of the MNTB also did not differ between control and NR mice, indicating that they were sampled from a similar frequency region ($p = 0.31$, Student's t-test).

In control animals, axonal pruning and elimination of boutons during the first week of auditory experience tonotopically sharpens the termination regions of individual MNTB axons in the LSO (Fig. 4-2 A, B). Around the time of hearing onset (P12-14), the 301 ± 29 boutons per axon located in the LSO cover 20 ± 1 % of LSO area and 21 ± 1 % of the LSO frequency axis. At P19-21, the average number of LSO boutons per MNTB axon is less than half of what it was one week earlier. The area of the LSO covered by boutons has also been reduced by half, while the spread has decreased by ~35 %, resulting in connections that are ~1.5 times more tonotopically precise than at P12-14.

Rearing animals in pulsed white noise did not affect the tonotopic refinement of anatomical MNTB-LSO connections. At P19-21, the majority of MNTB axons in NR animals were indistinguishable from age-matched controls (Fig. 4-2). Accordingly, the average number of boutons per MNTB axon in the LSO between control and NR axons did not differ ($p = 0.26$, Student's t-test; Fig. 4-3 A), nor did the spread of boutons along the LSO frequency axis ($p = 0.71$, Student's t-test; Fig. 4-3 B), nor the area of the LSO covered by boutons ($p = 0.34$, Student's t-test; Fig. 4-3 C). However, it is possible that noise-rearing could have influenced the

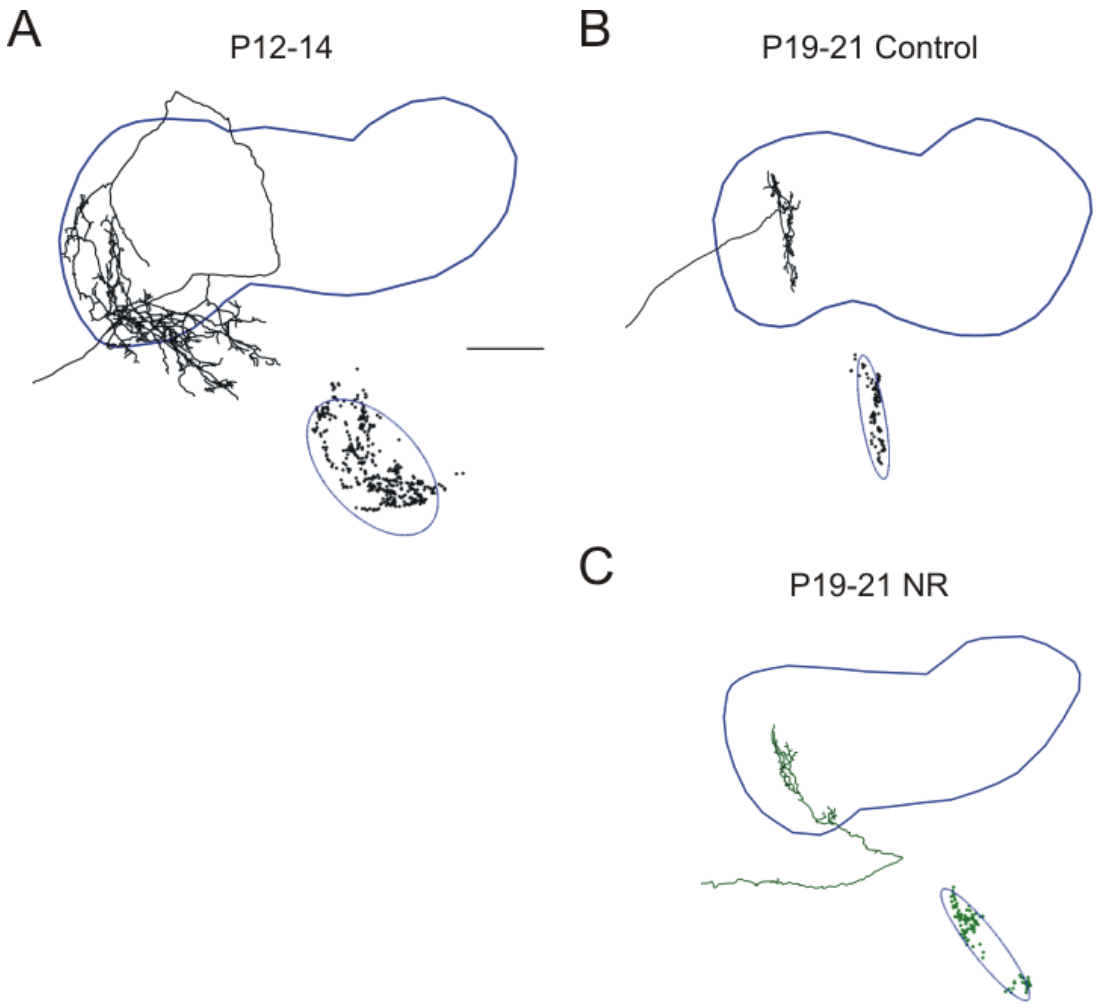

Figure 4-2. Pruning of MNTB axons in the LSO over post-hearing development is not impaired in NR animals.

(A) Representative reconstruction of a single MNTB axon in the LSO at P12-14. Solid blue line, outline of LSO; black line, MNTB axon; within inset: dots, location of boutons; thin blue line, ellipse fit to boutons. Dorsal is to the top and lateral to the right. Scale bar, 100 μm. (B) Representative reconstruction of the termination of a single MNTB axon in the LSO of a control animal at P19-21. Scale and conventions same as in (A). (C) Representative reconstruction of the termination of a single MNTB axon in the LSO of a NR animal at P19-21. Scale and conventions same as in (A) and (B), except that the axon and boutons are shown in green.

distribution of boutons in a manner that was not reflected in their spread along the frequency axis or the area they covered in the LSO. To test this possibility, I created heat maps that showed how the average density of boutons varied over different parts of the region of termination within the LSO (Fig. 4-3 D, F). To compare across populations, each axon was oriented in equivalent mediolateral and dorsoventral coordinate space using the slice midline as a guide. Within each experimental group, all the axons were then aligned on the bouton centroid to account for differences in the location of the termination within the LSO.

Maps of the average density of boutons revealed no obvious differences between control and NR axons at P19-21 (Fig. 4-3 D). In both cases termination regions were elongated dorsoventrally, consistent with the orientation of dendrites within isofrequency bands in the LSO (Rietzel and Friauf, 1998). Bouton density was highest in the center of termination regions, and gradually declined with distance from the centroid in both the mediolateral and dorsoventral direction. When the difference between the average distributions was plotted (Fig. 4-3 E), the differences tended to be negligible, never exceeding a gain or loss of ~2.5 boutons/0.17% LSO area. Out of the 265 bins that contained boutons, in only four cases was the average number of boutons per bin significantly different between control and NR axons ($p < 0.05$, Student's t-test). The distribution of NR animals, however, did seem to have a slightly lower and flatter peak.

Because axons with the highest number of boutons will have a greater influence on the average distribution than axons with smaller numbers of boutons, we also normalized each axon to its total number of boutons and looked at density as an average percentage of the total number of boutons per axon (Fig. 4-3 F). In this way the contribution of each axon is weighted equally within the average. The relative distributions changed very little compared to the absolute distributions, indicating that the average was reflective of the whole population of reconstructed

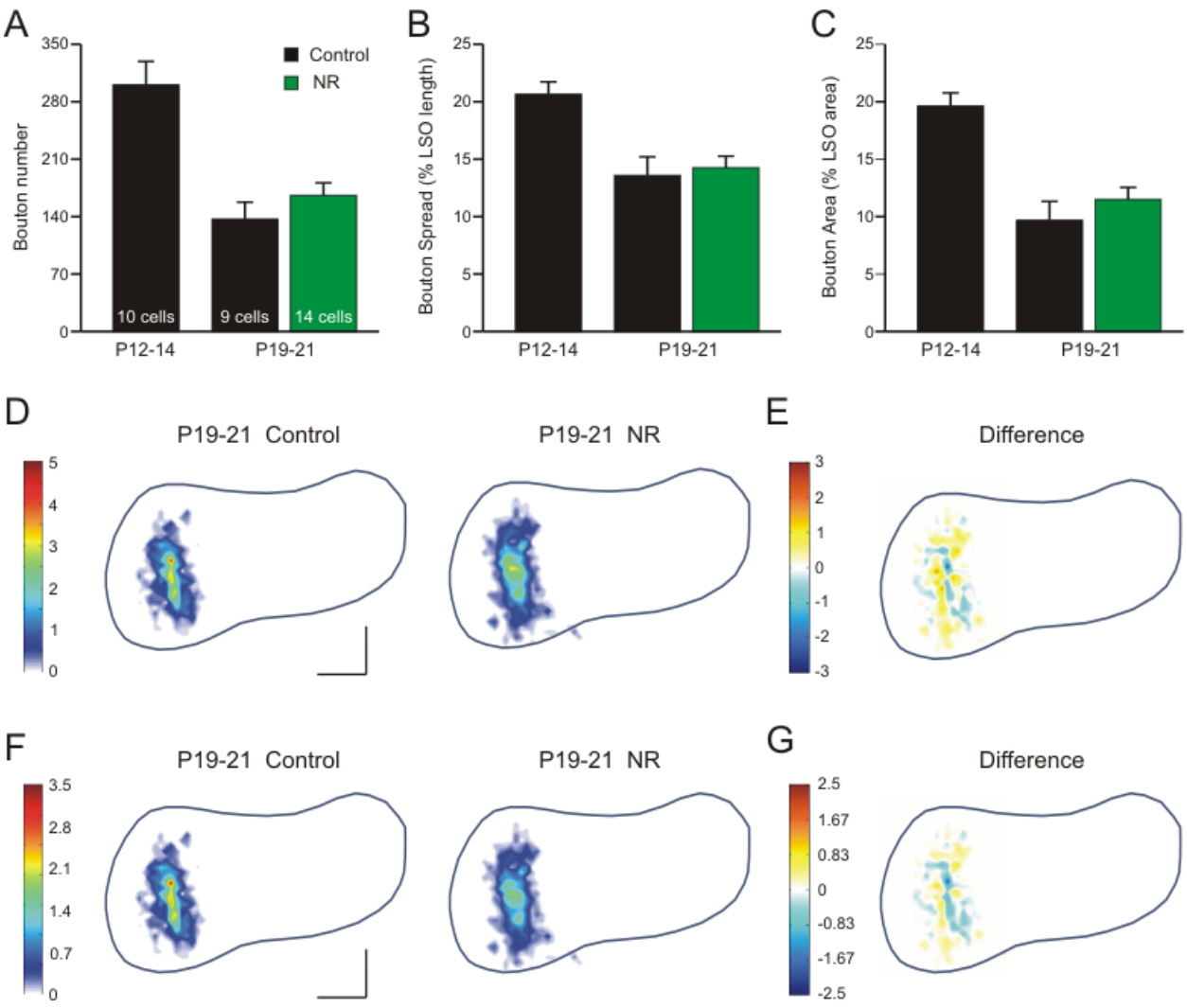
A
Bouton number
350
280
210
140
70
0
Control
NR
10 cells
9 cells
14 cells
P12-14
P19-21
B
Bouton Spread (% LSO length)
25
20
15
10
5
0
P12-14
P19-21
C
Bouton Area (% LSO area)
25
20
15
10
5
0
P12-14
P19-21
D
P19-21 Control
P19-21 NR
5
4
3
2
1
0
E
Difference
3
2
1
0
-1
-2
-3
F
P19-21 Control
P19-21 NR
3.5
2.8
2.1
1.4
0.7
0
G
Difference
2.5
1.67
0.83
0
-0.83
-1.67
-2.5

Figure 4-3.

Figure 4-3. Quantitative analysis of the distribution of the boutons of MNTB axons in the LSO of control and NR animals.

(A) Number of boutons located in the LSO per MNTB axon at postnatal day (P) 12-14 and P19-21 in control (black) animals and P19-21 in noise-reared (NR; green) animals. Data at P12-14 are shown to illustrate developmental changes. Data show mean ± s.e.m. for n = 10 control axons from 8 animals at P12-14, n = 9 control axons from 8 animals at P19-21, and n = 14 NR axons from 11 animals at P19-21. (B) Spread of the boutons of single MNTB axons along the LSO frequency axis. Conventions same as in (A). (C) Area of the LSO covered by the boutons of single MNTB axons. Conventions same as in (A) and (B). (D) Heat maps of absolute average bouton density per MNTB axon in the LSO for (left) control and (right) NR animals at P19-21. Color bar, average number of boutons per 0.17% LSO area; scale bars, 20 % mediolateral LSO length and 40 % dorsoventral height; dorsal is to the top and lateral to the right. (E) Heat map of the difference in the absolute average density of boutons per MNTB axon in the LSO between control and NR animals at P19-21. Warm colors indicate an increase with noise-rearing; cool colors indicate a decrease with noise-rearing. Color bar, average change in bouton number per 0.08 % LSO area. Scale and orientation same as in (D). (F) Heat maps of relative average bouton density per MNTB axon in the LSO for (left) control and (right) NR animals at P19-21. Color bar, average percentage of the total number of boutons per axon per 0.17 % LSO area; scale and orientation same as in (D) and (E). (G) Heat map of the difference in the relative average density of boutons per MNTB axon in the LSO between control and NR animals at P19-21. Warm colors indicate an increase with noise-rearing; cool colors indicate a decrease with noise-rearing. Color bar, average change in the percentage of the total number of boutons per axon per 0.17 % LSO area. Scale and orientation same as in (D), (E), and (F).

axons rather than being dominated by the characteristics of the axons with the highest numbers of boutons. Differences between the control and NR distributions were again very small (Fig. 4-3 G), with differences in only 3 bins out of 265 reaching statistical significance ($p < 0.05$, Student's t-test).

Again, the relative NR distribution appeared to have a slightly lower and flatter peak than the control distribution. A greater number or proportion of boutons at the peak of the density distribution could have implications for the strength of the input to that portion of the termination region, which could influence the flow of information between the MNTB and LSO. It could also indicate a subtle change in tonotopic organization if each axon's boutons were more evenly distributed across frequency space, rather than being more concentrated at a single location. However, because the individual density distributions were aligned in mediolateral and dorsoventral space to create the average heat maps, it is possible that slight variations in the orientation of the termination bands due to curvature of the LSO frequency axis could distort the true spread of the distribution along the frequency axis. The largely descriptive heat maps also make it difficult to assess whether qualitative differences in the overall shape of the distribution, such as the slightly smaller and flatter peak, are statistically significant.

Therefore, in order to more quantitatively compare the shape and tonotopic specificity of the distribution of boutons, I compressed the data in the longitudinal dorsoventral dimension and plotted the cumulative density function (CDF) of average bouton number (Fig. 4-4 A), as well as histograms of absolute bouton number (Fig. 4-4 B) and the relative proportion of the total number of boutons per axon (Fig. 4-4 C), all with respect to distance from the centroid along the LSO frequency axis.

Consistent with the gradual decline in density with distance from the centroid seen in the heat maps, the CDFs were largely linear. They were also not significantly different between control and NR animals. ($p = 0.92$; K-S test). There was little evidence that boutons were less likely to be located in the tonotopic center of the termination in NR animals, which would be the case if the spatial distribution had a significantly smaller and flatter peak.

This can be seen more clearly in the histograms of absolute (Fig. 4-4 B) and relative (Fig. 4-4 C) numbers of boutons with respect to distance from the centroid along the LSO frequency axis. The smoothed distributions were well fit with Gaussian functions (control: $R^2 = 0.96 \pm 0.01$ for both absolute and relative distributions; NR: $R^2 = 0.94 \pm 0.02$ for both absolute and relative distributions). For both the absolute and relative distributions, the average Gaussians did not differ significantly between control and NR animals in maximum height, location of the maximum height along the frequency axis, or the width of the Gaussian at half its maximum height ($p > 0.05$, Student's t-test). The width at the base of the Gaussians also corresponded well with the tonotopic spread of boutons measured with the ellipse-fitting (Fig. 4-4 B).

Taken together, our quantitative analyses of the projection of individual MNTB axons in the LSO of NR animals indicate that rearing in pulsed white noise did not influence anatomical refinement. However, although the majority of NR axons ($n = 14$ out of 17) looked indistinguishable from control axons at P19-21, a small number ($n = 3$) exhibited double-banded terminations in the LSO (Fig. 4-5). In these cases, axons tended to terminate in two distinct frequency regions. Each of the bands in double-banded axons was elongated across the frequency axis, similar to single-banded axons. The double-banded axons also had similar numbers of boutons in the LSO as the population of P19-21 control axons ($p = 0.97$, Student's t-test), and the single-banded NR axons ($p = 0.43$, Student's t-test), indicating that an equal

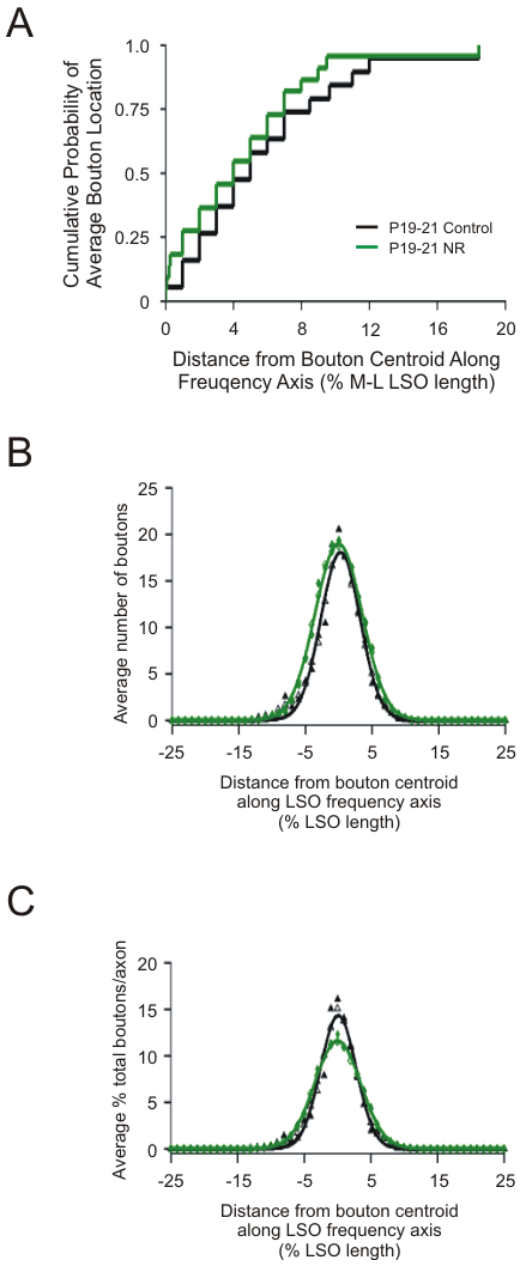

Figure 4-4. Distribution of boutons along the LSO frequency axis in NR animals.

(A) Cumulative probability function describing the cumulative likelihood that boutons will be found at a location some distance from the bouton centroid along the LSO frequency axis in control (black) and NR (green) axons at P19-21. The functions did not differ significantly ($p > 0.05$, Kolmogorov-Smirnov test). (B) Absolute distribution of boutons along the LSO frequency axis in control (black) and NR (green) axons at P19-21. Closed symbols represent population means; open symbols represent population means smoothed by a 3 bin-wide moving average; lines represent the Gaussian fit to the smoothed data. (C) Relative distribution of boutons along the LSO frequency axis in control (black) and NR (green) axons at P19-21. Conventions same as in (B).

number of boutons was distributed between the two bands as was normally found in a single band. This is consistent with the idea that pruning serves to regulate the number of synapses each axon is capable of supporting. Because of the spatial separation between the two termination regions, the boutons of the double-banded NR axons were spread across a significantly greater proportion of the LSO frequency axis ($p = 0.003$, Student's t-test) and covered a greater proportion of the LSO ($p = 0.01$, Student's t-test). The proportion of the frequency axis spanned by the boutons of double-banded NR axons was also significantly greater than at P12-14 ($p = 0.01$, Student's test). Somata of NR MNTB neurons with double-banded axons did not differ in their location along the MNTB frequency axis from the location of the somata of NR neurons without double-banded axons ($p= 0.15$, Student's t-test). Therefore, it is unlikely that the presence of double-banded termination areas was due to a difference in tonotopic location.

Adding the three double-banded axons to the population of other NR axons did not make any changes in tonotopic specificity statistically significant for the entire population of NR axons. Nevertheless, while the double-banded axons were uncommon in the NR population, they were never observed in the population of control axons, suggesting that pulsed noise-rearing may have had an effect on a small subset of MNTB axons.

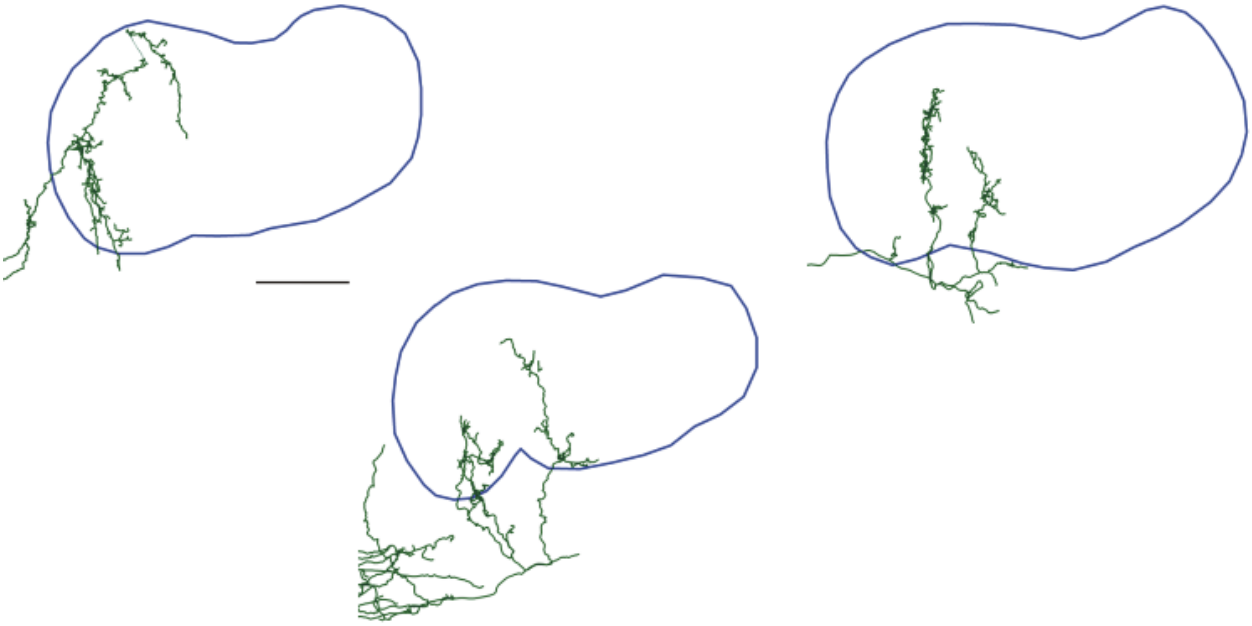

Figure 4-5. Double-banded terminations were observed for a small number of MNTB axons in NR animals.

A small number of MNTB axons in NR animals (n = 3) showed double-banded terminations in the LSO at P19-21 that were not observed in the population of P19-21 control axons. Solid blue line, outline of LSO; green line, MNTB axon. Dorsal is to the top and lateral to the right. Scale bar, 100 μm.

4.4 DISCUSSION

In the majority of NR axons, rearing in pulsed white noise had no effect on the refinement of MNTB axons in the LSO; at P19-21, axons had the same number of boutons and covered the same proportion of the LSO frequency axis as those in mice reared in a normal acoustic environment. The presence of normal pruning in noise-reared animals supports the idea that the pre-hearing phase of spontaneous activity and synaptic silencing plays a more important role than the pattern of sound-evoked activity in determining the tonotopic specificity of MNTB axons in the LSO.

4.4.1 Rearing in pulsed white noise

Pulsed white noise is expected to eliminate or greatly reduce the spectrotemporal structure of sounds present in a normal acoustic environment, repetitively entraining auditory nerve fibers representing a wide range of frequencies to fire synchronously. Spatio-temporally patterned neuronal activity is thought to play a central role in all aspects of topographic map refinement (Antonini and Stryker, 1993; Penn et al., 1998; Stellwagen and Shatz, 2002; Weliky, 2000; Wong, 1999), including tonotopic maps in the auditory system (Kandler et al., 2009; Sanes and Friauf, 2000). In the visual system, eliminating spatio-temporal variation in retinal activity via strobe-rearing disrupts the refinement of retinal axons in Xenopus optic tectum (Brickley et al., 1998), the sharpening of regenerating retinotectal connections in goldfish after transection of the optic nerve (Schmidt and Eisele, 1985), and the development of directional selectivity in the superior colliculus (Chalupa and Rhoades, 1978). Therefore, if the mechanisms responsible for

tonotopic refinement of MNTB-LSO connections depend similarly on the spatio-temporal structure of sound-evoked activity, this manipulation should disrupt the process.

Consistent with this hypothesis, rearing mice in pulsed white noise during early development has been shown to disrupt the normal developmental sharpening of frequency selectivity in primary auditory cortex, leading to less precise tonotopic organization and frequency response selectivity in the adult (Zhang et al., 2002). Similarly, inferior colliculus neurons in click-reared mice have broader tuning curves at P19-24 than those of mice reared in a normal acoustic environment (Sanes and Constantine-Paton, 1983).

While our noise-rearing protocol differed slightly from the protocols employed in the above studies, namely using pulses of slightly longer duration, presented at a slightly slower rate, the key components of the acoustic stimuli were maintained. Noise pulses were presented at a sound level and during a developmental window shown to be sufficient to prevent the maturation of frequency tuning in central auditory neurons. Pulses also covered a wide frequency spectrum to ensure synchronous firing was elicited across a large proportion of auditory afferents. Finally, pulses were presented pseudorandomly to avoid adaptation effects, and at a rate slightly slower than the rates of click presentation shown to cause attenuation of compound action potential amplitudes in the cochlear nucleus and inferior colliculus (Sanes and Constantine-Paton, 1985a, b), suggesting that a significant proportion of auditory afferents would continue to be entrained by the pulse stimuli over the week-long period of stimulus presentation.

Therefore, it is unlikely that the lack of an effect in the current study is due to a failure of the noise-rearing stimulus to disrupt the normal activity pattern of auditory afferents. However, *in vivo* recordings of the response of MNTB neurons to the pulsed white noise stimulus in NR animals would be required to absolutely confirm this. It is also possible that the cue(s) necessary

for refinement were still present in the acoustic environment of NR mice. For example, binaural cues, such as interaural time and sound level differences, were likely still available in the environment of pulsed white noise. Since I cannot be sure that rearing mice in another type of experimental acoustic environment would not impair refinement of anatomical MNTB-LSO connections, additional experiments that adjust the parameters of the acoustic environment would be necessary to more definitively pinpoint the characteristics of neuronal activity, if any, that are important for anatomical refinement.

4.4.2 Instructive or permissive role of sound-evoked activity

That tonotopic refinement of MNTB axons takes place normally in NR animals suggests that the spectrotemporal structure of normal sound-evoked activity does not play an instructive role in the tonotopic sharpening of MNTB axons in the LSO. Consistent with this idea, anatomical refinement is severely impaired in α9 KO mice despite seemingly normal hearing, indicating that the pattern of activity elicited by normal auditory experience cannot overcome the effect of disrupted functional refinement before hearing onset (Chapter 3).

However, it remains unclear whether any cochlear-generated activity after hearing onset is necessary for the sharpening. It is possible that a minimum level of sound-evoked or spontaneous activity is sufficient to facilitate refinement, without the pattern of the activity being important. Previous attempts to abolish all cochlear-generated activity after hearing onset usually did so at a time that could also affect pre-hearing spontaneous activity and functional refinement. As a result, any impairments of refinement that happened as a result are difficult to interpret solely as a consequence of the lack of sound-evoked activity. Therefore, additional studies that abolish cochlear-generated activity only after the pre-hearing phase of functional

silencing is completed are needed to determine whether cochlear-generated activity during the third postnatal week is necessary for post-hearing anatomical refinement.

4.4.3 Anatomical vs. physiological refinement

Normal pruning and refinement of MNTB axons in the LSO in NR mice was surprising in light of the numerous studies showing that the maturation of tuning and response properties of midbrain and cortical auditory neurons can be influenced by alterations of the acoustic environment during early development (Sanes and Constantine-Paton, 1983; Zhang et al., 2002, 2001; Zhou and Merzenich, 2008). In these studies however, the effects of manipulating the acoustic environment were assessed electrophysiologically, usually by determining the tuning curve of recorded neurons and mapping tonotopy based on the neurons' best frequency. In contrast, I investigated the anatomical specificity of a single input to a brainstem nucleus, the projection from the MNTB to the LSO. While it is true that ascending connections influence neuronal tuning curves and the mapping of best frequency in the inferior colliculus and primary auditory cortex, plasticity in the synaptic strength of local circuits, especially inhibitory networks, may also contribute to the changes induced by development in an altered acoustic environment. Thus it is possible that previously observed alterations in tuning in noise-reared animals could take place in the absence of any changes in the anatomical structure of excitatory afferents.

4.4.4 Is the MNTB-LSO circuit unique?

Previous anatomical studies have investigated the effects of noise-rearing in the medial superior olive (MSO) of gerbils, another brainstem nucleus involved in sound localization. Like the LSO, the MSO receives inhibitory input via the ipsilateral MNTB, as well as excitatory input from each ear via the ipsi- and contralateral cochlear nucleus. During early post-hearing development, glycinergic inputs and the axonal endsegments of MNTB axons become more concentrated near the soma rather than the dendrites of MSO neurons, a maturation of inhibition that is thought to be important for the computation of interaural time differences (Kapfer et al., 2002; Werthat et al., 2008). There is also a small degree of refinement of MNTB axonal endsegments along the dorsoventral MSO frequency axis during the same time period (Werthat et al., 2008). Both these changes can be disrupted by rearing animals in moderate intensity omnidirectional white noise. Since omnidirectional white noise greatly reduces binaural cues (Withington-Wray et al., 1990), which were likely still present during pulsed noise rearing, the maintenance of binaural cues may explain why pruning was spared in mice raised in pulsed white noise. It would be interesting to investigate whether refinement of MNTB axons in the LSO of mice would be affected by a similar manipulation of binaural cues during development, perhaps by eliminating the interaural intensity differences encoded by LSO neurons. Nevertheless, even though these studies certainly indicate that the refinement of MNTB axons during development can be influenced by altering the acoustic environment, at least in the gerbil MSO, it is unclear whether results from gerbil MSO can be directly applied to the mouse LSO, since a key aspect of refinement, the developmental restriction of inhibitory inputs to MSO neuronal somata, does not occur in rodents not specialized for low frequency hearing (Kapfer et al., 2002).

The MNTB-LSO circuit may also be unique in that circuit refinement takes place in two distinct stages confined to different development periods. In Chapter 2, I suggested that the distinct stages of MNTB-LSO refinement might be created by changes in the characteristics of synaptic transmission during development (again, this issue will be further explored in the General Discussion). As a result, the mechanisms underlying each form of refinement might only be available during certain critical windows of development. Pruning of MNTB axons in the LSO depends critically on functional refinement and the pattern of pre-hearing spontaneous activity. Therefore it is possible that the reason pruning is not disrupted by NR is that the pattern of pruning is determined by events that take place before hearing onset, which are unaffected by NR. Similarly, activity-dependent mechanisms necessary to influence the process may no longer be available during early auditory experience due to changes in the nature of synaptic transmission. If this is the case, the structure of sound-evoked activity may not be important because, no matter what the pattern of activity generated, the sequence of events leading to synapse elimination are already in motion, and the mechanisms necessary to influence the process are no longer accessible.

It is unknown whether functional refinement also precedes anatomical reorganization of inhibitory synapses in the gerbil MSO. And beyond the transition from depolarization to hyperpolarization, it is also unknown whether inhibitory synaptic transmission undergoes a similarly complex transformation during development. Thus it is possible that the refinement of inhibitory synapses in the MSO relies on a different complement of plasticity mechanisms than refinement in the LSO, which could influence its susceptibility to alterations of the normal acoustic environment.

4.4.5 Double-banded axons

Intriguingly, noise-rearing did seem to have an effect on a subset of MNTB axons, in that a small number of axons in NR animals exhibited double-banded terminations. Though the number of these axons was small (n = 3), they were never observed in mice reared in a normal acoustic environment at any age, suggesting they may be the result of noise-rearing. The three double-banded axons were also found in three different animals, each from different litters, indicating that the double bands were not an anomaly specific to a single case. In one case, a neuron filled in the contralateral MNTB of the same slice had a normal single-banded axon. The weight of animals in which double-banded axons were found also did not differ from the rest of the population of NR animals ($p = 0.5$, Student's t-test).

It is unclear what may have caused a small subset of MNTB axons to be susceptible to NR in a manner that other MNTB axons were not. The location of the soma along the MNTB frequency axis in double-banded NR axons did not differ from the somatic location of non-doubled-banded NR axons or control axons, however. So it is not likely to be the result of a simple change in the frequency represented by the neuron, though it is possible that small variations in the characteristics of the noise stimulus could have interacted with individual MNTB neurons in unique ways.

Perhaps the most obvious explanation for the double-banded terminations is that NR resulted in the stabilization of two portions of the axon, whereas normally only one portion would be maintained. However, the proportion of the frequency axis spanned by the boutons of double-banded NR axons was significantly greater than that spanned by boutons at P12-14, suggesting that NR did not simply alter the normal pattern of axonal pruning such that the medial- and lateral-most regions of the termination were both maintained. Instead, the increased

spread suggests that the axon grew into a previously unoccupied frequency region over the course of development in the pulsed white noise, at the same time other portions of the termination were being pruned. It is possible that axonal growth occurs concurrently with pruning during normal post-hearing development, but that natural sound-evoked activity patterns prevent axons from successfully invading new, less tonotopically precise areas. In the presence of pulsed white noise, competitive pressure could be reduced since all axons are likely active simultaneously. From the perspective of the postsynaptic LSO neuron, there could be few differences in the activity pattern to differentiate the input of a tonotopically correct MNTB neuron from the input of a newly connected, less tonotopically precise MNTB neuron. Still, the small number of double-banded axons indicates that NR impacts only a subset of MNTB neurons. Because double-banded axons seem to divide a similar total number of boutons between the two bands of the termination as axons normally distribute in one, it may be that only axons with an unusually small number of boutons around the time of hearing onset have the resources to successfully invade and elaborate in a new tonotopic region.

Because I observed such a small number of double-banded NR axons, it is unclear how much influence they would have in the behaving animal. However, MNTB axons with secondary projections have been observed in the gerbil LSO at P6-9 and 10-13 (Sanes and Siverls, 1991). A small proportion of LSO neurons in young animals have also been shown to have inhibitory response areas with more than one discrete range of frequencies (Sanes and Rubel, 1988). Neurons with two distinct frequency regions have also been observed in the inferior colliculus (Sanes and Constantine-Paton, 1985b), a major projection site of the LSO. If double-banded axons in only a small number of MNTB neurons contribute to this relatively rare response type in the normal animal, it may be possible that I simply missed seeing them in my

relatively small sample of axons in normally-reared animals. It is also possible that noise-rearing increased the proportion of MNTB axons with this type of termination, making them more likely to be sampled in the NR population.

4.4.6 Conclusion

Rearing in pulsed white noise had no effect on the refinement of the majority of MNTB axons in the LSO. The absence of impaired pruning in NR animals suggests that the spectrotemporal structure of normal sound-evoked activity does not play an instructive role in post-hearing anatomical refinement and is consistent with the idea that the pre-hearing phase of spontaneous activity and synaptic silencing may play a more important role than sound-evoked activity in determining the tonotopic specificity of MNTB axons in the LSO.

5.0 FREQUENCY DISCRIMINATION IS IMPAIRED IN FUNCTIONALLY DE-EFFERENTED A9 KNOCKOUT MICE

5.1 INTRODUCTION

Among sensory systems, the auditory system is unique because its sensory structure, the cochlea, receives abundant efferent innervation. In mature animals, acetylcholine released by medial olivocochlear (MOC) fibers activates α9/α10-containing acetylcholine receptors on outer hair cells (OHCs; Elgoyhen et al., 1994; Elgoyhen et al., 2001). The resulting calcium influx activates calcium-dependent potassium channels, hyperpolarizing the OHC (Goutman et al., 2005). Changes in OHC membrane potential induce an electromotile response that provides mechanical feedback to the basilar membrane. Thus a primary function of efferent inhibition is to adjust the gain of the cochlear amplifier (Dallos et al., 1997; Guinan, 1986; Housley and Ashmore, 1991; Kim, 1986).

Before the onset of hearing, however, MOC fibers transiently synapse onto α9-containing acetylcholine receptors on inner hair cells (IHCs; Bruce et al., 2000; Luo et al., 1998; Simmons and Morley, 1998). Also prior to hearing onset, spontaneous depolarization of IHCs by ATP generates calcium action potentials and the release of glutamate onto primary auditory neurons, triggering coordinated bursts of action potentials in the auditory nerve (Tritsch et al., 2007). Because downstream connections of the auditory nerve are already functional days before birth

(Kandler and Friauf, 1995; Kotak and Sanes, 1995; Wu and Oertel, 1987), patterned spontaneous activity appears to be transmitted along the ascending auditory pathway, where it shapes the firing of central auditory neurons even before they respond to sound (Fig. 1-4; Tritsch et al., 2010). Because acetylcholine released by MOC fibers can inhibit the spontaneous firing of IHCs (Glowatzki and Fuchs, 2000), the efferent system likely plays an additional role in the developing auditory system by contributing to the patterning of spontaneous activity.

Evidence for this hypothesis can be seen in the functionally de-efferented α9 KO mice, which carry a null mutation for the α9 subunit of the acetylcholine receptor (Vetter et al., 1999). In these mice the efferent pathways are intact, but hair cells cannot respond to the release of acetylcholine because they lack the necessary receptor subunit (Fig. 1-3). In the absence of cholinergic transmission in the cochlea, spontaneous activity recorded in medial nucleus of the trapezoid body (MNTB) neurons of α9 KO mice does not show the same fine temporal structure as that of controls (Fig. 1-4). As a result, these mice show impaired refinement and reduced tonotopic specificity in the connections between the MNTB and its postsynaptic target, the lateral superior olive (LSO; Fig. 1-5, Chapter 3). Because the output of this circuit is determined by the convergence of frequency-specific inputs, the imprecise representation of frequency is likely to pass downstream and influence processing in higher auditory centers like the inferior colliculus, the primary integration center of the midbrain.

Despite these central abnormalities, α9 KO mice do not show generalized deficits in the detection and discrimination of auditory signals; they have normal tone detection and intensity discrimination thresholds (May et al., 2002). However, perceptual behaviors that should depend on precise frequency tuning have never been tested in these mice. Impaired tonotopic precision in the MNTB-LSO pathway and perhaps other downstream auditory pathways as well, predicts

deficits in frequency discrimination. To test this hypothesis, I used prepulse inhibition of the acoustic startle response to determine whether reduced tonotopic precision is accompanied by impaired frequency discrimination in α9 KO mice, indicating that efferent cholinergic transmission in the cochlea plays a role in this important aspect of auditory perception.

5.2 MATERIALS AND METHODS

5.2.1 Experimental animals

Experiments were carried out on α9 KO mice (gift of D. Vetter, Tufts University), which are homozygous for a null deletion of the α9 nAChR gene (Vetter et al., 1999). Mice of the same genetic background, 129S6/SvEv (also obtained from D. Vetter), were used as a control. Mice were maintained on a 12 hour light/dark cycle and provided food and water *ad libitum*. Both sexes were used for testing. Testing was either conducted just after hearing onset, at postnatal day (P) 14, or post-puberty, at P50. Mice tested at a young age were not tested again at a later time point, and mice tested for frequency discrimination were not also tested for intensity discrimination, or vice versa. All experimental procedures were in accordance with NIH guidelines and approved by the Institutional Animal Care and Use Committee at the University of Pittsburgh.

5.2.2 Testing frequency discrimination

Frequency discrimination testing was performed using an apparatus and methods more thoroughly described in Appendix A. Briefly, the mouse was placed in the enclosure at the start of each session and allowed to acclimate to a constant background tone (f_1: 16 kHz, 70 dB SPL) for five minutes. The acclimation period was then followed by "prepulse" and "startle only" trials. In prepulse trials, the prepulse stimulus comprised a change in frequency consisting of a 1 ms linear ramp from the background tone, f_1, to the prepulse tone, f_2, also at 70 dB SPL. The change from background, f_1, to prepulse frequency, f_2, took place in variable steps of size Δf, such that $f_2 = f_1 - \Delta f$. f_2 was maintained for an 80 ms inter-stimulus interval (ISI). The ISI was then followed by the startle-eliciting stimulus: a 40 ms long, 120 dB SPL burst of white noise. At the conclusion of the startle stimulus, f_1 was presented again until the prepulse stimulus of the next trial. In startle only trials, the prepulse stimulus consisted of a 1 ms ramp from f_1 to f_1, and thus maintained the command to change frequency, while not actually introducing a frequency change. All trials were randomly separated by an 8-25 second inter-trial interval (ITI) to prevent the animal from anticipating presentation of the startle stimulus. A trial schematic is shown in Figure 5-1.

Trials were divided into three blocks. Block one consisted of a series of startle only trials to allow for short-term habituation to the startle stimulus. Block two contained prepulse trials randomly interleaved with an equal number of startle only trials. Prepulse trials were made up of seven classes, 10 trials each, where f_2 = 15.92, 15.68, 15.47, 15.2, 14.4, 13.34, and 12.0 kHz. Block three consisted of a short series of startle only trials to check for habituation over the course of the session.

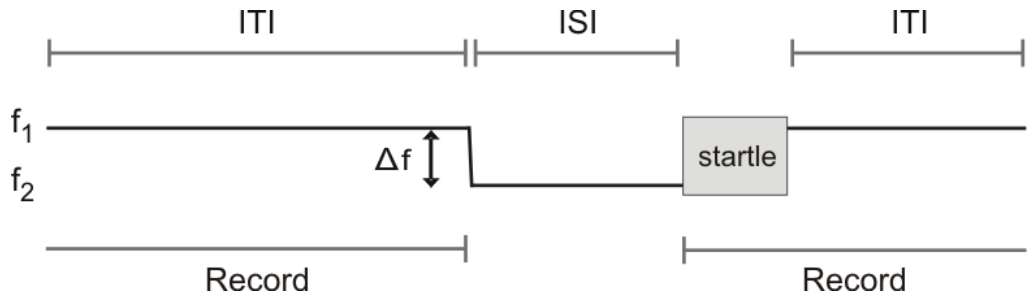

Figure 5-1. Schematic of trials used to test frequency discrimination.

f_1, background frequency; f_2, prepulse frequency; Δf, frequency change; ITI, inter-trial interval; ISI, inter-stimulus interval.

During each trial the vertical force exerted by the animal on the platform was measured during two 500 ms recording windows. The first recording window occurred immediately before the prepulse stimulus and provided a gauge of the animal's baseline activity. The second recording window began at the onset of the startle stimulus and measured the startle response of the animal to the white noise burst.

5.2.3 Testing intensity discrimination

Intensity discrimination testing was performed using the same apparatus and a procedure very similar to that used for frequency discrimination testing. However, rather than a change in sound frequency, the prepulse stimulus for intensity discrimination comprised a change in sound intensity. 70 dB SPL white noise was used as the background, i_1. The prepulse stimulus for prepulse trials comprised an intensity change of the background white noise, i_1, to the prepulse intensity, i_2, in variable steps of size Δi, such that $i_2 = i_1 + \Delta i$. Again, in startle only trials, the prepulse stimulus consisted of a transition from i_1 to i_1, maintaining the command to change intensity, while not actually introducing an intensity change. The same acclimation period, startle stimulus, ISI, and randomized ITIs as those used for frequency discrimination testing were used for intensity discrimination testing. The same block design was also employed, with blocks one and three consisting of startle only trials, and block two containing the same proportion of prepulse trials randomly interleaved with an equal number of startle only trials. Prepulse trials were made up of five classes, 10 trials each, where i_2 = 74, 78, 82, 86, and 90 dB SPL. A schematic of trials for intensity discrimination is shown in Fig. 5-4 A.

5.2.4 Data analysis

Data from frequency discrimination and intensity discrimination testing were analyzed separately. For each trial, the startle response was defined as the maximum force exerted during the startle recording period minus the background force, which was defined as the root-mean-square of the force exerted during the background recording period of that trial.

For each animal, startle responses were averaged across each class of prepulse trials and startle only trials. For each class of prepulse trials the average percent inhibition was calculated by subtracting the average prepulse response amplitude from the average startle only response amplitude and normalizing it to the average startle only response amplitude. One-way ANOVA (Sigmastat, Systat Software, Chicago, IL) was used to determine if the magnitude of the prepulse frequency change had a significant effect on startle response amplitude. Prepulse frequency changes that caused significant inhibition of the startle response were identified using a one-sample t-test against zero. Discrimination threshold was defined as the smallest frequency change to significantly inhibit the ASR. Within a single trial type, ASR amplitude of control and α9 KO mice were compared using a two-tailed Student's t-test. An alpha level of 0.05 was used to determine statistical significance for all tests.

Using real-time webcam images, trials in which the animal was moving spontaneously between trials or did not have its feet flat on the floor of the housing were excluded from analysis. Trials in which the mean background load exceeded two standard deviations of the sessions' average background load were also excluded.

5.3 RESULTS

5.3.1 Impaired frequency discrimination in α9 KO mice at P14

At P14, both control and α9 KO mice showed a reliable ASR in response to the startle stimulus (Fig. 5-2). When the startle stimulus was presented alone, without a preceding prepulse, the average response amplitude did not differ significantly between control and α9 KO mice (control: 0.68 ± 0.04, α9 KO: 0.70 ± 0.03; $p = 0.60$, Student's t-test; Fig. 5-2 A). Equivalent ASR waveform and magnitude in control and α9 KOs indicate that startle circuitry functions normally in α9 KO mice.

Preceding the startle stimulus with a change in frequency inhibited the ASR in both control and α9 KO mice (Fig. 5-2 H). As the prepulse frequency change grew larger, the amount of inhibition elicited increased, eventually reaching a plateau at around 60 % inhibition. In both control and α9 KO mice, prepulse magnitude had a significant effect on ASR magnitude ($p < 0.001$ in both control and α9 KO, one-way ANOVA). However, the amount of inhibition elicited by small negative frequency changes (0.5 – 10 %) was significantly less in α9 KO mice. In contrast, α9 KO and control mice showed equivalent inhibition for large frequency changes (16.6 and 25 %), indicating that α9 KO mice were less able to detect small changes in frequency, though their ability to discriminate between more widely-separated tones remained intact. Because α9 KO mice showed PPI comparable to control animals for large frequency changes, it is unlikely that alterations in PPI circuitry are responsible for the reduced inhibition elicited by small frequency changes in α9 KO mice. α9 KO mice also had larger discrimination thresholds. While control mice showed significant inhibition of the ASR for frequency changes as small as

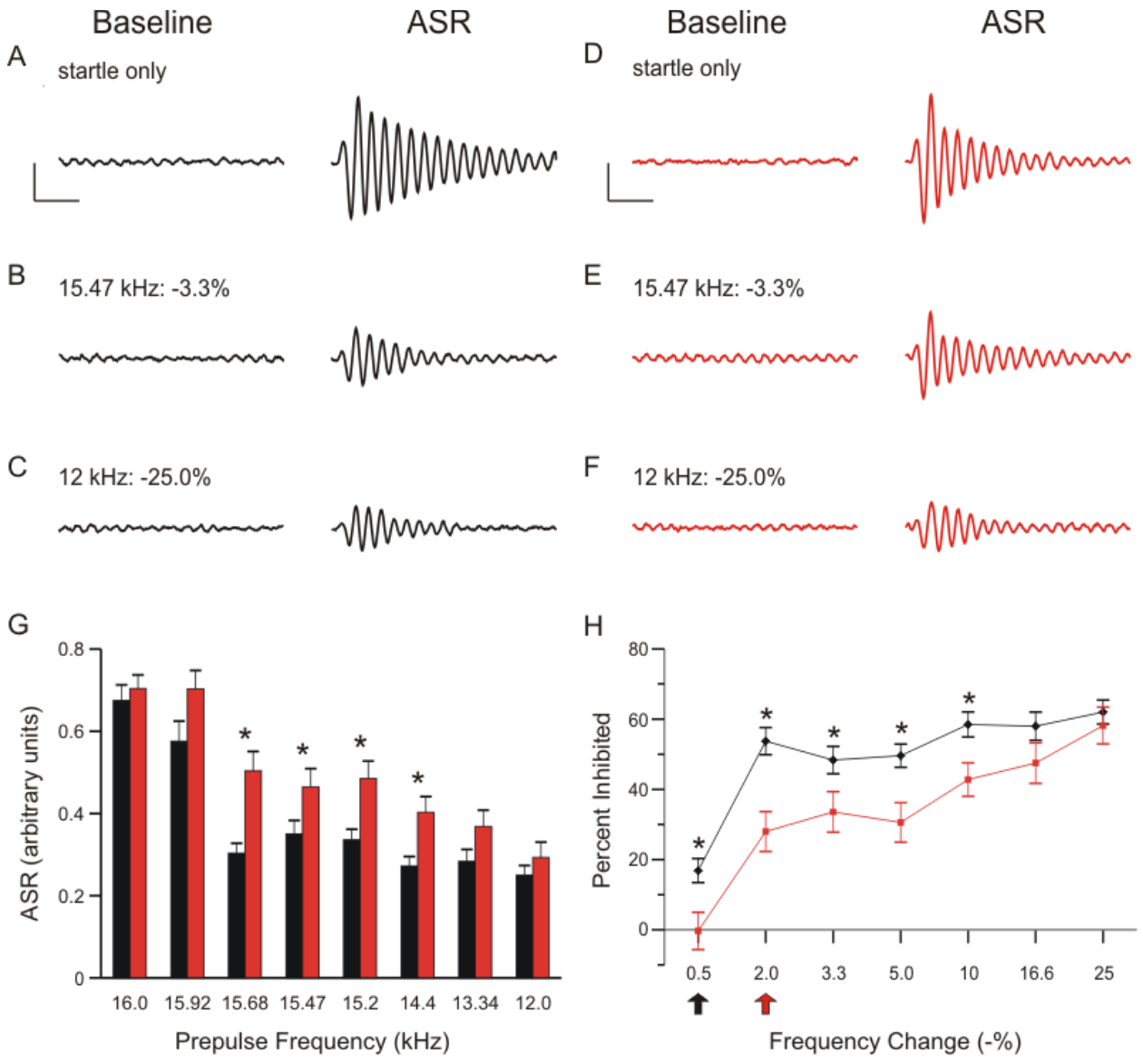
Baseline
ASR
A
startle only
B
15.47 kHz: -3.3%
C
12 kHz: -25.0%
Baseline
ASR
D
startle only
E
15.47 kHz: -3.3%
F
12 kHz: -25.0%
G
ASR (arbitrary units)
0.8
0.6
0.4
0.2
0
16.0
15.92
15.68
15.47
15.2
14.4
13.34
12.0
Prepulse Frequency (kHz)
H
Percent Inhibited
80
60
40
20
0
0.5
2.0
3.3
5.0
10
16.6
25
Frequency Change (-%)

Figure 5-2.

Figure 5-2. At P14, α9 KO mice show impaired PPI for small, but not large, changes in frequency.

(A-F) Examples of baseline activity and acoustic startle response for control (black; A-C) and α9 KO (red; D-F) mice. Traces represent the force measured on the platform during the first 500 ms recording period, "baseline," and force measured during the second 500 ms recording period, "ASR" for (A,B) startle only trials and (C-F) prepulse trials with frequency steps of increasing size. Prepulse trials are labeled with the frequency of the prepulse and magnitude of the resulting frequency change. For each trial, the maximum force recorded during the second recording period, in either the positive or negative direction, was reported as the ASR. Scale bars, 0.4 arbitrary units of force, 100 ms. (G) Average ASR for control (black) and α9 KO (red) mice for each trial type. Asterisks indicate that ASR magnitude for α9 KO mice is significantly different than ASR magnitude for control mice for that class of trials ($p<0.05$, Student's t-test). Data represent mean ± s.e.m.; n = 20 control and 13 α9 KO animals. (H) Percent inhibition of the ASR caused by a prepulse frequency change of various magnitudes. Arrows indicate discrimination threshold, the smallest frequency change that caused significant inhibition of the ASR ($p < 0.05$, one-way t-test against zero) for control (black) and α9 KO (red) animals. Data represent mean ± s.e.m.; n = 20 control and 13 α9 KO animals.

0.5 %, in α9 mice the ASR was not significantly inhibited until the preceding frequency change reached 2 %.

5.3.2 Impaired frequency discrimination in α9 KO mice at P50

Because the auditory system is still developing at P14, I was interested in whether the impaired frequency discrimination observed in α9 KO mice soon after hearing onset would persist into maturity or whether plastic mechanisms might be able to compensate for the deficits. It is also unknown whether the loss of precision in tonotopic maps persists past the age of P21. We therefore tested frequency discrimination in mature animals at P50.

At P50, average ASR amplitude was larger in both control and α9 KO mice, consistent with the increased weight of the animals (Fig. 5-3). However, the increase in ASR amplitude was greater in control than in α9 KO mice, such that the mean startle only ASR was significantly larger in P50 control mice than in P50 α9 KO mice (control: 2.77 ± 0.16, α9 KO: 2.22 ± 0.13; $p = 0.02$, Student's t-test). This change cannot be accounted for based on the weight of the animals because weight did not differ significantly between control and α9 KO mice (P50 control: 21.5 ± 0.8 g, P50 α9 KO: 21.8 ± 0.8 g; $p = 0.80$, Student's t-test). Compound action potential (CAP) threshold sensitivity is unchanged in α9 KO mice (He et al., 2004; Vetter et al., 1999), and chronic de-efferentation does not seem to affect afferent innervation of either inner or outer hair cells (Liberman et al., 2000). Thus it is unlikely that changes in the afferent system are responsible for reduced startle only ASR amplitude in α9 KO mice, though a similar reduction in startle only ASR amplitude was also seen in P50 α9 KO mice in the intensity discrimination task (data not shown). However, because the relative degree of PPI remains constant despite changes in the magnitude of the startle only ASR (Ison et al., 1997), the reduced startle only ASR in α9

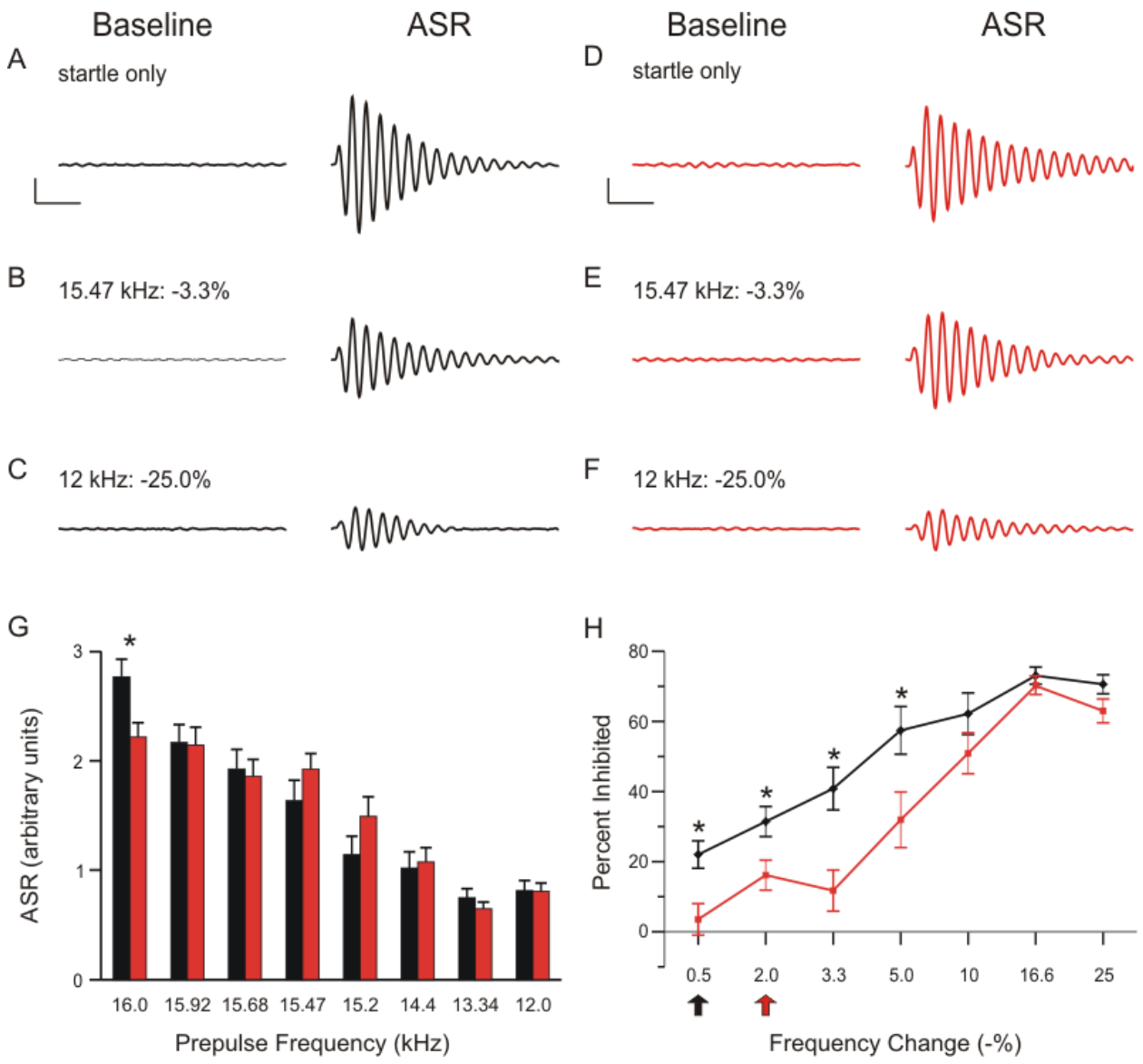
Baseline
ASR
A
startle only
B
15.47 kHz: -3.3%
C
12 kHz: -25.0%
D
Baseline
ASR
startle only
E
15.47 kHz: -3.3%
F
12 kHz: -25.0%
G
ASR (arbitrary units)
0
1
2
3
*
16.0
15.92
15.68
15.47
15.2
14.4
13.34
12.0
Prepulse Frequency (kHz)
H
Percent Inhibited
0
20
40
60
80
*
*
*
*
0.5
2.0
3.3
5.0
10
16.6
25
Frequency Change (-%)

Figure 5-3.

Figure 5-3. At P50, α9 KO mice continue to show impaired PPI for small, but not large, changes in frequency.

(A-F) Examples of baseline activity and acoustic startle response for control (black; A-C) and α9 KO (red; D-F) mice. Traces represent the force measured on the platform during the first 500 ms recording period, "baseline," and force measured during the second 500 ms recording period, "ASR" for (A,B) startle only trials and (C-F) prepulse trials with frequency steps of increasing size. Prepulse trials are labeled with the frequency of the prepulse and magnitude of the resulting frequency change. For each trial, the maximum force recorded during the second recording period, in either the positive or negative direction, was reported as the ASR. Scale bars, 1.0 arbitrary units of force, 100 ms. (G) Average ASR for control (black) and α9 KO (red) mice for each trial type. Asterisks indicate that ASR magnitude for α9 KO mice is significantly different than ASR magnitude for control mice for that class of trials ($p<0.05$, Student's t-test). Data represent mean ± s.e.m.; n = 15 control and 12 α9 KO animals. (H) Percent inhibition of the ASR caused by a prepulse frequency change of various magnitudes. Arrows indicate discrimination threshold, the smallest frequency change that caused significant inhibition of the ASR ($p < 0.05$, one-way t-test against zero) for control (black) and α9 KO (red) animals. Data represent mean ± s.e.m.; n = 15 control and 12 α9 KO animals.

KO mice is unlikely to influence the results of discrimination testing.

As at P14, at P50 preceding the startle stimulus with a change in frequency inhibited the ASR in both control and α9 KO mice, with a significant effect of prepulse magnitude on ASR amplitude ($p < 0.001$ in both control and α9 KO, one-way ANOVA). However, because the startle only ASR was reduced in α9 KO mice, the magnitude of the ASR elicited by any of the prepulse frequency changes tested (15.92 – 12.0 kHz) did not differ between control and α9 KO mice (Fig. 5-3 G). Nonetheless, ASR amplitude in control mice declined more rapidly when the startle stimulus was preceded by frequency changes of increasing magnitude. As a result, small negative changes in frequency (0.5 - 5.0 %) elicited significantly less inhibition of the ASR in α9 KO mice than in controls, consistent with the impaired discrimination observed in α9 KO mice at P14. Accordingly, the discrimination threshold of P50 α9 KO mice was again larger than that of age-matched controls (control: 0.5 %, α9 KO: 2.0 %).

5.3.3 Intensity discrimination is not impaired in α9 KO mice

I hypothesized that frequency discrimination would be impaired in α9 KO mice due to their deficits in central tonotopic specificity (Fig. 4; Chapter 3). I did not expect to see generalized deficits for other types of auditory discriminations, since adult α9 KO mice are normal in their ability to detect a pure tone and discriminate its intensity when trained on a conditioning paradigm (May et al., 2004). Therefore, to further show that the deficits in frequency discrimination observed in α9 KO mice were not related to more generalized deficits in PPI, I modified the PPI protocol that was previously used to test frequency discrimination to also test intensity discrimination. By replacing the prepulse frequency change with a prepulse intensity

change (Fig. 5-4 A), I tested whether α9 KO mice show normal intensity discrimination using PPI.

At both P14 and P50, control and α9 KO mice showed equivalent levels of inhibition at each of the intensity changes tested (Fig. 5-4 B,C), indicating that the ability of α9 KO mice to discriminate intensity, as shown previously (May et al., 2002), remains intact. Both control and α9 KO mice at P14 and P50 were capable of discriminating changes in white noise intensity as small as 4 dB SPL, a change in sound level of less than 6 %. The specificity of discrimination deficits in α9 KO mice for frequency, and not intensity, along with the fact that they show equivalent levels of inhibition for large frequency changes, indicates that a generalized deficit in PPI can not explain the impaired frequency discrimination of α9 KO mice at P14 and P50.

5.3.4 Age-related changes in PPI

For both control and α9 KO mice, the amount of inhibition elicited did not increase as rapidly with frequency changes of increasing magnitude at P50 as it did at P14 (Fig. 5-2 H vs. Fig. 5-3 H). While the amount of inhibition elicited by the smallest frequency change (0.5 %) did not differ for either control or α9 KO mice between P14 and P50, the amount of inhibition for the next-largest frequency change (2.0 %) was much greater at P14 than at P50 for both control and α9 KO mice. For example, in P14 control mice, the amount of inhibition elicited by a 2.0 % change (54 ± 4 %) was already ~87 % of the maximum inhibition (62 ± 3 %). At P50, the same frequency change only elicited inhibition that was ~42 % of the maximum, about half of what it was at P14. As a result, the amount of PPI elicited by a 2.0 % frequency change did not differ from the amount elicited by a 25 % frequency change ($p = 0.12$, Student's t-test). The same relationship held true for α9 KO mice as well, with ~ 48% of the maximum inhibition elicited by

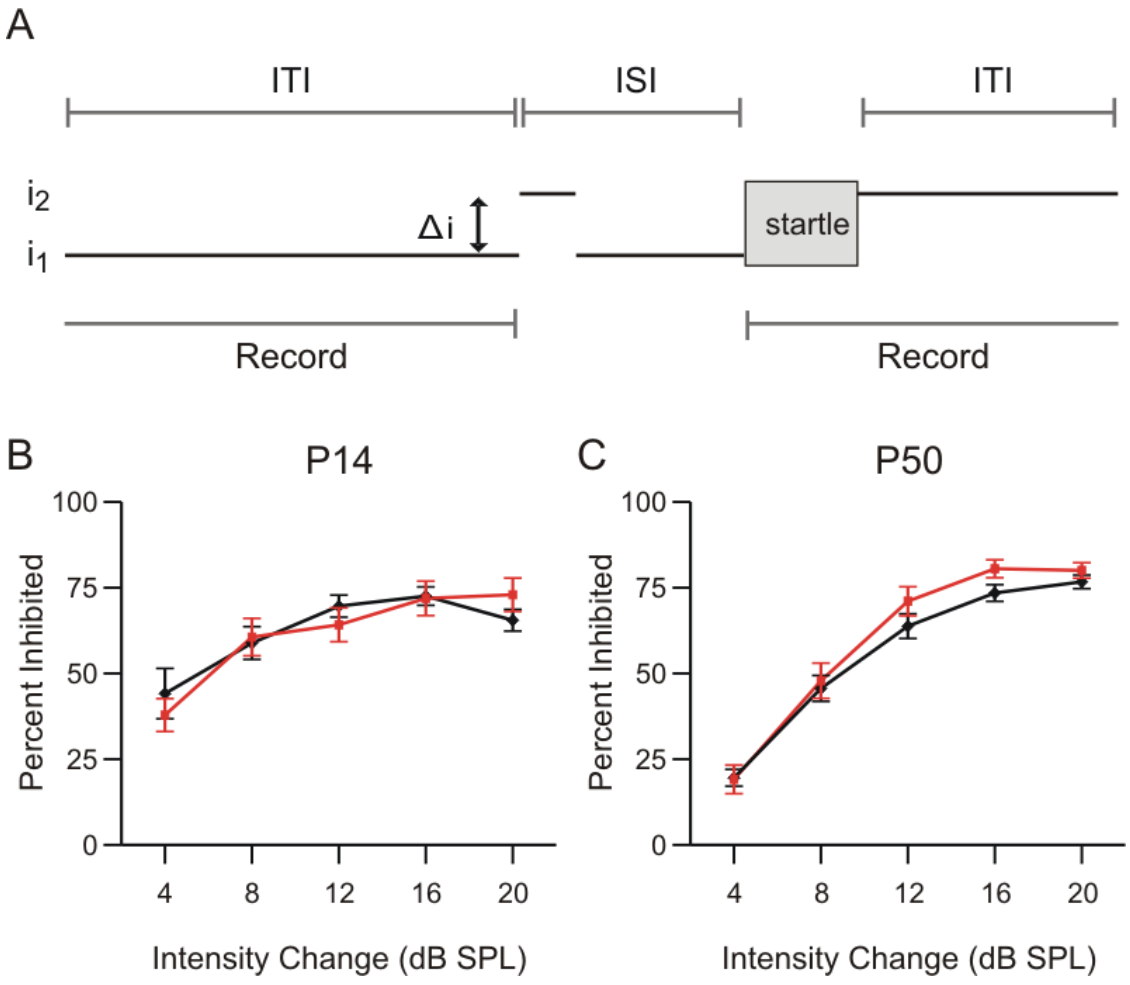

Figure 5-4. Intensity discrimination is not impaired in α9 KO mice.

(A) Schematic of trials used to test intensity discrimination. i_1, background intensity; i_2, prepulse intensity; Δi, intensity change; ITI, inter-trial interval; ISI, inter-stimulus interval. (B, C) Percent inhibition of the ASR caused by a prepulse intensity change of various magnitudes in control (black) and α9 KO (red) mice at (B) P14 and (C) P50. Data represent mean ± s.e.m.; n = 13 control and 15 α9 KO animals at P14; n = 20 control and 12 α9 KO animals at P50.

a 2.0 % frequency change at P14, but only ~23 % at P50. A similar age-related trend was also evident in the intensity discrimination data, with a 4 dB SPL intensity change eliciting significantly more inhibition at P14 than at P50 (Fig. 5-4 B, C; $p < 0.001$, Student's t-test), in both control and α9 KO mice. Increased inhibition between the second and third postnatal weeks has also been observed in PPI studies of the ASR in rats (Parisi and Ison, 1979).

5.4 DISCUSSION

Using prepulse inhibition of the acoustic startle response, we showed that α9 KO mice have deficits discriminating small, but not large, changes in frequency. These deficits are present soon after hearing onset (P14) and persist into maturity (P50). The discrimination deficits are specific to frequency, since α9 KO mice at both P14 and P50 could discriminate intensity as well as age-matched controls. To my knowledge, this is the first deficit in auditory perception exhibited by α9 KO mice. Work in Chapter 3 showed that disruption of the efferent system in α9 KO mice produces abnormalities in the development of the central auditory system's representation of frequency (see also Fig. 1-5). The impaired frequency discrimination of α9 KO mice therefore provides a critical link between the degree of precision of a neural circuit to behavioral performance, and highlights a role of the MOC efferent system in auditory perception.

5.4.1 PPI in α9 KO mice

The primary acoustic startle circuit consists of an initial auditory relay involving the auditory nerve, cochlear root neurons, and cochlear nucleus complex. If the acoustic stimulus is sufficiently intense, giant neurons in the caudal pontine reticular nucleus (PnC) are activated and mediate the startle response via output to spinal and brainstem motor neurons. The prepulse is believed to exert its inhibitory effect through cholinergic neurons in the pedunculopontine reticular nucleus (PRN), which inhibit the startle-activating neurons of the PnC. For an acoustic prepulse such as a frequency change, the ascending auditory pathway is thought to send projections to the superior colliculus (SC), where information about tactile or visual prepulses also enters the PPI pathway. Information about the prepulse then passes to the PRN, inhibiting the startle response (Fig. 5-5; Koch and Schnitzler, 1997).

The inferior colliculus (IC) is believed to be a critical relay in acoustic PPI. In rats with IC lesions, auditory prepulses are no longer effective in reducing startle amplitude, although the effect of visual prepulses is unaffected by the lesion (Leitner and Cohen, 1985). Conversely, IC stimulation mimics the effect of a prepulse, inhibiting the ASR (Li et al., 1998). Portions of the IC provide direct input to the middle and deep layers of the SC (Covey et al., 1987; Druga and Syka, 1984; Frisina et al., 1997), which then projects to the PRN (Steininger et al., 1992). Almost all ascending auditory pathways synapse in the IC, including those from the LSO (Glendenning et al., 1992; Glendenning and Masterton, 1983), making it a major site for the integration of monaural, binaural, and frequency characteristics of sound. Thus impaired tonotopy in the MNTB-LSO pathway is in a prime position to influence the way the prepulse is processed in the IC. The IC also receives input from descending auditory pathways, but because

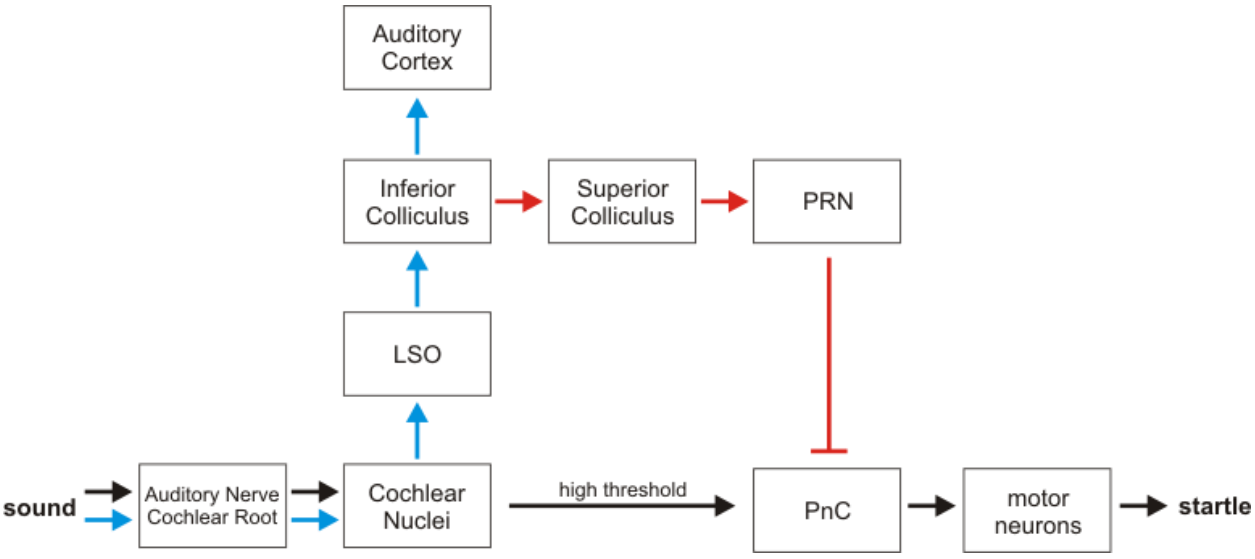

Figure 5-5. Simplified schematic of acoustic startle and PPI circuits.

Acoustic stimuli enter the auditory pathway. If the stimulus is intense enough, it activates neurons in the PnC, generating the ASR. If it is not intense enough, like a prepulse, then it may inhibit the startle through the inhibitory effect of PRN neurons on the PnC. The ascending auditory pathway is represented in blue, the primary startle circuit in black, and the PPI circuit in red. LSO, lateral superior olive; PRN, pedunculopontine reticular nucleus; PnC, caudal pontine reticular nucleus. Adapted from Koch and Schnitzler, 1997.

acoustic prepulses can still inhibit the ASR in decerebrate animals (Davis and Gendelman, 1977), cortical input is not necessary for either the mediation of PPI or processing of the prepulse.

In α9 KO mice, motor pathways involved in the ASR should be unaffected, since muscle-type nicotinic acetylcholine receptors at the neuromuscular junction contain α1 subunits (Kalamida et al., 2007). Processing of the intense, broadband startle stimulus should also be unaffected, since α9 KO mice have normal threshold sensitivity, no obvious hearing deficits, and normal compound action potential responses to stimuli of increasing intensity (May et al., 2002; Vetter et al., 1999). Accordingly, the ASR in α9 KO mice was normal when the startle stimulus was presented alone, with only a slight reduction in amplitude at P50 compared to controls. Similarly, the primary pathway believed to mediate PPI, the inhibitory effect of cholinergic input from the PnC to PRN would also not be affected by the knockout, since the inhibition is mediated by muscarinic receptors (Koch et al., 1993). Consistent with this assertion, PPI elicited by intensity changes and large frequency changes was normal in α9 KO mice. Therefore, the reduced inhibition elicited by small frequency changes in α9 KO mice is most likely due to a change in processing of the prepulse.

5.4.2 Link to tonotopic organization

Frequency discrimination deficits in α9 KO mice likely stem from their less precise tonotopic organization. At P14, the tonotopic representation of frequency is less precise in α9 KO mice due to impaired sharpening of functional connections in the MNTB-LSO circuit of the auditory brainstem (Fig. 1-5; Chapter 3). Outside a small body of evidence that indicates frequency-selective neurons in primate auditory cortex are important for fine-grained pitch discrimination

(Tramo et al., 2005; Tramo et al., 2002), the neural code for frequency discrimination is still largely unknown. However, it is likely that a loss of precision in the representation of frequency early in the afferent stream affects processing in higher order auditory integration centers needed for perceptual discrimination. Importantly, large-scale tonotopy remains intact in α9 KO mice, with high frequency LSO neurons still receiving inputs restricted to high frequency regions of the MNTB. In contrast, the proportion of MNTB frequency space covered by the inputs to a single LSO neuron is over 50 % larger in α9 KO mice. The specific loss of fine-scaled tonotopic precision around the time of hearing onset is consistent with the behavioral frequency discrimination data; α9 KO mice could not discriminate small changes in frequency, but showed normal abilities to discriminate large frequency changes.

It is not known whether the reduced tonotopic specificity of functional connections in α9 KO mice persists into adulthood, though a similar reduction in the tonotopic precision of anatomical connections is found at P21 (Chapter 3). Since α9 KO mice at P50 show frequency discrimination deficits comparable to those at P14, it is likely that deficits in central tonotopy are also still present at P50.

Previous links between tonotopic map changes and frequency discrimination have been made in the context of auditory plasticity. Cochlear damage and hearing loss, for example, are known to produce rearrangements of tonotopic maps in the brain. More specifically, the neural representation of the frequency specific to the edge of the lesion or area of hearing loss is enlarged (cat IC: Kamke et al., 2003; cat cortex: Rajan et al., 1993; guinea pig cortex: Robertson and Irvine, 1989; macaque cortex: Schwaber et al., 1993). In human patients with steeply-sloped hearing loss, frequency discrimination thresholds are improved specifically for frequencies at or near the cut-off frequency of the hearing loss (McDermott et al., 1998; Thai-Van et al., 2003;

Thai-Van et al., 2002), suggesting that local improvement in thresholds near the cut-off frequency are related to its enhanced neural representation (McDermott et al., 1998). Though I cannot assert that a causal relationship exists between the loss of tonotopic precision and impaired frequency discrimination based on the present study alone, the results are consistent with mounting evidence, even in humans (Dietrich et al., 2001), that indicates there is a strong link between the two.

5.4.3 Anti-masking effects of MOC efferents

The efferent system can enhance cochlear responses when signals are presented in noise, a process that is thought to contribute to the ability to hear in noisy backgrounds (Dewson, 1968; Kawase and Liberman, 1993; Trahiotis and Elliott, 1970; Winslow and Sachs, 1988). When a background sound is presented shortly before the presentation of a signal such as a tone, the response to the signal is reduced as compared to the response to the signal presented alone, a phenomenon known as forward masking. But when the MOC efferent system is activated, either through electrical stimulation or the presentation of contralateral noise, the masking effect (i.e. the reduction of the response to the signal due to the background sound) is reduced. This anti-masking effect of MOC efferents is attributed to the fact that auditory nerve fiber (ANF) responses adapt to the presence of the masker, causing them to be less responsive to the subsequent presentation of the signal. MOC activity, however, can suppress the response to the masker, decreasing adaptation levels, and thus indirectly increasing the ANF response to the signal (Kawase and Liberman, 1993). In the frequency discrimination tasks, it is possible that the constant background had a forward masking effect on the prepulse, an effect that would be equivalent in control and α9 KO mice. If MOC efferents were active during the ITI in the

control mice, but not α9 KO mice, the anti-masking effects could increase the response to the prepulse in controls, but not α9 KOs, thereby contributing to their frequency discrimination deficits. Although such an effect is possible, it is unlikely to be the case.

First, it is unclear whether MOC efferents would be active during the frequency discrimination task at the time when their activity could increase the response to the prepulse. In intact animals MOC feedback is sound-evoked. So in typical studies of the anti-masking effects of efferent activity, MOC feedback is actively recruited by either direct stimulation or the presentation of noise to the contralateral ear during the presentation of the masker to the ipsilateral ear (Bonfils et al., 1987; Kawase and Liberman, 1993; Winslow and Sachs, 1988). Signal presentation is then timed so as to coincide with the period of MOC activity, since the effects of MOC feedback decay with a time constant of ~80 ms after cessation of activity (Warren and Liberman, 1989). In our study, MOC activity was never directly elicited before presentation of the prepulse. Similarly, in studies of MOC effects that did not actively recruit their activity, but instead looked at the difference in responses between control animals and those de-efferented by transection of the OC bundle, the masker was typically turned on shortly before the signal (10s to 100s of ms), providing an onset response to activate MOC fibers. In our study, there was no onset response shortly before the prepulse because the background tone was constant throughout the 8-25 s ITI. Therefore it is unclear whether the MOC system would even be active enough shortly before the prepulse to provide significant anti-masking effects.

In addition, the magnitude of anti-masking effects tends to diminish with increasing masker levels, because the ANF responses to the background masker begin to saturate with increasing sound level. Since MOC feedback cannot significantly reduce the response to the masker if the response is saturated, there is no de-adaptation, and no indirect increase in the

response to the signal. In a forward masking paradigm, anti-masking effects were already almost gone at masker levels of ~60 dB (Kawase and Liberman, 1993), which is less than the 70 dB SPL used in the current study. Therefore it is likely that even if MOC efferents were active before the prepulse in the frequency discrimination task, their anti-masking effects would be negligible.

Consistent with this idea, α9 KO mice had no deficits discriminating intensity using PPI. Since the intensity discrimination was also tested using a continuous background at the same sound level (70 dB SPL) and presented for the same period of time (8-25 s ITI) as that used to test frequency discrimination, it is just as likely that the background would have a forward-masking effect on the prepulse in the intensity discrimination task as in the frequency discrimination task. The lack of deficits in α9 KO mice suggests that MOC-mediated anti-masking effects were not a factor in their performance in either intensity or frequency discrimination using PPI. The presence of background sound also did not impair the ability of α9 KO mice to detect or discriminate the intensity of a tone when tested using an operant conditioning paradigm (May et al., 2002).

It therefore seems unlikely that the deficits of α9 KO mice in frequency discrimination were the result of the loss of MOC-mediated anti-masking effects in processing the prepulse. Furthermore, because behavioral frequency discrimination in cats was unaffected by acute OC bundle transection (Igarashi et al., 1979b), it is even more likely that the deficits arise from the loss of efferent effects during development, and their influence on tonotopic refinement. However, the potential effects of masking could be definitively tested by surgically transecting the OC bundle at the midline in a control mouse, eliminating MOC-mediated anti-masking effects. If frequency discrimination is unchanged, it would support the hypothesis that the lack

of peripheral MOC effects does not contribute to impaired frequency discrimination in α9 KO mice.

5.4.4 Efferent effects on mechanical tuning

It has been suggested that the efferent system may influence frequency tuning in the cochlea as well, which could also contribute to the frequency discrimination deficits of α9 KO mice. Acute sectioning of the efferent bundle in rats, for example, causes a 30 % reduction of the sharpness of compound action potential tuning curves measured with a simultaneous tone-on-tone masking paradigm, with no effect on thresholds (Carlier and Pujol, 1982; Dallos and Cheatham, 1976). However, subsequent studies in guinea pigs showed that de-efferentation did not affect single-unit tuning curves (Bonfils et al., 1986), indicating that the reduced tuning observed using the masking paradigm resulted from the loss of masking effects, and that the crossed (primarily MOC) efferents do not produce sharp cochlear tuning. Consistent with this interpretation, complete de-efferentation in adult cats, whether acutely or chronically, has no effect on either the tuning or sensitivity of auditory nerve fibers (Liberman, 1990; Warren and Liberman, 1989).

In cats chronically de-efferented since P2-4, however, auditory nerve fibers show elevated thresholds and, for a small proportion of fibers with characteristic frequencies between ~10-25 kHz, slightly reduced sharpness of tuning (Walsh et al., 1998). The authors attribute these abnormalities to a loss of normal OHC function in the absence of efferent innervation, suggesting that the efferent system may play a special role in the development of the OHCs' contribution to active cochlear mechanics. Functionally de-efferented α9 KO mice, however, show normal cochlear sensitivity and motile OHCs (He et al., 2004; Vetter et al., 1999), suggesting that OHC function is largely normal in these mice. The type of interaction between

the OHCs and MOC fibers necessary for OHC maturation is unknown, although it is possible that the continued presence of efferent fibers beneath the OHCs and the release of neurotransmitter, which are maintained in α9 KOs but lost in surgically de-efferented animals, might play a role.

Because the tuning of auditory nerve fibers has not been determined in α9 KO mice, I cannot completely exclude a potential contribution of reduced mechanical tuning to the impaired frequency discrimination we observed. However, reductions in the tuning of auditory nerve fibers in chronically de-efferented cats were small even for the small proportion of fibers for which they were significant. Therefore, even in the unlikely case mechanical tuning is reduced for some frequencies in α9 KO mice, it is likely its contribution to frequency discrimination deficits would be negligible.

5.4.5 Comparison of thresholds

When defined as the smallest frequency change to significantly inhibit the ASR, I found discrimination thresholds of 0.5 % in control mice at both P14 and P50. While it is difficult to directly compare the threshold we obtained with a reflex response to behavioral thresholds obtained via operant conditioning paradigms, this is just slightly lower than a frequency discrimination limens of ~0.8 % found in house mice at 16-20 weeks of age (Ehret, 1975) and of 1.25-5 % in cats (Butler et al., 1957; Igarashi et al., 1979b).

Similarly, in the intensity discrimination test, both control and α9 KO mice were capable of detecting intensity changes of 4 dB SPL, or ~6 %, which is consistent with the behavioral pure tone intensity discrimination threshold found in cats, ~5 % (Igarashi et al., 1979a). However, it is lower than the discrimination threshold of ~15 % found in the same mice when they were

trained to move from the listening to the response compartment of a chamber upon detecting an increase in the intensity of a 16 kHz tone (May et al., 2002). Although differences in stimuli, sound level, and animal age must all be taken into account, because PPI is based on a reflex and therefore less influenced by cognitive factors like motivation, attention, and learning, it is likely thresholds obtained with PPI are more reflective of sensory thresholds.

5.4.6 Maturation of PPI circuitry

In control and α9 KO mice, in both the frequency and intensity discrimination tasks, larger changes from background were required to elicit maximum levels of inhibition at P50 as compared to P14. Taken together, these data suggest that the dynamic range of prepulse inhibition increases with development between P14 and P50. Consistent with this idea, maximum levels of inhibition were slightly elevated at P50 in both control and α9 KO mice for frequency and intensity discrimination. Since the developmental change in the PPI function was independent of both genotype and type of discrimination task, it may reflect maturation of the circuitry underlying prepulse inhibition. Similarly, Parisi and Ison (1979) found that PPI levels increase between the second and third postnatal weeks, independent of the modality of the prepulse and experience with the PPI paradigm. The increase was also observed when the prepulse comprised the same acoustic stimulus as the startle, indicating that the effect was due to maturation of central inhibitory mechanisms, rather than an increase in peripheral acuity.

Both muscarinic and $GABA_B$ metabotropic receptors have been implicated in the inhibition of giant neurons in the caudal pontine reticular nucleus responsible for attenuating the ASR (Fendt et al., 2001). Because GABAergic signaling undergoes many changes during development (Lujan et al., 2005; Owens and Kriegstein, 2002), maturation of inhibitory

signaling in the PPI pathway may contribute to age-related changes in the degree of ASR inhibition elicited by prepulse stimuli of varying magnitude. PPI is also modulated by a diverse array of forebrain circuits, including the hippocampus, medial prefrontal cortex, amygdala, and nucleus accumbens (reviewed in Swerdlow et al., 2001). While these regions do not mediate PPI, maturation of such modulatory systems, as well as additional prefrontal regions involved in sensorimotor gating (Koch, 1999), could also contribute to developmental changes in the expression of PPI.

6.0 GENERAL DISCUSSION

6.1 TWO STAGES OF REFINEMENT

By comprehensively mapping the tonotopic precision of individual MNTB axons in the LSO over the first three weeks of postnatal development in a mouse strain in which functional silencing has already been characterized (Kim, 2004; Kim and Kandler, 2010), I showed that pruning and anatomical reorganization of MNTB axons does not accompany synaptic silencing before the onset of hearing. The lack of anatomical refinement before hearing indicates that frequency-specific silencing of synapses is not reflected in the distribution of the boutons of individual MNTB axons along the frequency axis of the LSO and provides strong evidence that functional silencing and anatomical pruning are two distinct phases in the tonotopic refinement of MNTB-LSO connections. The fact that synaptic silencing is not immediately followed by axonal pruning suggests that silencing and pruning may rely on different mechanisms. The restriction of both of these processes to distinct periods of development further suggests that the underlying mechanisms may only be available at specific developmental stages. In support of this hypothesis, synaptic transmission at MNTB-LSO connections undergoes fundamental changes during development. As a result, specific characteristics of transmission characterize both the pre-hearing period of synaptic silencing and post-hearing period of axonal pruning (Fig. 6-1).

	Synaptic Silencing (1st postnatal week)	Synaptic Strengthening (2nd postnatal week)	Axonal Pruning (3rd postnatal week)
Activity	Spontaneous Bursts	Spontaneous Bursts	Structured Sound-evoked
Primary Neurotransmitter	GABA	GABA/Glycine	Glycine
GABA/glycine Effect	Depolarizing	Hyperpolarizing	Hyperpolarizing
Glutamate Co-release	Yes	Reduced	Unknown

Figure 6-1. Summary of the changes that take place in the characteristics of synaptic transmission at MNTB-LSO synapses during early postnatal development.

6.1.1.1 The period of synaptic silencing

During the period of synaptic silencing, release of the inhibitory neurotransmitters GABA and glycine from MNTB terminals causes depolarization of the postsynaptic LSO neuron, rather than hyperpolarization (Kandler and Friauf, 1995; Kotak et al., 1998). Depolarization is due to a high intracellular chloride concentration in immature LSO neurons. Consequently, the chloride reversal potential is more positive than the resting potential and activation of glycine and $GABA_A$ receptors causes calcium eflux instead of influx (Ehrlich et al., 1999; Kakazu et al., 1999). Depolarizing GABA/glycinergic synapses can activate voltage-gated calcium channels and trigger action potentials in LSO neurons (Kullmann et al., 2002; Kullmann and Kandler, 2008, 2001), which is important for plasticity in many GABA- and glycinergic synapses (Kotak and Sanes, 2000; Luscher and Keller, 2004; Magnusson et al., 2008). A depolarizing effect of GABA/glycinergic synapses could thus provide developing MNTB-LSO synapses access to calcium-dependent signaling cascades that commonly underlie plasticity of excitatory synapses and are also known to be important in many forms of inhibitory synaptic plasticity as well (Gaiarsa et al., 2002).

Additional possibilities for plasticity result from the fact that immature MNTB terminals express the vesicular glutamate transporter 3 and also release glutamate in addition to GABA and glycine (Gillespie et al., 2005). Glutamate co-release at MNTB-LSO synapses can activate postsynaptic NMDA receptors and is most prevalent in the period of synaptic silencing during the first postnatal week, when depolarizing GABA/glycine responses can contribute to removal of the voltage-dependent magnesium block. Furthermore, while mature MNTB terminals are almost exclusively glycinergic, during early development they are primarily GABAergic. The transition in inhibitory neurotransmitter phenotype is gradual, but is largely complete around

hearing onset (Kotak et al., 1998; Nabekura et al., 2004). GABA specifically is involved in long-term depression of MNTB-LSO synapses (Chang et al., 2003; Kotak and Sanes, 2003), which is also less prevalent after hearing onset, so the transient GABAergic phenotype may also contribute to synaptic silencing and functional refinement.

In the spinal cord, mixed GABA/glycinergic synapses induce postsynaptic currents that are larger in amplitude and longer in duration than those that use only one of the transmitters individually (Keller et al., 2001), and blocking the GABAergic component of inhibitory postsynaptic currents (IPSCs) reduces the ability of inhibitory postsynaptic potentials to prevent brainstem motor neuron firing (Russier et al., 2002), suggesting that the synergistic action of GABA and glycine may be important for optimizing inhibition. Early GABAergic responses also tend to decay more slowly than their glycinergic counterparts (Gao et al., 2001; Jonas et al., 1998; Kotak et al., 1998; Nabekura et al., 2004; O'Brien and Berger, 1999; Russier et al., 2002), enabling fine-tuning of the time course of inhibition. The addition of longer duration GABAergic responses could also broaden the window for synaptic integration (Akerman and Cline, 2007), which could have especially important implications for refinement of the MNTB-LSO pathway, by modulating which synapses are identified for silencing or strengthening.

Thus before hearing onset, all of the necessary cellular and molecular components are available for patterned spontaneous activity to sharpen tonotopic MNTB-LSO connections. According to this hypothesis, the specific temporal structure of the activity pattern is important in recruiting the plasticity mechanisms responsible for weakening tonotopically incorrect inputs and strengthening tonotopically correct inputs. Induction of long-term potentiation (LTP) and long-term depression (LTD) in a variety of *in vitro* and *in vivo* systems has been shown to depend on the temporal order of pre- and postsynaptic activity (Caporale and Dan, 2008; Dan

and Poo, 2006). The induction of LTP and LTD also frequently depends on the activation of NMDA receptors and a rise in postsynaptic calcium levels (Malenka and Bear, 2004). In the LSO, LTD of inhibitory postsynaptic potentials and currents by low frequency stimulation also depends on postsynaptic calcium (Kotak and Sanes, 2000). Consistent with the fact that the normal spectrotemporal structure of sound-evoked activity is not required for bouton elimination and anatomical refinement, LTD declines with age post-hearing. Thus despite the fact that a specific learning rule has yet to be determined, the precise pattern of pre-hearing spontaneous activity, but not post-hearing sound-evoked activity, may be important for the refinement of developing MNTB-LSO connections because spike timing-dependent plasticity mechanisms play an important role in re-shaping the pathway specifically before hearing onset. Accordingly, the synaptic silencing and strengthening responsible for functional refinement are impaired in α9 KO mice, in which the temporal pattern of pre-hearing spontaneous activity is less structured.

6.1.1.2 The period of anatomical pruning and bouton elimination

With the abundance of mechanisms available for plasticity during the first postnatal week, it is easy to see how functional connections could be refined even before hearing onset. However, it is less clear why pruning of MNTB axons and elimination of boutons does not immediately follow. At the neuromuscular junction, it takes less than one day for a muscle fiber to become singly innervated once the strength of its inputs have diverged and differ by at least 4-fold (Colman et al., 1997). Because the strength of single MNTB inputs to LSO neurons increase 14-fold between P1 and P12, and synapse silencing is largely complete by P8, it would seem likely that a similarly large strength differential would be achieved well before the period of early auditory experience when anatomical pruning actually takes place.

If such a strength differential is important for axonal pruning at inhibitory MNTB-LSO synapses, however, it may be that by the time a sufficient differential is achieved, the plasticity mechanism necessary for the anatomical elimination of MNTB boutons is lost, possibly due to the changes in synaptic transmission described above. Alternatively, it may be that the necessary mechanism is not lost, but that anatomical elimination is dependent on a mechanism that is only available after hearing onset. The onset of sound-evoked activity might then either restore or first make the critical mechanism available, possibly through the pattern of activity generated by sound.

6.1.1.3 The functional map as a template for anatomical refinement

Delaying anatomical changes until after the onset of sensory experience might also seem advantageous, as it provides the opportunity for real-world experience to fine-tune the connections. In the midbrain auditory localization pathway of the barn owl, for example, displacement of the visual field via prism-rearing causes a shift of auditory receptive fields to match the new visual receptive fields induced by the prisms. This shift is achieved through the growth of new adaptive connections. However, the initial connections are anatomically maintained, despite the fact that they are no longer functionally relevant. The maintenance of the original pathway enables animals to behaviorally recover once the prisms are removed (Knudsen et al., 2000). In the case of the MNTB-LSO pathway, maintaining anatomical connections until after hearing onset could allow adjustments based on the characteristics of the acoustic environment to be made before the functionally-defined map is cemented anatomically.

However, impaired anatomical refinement in α9 KO mice, despite a lack of hearing abnormalities, indicates that normal auditory experience cannot override or correct the effects of reduced functional refinement before hearing. The map of functional connections set up by

synapse silencing and strengthening thus seems to serve as a template that determines the final pattern of anatomical connections as well.

6.1.1.4 Reading the template – the role of sound-evoked activity

Because activity blockade studies have not yet clearly prevented sound-evoked activity after hearing onset without also blocking the later portion of the period of spontaneous activity before hearing onset, we cannot be absolutely sure that sound-evoked activity is absolutely necessary to "read the template" and transform tonotopically precise functional connections into tonotopically precise anatomical connections. However, the delay of anatomical pruning until after hearing onset suggests that sound-evoked activity does play a role, though most likely not an instructive one. Normal bouton elimination and refinement in NR animals, regardless of the spatio-temporal synchronization of auditory input, further indicates that the specific pattern of sound-evoked activity is not the key factor. It could be that a minimum level of activity is all that is required. Alternatively, coincident activation of both excitatory and inhibitory inputs to LSO neurons through binaural synchrony could be important. This type of bilaterally-coordinated activity should still be present in NR animals. Determining whether anatomical refinement proceeds normally in animals reared with disynchronous binaural input would provide important insight as to whether this is the case.

Nevertheless, it remains unclear exactly how the functional template is manifested anatomically, and whether boutons anatomically eliminated from individual MNTB axons after hearing onset correspond to inputs that were functionally disconnected from postsynaptic partners in the LSO. In the control case, the portion of the MNTB that provides functional input to a single LSO neuron is reduced by ~45 %, from ~35 % to ~18 % of the length of the MNTB before hearing onset. After hearing onset, the spread of the boutons of individual MNTB axons

along the LSO frequency axis is also reduced by a similar amount, from ~21 % to ~14 % LSO length. But while the pattern of input silencing was frequency-specific and seemed to only eliminate connections that would contribute to narrowing the input map, the pattern of bouton elimination was not; many more boutons were eliminated from regions that did not cause a reduction in spread than boutons were eliminated from regions that did.

Although the elimination of boutons from individual MNTB axons cannot be directly equated to the disconnection of multiple MNTB axons from individual LSO neurons, it seems likely that the addition of boutons to individual MNTB axons correlates with the strengthening of maintained, tonotopically correct single fiber inputs to LSO neurons, especially since a major component of strengthening is the addition of release sites to individual MNTB axons (Kim and Kandler, 2010). And since bouton addition was selective for the center of termination regions, it seems likely that the central connections were the most tonotopically correct. Accordingly, it is unlikely that boutons that were eliminated from the center of termination regions after hearing onset could correspond only to tonotopically incorrect synapses, those that would have been functionally silenced. Furthermore, in α9 KO mice, functional connections were narrowed and inputs eliminated before hearing onset, although to a lesser extent than in controls, yet no anatomical sharpening occurred after hearing, suggesting that not all of the silenced inputs were anatomically eliminated. Thus it may be that the tonotopic precision of anatomical connections does not follow directly from the functional template through the sole elimination of silent inputs. Instead, anatomical pruning may be a process that acts on the template of functional connectivity, but is not the direct manifestation of it. Accordingly, if the strength of connections influences pruning, the degree of strengthening that takes place before hearing may be just as

important as the pattern of synaptic silencing in determining the tonotopic precision of MNTB axons in the LSO after hearing.

6.2 COMPARISON WITH REFINEMENT IN OTHER SYSTEMS

In some ways the tonotopic refinement of developing MNTB-LSO connections is similar to the ways in which circuits are refined in other systems. MNTB inputs that were maintained were strengthened, for example, similar to the increase in strength of "winning" motor neurons at the neuromuscular junction (Colman and Lichtman, 1993) and climbing fibers in the cerebellum (Kano and Hashimoto, 2009). Strengthening was due to a small increase in quantal size and larger increase in the number of release sites (Kim and Kandler, 2010), similar to changes at retinogeniculate synapses during the period of input elimination (Chen and Regehr, 2000). Although it is unknown whether MNTB-LSO synapses are weakened before being silenced, it seems likely given that long-term depression has been shown to occur at MNTB-LSO synapses during the period of silencing (Kotak and Sanes, 2000) and that long-term depression has been implicated as a step in silencing unused inputs in somatosensory cortex (Allen et al., 2003; Celikel et al., 2004).

In contrast, the delay between pre-hearing synaptic silencing and post-hearing axonal pruning is distinct from similar processes in excitatory systems, where synapse weakening is generally rapidly followed by axon withdrawal and structural elimination (Antonini and Stryker, 1993; Colman et al., 1997; Lu and Trussell, 2007). At the neuromuscular junction, changes in the structure and function of the synapses of a motor neuron occur in parallel. Furthermore, the terminals of competing axons seem to be functional up until the axons withdraw, suggesting that

terminal elimination leads to a loss of function, rather than the loss of function preceding axon withdrawal and the loss of terminals (Balice-Gordon and Lichtman, 1993; Lichtman et al., 1985; Wyatt and Balice-Gordon, 2003). This is the opposite of what happens at MNTB-LSO connections, where inputs are first silenced, but are then maintained anatomically for an extended period of time before elimination.

The fact that synchronizing sound-evoked activity had no effect on the number of boutons eliminated is also very different from the effects of synchronous activity in other systems. In the developing visual system, for example, synchronous activity allows more synapses to be maintained, as it is thought to level the playing field among competing inputs (LeVay et al., 1980). The same is true at the neuromuscular junction, as artificially synchronizing activity among motor neurons prolongs the period of multiple innervation (Busetto et al., 2000). In contrast, normal elimination in NR animals suggests that after hearing onset in the MNTB-LSO system, axons are no longer actively competing for postsynaptic partners based on spectrotemporal variations in their activity pattern, although the special case of double-banded axons may contradict this conclusion.

While it is clear that refinement of inhibitory MNTB-LSO connections differs in some fundamental ways from the refinement of excitatory connections, it is largely unknown whether refinement of other inhibitory networks proceeds through a similar sequence of events. Even in the MSO, where MNTB axons are similarly refined (Werthat et al., 2008), it is unknown whether functional changes precede the anatomical rearrangment of synapses. Additional studies are needed to determine whether the unifying characteristics of inhibitory transmission, such as its depolarizing effect during early development and the importance of calcium for plasticity, will

translate into similarities in the refinement of inhibitory networks across diverse regions of the brain.

6.3 A NEW ROLE FOR THE MOC EFFERENT SYSTEM DURING DEVELOPMENT

α9 KO mice have a less temporally structured pattern of pre-hearing spontaneous activity due the loss of cholinergic transmission between medial olivocochlear (MOC) fibers and cochlear hair cells (HCs). As a result, pre-hearing refinement of functional MNTB-LSO connections through synapse silencing and strengthening is impaired. Here I showed that refinement of anatomical MNTB-LSO connections through the elimination of boutons from individual MNTB axons after hearing onset is also impaired in α9 KO mice. Furthermore, reduced tonotopic precision was accompanied by impaired discrimination of small, but not large, changes in the frequency of sound.

Historically, the transient stop by MOC efferents at IHCs before hearing was thought to be part of a developmental "waiting period" (Simmons et al., 1996). In this scheme IHCs primarily served as an intermediate target for MOC fibers as they waited for their final target, OHCs, to mature, a process similar to the waiting period of thalamocortical axons at the subplate before reaching their target neurons in cortical layer 4 (Ghosh et al., 1990). This type of developmental pattern was thought to stem partly from the shared embryonic origin of MOC neurons with facial branchial motor neurons (Bruce et al., 2000). As a result of this common ancestry, they were proposed to share a similar developmental pattern involving the precocious synthesis of acetylcholine prior to target innervation and the subsequent reorganization of

synapses, which in MOC fibers progressed from the innervation of IHCs only, to dual IHC and OHC innervation, to the final innervation pattern of OHCs only (Simmons, 2002).

When subsequent studies revealed functional cholinergic receptors on immature IHCs and an inhibitory effect of acetylcholine on spontaneous calcium spikes in IHCs (Glowatzki and Fuchs, 2000; Katz et al., 2004), it was proposed that inhibition of spontaneous IHC firing by MOC-mediated acetylcholine release could impose rhythmicity onto activity patterns even before the auditory system could respond to sound, providing a mechanism for the developmental refinement of central connections. Testing this hypothesis, however, required well-defined manipulations of the activity pattern *in vivo*, manipulations that were unachievable in the currently available deaf mouse strains and methods of activity blockade. α9 KO mice provided the first experimental evidence that cholinergic transmission in the cochlea does indeed play a critical role in the tonotopic refinement of an inhibitory pathway in the brainstem, most likely through its role in shaping spontaneous activity patterns before hearing.

A role of spontaneous activity in the development of central connections is not new. It has been well-characterized in the developing visual system (Huberman, 2007; Huberman et al., 2008; Wong, 1999), neuromuscular junction (Wyatt and Balice-Gordon, 2003), and in the cerebellum (Kano and Hashimoto, 2009). Its effects can even be cross-modal; spontaneous muscle twitches in neonatal animals produce spatially-confined activity bursts in primary somatosensory cortex, a process that is believed to contribute to the development of maps of body representations and sensorimotor coordination in the adult (Khazipov et al., 2004). The process is so ubiquitous that activity-dependent refinement is now considered a general principle for the developmental organization of neural circuits (Zhang and Poo, 2001). However, the unique organization of the auditory system, in which its sensory structure and source of

spontaneous activity, the cochlea, receives direct efferent innervation, provides a novel mechanism whereby central neurons can participate in shaping their own organization by modulating spontaneous activity patterns at the periphery.

In the spinal cord, for example, rhythmic spontaneous activity patterns originate from interneurons and contribute to pathfinding decisions in motor neuron axons (Hanson and Landmesser, 2006; Hanson et al., 2008), but the timing of activity is not influenced by the recurrent collaterals of the motor neurons (O'Donovan, 1999). Similarly, in the visual system, spontaneous retinal waves important for the development and refinement of central visual circuits are generated by cells and circuits intrinsic to the retina (Huberman, 2007; Huberman et al., 2008; Wong, 1999). And while the activity pattern can be modulated by descending and reciprocal connections, the modulation occurs within central circuits, not at the retina itself. Only in the auditory system does efferent feedback act to modify spontaneous activity patterns at their source.

Still, descending modulation of activity patterns can add useful information not present in the original pattern. In the lateral geniculate nucleus, the spontaneous activity pattern inherited from the retina is re-shaped by reciprocal connections between the thalamus and cortex, producing binocular correlations not present based on retinal drive alone (Weliky, 2000). The MOC efferent system may perform a similar function in the auditory system by creating binaural correlations between the activity patterns generated independently in each cochlea. While the majority of MOC neurons provide feedback to the cochlea from which they receive afferent input, a significant portion (about 1/3) project to the opposite cochlea (Liberman and Brown, 1986), forming an intercochlear effector pathway. MOC neurons also exhibit sharp frequency tuning (Liberman, 1988) and have limited terminations along the length of the cochlea that

correspond to their characteristic frequency (Liberman and Brown, 1986). Thus in addition to imposing additional structure on the timing of spontaneous bursts by IHCs, cholinergic feedback from the MOC fibers may serve an additional function in synchronizing the spontaneous activity of tonotopically matched regions in both cochleas.

Binaural correlations in spontaneous activity could contribute to aligning the tonotopic maps of CN- and MNTB-LSO connections, which is already present at hearing onset (Sanes and Rubel, 1988). Furthermore, if bilateral interaction between CN and MNTB inputs contributes to frequency-specific input silencing before hearing, than impaired functional refinement in α9 KO mice may also reflect the loss of the binaural synchronization component of MOC function, in addition to the loss of its effect on fine temporal structure. Testing whether the excitatory and inhibitory tuning curves of LSO neurons are less well matched in α9 KO mice would provide insight into whether or not this is the case.

Finally, the fact that α9 KO mice exhibit impairments in frequency discrimination indicates that cholinergic transmission in the cochlea plays a role in auditory perception, most likely through its role in the development of precise tonotopy. In humans, good phonological processing and literacy seem to depend on good frequency discrimination skills (Halliday and Bishop, 2005), and patients with specific reading disability (dyslexia) often show impairments in frequency discrimination (Ahissar et al., 2000). Interestingly, patients with learning disabilities (Garinis et al., 2008) and auditory processing disorders (Muchnik et al., 2004) also seem to have abnormal MOC function, showing unusual or weak suppression of transient evoked otoacoustic emissions by the presentation of contralateral noise. In the past, the link between MOC function and auditory processing and learning disorders was based on its contribution to the detection of signals in noise (Micheyl and Collet, 1996). The frequency discrimination deficits observed in

α9 KO mice, however, suggest that the effect of the MOC system in refining central tonotopy during early development might also contribute to deficits in auditory perception.

APPENDIX A

CATALOG OF CELLS AND RECONSTRUCTED AXONS USED FOR QUANTITATIVE ANALYSIS

This appendix contains the reconstructed axons of all MNTB neurons in the LSO that were used for quantitative analysis in Chapters 2, 3, and 4. Axons are shown in black, while nuclei are outlined in grey with the more medial MNTB to the left and the LSO to the right. All reconstructions follow the scaling as shown.

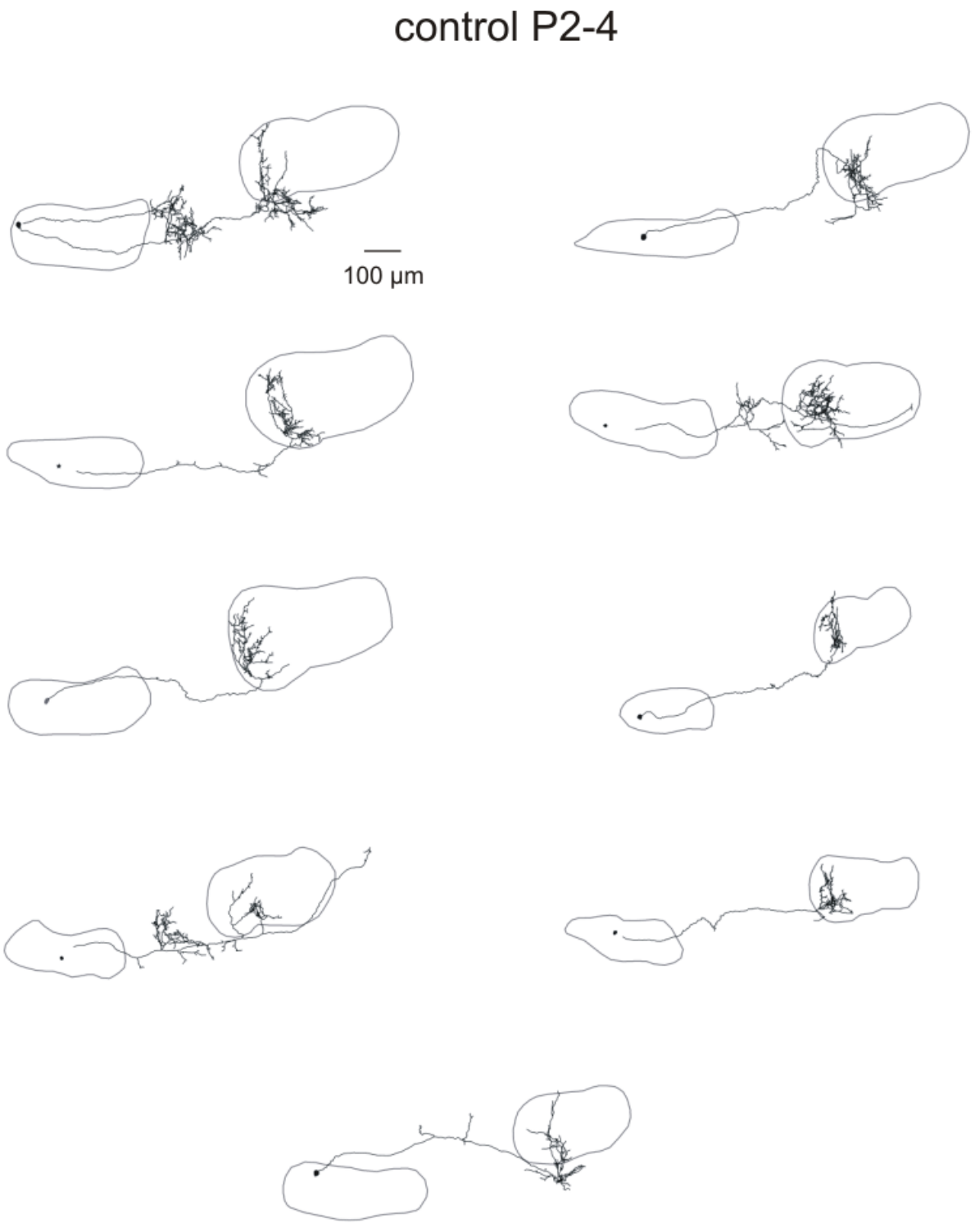

Figure A1. Reconstructed control axons at P2-4.

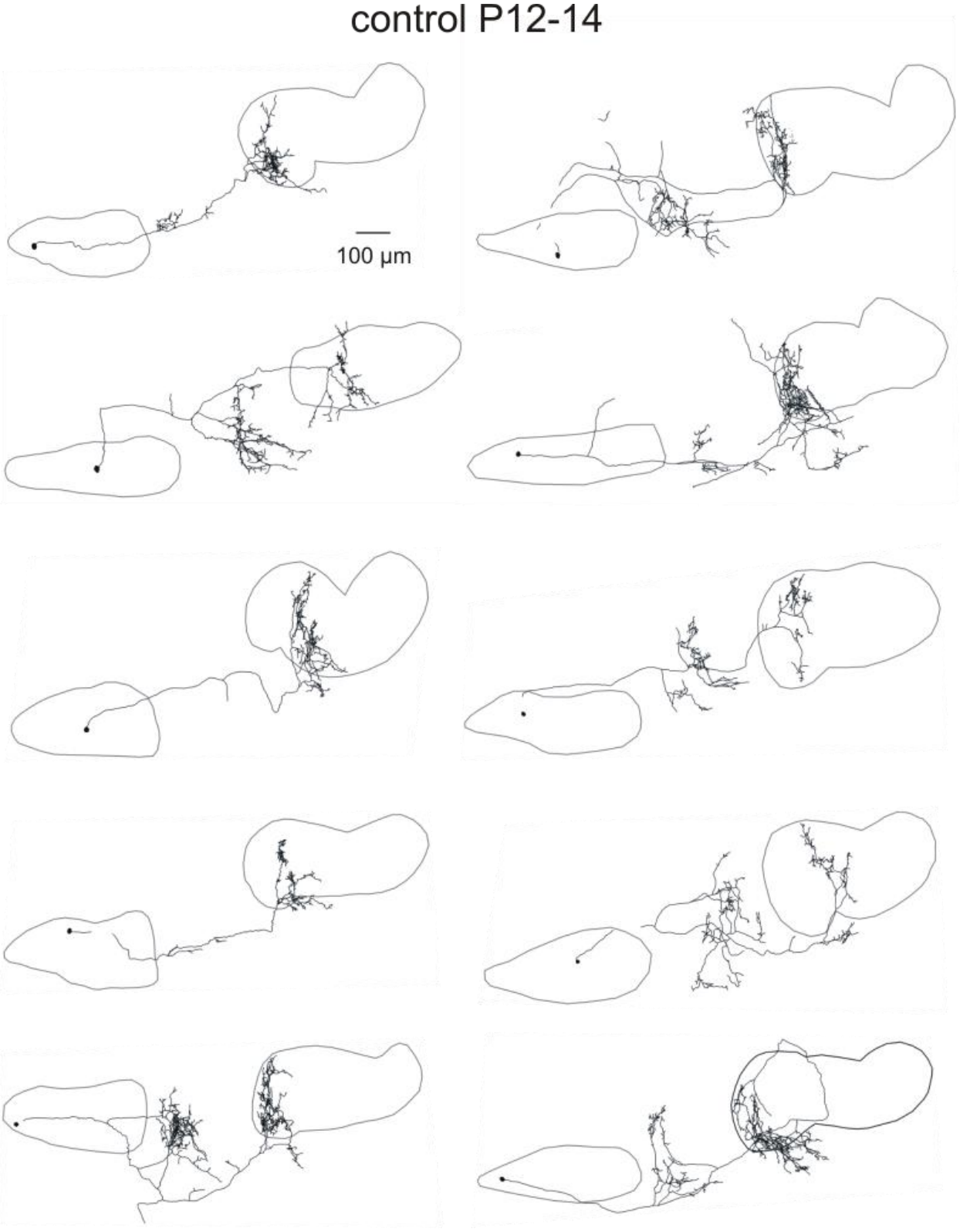

Figure A2. Reconstructed control axons at P12-14.

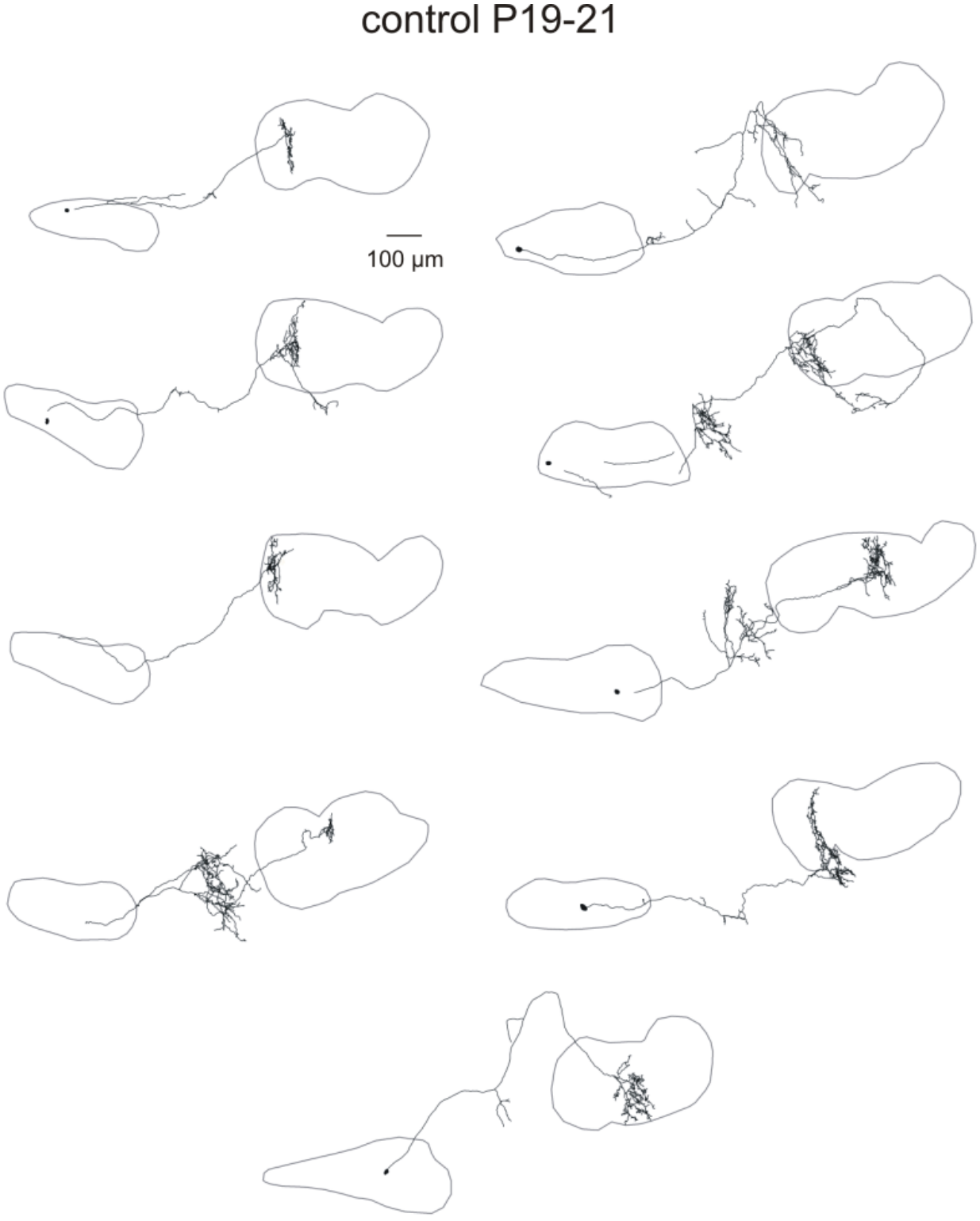

Figure A3. Reconstructed control axons at P19-21.

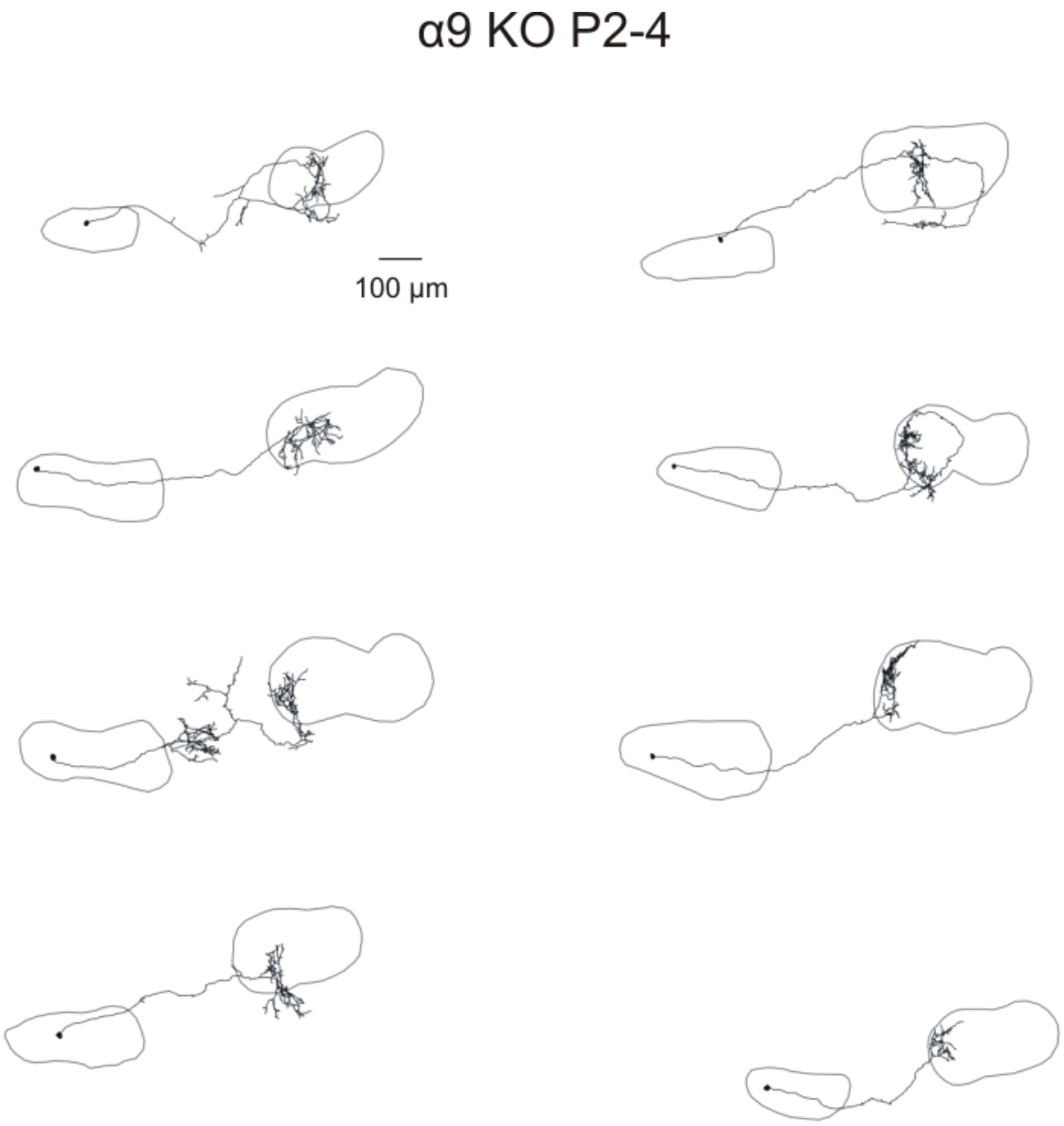

Figure A4. Reconstructed α9 KO axons at P2-4.

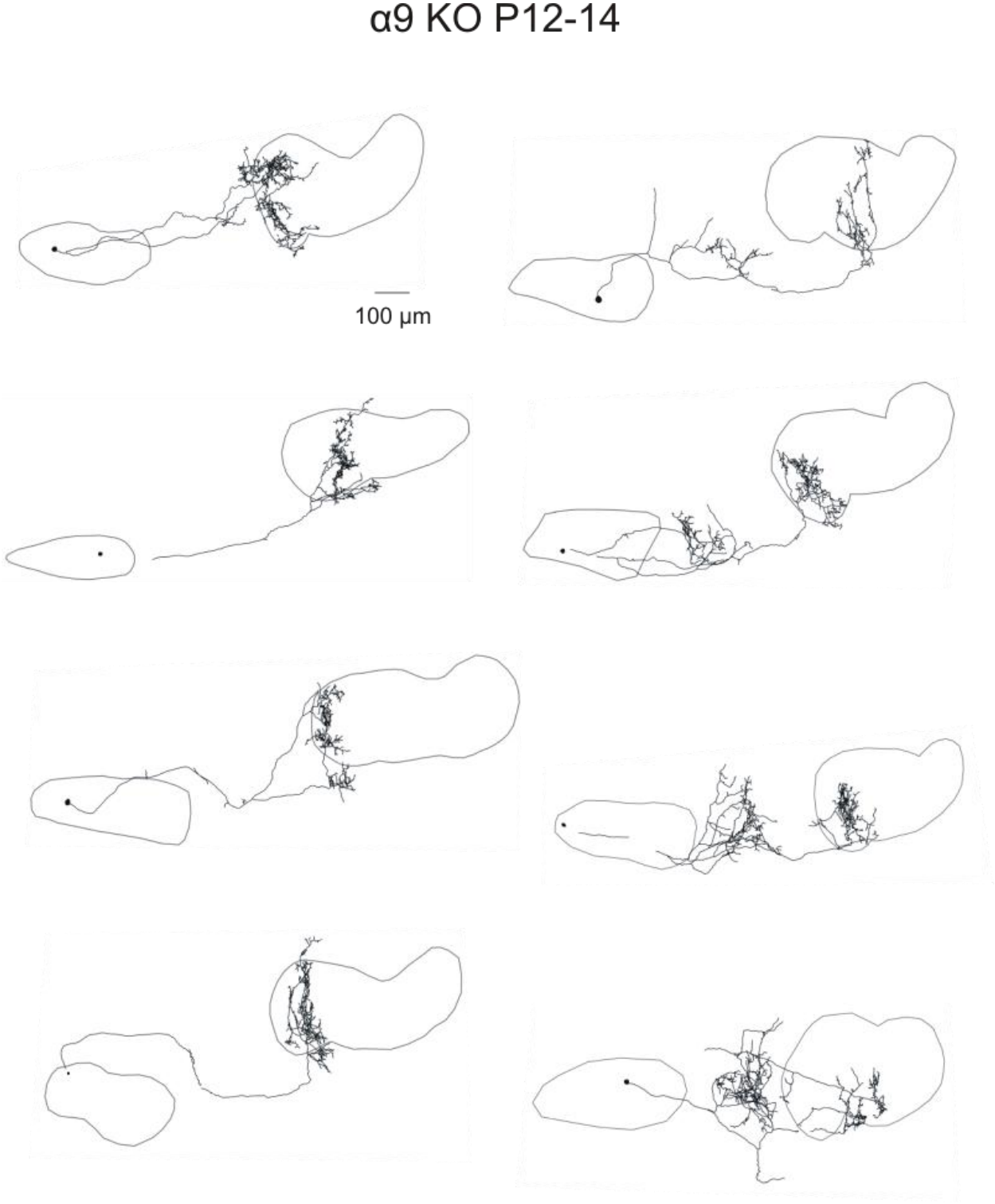

Figure A5. Reconstructed α9 KO axons at P12-14.

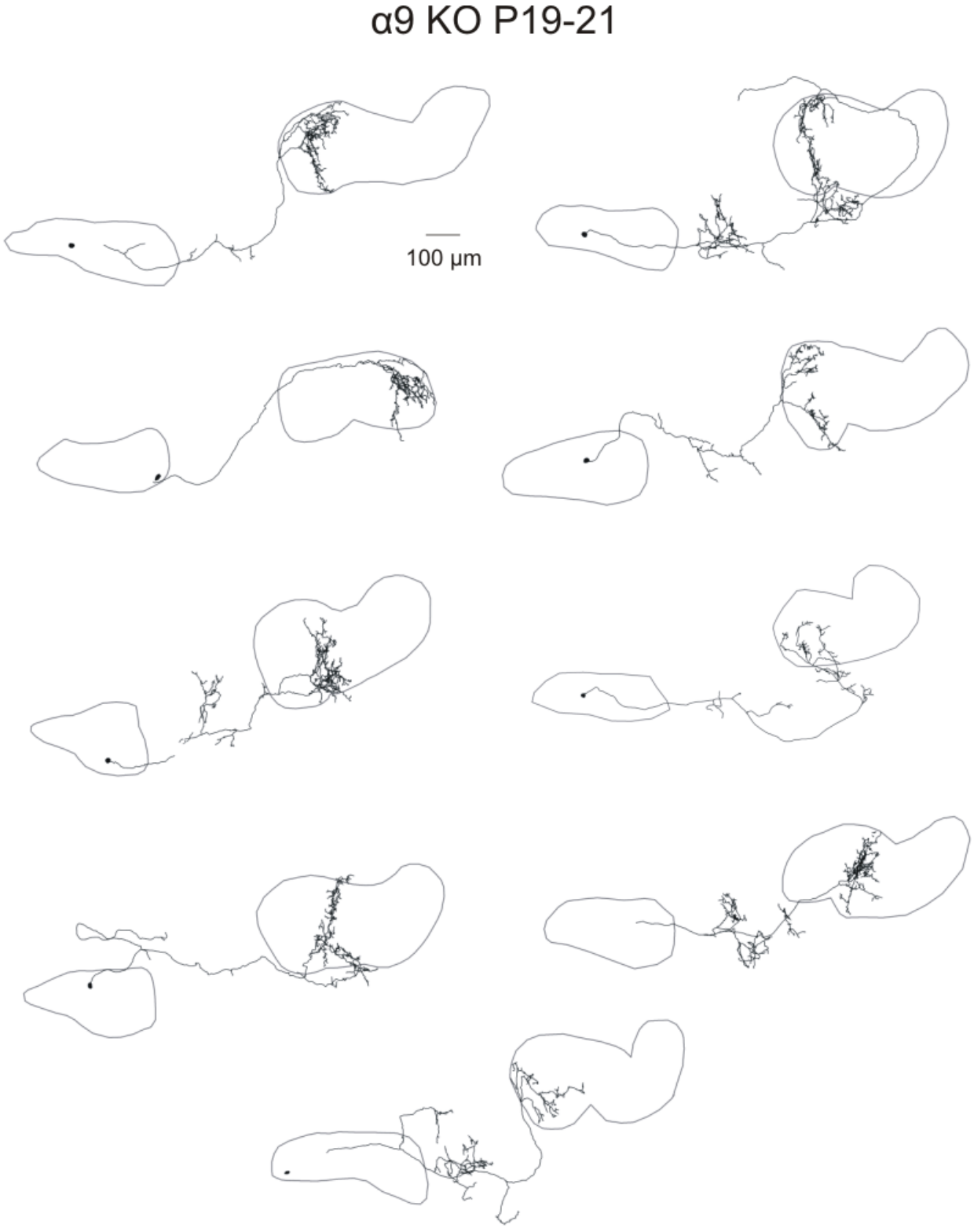

Figure A6. Reconstructed α9 KO axons at P19-21.

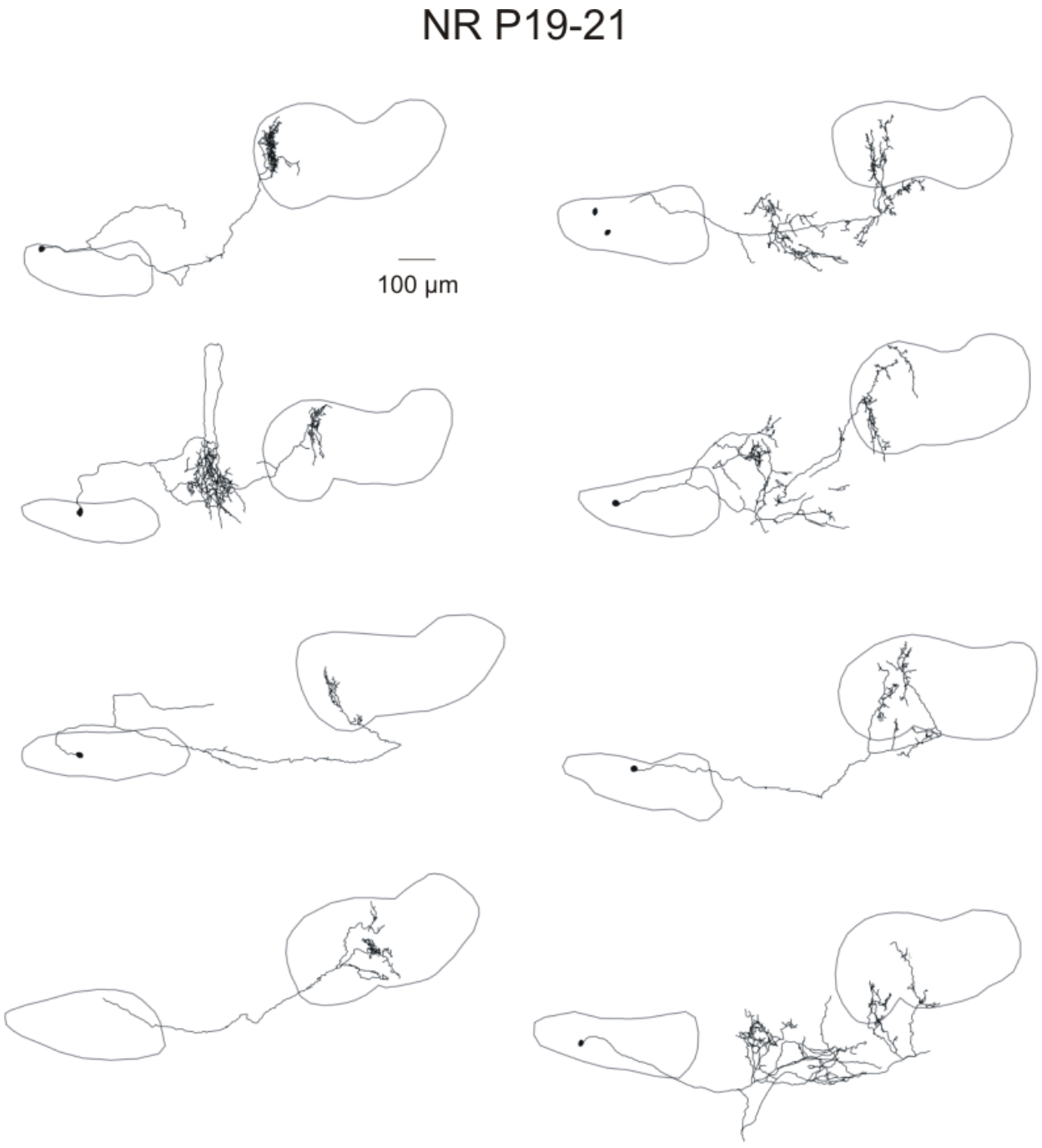

Figure A7. Reconstructed axons of noise-reared animals at P19-21, from litters one and two.

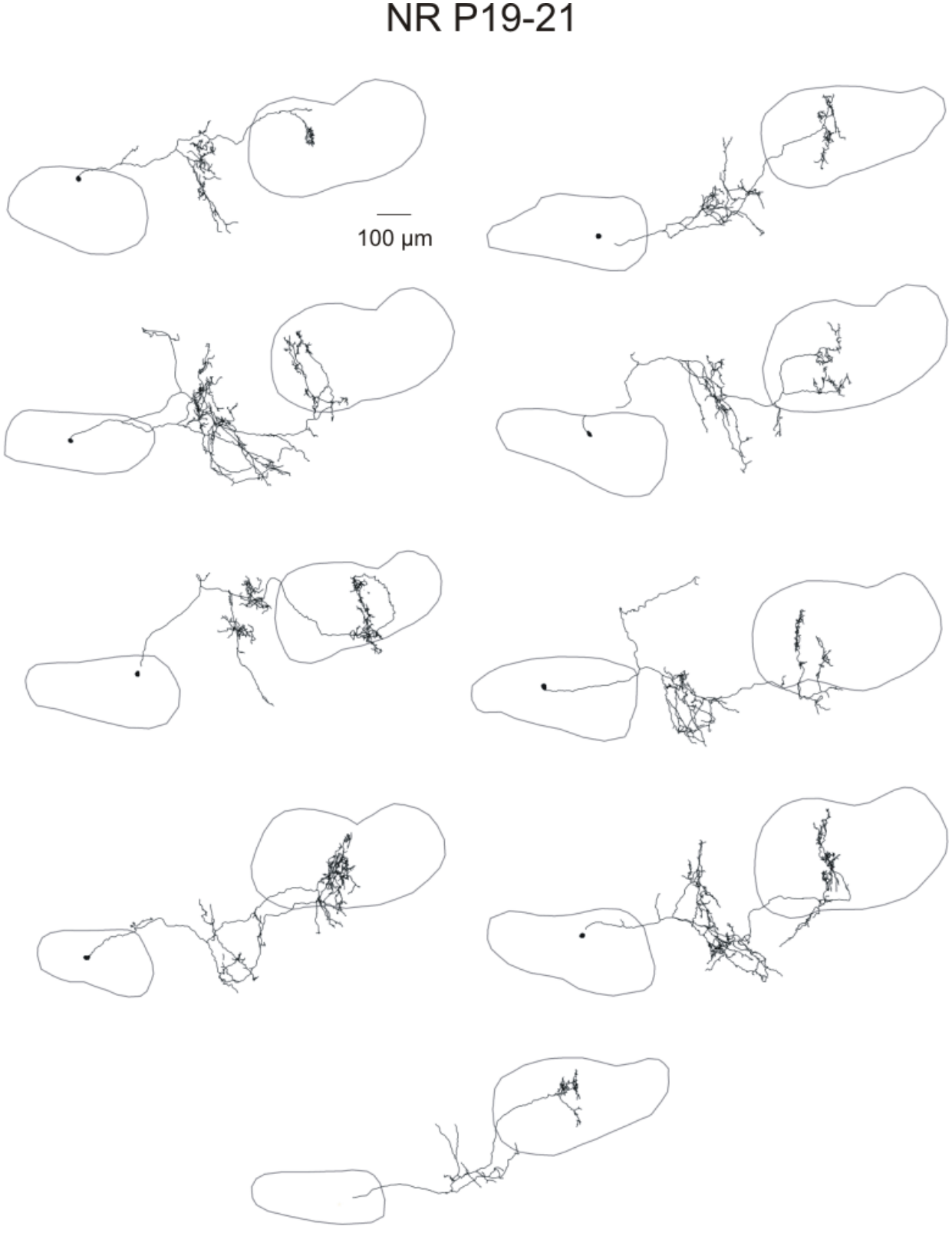

Figure A8. Reconstructed axons from noise-reared animals at P19-21, from litters three and four.

	number of cells	number of animals	number of litters
Control P2-4	9	6	6
Control P12-14	10	8	7
Control P19-21	9	8	7
α9 KO P2-4	9	8	5
α9 KO P12-14	8	6	4
α9 KO P19-21	9	8	7
NR P19-21	17	13	4

Figure A9. Number of cells, animals, and litters in each experimental group.

APPENDIX B

AN ACOUSTIC STARTLE-BASED METHOD OF ASSESSING FREQUENCY DISCRIMINATION IN MICE

A version of Appendix B is currently under revision for publication as a Short Communication by A. Clause, T. Nguyen, and K. Kandler in the Journal of Neuroscience Methods. T. Nguyen helped to design the software and hardware systems, while I contributed to study design, collected and analyzed the data, and wrote the manuscript.

B.1 ABSTRACT

The acoustic startle response (ASR) is a reflexive contraction of skeletal muscles in response to a loud, abrupt acoustic stimulus. ASR magnitude is reduced if the startle stimulus is preceded by a weaker acoustic or non-acoustic stimulus, a phenomenon known as prepulse inhibition (PPI). PPI has been used to test various aspects of sensory discrimination in both animals and humans. Here we show that PPI of the ASR is a reliable method of assessing frequency discrimination. We describe the apparatus and its performance testing frequency discrimination in young CD1 mice, whose ability matches that of humans. Compared to classical conditioning paradigms, PPI

of the ASR is less time consuming, produces robust results, and can be used without training even in young animals. This approach can be used to investigate the neuronal mechanisms underlying frequency discrimination, its maturation during development, and its relationship to tonotopic organization.

B.2 INTRODUCTION

The ability to discriminate between frequencies is a key function of the auditory system. Vocal communication in particular depends on the ability to detect and encode fast changes in the spectral characteristics of sound. In humans, frequency discrimination skills have been linked to good phonological processing and literacy (Halliday and Bishop, 2005), while patients with specific reading disability (dyslexia) often show impairments in frequency discrimination (Ahissar et al., 2000). People with sensorineural hearing loss also show difficulty discriminating between pure tones (Gengel, 1973; Halliday and Bishop, 2005; Nelson and Freyman, 1986), which may contribute to accompanying problems with speech perception and language development.

Due to the ease of genetic manipulation, mice have become a preferred animal model for understanding auditory processing disorders. Many hearing abilities and auditory functions are also well understood in the mouse (Dooling and Hulse, 1989; Willott, 1983, 2001). As a result, establishing a reliable behavioral test for a particular auditory function in mice offers the possibility to link a specific neuronal substrate to that function. Furthermore, it provides the opportunity to investigate how defined changes in auditory circuitry influence a particular auditory function, or how they might ameliorate identified hearing deficits.

Frequency discrimination is easily assessed in humans, even in young children and patient groups like those with dyslexia, cochlear implants, and hearing loss. However, current methods of assessing frequency discrimination in rodents depend on intricate and time-consuming conditioning paradigms (Kurt and Ehret, 2010; Ono et al., 2006) that are also influenced by confounding issues related to learning and motivation. These conditioning paradigms cannot be utilized in very young animals due to the training required, and may be difficult to use in animals with rapidly changing auditory thresholds, such as models of progressive hearing loss.

To circumvent these issues, we developed a method of assessing frequency discrimination in mice based on prepulse inhibition of the acoustic startle response (ASR). The acoustic startle is a reflexive motor response to an unexpected loud auditory stimulus that manifests behaviorally as a swift contraction of skeletal muscles (Hoffman and Ison, 1980). In humans, the ASR is usually quantified via eyeblink measures (Ison and Pinckney, 1983), while in rodents it is measured by placing the animal on a platform that transmits the downward force produced by the reflex. In rats, the ASR is typically elicited by stimuli >80 decibels (dB) above auditory thresholds (Pilz et al., 1987).

The ASR is attenuated when a weak pre-stimulus, or prepulse, is presented just prior to the startle-eliciting stimulus, a phenomenon known as prepulse inhibition (PPI; Ison et al., 1973). Because inhibition depends solely on the ability to detect and process the prepulse, PPI provides a useful means of assessing acoustic detection and discrimination. Since it is reflexive, PPI also largely eliminates confounds due to motivation and attention. Finally, as no training is required, PPI can also be used on young animals as soon as they can hear (Parisi and Ison, 1979), providing a useful tool for developmental studies.

In the past, PPI paradigms have been successfully used to assess several aspects of complex auditory processing in rodents, including gap detection (Turner et al., 2006), speech sounds (Floody et al., 2010), and tone saliency (Carlson and Willott, 1996). Here we describe and characterize an easy, highly reliable method of assessing frequency discrimination in mice, using a change in the frequency of a background tone as the prepulse stimulus. This approach will be useful not only for understanding this particular aspect of auditory perception, but also for understanding its neural mechanisms.

B.3 MATERIALS AND METHODS

B.3.1 Animals

Experiments utilized fourteen CD1 female mice (Charles River, Wilmington, MA), ten for testing frequency discrimination and four for auditory brainstem responses. Mice were received at four weeks of age and allowed to acclimate to the animal facility for ~one week before being tested at five weeks of age. Mice were maintained on a 12 hour light/dark cycle and provided food and water *ad libitum*. All experimental procedures were in accordance with NIH guidelines and approved by the Institutional Animal Care and Use Committee at the University of Pittsburgh.

B.3.2 Apparatus and hardware

The production of precise acoustic stimuli is essential for testing auditory function and behavior. However, we found that commercial acoustic startle equipment introduces unexpected sounds and/or silent gaps. Such acoustic artifacts usually arise when the software transitions between stimuli and reinitializes the sound card. To avoid such artifacts, we "compose" and save the complete sequence of acoustic stimuli in a single audio file. When played back during an experiment, the sound card is initialized only once, at the beginning of each testing session, thereby eliminating sound card initialization-induced acoustic transients during actual testing. The audio file is created using software written in the LabView® programming language[1] (National Instruments, TX) and saved as a waveform audio file (WAV).

A schematic of the experimental setup is illustrated in Figure B1. Channel L of the sound card (LynxTwo-A, Lynx Studio Technology, CA) is connected to an audio amplifier (AMP110, AudioSource, OR) to drive the loudspeaker. Channel R is connected to the analog-to-digital converter to trigger data acquisition (NI USB-6211, National Instruments, TX). The loudspeaker is a planar isodynamic tweeter (RT2H-A, HiVi, CA) that has high-power output (60 W maximum), relatively flat frequency response (1.7 - 25 kHz), and uniformly distributed sound energy. To minimize changes in sound intensity at the animal's ears due to changes in its position, a custom-made housing was constructed using fine plastic mesh and Lego® parts to constrain animal motion. The housing rests upon a load-cell platform (E45-11, Coulbourn Instruments, PA) whose output is filtered and amplified (LP122, Grass Technologies, RI), and then digitized before being sent to the computer for storage and analysis. The speaker is placed

[1] Source-code available upon request.

in front of the animal to minimize standing-wave resonances. The speaker, housing, and platform are placed inside an anechoic chamber (ENV-022SD, Med Associates, VT) along with a webcam and infrared light used for animal monitoring.

All acoustic stimuli were calibrated with a ¼" diameter microphone (4939, Brüel & Kjær, Denmark) placed at the level of the animals' ear within the housing. Microphone signals were sent to a signal conditioning amplifier (Nexus 2690-A-OS1, Brüel & Kjær, Denmark) and analyzed using commercial software (SoundCheck, Listen, MA, USA). Figure B1 shows the frequency spectra of ambient noise within the chamber (B), the 16 kHz pure tone used as the background during frequency discrimination testing (C), and the high-intensity white-noise stimulus used to elicit the ASR (D).

B.3.3 Testing frequency discrimination

At the start of each session, the mouse was placed in the housing and allowed to acclimate to a constant background tone (f_1: 16 kHz, 70 dB SPL) for five minutes. The acclimation period was followed by "prepulse" and "startle only" trials. In prepulse trials (Fig. B1 E), the prepulse stimulus comprised a frequency change consisting of a 1 ms linear ramp from the background tone, f_1, to the prepulse tone, f_2, also at 70 dB SPL. The frequency change took place in variable steps of size Δf, such that $f_2 = f_1 - \Delta f$. WAV file values during the frequency ramp show a smooth transition from f_1 to f_2 (Fig. B1 F). f_2 was maintained during the 80 ms inter-stimulus interval (ISI), then followed by the startle stimulus, a 40 ms white noise burst at 120 dB SPL. Following the startle stimulus, f_1 was presented again until the prepulse of the next trial. In startle only trials, the prepulse consisted of a 1 ms ramp from f_1 to f_1, and thus maintained the ramp

command while not actually introducing a frequency change. All trials were separated randomly by an inter-trial interval (ITI) ranging from 8-25 seconds.

Trials were divided into three blocks. The first block comprised a series of startle only trials to allow for short-term habituation to the startle stimulus. The second block contained prepulse trials randomly interleaved with an equal number of startle only trials. Prepulse trials were made up of seven classes, where f_2 = 15.92, 15.68, 15.47, 15.2, 14.4, 13.34, and 12.0 kHz, corresponding to frequency changes of 0.5, 2.0, 3.3, 5.0, 10, 16.6, and 25 %, respectively. Negative frequency changes were used because mice show greater inhibition to downward frequency sweeps than to upward sweeps (Allen et al., 2008). The last block consisted of a final series of startle only trials to test for habituation over the course of the session.

The vertical force exerted by the animal on the platform was measured during two 500 ms recording periods within each trial (Fig. B1 E). The first recording period occurred immediately before the prepulse and provided a gauge of the animal's baseline activity (Fig. B2 A-D "Baseline"). The second recording period began at startle stimulus onset and measured the ASR (Fig. B2 A-D "ASR").

B.3.4 Data analysis

The ASR for each trial was defined as the maximum force exerted during the startle recording period minus the background force, defined as the root-mean-square of the force exerted during that trial's background recording period (Fig. B2 A-D).

Using the real-time webcam, trials in which the animal showed spontaneous movement or had its feet off the floor of the housing were excluded from analysis. Trials in which the

background force exceeded two standard deviations of the session's mean background force were also excluded.

For each animal, ASRs were averaged across startle only trials and each class of prepulse trials. The mean percent inhibition was then calculated for each class of prepulse trial by subtracting the mean prepulse response amplitude from the mean startle only response amplitude and normalizing to the mean startle only response amplitude. One-way ANOVA (Sigmastat, Systat Software, Chicago, IL) was used to determine if the magnitude of the prepulse frequency change had a significant effect on ASR amplitude. Prepulse frequency changes that caused significant inhibition of the startle response were identified using a one-sample t-test against zero. Discrimination threshold was defined as the smallest frequency change to significantly inhibit the ASR. An alpha level of 0.05 was used to determine statistical significance for all tests.

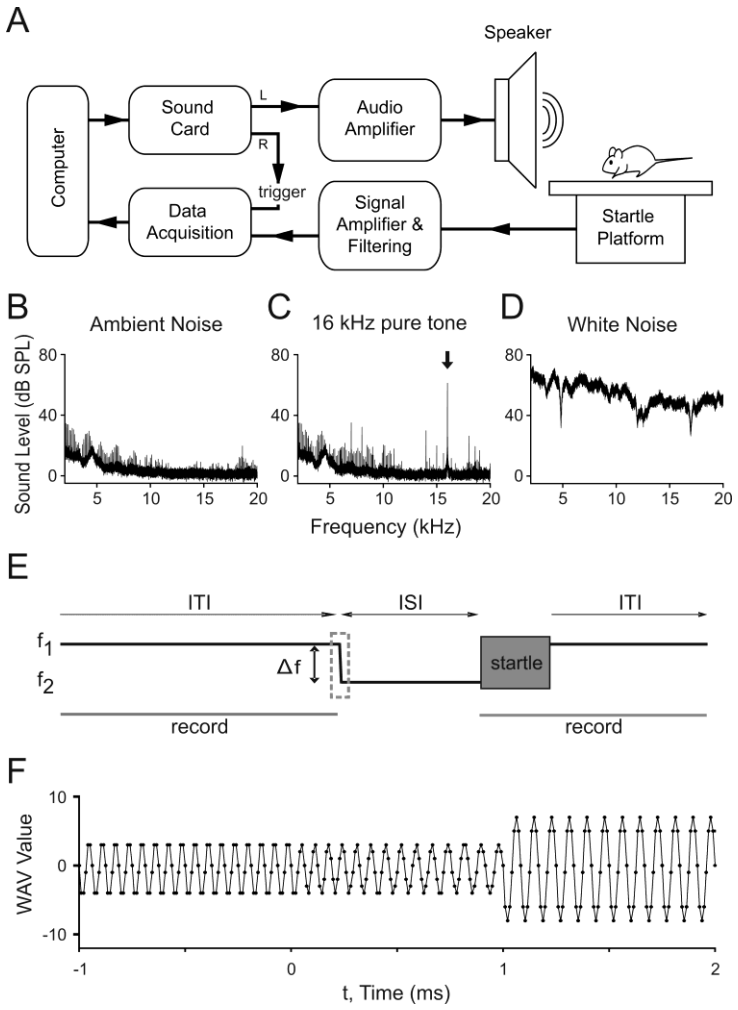

Figure B1. Acoustic startle apparatus for frequency discrimination.

(A) Schematic of apparatus. (B-D) Frequency spectra measured at the animal's ear inside the housing within the anechoic chamber. (B) Ambient noise, (C) 16 kHz tone at 70 dB SPL used as the background frequency, and (D) white noise at 100 dB SPL. To protect the speaker during the 10 s sound delivery required for acquisition of the frequency spectra, white noise was delivered at 100 dB SPL, rather than the 120 dB SPL used to elicit the ASR. Arrow in (C) indicates the 70 dB SPL peak at 16 kHz. (E) Trial schematic. Dashed rectangle denotes portion of trial shown in (F). ITI, inter-trial interval; ISI, inter-stimulus interval; f_1, background frequency; f_2, prepulse frequency; Δf, frequency change. (F) Portion of example WAV showing the transition between f_1 (16 kHz) and f_2 (here, 12 kHz) that begins at t = 0. The increase in WAV value between f_1 and f_2 is due to the increase in power necessary to maintain a constant sound intensity for both frequencies. Each point in the waveform represents the value written to the WAV file for delivery to the soundcard.

B.4 RESULTS

CD1 mice showed a reliable ASR, with an average response of 0.66 ± 0.08 when the startle stimulus was presented alone, without a preceding prepulse (Fig. B2 A, E). Preceding the startle stimulus with a shift in frequency from the background tone caused reliable inhibition of the ASR (Fig. B2), with the magnitude of the change having a significant effect on ASR amplitude (One-way ANOVA; $p < 0.001$). As the difference between the background and prepulse frequencies increased, so did the amount of inhibition elicited, attaining a maximum of 65 ± 3 % inhibition for a frequency shift of 10 %. The degree of inhibition reached a plateau around 65 %, indicating a limit on the amount of inhibition possible. The relationship between frequency change magnitude and extent of PPI is consistent with previous findings that the degree of inhibition is related to the ease with which the prepulse is detected (Ison and Hoffman, 1983; Leitner et al., 1993).

The smallest frequency change, 0.5 %, did not significantly inhibit the ASR ($p > 0.05$, one-sample t-test against zero), suggesting this change is below discrimination threshold, at least to the extent required to inhibit the ASR. The smallest frequency change to significantly inhibit the ASR was a shift to 15.68 kHz, or a 2 % decrease in frequency. By our definition, this is the threshold for frequency discrimination in 5 week-old CD1 mice (Fig. B2 F).

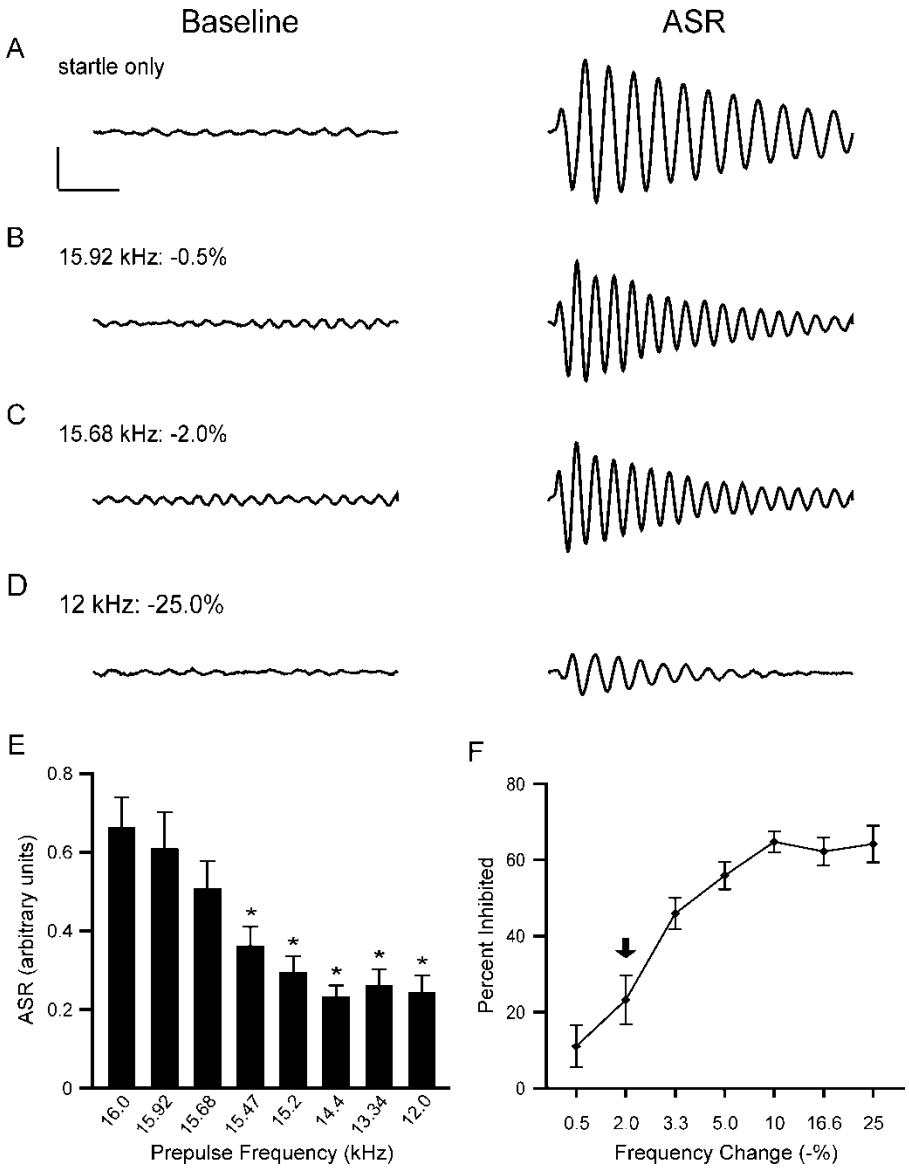

Figure B2. Inhibition of the ASR by a preceding frequency change.

Traces represent the force measured on the platform during the first recording period, "baseline," and second recording period, "ASR". Examples of (A) startle only and (B-D) prepulse trials. For each trial, the maximum force recorded during the second recording period, positive or negative, was reported as the ASR. Scale bars, 0.4 arbitrary units of force, 100 ms. (E) Mean ASR for each trial type. Asterisks indicate that ASR magnitude is significantly different from that of the startle only ASR ($p < 0.05$, corrected for multiple comparisons). (F) Inhibition of the ASR by a prepulse frequency change of various magnitudes. Arrow indicates discrimination threshold ($p < 0.05$, one sample t-test against zero). Data represent mean ± s.e.m.; n = 10 animals.

6.4 DISCUSSION

To use PPI to assess frequency discrimination, the frequency change must be the only change in the acoustic environment preceding the startle stimulus. Any additional cues (e.g. acoustic transients or intensity change) could also function as a prepulse, making it impossible to attribute attenuation of the ASR solely to the frequency change.

We avoided acoustic transients by pre-composing our stimuli and using a ramp that was long enough to allow a smooth transition between frequencies (Fig. B2 F), but still steep enough to produce robust PPI (Fig. B2). ASR amplitude was also the same whether or not startle only trials included a 16 to 16 kHz ramp command, indicating that transition-induced acoustic transients did not contribute to the observed PPI. To ensure that sound intensity remained constant, even within the startle chamber's enclosed environment, we prevented intensity changes resulting from standing-wave resonances through positioning of the loudspeaker and by constraining the animals' position. We also compensated for slight differences in loudspeaker sensitivity at different frequencies by precisely calibrating our pure tones at the level of the animals' ear. Finally, we used auditory brainstem responses (n = 4) to confirm that hearing thresholds in our CD1 mice were frequency-independent over the range of frequencies used for discrimination testing (10-18 kHz; data not shown), as reported previously (Shone et al., 1991). Thus, we are confident that a change in intensity, or in tone audibility, and therefore perceived intensity, also did not contribute to the observed inhibition.

Our results demonstrate that frequency discrimination can be efficiently and reliably assessed in mice using PPI. Unlike time-consuming conditioning paradigms, results from each animal were obtained in a single testing session, in less than one hour. Due to the reflexive nature of the behavioral response, frequency discrimination thresholds obtained with PPI are

independent of motivation and learning and thus more likely to reflect perceptual thresholds. In fact, for gap detection, thresholds in mice defined using PPI correspond well with those measured in humans using psychophysical techniques (humans: Forrest and Green, 1987; mice: Ison, 2001).

The 64 ± 4 % inhibition elicited by a 25 % frequency change we measured is consistent with the 60 % inhibition reported in a previous PPI study that used a comparably-sized transition (between one octave-wide bands of random noise centered on frequencies of 4.5 kHz to 3.18 kHz; Stitt et al., 1974). However, by comparing the inhibition elicited by frequency changes of various magnitudes, we could also determine discrimination thresholds. Using PPI, we found a discrimination threshold of 2 % in 5 week-old CD1 mice. This threshold is similar to that of cats (1.25-5 %; Butler et al., 1957) and humans (1.5-3 %; Bonnel et al., 2010; Johnsrude et al., 2000). Thus, like gap detection, mice and humans show comparable abilities to discriminate frequency.

Nevertheless, a threshold of 2 % is much lower than the changes typically used in conditioning studies of frequency discrimination. For example, when trained on a go/no-go avoidance discrimination learning paradigm, mice can successfully discriminate between 7 and 12 kHz pure tones (Kurt and Ehret, 2010). Similarly, rats can discriminate between frequencies separated by ½ and full octaves (Ono et al., 2006). While consistent with these previous findings, our results indicate that mice are capable of very fine-grained frequency discriminations.

As a reliable test of frequency discrimination, PPI provides a useful tool to investigate the neuronal mechanisms underlying pitch discrimination, its maturation during development, and its relationship to tonotopic organization. The straightforward design of the apparatus, together with

the robustness of the reflexive behavioral response, provides the opportunity to establish frequency discrimination tests in laboratories with minimal experience in animal behavior.

APPENDIX C

LACK OF REFINEMENT OF MEDIAL NUCLEUS OF THE TRAPEZOID BODY AXON COLLATERALS IN THE SUPERIOR PARAOLIVARY NUCLEUS

C.1 INTRODUCTION

The superior paraolivary nucleus (SPON) is one of the most prominent of the many periolivary nuclei of the superior olivary complex (SOC). Located in the auditory brainstem, the SOC is the site of the first major binaural interactions. While the role of the primary SOC nuclei - the medial nucleus of the trapezoid body (MNTB), medial superior olive (MSO), and lateral superior olive (LSO) - in the azimuthal sound localization pathway has been well-characterized, the functional role of the SPON in auditory processing is much less clear.

SPON neurons are GABAergic (Kulesza and Berrebi, 2000) and provide a major source of topographically-organized inhibitory input to all three subdivisions of the ipsilateral inferior colliculus (IC), along with a sparse projection to the contralateral dorsal cortex (Saldana et al., 2009). While GABAergic inhibition is known to be critical in shaping the response properties of IC neurons (Caspary et al., 2002; Casseday et al., 1994; Palombi and Caspary, 1996; Park and Pollak, 1993; Yang et al., 1992), SPON neurons themselves tend to show heterogeneous responses to sounds. In the gerbil, cells show both monaural and binaural responses, and

sustained as well as phasic discharge patterns (Behrend et al., 2002; Dehmel et al., 2002), while in the rat the vast majority of neurons only respond to stimuli presented to the contralateral ear and show primarily offset activity (Kulesza et al., 2003).

Excitatory input to SPON neurons comes from octopus and multipolar cells in both posteroventral cochlear nuclei (Friauf and Ostwald, 1988; Thompson and Schofield, 2000; Thompson and Thompson, 1991; Warr, 1972). They also receive substantial inhibitory input from MNTB principal cells on the ipsilateral side (Banks and Smith, 1992; Kuwabara and Zook, 1991; Sommer et al., 1993). MNTB inputs to the SPON, like its input to other SOC nuclei, are organized topographically according to frequency (tonotopically). Although topography in the SOC is generally already present soon after birth (Kandler and Friauf, 1993), the organization of MNTB inputs to its other SOC targets undergoes significant tonotopic refinement during early postnatal development. In the LSO, pruning and synapse elimination result in a reduction of the number of boutons per axon, and in their spread along the LSO frequency axis. These anatomical changes correspond to an increase in the frequency specificity of the projection (Chapter 2; Sanes and Siverls, 1991). Similarly, in the MSO, MNTB axonal endsegments are eliminated and redistributed so as to cover a smaller portion of the frequency axis (Werthat et al., 2008). In each case, anatomical changes were observed after the onset of hearing.

Inhibition from the MNTB has a key role in establishing the response properties of neurons in both the MSO and LSO. In each case, the inhibitory inputs must be matched tonotopically with excitatory inputs for the frequency-specific computation of interaural time and intensity differences and thus the neurons' function in sound localization. As a result, it has been hypothesized that tonotopic refinement is more prominent in binaural sound localization circuits

than in other regions, such as the cochlear nucleus, where the monaural inputs do not need to be aligned with inputs from the contralateral ear (Kandler et al., 2009).

SPON neurons also receive tonotopically-organized excitatory and inhibitory inputs, and inhibition from the MNTB plays a similarly profound role in shaping their response properties (Behrend et al., 2002; Kulesza et al., 2003). However, it is unknown whether MNTB inputs to the SPON undergo a similar degree of tonotopic reorganization. This question is especially interesting since individual MNTB axons often project to multiple target nuclei in the SOC, including the MSO, LSO, and SPON, raising the possibility that the collaterals of a single axon may undergo target-specific refinement. Here we address this question by reconstructing the axons of individual MNTB neurons and quantitatively examining their terminations in the SPON during the same period of early postnatal development when refinement has been observed in other target nuclei.

C.2 MATERIALS & METHODS

C.2.1 Experimental Animals

All experiments were performed using mice of the strain 129S6/SvEv (gift of D. Vetter, Tufts University) at the following ages: soon after birth, postnatal day (P) 2-4, around the time of hearing onset, P12-14, or following one week of auditory experience, P19-21. All experimental procedures were in accordance with NIH guidelines and were approved by the Institutional Animal Care and Use Committee at the University of Pittsburgh.

C.2.2 Acute Slice Preparation

Mice were anesthetized with isoflurane (Piramal Healthcare, Eagle, ID), decapitated, and the brain removed and bathed in ice-cold artificial cerebrospinal fluid (ACSF; composition in mM: 124 NaCl, 26 $NaHCO_3$, 10 glucose, 5 KCl, 1.25 KH_2PO_4, 1.3 $MgSO_4$, 2 $CaCl_2$, pH 7.4 when aerated with 95% O_2/5% CO_2). ACSF for slice preparation also included 1 mM kynurenic acid to prevent excitotoxicity. Three hundred fifty μm thick coronal brain slices were then prepared with a vibratome (Leica VT 1200). Slices containing the MNTB and SPON were transferred to an interface chamber with aerated aCSF, warmed to room temperature, and incubated for 1 hour. Slices from P19-21 animals were incubated at 32°C. After incubation, slices were maintained at room temperature until used.

C.2.3 Electrophysiology & Intracellular Fills

Slices were transferred to a submerged-type recording chamber continuously perfused with aerated aCSF. Individual neurons within the MNTB were recorded in whole-cell configuration for approximately 30 minutes with 8-15 MΩ pipettes filled with an internal solution containing (in mM) 100 K-gluconate, 11 EGTA, 10 KCl, 1 $MgCl_2$, 1 $CaCl_2$-H_2O, 10 Hepes, 0.3 Na-GTP, 2 Mg-ATP, 0.1 Alexa Fluor 568 hydrazide (Invitrogen, Carlsbad, CA), and 0.5% biocytin (pH 7.2, 280 mOsm/L). Alexa 568 was included in the pipette for immediate identification of axons cut during slicing. Pipettes were pulled from borosilicate glass capillary tubes (outer diameter 1.5 mm, inner diameter 1.10 mm, 10 cm length; Sutter Instrument Co., Novato, CA) using a Sutter model P-97 puller. Voltage responses to current steps were recorded and used to electrophysiologically confirm MNTB cell identity. Cell viability was monitored by eliciting a

spike in response to depolarizing current injection. After the 30-minute holding period, slices were then incubated in the interface chamber for approximately one hour at room temperature before being fixed in 4 % paraformaldehyde in 0.01 M phosphate-buffered saline (PBS) for 1-7 days and transferred to 30 % sucrose in PBS for cryoprotection.

C.2.4 Histology

Slices from P12-14 and P19-21 animals were cryo-sectioned approximately in half using a sliding, freezing microtome (Microm HM 430). Slices from P2-4 animals were not re-sectioned. All sections were sequentially frozen on dry ice and thawed three times before being treated with 10 % methanol and 3 % H_2O_2 in PBS for 30 min. Sections were washed in PBS and then incubated in blocker (2 % normal goat serum and 0.2 % Triton X-100 in PBS) for 4 hr before being reacted with an avidin-biotin reagent (ABC Elite Kit, Vector Laboratories, Burlingame, CA) in blocker for 2 hr at room temperature and then overnight at 4ºC. Sections were then washed in PBS and reacted with 0.05 % diaminobenzidine-tetracholoride (DAB; Sigma, St. Louis, MO) in a solution containing 1 % $CoCl_2$, 1 % $Ni(NH_4)_2SO_4$, and 0.3 % H_2O_2 in PBS. Sections were washed in PBS, mounted on gelatinized glass slides, dehydrated in an ethanol/xylene series, and coverslipped with Permount (Fisher Scientific, Fair Lawn, NJ).

C.2.5 Axon Reconstruction

Complete axonal arbors within the SPON were reconstructed using a Neurolucida system (MBF Bioscience, Williston, VT). Putative synaptic boutons were identified and marked based on their characteristic round shape and diameter greater than 2x the width of the parent axon. While the

complete axon was usually reconstructed, only portions within the SPON were analyzed. To ensure analyzed arbors were complete, cells with axon branches within the SPON that were cut during slicing (identified by a large bulbous axonal ending at the slice surface) were discarded from analysis. Reconstructions and analysis were performed blind to age, although slices at P2-4 were generally noticeably smaller than those at P12-14 or P19-21. For analysis, 3-dimensional reconstructions were flattened rostro-caudally into a 2-dimensional, mediolaterally- and dorsoventrally-defined Cartesian coordinate system.

C.2.6 Quantitative Analysis of Reconstructed Axons

Neurolucida Explorer (MBF Bioscience, Williston, VT) was used for basic analysis of reconstructions, including the calculation of cross-sectional nucleus area, and the length of axon and number of boutons within the SPON, the location of the soma in the MNTB measured from its medial edge, and the location of the bouton centroid in the SPON measured from its medial edge. It was also used to calculate bouton area using the circumscription method, and tonotopic spread using the longitudinal method.

To estimate bouton area using the circumscription method, boutons located within the confines of the SPON were manually circumscribed and the area of the circumscribed region computed (an example is depicted graphically in Fig. C4 A). Because this method is based on the inclusion of every bouton, it is easily skewed by the presence of a few boutons outside the main region of termination. The SPON increases significantly in size during pre-hearing development (Fig. C3 D). Therefore, in order to compare across age groups, the calculated bouton area was also normalized to the size of the SPON and expressed as a percentage of SPON cross-sectional area.

To estimate tonotopic specificity, the spread of boutons along the putative frequency axis was calculated using the longitudinal method. First, the longitudinal axis of the group of boutons was defined by eye. Then the distance between the two most peripherally-located boutons was measured along a line oriented perpendicularly to the longitudinal axis (an example is depicted graphically in Fig. C5 A). Again, this method includes all boutons within the SPON and can be strongly influenced by the presence of a small number of boutons separate from the main termination. Thus the longitudinal method is likely to provide more of a minimum estimate of tonotopic specificity. To account for changes in SPON size, and more accurately express tonotopic specificity as a portion of the available frequency space, spread was also expressed as a percentage of the mediolateral SPON length.

The statistical significance of age group differences was assessed using a two-tailed Student's t-test.

C.2.7 Ellipse-fitting

Due to the sensitivity of the circumscription and longitudinal methods to boutons located outside the main region of termination, I also developed a second method of estimating bouton area and tonotopic spread to verify our results. In order to capture the elongated shape of the termination zones (see Fig. C1), I chose to fit an ellipsoid to the bouton coordinates that maximized the density of boutons within the confines of the ellipse. Because the shape, orientation, and size of the ellipse were objectively determined to maximize density, boutons located outside the main termination region were not always included. As a result, this method is much less likely to be influenced by the presence of outliers.

Custom-written LabView (National Instruments, TX) programs were used to extract the Cartesian coordinates of boutons located with the SPON from Neurolucida ASC files. A minimum volume enclosing ellipsoid was then fit to these coordinates using custom-written MATLAB (Mathworks, Natick, MA) scripts based on the Khachiyan Algorithm. The area of the ellipse was then used as a measure of bouton area (see Fig. C4 B for a representative example). The ellipse axis that was most closely oriented mediolaterally was defined as the putative SPON frequency axis. The diameter of the ellipse along the frequency axis was used as a measure of bouton spread, or tonotopic specificity (see Fig. C5 B for a representative example). Again, the statistical significance of age group differences was assessed using a Student's t-test.

C.2.8 Polar Plots

Custom-written LabView programs were used to compute the location of the centroid (center of mass) of boutons found within the SPON. The centroid was then used as the origin of a polar coordinate system used to subdivide the termination area into octants, with major axes oriented dorsoventrally and mediolaterally. For each axon, both the number of boutons and percentage of the total number of boutons per axon within each octant were calculated. The data for all of the axons in each age group were then averaged and the means plotted.

C.2.9 Density Heat Maps

Within Neurolucida, the boutons of each reconstructed axon were overlaid with a 2-dimensional grid comprised of 59.3 μm^2 (at P2-4) or 100 μm^2 (at P12-14 and P19-21) bins. The bin size was chosen to encompass a constant proportion of SPON area (~0.14 %) at each of the ages studied.

The grid covered the total area of the SPON and was positioned consistently in relation to the bouton centroid of each axon. As a result, the data from each axon were aligned at the bouton centroid, to account for differences in the location of the termination within the SPON and along its frequency axis. Neurolucida Explorer was used to compute the number of boutons per bin, which were also normalized to the total number of SPON boutons per axon and expressed as a percentage of the total bouton number.

Custom LabView programs were then used to sort both the number of boutons per bin and the percent of the total bouton number per bin into vector and matrix formats that maintained the geographical position of the boutons in mediolaterally- and dorsoventrally-defined space. The vector data for all of the axons in each age group were averaged and the means converted into matrix form. The mean matrix data (absolute and normalized) was then plotted as a heat map of average bouton density using MATLAB. To better illustrate developmental changes in the distribution of boutons, the difference between the P12-14 and P2-4 averages and P19-21 and P12-14 averages ("pre-hearing change" and "post-hearing change," respectively) was also plotted, again for both absolute and normalized data.

For presentation purposes, the average and difference maps were positioned medially within a representative outline of the SPON, to reflect the position of the majority of termination regions, though the actual location of individual axon terminations within the SPON varied.

C.2.10 Density of Boutons Along the SPON Frequency Axis

Histograms and cumulative density functions (CDFs) of bouton density along the SPON frequency axis were generated in MATLAB. First, the Cartesian coordinates of each axon's boutons were rotated around the centroid by an angle theta, which was defined by the orientation

of its fitted ellipse. As a result, the horizontal axis of the coordinate system now corresponded to the putative SPON frequency axis, rather than mediolateral space, with an origin at the bouton centroid. The frequency axis was then divided into 2.21 μm- (at P2-4) or 2.85 μm- (at P12-14 and P19-21) wide bins that corresponded to a constant 1 % of the mediolateral length of the SPON. For each axon, counts of the number of boutons per bin were computed and again normalized to the total number of SPON boutons per axon and expressed as a percentage of the total bouton number. The absolute and normalized histogram data for all of the axons in each age group were then averaged.

For CDF plots, the histogram data of average bouton density were collapsed in the mediolateral dimension and plotted as the cumulative likelihood that a bouton, on average, would be located some distance from the centroid along the SPON frequency axis. Again, distances were expressed as a percentage of the mediolateral length of the SPON. Statistical significance of group differences was assessed using the Komolgorov-Smirnoff test.

For the presentation of histograms, the average data were smoothed with a 3 bin-wide moving average, and then fit with the Gaussian function $f(x) = a1*\exp(-((x-b1)/c1)^2)$, where a1 = the maximum height and b1 = the x-coordinate at maximum height. c1 is related to width such that full width at half the maximum height (FWHM) = 2*c1*sqrt(log(2)).

To gauge statistical significance, each axon's histogram data was also smoothed and fit with a Gaussian. The descriptive characteristics a1, b1, and FWHM of the individual Gaussians were then averaged for all of the axons of each age group and the statistical significance of age group differences assessed using a two-tailed Student's t-test.

C.3 RESULTS

By holding MNTB neurons in whole-cell configuration and allowing biocytin to diffuse from the pipette into the cell, we were able to visualize the complete axonal arbor, including fine branches and the round swellings we identified as putative synaptic boutons at each of the ages studied (Fig. C1). MNTB axons with collaterals in the SPON often also continued on to terminate in the LSO. Here I will discuss only terminations within the SPON.

I first wanted to confirm that the MNTB neurons selected for filling at each of the experimental ages of interest were drawn from approximately the same frequency region of the MNTB, so that any changes in the tonotopic specificity of the MNTB-SPON projection seen with development could not be attributed to differences in the specificity of the representation of certain portions of the frequency axis over others. I found no significant difference in the location of filled MNTB cell bodies along the mediolateral length of the SPON between the ages studied (P2-4, 12-14, and 19-21; Student's t-test), indicating that all of the MNTB neurons were drawn from approximately the same portion of the frequency axis (Fig. C2 A). I also found no significant differences in the location of the bouton centroid, the center of mass of each MNTB axon's termination in the SPON, along the mediolateral axis of the SPON, indicating that MNTB axons at all ages terminated in approximately the same frequency region of the SPON (Fig. C2 B).

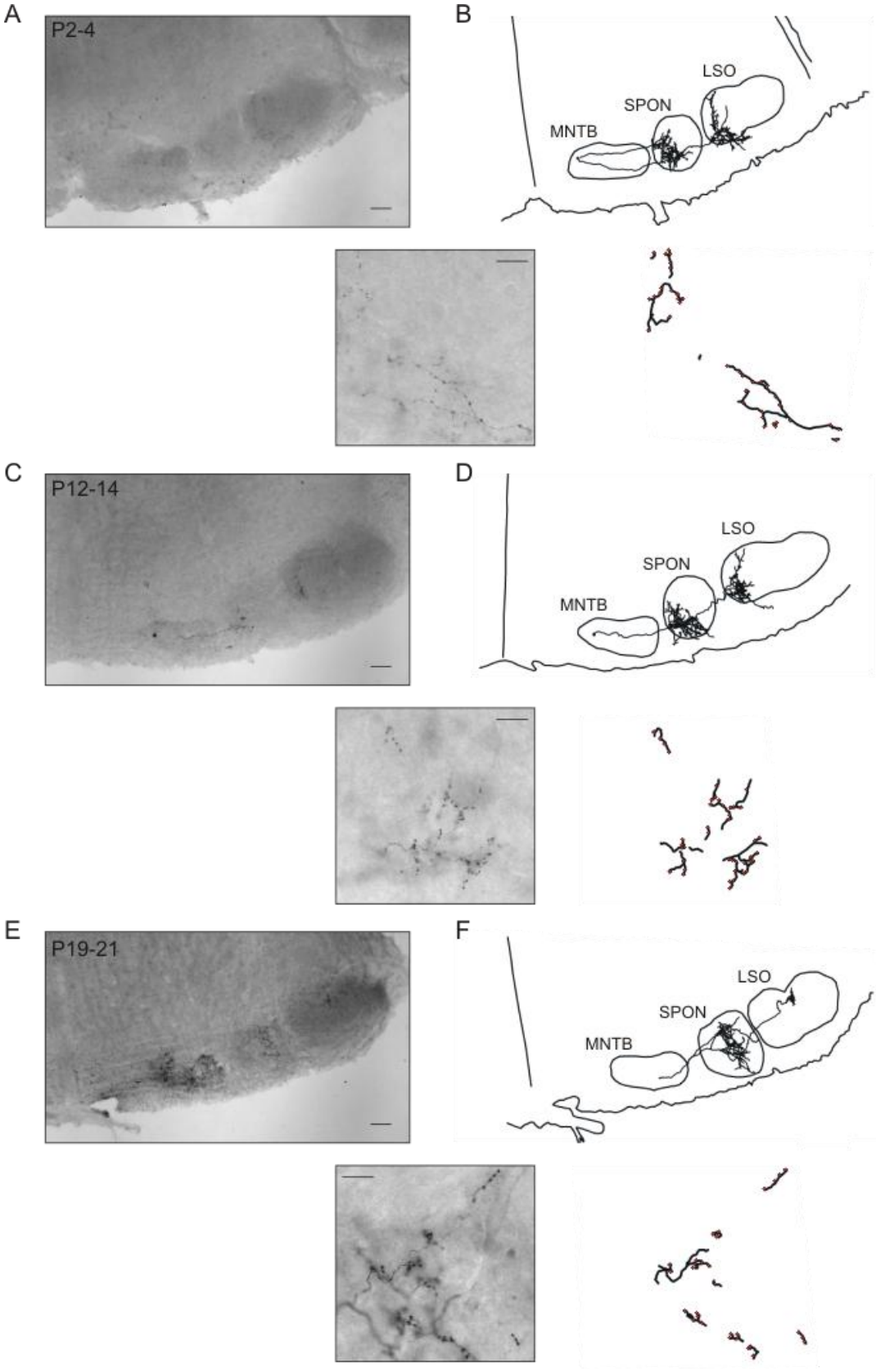
A
P2-4
B
LSO
SPON
MNTB
C
P12-14
D
LSO
SPON
MNTB
E
P19-21
F
LSO
SPON
MNTB

Figure C1.

Figure C1. MNTB axons and boutons in the SPON over development.

(A-B) P2-4. (A) Upper left micrograph shows low magnification view of whole section. Dorsal is to the top and medial is to the left. Scale bar, 100 µm. Lower right shows high level magnification of a portion of the MNTB axon and its boutons in the SPON within a single focal plane. The axon appears discontinuous as it moves in and out of the focal plane. Scale bar, 20 µm. (B) Reconstruction of the regions shown in the micrographs in (A). Scale same as in (A). In the reconstruction of the high magnification region, boutons are designated by red dots. (C-D) P12-14. Scale and conventions same as in (A) and (B). (E-F) P19-21. Scale and conventions same as in (A) and (B). MNTB, medial nucleus of the trapezoid body; SPON, superior paraolivary nucleus; LSO, lateral superior olive.

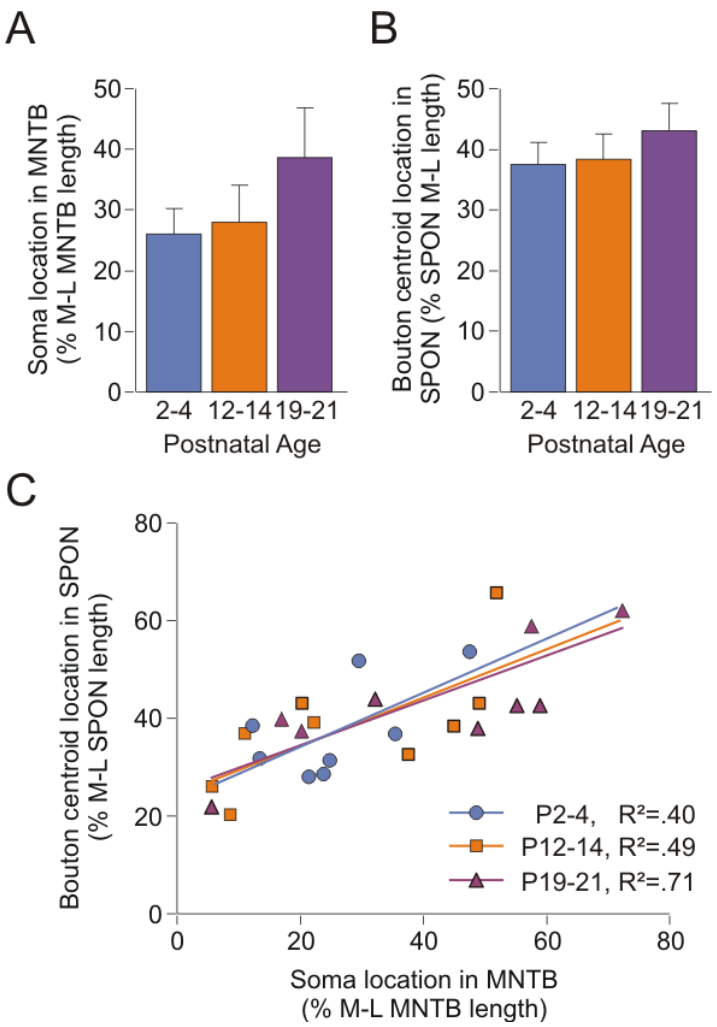

Figure C2. The MNTB-SPON projection is topographically organized throughout early development.

(A) Average soma location of filled neurons within the MNTB, normalized to the mediolateral length of the MNTB. (B) Average location of the bouton centroid of MNTB axons in the SPON, normalized to the mediolateral length of the SPON. (C) Correlation of soma location in the MNTB with bouton centroid location in the SPON. At each of the ages studied the MNTB-SPON projection shows topographic organization, with a positive correlation between the location of MNTB cell bodies and bouton centroids along the mediolateral dimension of the MNTB and SPON, respectively. However, the topographic relationship, as measured by the slope of the linear regression line, did not change over the first three weeks of postnatal development.

Consistent with previous reports (Banks and Smith, 1992), I found the projection from the MNTB-SPON to be topographically organized, showing a positive correlation between the location of the MNTB neuron's soma along the mediolateral axis of the MNTB and the location of the center of its termination, the bouton centroid, along the mediolateral axis of the SPON (Figure C2 C). This organization is established early as it is already present soon after birth at P2-4, and is maintained through hearing onset and early auditory experience until at least P21. Although the correlation did not quite reach statistical significance at P2-4 ($p = 0.09$, Pearson Correlation), the topographic relationship between soma location and bouton centroid location, as measured by the slope of the linear regression line, did not change significantly over development (Glantz, 2002).

We next investigated whether the strength of the connection, as measured by the number of boutons per MNTB axon found in the SPON, changed with development. From soon after birth to the time of hearing onset, the average number of SPON boutons per MNTB axon increased more than 2.5 times, from 108 ± 20 boutons at P2-4 to 282 ± 34 boutons at P12-14 ($p = 0.001$, Student's t-test; Fig. C3 A). This is comparable to the almost 2.5-fold increase seen in the number of LSO boutons/MNTB axon over the same period (Chapter 2). However, the number of SPON boutons then remained constant over the first week after hearing onset, rather than decreasing again as in the LSO. Since many MNTB axons send collaterals to both the SPON and LSO, a lack of pruning in the SPON suggests that the elimination of boutons from MNTB axon collaterals is target-specific. The addition of boutons also did not seem to be accompanied by growth of MNTB axons, since axonal length within the SPON did not change significantly between P2-4 and P12-14 (Fig. C3 B), even when normalized to SPON area to account for growth of the SPON nucleus itself (Fig. C3 C).

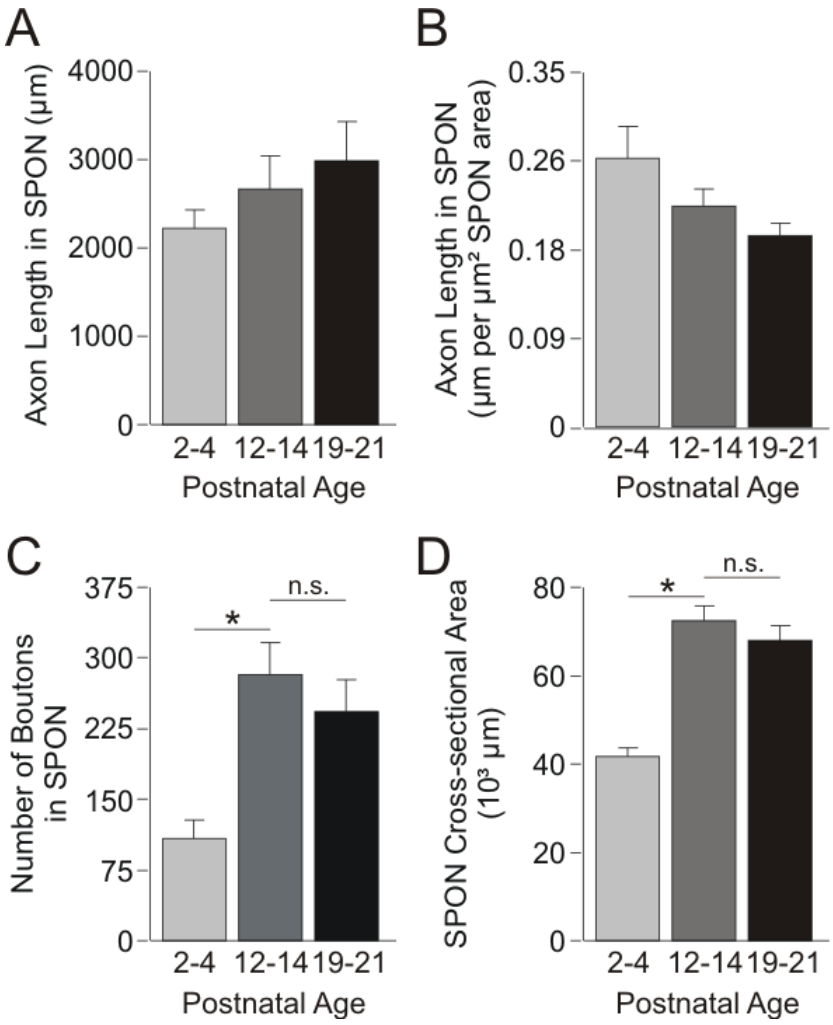

Figure C3. Characteristics of individual MNTB axons in the SPON over development.

(A) Average number of boutons in the SPON per MNTB axon. A significant number of boutons were added before the onset of hearing, between P2-4 and P12-14 ($p = 0.001$, Student's t-test), but the number of boutons in the SPON per MNTB axon did not change significantly after hearing onset (P12-14 to P19-21; $p > 0.05$, Student's t-test). (B) Absolute length of MNTB axon branches in the SPON. (C) Relative length of MNTB axon branches in the SPON (normalized to SPON cross-sectional area). Asterisk, $p < 0.05$; n.s., not significant.

Because MNTB neurons must project to the correct frequency region of the SPON, portions of the axon may have to cross expanses of the SPON simply to reach their target neurons. Thus the presence of an axonal segment within the confines of the SPON does not necessarily signify that synaptic transmission is taking place. This makes it difficult to use axonal measurements as a measure of the tonotopic specificity. Therefore, to investigate whether the tonotopic specificity of the MNTB-SPON projection, like that of the MNTB-LSO (Chapter 2), changes with development, we used the location of boutons rather than axons as a measure of connectivity.

To estimate the area of the SPON covered by the boutons of individual MNTB axons, I both circumscribed the bouton area ("circumscription method") and calculated the area of an ellipse that was fit to the boutons ("ellipse-fitting;" see Materials and Methods). While both provide a measure of bouton area, each measurement is slightly different in the characteristics of the termination it most reflects. While the circumscribed area may be more exact, it is also more easily influenced by the presence of a few boutons on the periphery of the termination. In contrast, the fitted ellipse is less influenced by outliers and thus is more likely to capture the gestalt of the termination region, though it may also be more likely to overestimate the area than the circumscription method. An example of each of these methods is shown in Figure C4 A and B.

In absolute terms, there is a trend for the area covered by boutons to increase over the first three weeks of development (Fig. C4 C, D). However, this increase is only statistically significant between P2-4 and P12-14 when measured using the area of the fitted ellipse. In addition, even if the boutons do cover a significantly greater area at P12-14 than they did at P2-4, this does not necessarily mean they cover a significantly greater proportion of the SPON, since

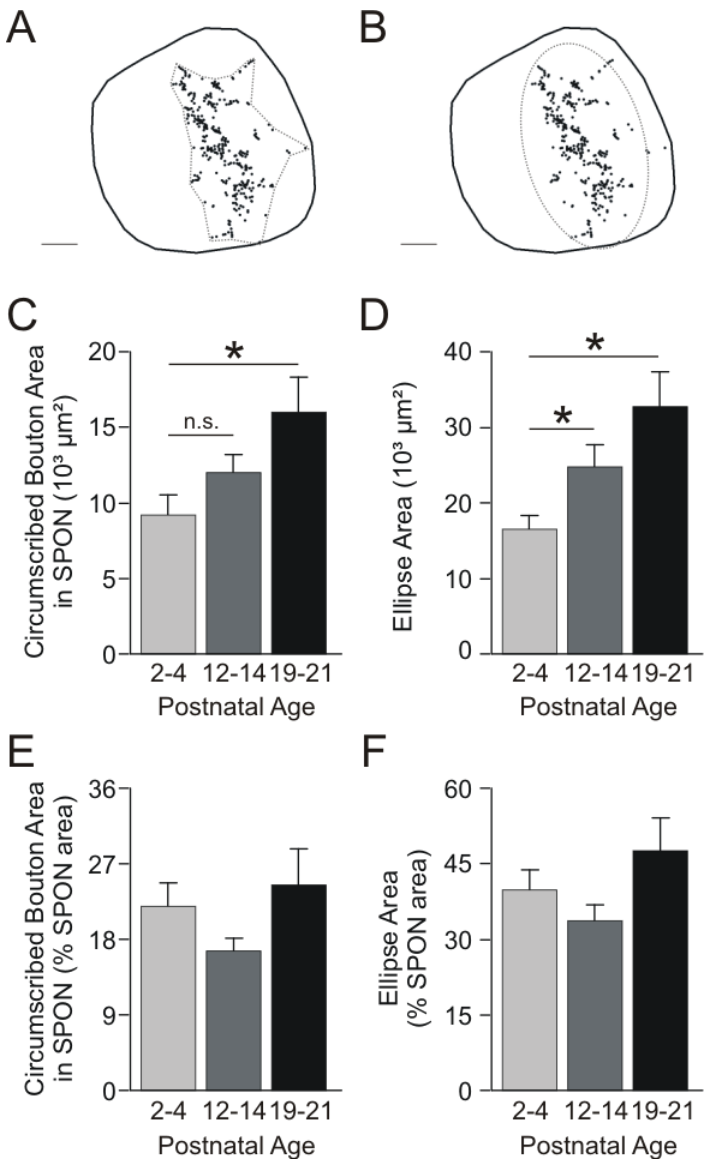

Figure C4. Area of the SPON covered by the boutons of individual MNTB axons over development.

(A) Calculation of bouton area by circumscribing the field of SPON boutons (see Materials and Methods), using the boutons of a representative P12-14 axon as an example. Solid black line, outline of SPON; black dots, location of boutons; dotted grey line, circumscribed bouton area. Scale bar, 50 µm. (B) Calculation of bouton area by fitting an ellipse to boutons within the SPON (see Materials and Methods), using the same axon shown in (A). Solid black line, outline of SPON; black dots, location of boutons; dotted grey line, fitted ellipse. Scale bar, 50 µm. (C) Absolute bouton area in SPON using circumscription method described in (A). (D) Absolute bouton area in SPON using ellipse-fitting method described in (B). (E) Relative circumscribed bouton area in SPON. (F) Relative bouton area in SPON using ellipse-fitting. Asterisk, $p < 0.05$, Student's t-test; n.s., not significant.

the SPON also increases in size significantly during pre-hearing development (Fig. C3 D). To account for growth of the SPON, I also normalized bouton area to the area of the SPON itself, so that it is expressed as a percentage of SPON area. This normalized value more accurately represents the proportion of the SPON covered by the boutons of a single MNTB axon. When normalized in this manner, I found no significant change in the percentage of the SPON covered by boutons over the course of development (circumscribed area: Fig. C4 E; ellipse area: Fig. C4 F). This is in sharp contrast with what happens to MNTB axon collaterals in the LSO, where the percentage of the LSO covered by boutons is reduced by half during the first week after hearing onset (Chapter 2), and provides additional evidence that refinement of MNTB axon collaterals is target-specific.

However, tonotopic specificity is most accurately described as the proportion of frequency space occupied by the projection, not necessarily as a percentage of nucleus area. Therefore I also wanted to measure the spread of boutons along the SPON frequency axis, which is slightly tilted, but oriented primarily mediolaterally (Kulesza et al., 2003). To estimate spread, and thus tonotopic specificity, I again employed two complementary measures. First, I defined the longitudinal axis of the group of boutons by eye, and then measured the distance between the two most peripherally-located boutons along a line oriented orthogonal to the longitudinal axis (Fig. C5 A). Like the circumscription method employed for measuring bouton area, this measure is sensitive to outliers and the subjective definition of the longitudinal axis. Therefore I also employed the ellipse-fitting method and used the diameter of the fitted ellipse as the measure of tonotopic spread (Fig. C5 B). Because the orientation of the ellipse and inclusion or exclusion of individual boutons is mathematically chosen so as to maximize bouton density within the ellipse, this measure is objective and again less sensitive to outliers. However, both methods produced

the same results regarding statistically significant changes in tonotopic specificity during development, and so are discussed together below.

I did not observe any changes in the spread of boutons along the SPON frequency axis during pre-hearing development (Fig. C5 C-F). Though the normalized spread of boutons decreased between P2-4 and P12-14, the reduction was not significant ($p > 0.05$, Student's t-test). Thus the tonotopic specificity of the connections of the MNTB with the SPON, like those with the LSO (Chapter 2), appears to remain constant during pre-hearing development. In contrast, during the first week of auditory experience, tonotopic spread actually increased significantly. Since the size of the SPON remains constant over this period, this increase is seen in both the absolute spread, and the relative spread expressed as a percentage of the mediolateral length of the SPON. However, spread did not differ significantly between P2-4 and P19-21 (relative spread: $p = 0.51$, relative ellipse diameter: $p = 0.37$, Student's t-test). Therefore the significant increase in spread seen between P12-14 and P19-21 may be an artifact that reflects the non-significant decrease in spread observed between P2-4 and P12-14, rather than a true developmental change in tonotopic specificity. Nevertheless, regardless of whether the tonotopic specificity of the MNTB-SPON projection remained constant or decreased during post-hearing development, it contrasts with the increase in specificity observed for the MNTB collaterals to other SOC nuclei (Chapter 2; Sanes and Siverls, 1991; Werthat et al., 2008).

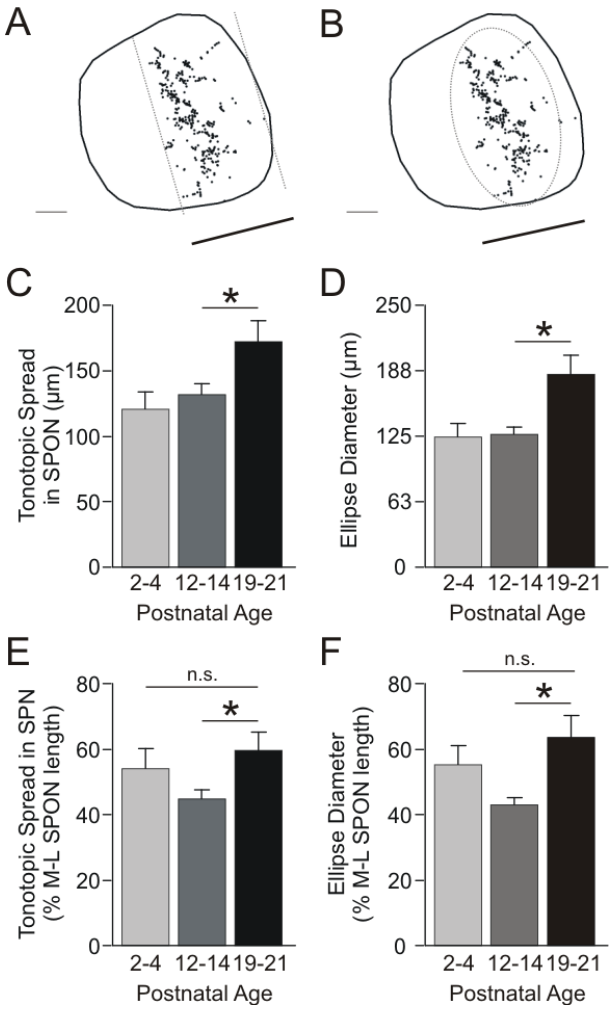

Figure C5. Tonotopic spread of MNTB boutons in the SPON over development.

(A) Calculation of tonotopic spread as the maximum distance between boutons along a line oriented perpendicular to the longitudinal axis of the bouton field (see Materials and Methods), using the boutons of the same representative P12-14 axon shown in Figure 31. Thin solid black line, outline of SPON; black dots, location of boutons; dotted grey lines, longitudinal axis; thick solid black line, tonotopic spread. (B) Calculation of tonotopic spread using the ellipse-fitting method (see Materials and Methods), utilizing the same axon shown in (A). Thin solid black line, outline of SPON; black dots, location of boutons; dotted grey line, fitted ellipse; thick solid black line, tonotopic spread measured as ellipse diameter. (C) Absolute tonotopic spread of boutons in SPON using the longitudinal method described in (A). (D) Absolute tonotopic spread of boutons in SPON using the ellipse-fitting method described in (B). (E) Relative tonotopic spread of boutons in SPON using longitudinal method. (F) Relative tonotopic spread of boutons in SPON using ellipse-fitting method. Asterisk, $p < 0.05$, Student's t-test; n.s., not significant.

Because it has been proposed that the response properties of inhibitory SPON neurons may contribute to the directional selectivity of IC neurons for frequency-modulated sweeps (Pollak et al., 2010), I was interested to determine whether the boutons were evenly distributed across frequency space, or whether there was a bias for the high or low frequency portions of the termination region. To do so, I first created polar plots of the average location of boutons within the SPON relative to each axon's center of the termination, the bouton centroid, and the mediolateral and dorsoventral axes of the SPON (Fig. C6). Overall, the shape of the distribution did not seem to change over development; it remained elongated dorsoventrally, with an approximately 22° medial rotation. Based on the orientation of MNTB bouton fields, the SPON frequency axis is likely to run primarily mediolaterally, but with a slight dorsal slant. This is consistent with the finding of dorsomedially to ventrolaterally tilted isofrequency contours in the SPON of the rat (Kulesza et al., 2003). When plotting absolute bouton numbers, the smaller number of boutons per P2-4 axons is evident (Fig. C6 A). However, the distribution of boutons among octants appears similar to the distributions at P12-14 and P19-21. This can be seen more clearly by expressing the distribution of boutons among octants as a percentage of the total number of boutons per axon (Fig. C6 B). In this case, the only significant difference between the distributions at the ages studied is that there are significantly more boutons located in the more lateral of the ventrolateral octants at P2-4 than there are at P12-14 ($p < 0.05$, Student's t-test). But at all ages the boutons were distributed in longitudinal bands, with no apparent bias towards either the high or low frequency sides of the termination.

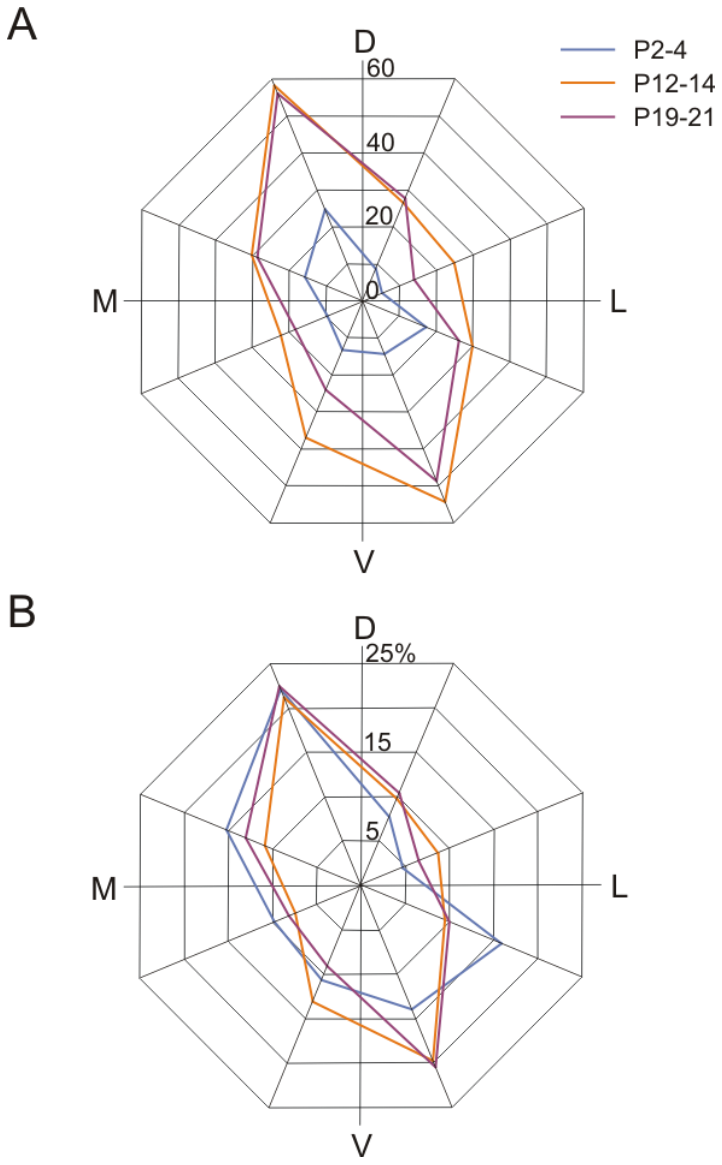

Figure C6. Polar plots of the distribution of the boutons of individual MNTB axons in the SPON around the bouton centroid.

(A) Absolute distribution of boutons around the centroid. Radial coordinates denote the average number of boutons found within the corresponding octant. (B) Relative distribution of boutons around the centroid. Radial coordinates denote the average percentage of the total number of boutons per axon found within the corresponding octant. D, dorsal; L, lateral; V, ventral; M, medial.

Nonetheless, I was interested to know more about the distribution of boutons within the region of termination, and whether there were any changes in the pattern of distribution over development. For example, changes in the distribution of boutons from 'hotspots' to a more even distribution, or vice versa, could have important implications for the transfer of information between the MNTB and SPON, even in the absence of changes in the tonotopic specificity of the projection. There might also be differences in the distribution of boutons in the dorsoventral dimension during different development stages.

To look more in depth at the distribution of boutons, I first oriented each axon in equivalent mediolateral and dorsoventral coordinate space, using the slice midline as a guide, and then aligned the bouton centroids of each axon (see Materials and Methods). I then created heat maps to show how the average density of boutons varied over different parts of the region of termination (Fig. C7). In order to compare density maps across development, I always plotted bouton density as a percentage of total SPON area, rather than absolute area, to account for the smaller size of the SPON at P2-4.

I first looked at the distribution of boutons in terms of absolute numbers (Fig. C7 A). At all ages the distribution of boutons was relatively smooth, rather than highly patchy. Density tended to be higher in the center and decline gradually with distance from the aligned centroids. In fact, the distributions were shaped much like 2-dimensional elliptical Gaussians, with the major axis running orthogonal to the largely mediolateral frequency axis, consistent with polar plots. At no age did there appear to be a dorsoventral gradient in the distribution of boutons.

Density was most constant across the areas of termination at P2-4. However, during pre-hearing development, when the number of boutons more than doubles, the addition of boutons seemed to be concentrated in the center of the termination regions, causing a noticeably larger

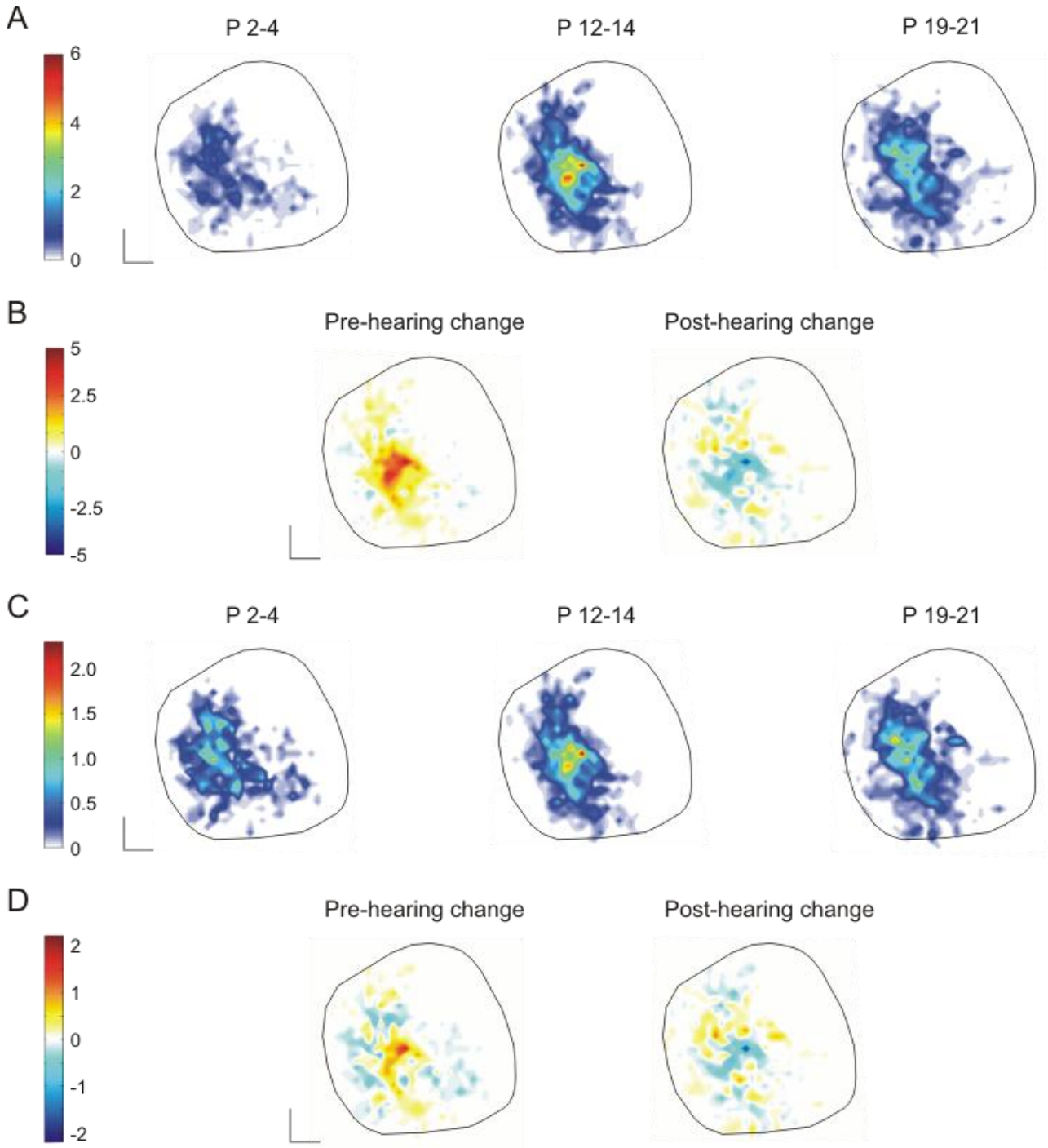
A
P 2-4
P 12-14
P 19-21
6
4
2
0
B
Pre-hearing change
Post-hearing change
5
2.5
0
-2.5
-5
C
P 2-4
P 12-14
P 19-21
2.0
1.5
1.0
0.5
0
D
Pre-hearing change
Post-hearing change
2
1
0
-1
-2

Figure C7.

Figure C7. Heat maps of the spatial density of MNTB boutons in the SPON over development.

(A) Average absolute density of boutons in the SPON at each developmental age. Color bar, average number of boutons per 0.14% SPON area; scale bars, 17.5% SPON mediolateral length and dorsoventral height; dorsal is to the top and lateral to the right. (B) Change in the absolute density of boutons over development. Pre-hearing change shows the difference between P2-4 and P12-14. Post-hearing change shows the difference between P12-14 and P19-21. Warm colors indicate an increase with development; cool colors indicate a decrease with development. Color bar, average change in bouton number per 0.14% SPON area; scale and orientation same as in (A). (C) Average relative density of boutons in the SPON at each developmental age. Color bar, average percentage of the total number of boutons per axon per 0.14% SPON area; scale and orientation same as in (A). (D) Change in relative density of boutons over development. Color bar, average change in percentage of the total number of boutons per axon per 0.14% SPON area; scale and orientation same as in (A).

peak in density. This can be seen more clearly in Figure C7 B, which shows the developmental change in bouton density. Between P2-4 and P12-14 many boutons were added within the same area, so density generally increased (indicated by warm colors), but the increase was clearly concentrated in the center of the termination bands. After hearing onset, the number of boutons did not change significantly, so there was a roughly equal mix of small positive and negative changes in density, though the loss appeared greatest near the central regions of peak density. As a result, although the large peak in density is still present at P19-21, it is slightly lower than it was at P12-14.

Because axons with the highest number of boutons will have a greater influence on the average distribution than axons with smaller numbers of boutons, we also normalized each axon to its total number of boutons and looked at density as an average percentage of the total number of boutons per axon (Fig. C7 C). When examined this way the general shape of the distributions does not change; density is still highest in the center and declines with distance from the centroid. The observed developmental changes are also still present, with a concentration of density at the center of termination bands during pre-hearing development and a mix of increasing and decreasing density over post-hearing development (Fig. C7 D), indicating that the results are reflective of the population as a whole and not dominated by a small number of axons with high numbers of boutons.

Though the density heat maps provide a valuable way of graphically depicting the distribution of MNTB boutons within the SPON, they are also largely descriptive. Therefore, I developed a more quantitative way of describing the shape and tonotopic specificity of the distributions. Because I found no evidence for a dorsoventral gradient, I compressed the data in the longitudinal dorsoventral dimension and plotted the CDF of average bouton number with

respect to distance from the centroid along the SPON frequency axis (Fig. C8). When examined this way, I found no significant differences in the distributions during either pre-hearing or post-hearing development (P2-4 v P12-14: p=0.74, P12-14 v P19-21: p=0.46; K-S test). This is consistent with the polar plots (Fig. C6 B) and especially the density maps (Fig. C7 C), where the distributions at all ages shared the same general shape, with a peak density located in the center that then declined gradually with distance from the centroid, a decline that is reflected by the largely linear slope of the majority of the CDF.

However, both the CDFs and density heat maps seemed to suggest that boutons are more concentrated near the centroid at P12-14 and P19-21 than they are soon after birth at P2-4. For example, at P12-14 and P19-21, 5 % of boutons can be found within 2 μm of the centroid, while at P2-4 the same 5 % are spread over twice the area. Therefore, I also converted the density heat maps to histograms that showed the distribution of boutons as a function of distance from the centroid along the SPON frequency axis (see Materials and Methods), again in terms of both absolute bouton number (Fig. C9 A), and as a percentage of the total number of boutons per axon (Fig. C9 B).

Consistent with the shape of the density heat maps, the histograms were well-fit with a Gaussian function (absolute: R^2 = 0.96 at P2-4, 0.99 at P12-14, and 0.97 at P19-21, normalized: R^2 = 0.95 at P2-4, 0.99 at P12-14, and 0.96 at P19-21). As seen in the heat maps, the distribution of absolute bouton number is flattest at P2-4. The pre-hearing addition of boutons to individual MNTB axons then seems to occur selectively at the center of termination bands, causing the maximum height of the Gaussian to increase by almost four times between P2-4 and P12-14. As a result, the FWHM of the Gaussian was reduced by ~1/3. Following one week of auditory experience the maximum height and FWHM did not change significantly (maximum height:

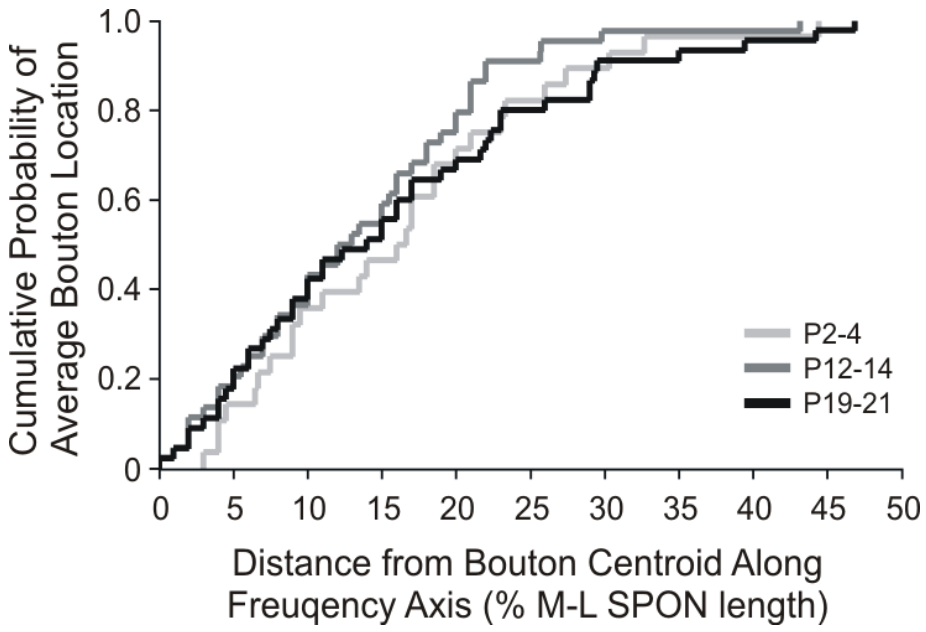

Figure C8. Cumulative density plot describing the distribution of boutons along the SPON frequency axis over development.

Cumulative probability function for each age group (P2-4, P12-14, and P19-21) describing the cumulative likelihood that boutons will be found at a location some distance from the bouton centroid. The functions did not change significantly over the first three weeks of postnatal development ($p > 0.05$, Kolmogorov-Smirnov test).

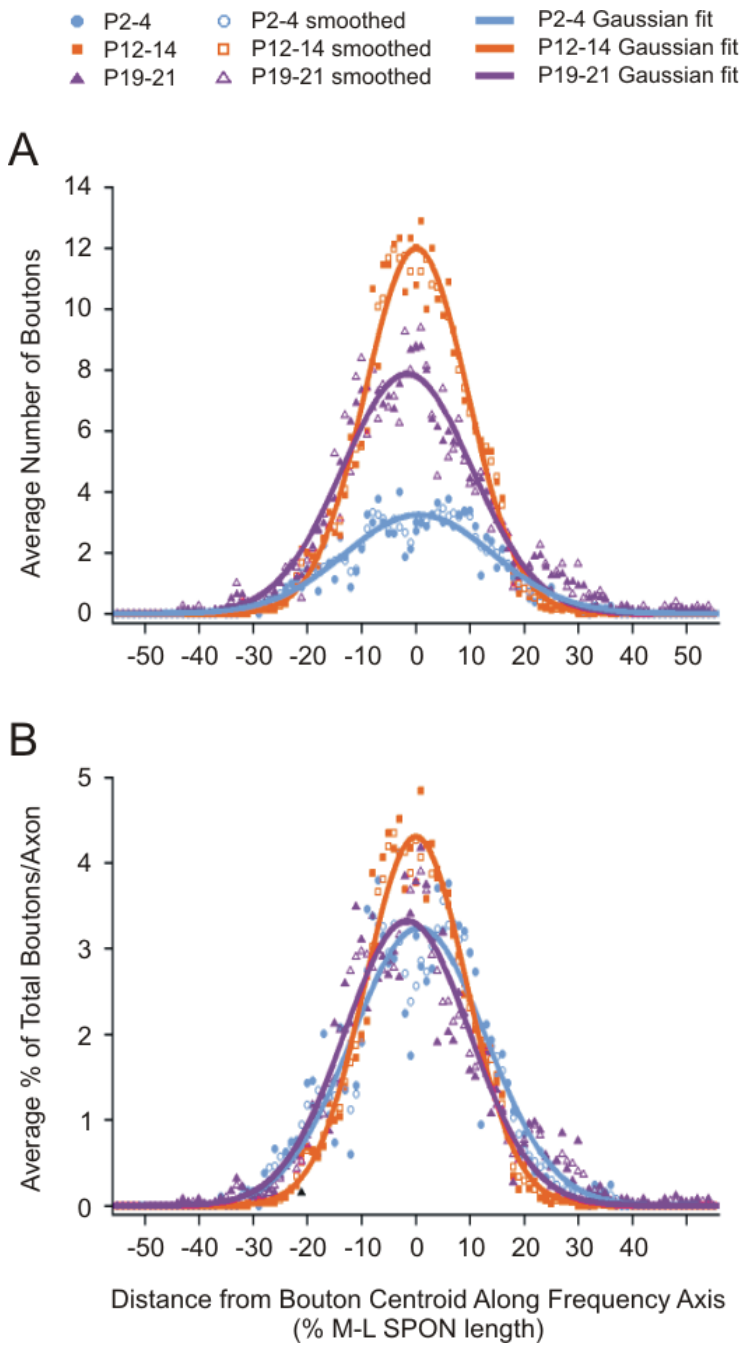

Figure C9. Distribution of boutons along the SPON frequency axis over development.

(A) Histogram showing the absolute distribution of boutons along the frequency axis. Negative distances, medial; positive distances, lateral. (B) Histogram showing the relative distribution of boutons along the frequency axis. Closed symbols represent population means, open symbols represent smoothed data points, lines represent Gaussians fit to the smoothed data.

p = 0.08, FWHM: p = 0.16, Student's t-test). At no point did the width of the base, which corresponds most closely to tonotopic spread, appear to change over development.

In terms of the percentage of the total number of boutons per axon, the histograms, like the heat maps, were very similar across ages. However, the same relationships were observed; at P12-14 the maximum height was significantly greater than at P2-4, though it did not differ significantly from the maximum height at P19-21. Accordingly, the FWHM was also significantly less at P12-14 than at P2-4, though again it did not change with post-hearing development. Thus during the two weeks of development before hearing onset, boutons are added to individual MNTB axons at the center of the termination region, causing a peak in bouton density.

In conclusion, I found a lack of tonotopic refinement of MNTB-SPON connections over early development, in contrast to the increased tonotopic specificity of MNTB axons in other SOC target nuclei.

C.4 DISCUSSION

Inhibitory input from the MNTB plays an important role in shaping the response properties of SPON neurons. In other SOC nuclei, MNTB inputs are pruned and reorganized after the onset of hearing such that they become more tonotopically precise. By quantitatively reconstructing the axons and boutons of individual MNTB axons in the SPON, I investigated whether MNTB-SPON connections, like those elsewhere in the SOC, undergo tonotopic refinement during early postnatal development.

Based on the location of MNTB boutons, I found the SPON frequency axis to be slightly tilted dorsomedially to ventrolaterally, consistent with previous work in the rat (Kulesza et al., 2003). At all ages boutons were distributed in longitudinal bands, with no apparent bias towards either the high or low frequency sides of the termination, or along the dorsoventral aspect of the isofrequency contour. Before the onset of hearing, the number of boutons in the SPON more than doubled, the addition of which appeared to be selective for the center of the termination bands, similar to what took place in the LSO (Chapter 2). The concentration of boutons in the center of the termination was maintained during the first week after hearing onset. However, the spread of boutons along the frequency axis never decreased, indicating that the MNTB-SPON projection does not become more tonotopically precise during early postnatal development, in contrast to the post-hearing refinement of MNTB axons observed in other SOC nuclei, the MSO and LSO.

Although it likely receives binaural excitatory and inhibitory inputs like the MSO and LSO, the SPON is not thought to play a role in sound localization (Behrend et al., 2002). Instead, the SPON may play a role in the encoding of sound duration; in particular, the offset responses of SPON units may contribute to duration tuning in the IC (Casseday et al., 1994). Input from the MNTB may be especially important for this aspect of SPON sound processing, since SPON neurons seem capable of firing only when released from inhibition. As a result, they tend to produce offset responses that are likely generated through a post-inhibitory rebound mechanism (Kulesza et al., 2003). However, because SPON units have wider frequency receptive fields than MNTB neurons and can generate offset responses throughout their response maps, highly frequency-specific inhibition may not be necessary to produce this type of response. As a result, MNTB inputs to the SPON may not need to be tonotopically refined,

whereas inputs to the LSO and MSO, where frequency-specific inhibition is very important, do become more tonotopically precise during early auditory experience.

We observed no tonotopic refinement of the MNTB-SPON pathway, yet it is known that collaterals of these same axons in the LSO are refined during the first week of auditory experience (Chapter 2). While the exact mechanism underlying refinement remains unclear, its target-specific nature indicates communication with the postsynaptic cell must be important. In the LSO, long term depression at MNTB synapses that depends on postsynaptic calcium and kinase signaling is likely to contribute to the developmental rearrangement of inhibitory inputs (Chang et al., 2003; Kotak and Sanes, 2000, 2002). Because synaptic plasticity has not yet been investigated in the SPON, it is possible SPON neurons lack the signaling components required for this type of plasticity.

BIBLIOGRAPHY

Ahissar M, Protopapas A, Reid M, Merzenich MM. Auditory processing parallels reading abilities in adults. Proc Natl Acad Sci U S A, 2000; 97: 6832-7.

Akerman CJ, Cline HT. Refining the roles of GABAergic signaling during neural circuit formation. Trends Neurosci, 2007; 30: 382-9.

Allen CB, Celikel T, Feldman DE. Long-term depression induced by sensory deprivation during cortical map plasticity in vivo. Nature neuroscience, 2003; 6: 291-9.

Allen P, Housel N, Yee S, Zenczak C, Ison J. Abstract #365: Response to sweeping frequency changes in the CBA/CaJ mouse model of presbycusis. Thirty-first Annual Midwinter Research Meeting of the Association for Research in Otolaryngology: Phoenix, AZ, 2008.

Antonini A, Stryker MP. Rapid remodeling of axonal arbors in the visual cortex. Science, 1993; 260: 1819-21.

Balice-Gordon RJ, Lichtman JW. In vivo observations of pre- and postsynaptic changes during the transition from multiple to single innervation at developing neuromuscular junctions. J Neurosci, 1993; 13: 834-55.

Banks MI, Smith PH. Intracellular recordings from neurobiotin-labeled cells in brain slices of the rat medial nucleus of the trapezoid body. J Neurosci, 1992; 12: 2819-37.

Behrend O, Brand A, Kapfer C, Grothe B. Auditory response properties in the superior paraolivary nucleus of the gerbil. J Neurophysiol, 2002; 87: 2915-28.

Bonfils P, Puel JL, Ores S, Pujol R. Modulation of the masking phenomenon by the crossed part of the medial olivocochlear bundle. Arch Otorhinolaryngol, 1987; 244: 198-203.

Bonfils P, Remond MC, Pujol R. Efferent tracts and cochlear frequency selectivity. Hear Res, 1986; 24: 277-83.

Bonnel A, McAdams S, Smith B, Berthiaume C, Bertone A, Ciocca V, Burack JA, Mottron L. Enhanced pure-tone pitch discrimination among persons with autism but not Asperger syndrome. Neuropsychologia, 2010; 48: 2465-75.

Born DE, Rubel EW. Afferent influences on brain stem auditory nuclei of the chicken: presynaptic action potentials regulate protein synthesis in nucleus magnocellularis neurons. J Neurosci, 1988; 8: 901-19.

Bosman LW, Takechi H, Hartmann J, Eilers J, Konnerth A. Homosynaptic long-term synaptic potentiation of the "winner" climbing fiber synapse in developing Purkinje cells. J Neurosci, 2008; 28: 798-807.

Boudreau JC, Tsuchitani C. Binaural interaction in the cat superior olive S segment. Journal of neurophysiology, 1968; 31: 442-54.

Brickley SG, Dawes EA, Keating MJ, Grant S. Synchronizing retinal activity in both eyes disrupts binocular map development in the optic tectum. J Neurosci, 1998; 18: 1491-504.

Bruce LL, Christensen MA, Warr WB. Postnatal development of efferent synapses in the rat cochlea. The Journal of comparative neurology, 2000; 423: 532-48.

Busetto G, Buffelli M, Tognana E, Bellico F, Cangiano A. Hebbian mechanisms revealed by electrical stimulation at developing rat neuromuscular junctions. J Neurosci, 2000; 20: 685-95.

Butler RA, Diamond IT, Neff WD. Role of auditory cortex in discrimination of changes in frequency. J Neurophysiol, 1957; 20: 108-20.

Cant NB, Casseday JH. Projections from the anteroventral cochlear nucleus to the lateral and medial superior olivary nuclei. The Journal of comparative neurology, 1986; 247: 457-76.

Caporale N, Dan Y. Spike timing-dependent plasticity: a Hebbian learning rule. Annu Rev Neurosci, 2008; 31: 25-46.

Carlier E, Pujol R. Sectioning the efferent bundle decreases cochlear frequency selectivity. Neurosci Lett, 1982; 28: 101-6.

Carlson S, Willott JF. The behavioral salience of tones as indicated by prepulse inhibition of the startle response: relationship to hearing loss and central neural plasticity in C57BL/6J mice. Hear Res, 1996; 99: 168-75.

Caspary DM, Palombi PS, Hughes LF. GABAergic inputs shape responses to amplitude modulated stimuli in the inferior colliculus. Hear Res, 2002; 168: 163-73.

Casseday JH, Ehrlich D, Covey E. Neural tuning for sound duration: role of inhibitory mechanisms in the inferior colliculus. Science, 1994; 264: 847-50.

Celikel T, Szostak VA, Feldman DE. Modulation of spike timing by sensory deprivation during induction of cortical map plasticity. Nature neuroscience, 2004; 7: 534-41.

Chalupa LM, Rhoades RW. Directional selectivity in hamster superior colliculus is modified by strobe-rearing but not by dark-rearing. Science, 1978; 199: 998-1001.

Chang EF, Merzenich MM. Environmental noise retards auditory cortical development. Science, 2003; 300: 498-502.

Chang EH, Kotak VC, Sanes DH. Long-term depression of synaptic inhibition is expressed postsynaptically in the developing auditory system. Journal of neurophysiology, 2003; 90: 1479-88.

Chen C, Regehr WG. Developmental remodeling of the retinogeniculate synapse. Neuron, 2000; 28: 955-66.

Chiu C, Weliky M. Spontaneous activity in developing ferret visual cortex in vivo. J Neurosci, 2001; 21: 8906-14.

Cohen-Cory S. The developing synapse: construction and modulation of synaptic structures and circuits. Science, 2002; 298: 770-6.

Colman H, Lichtman JW. Interactions between nerve and muscle: synapse elimination at the developing neuromuscular junction. Dev Biol, 1993; 156: 1-10.

Colman H, Nabekura J, Lichtman JW. Alterations in synaptic strength preceding axon withdrawal. Science, 1997; 275: 356-61.

Coomes DL, Schofield BR. Projections from the auditory cortex to the superior olivary complex in guinea pigs. The European journal of neuroscience, 2004; 19: 2188-200.

Covey E, Hall WC, Kobler JB. Subcortical connections of the superior colliculus in the mustache bat, Pteronotus parnellii. The Journal of comparative neurology, 1987; 263: 179-97.

Cramer KS. Eph proteins and the assembly of auditory circuits. Hearing research, 2005; 206: 42-51.

Dallos P, Cheatham MA. Compound action potential (AP) tuning curves. J Acoust Soc Am, 1976; 59: 591-7.

Dallos P, He DZ, Lin X, Sziklai I, Mehta S, Evans BN. Acetylcholine, outer hair cell electromotility, and the cochlear amplifier. J Neurosci, 1997; 17: 2212-26.

Dan Y, Poo MM. Spike timing-dependent plasticity: from synapse to perception. Physiol Rev, 2006; 86: 1033-48.

Davis M, Gendelman PM. Plasticity of the acoustic startle response in the acutely decerebrate rat. J Comp Physiol Psychol, 1977; 91: 549-63.

Dehmel S, Kopp-Scheinpflug C, Dorrscheidt GJ, Rubsamen R. Electrophysiological characterization of the superior paraolivary nucleus in the Mongolian gerbil. Hear Res, 2002; 172: 18-36.

Dewson JH. Efferent Olivocochlear Bundle: Some relationships to stimulus discrimination in noise. Journal of neurophysiology, 1968; 31: 122-30.

Dietrich V, Nieschalk M, Stoll W, Rajan R, Pantev C. Cortical reorganization in patients with high frequency cochlear hearing loss. Hear Res, 2001; 158: 95-101.

Dooling RJ, Hulse SH. The Comparative psychology of audition: perceiving complex sounds. L. Erlbaum Associates: Hillsdale, N.J., 1989.

Druga R, Syka J. Projections from auditory structures to the superior colliculus in the rat. Neurosci Lett, 1984; 45: 247-52.

Ehret G. Frequency and intensity difference limens and nonlinearities in the ear of the housemouse (Mus musculus) Journal of Comparative Physiology, 1975; 102: 321-36.

Ehrlich I, Lohrke S, Friauf E. Shift from depolarizing to hyperpolarizing glycine action in rat auditory neurones is due to age-dependent Cl- regulation. The Journal of physiology, 1999; 520 Pt 1: 121-37.

Elgoyhen AB, Johnson DS, Boulter J, Vetter DE, Heinemann S. Alpha 9: an acetylcholine receptor with novel pharmacological properties expressed in rat cochlear hair cells. Cell, 1994; 79: 705-15.

Elgoyhen AB, Vetter DE, Katz E, Rothlin CV, Heinemann SF, Boulter J. alpha10: a determinant of nicotinic cholinergic receptor function in mammalian vestibular and cochlear mechanosensory hair cells. Proc Natl Acad Sci U S A, 2001; 98: 3501-6.

Farinas I, Jones KR, Tessarollo L, Vigers AJ, Huang E, Kirstein M, de Caprona DC, Coppola V, Backus C, Reichardt LF, Fritzsch B. Spatial shaping of cochlear innervation by temporally regulated neurotrophin expression. J Neurosci, 2001; 21: 6170-80.

Fendt M, Li L, Yeomans JS. Brain stem circuits mediating prepulse inhibition of the startle reflex. Psychopharmacology (Berl), 2001; 156: 216-24.

Floody OR, Ouda L, Porter BA, Kilgard MP. Effects of damage to auditory cortex on the discrimination of speech sounds by rats. Physiol Behav, 2010; 101: 260-8.

Forrest TG, Green DM. Detection of partially filled gaps in noise and the temporal modulation transfer function. J Acoust Soc Am, 1987; 82: 1933-43.

Friauf E. Tonotopic Order in the Adult and Developing Auditory System of the Rat as Shown by c-fos Immunocytochemistry. The European journal of neuroscience, 1992; 4: 798-812.

Friauf E, Hammerschmidt B, Kirsch J. Development of adult-type inhibitory glycine receptors in the central auditory system of rats. The Journal of comparative neurology, 1997; 385: 117-34.

Friauf E, Ostwald J. Divergent projections of physiologically characterized rat ventral cochlear nucleus neurons as shown by intra-axonal injection of horseradish peroxidase. Experimental brain research. Experimentelle Hirnforschung, 1988; 73: 263-84.

Frisina RD, Walton JP, Lynch-Armour MA, Klotz DA. Efferent projections of a physiologically characterized region of the inferior colliculus of the young adult CBA mouse. J Acoust Soc Am, 1997; 101: 2741-53.

Gaiarsa JL, Caillard O, Ben-Ari Y. Long-term plasticity at GABAergic and glycinergic synapses: mechanisms and functional significance. Trends Neurosci, 2002; 25: 564-70.

Gao BX, Stricker C, Ziskind-Conhaim L. Transition from GABAergic to glycinergic synaptic transmission in newly formed spinal networks. Journal of neurophysiology, 2001; 86: 492-502.

Garinis AC, Glattke T, Cone-Wesson BK. TEOAE suppression in adults with learning disabilities. Int J Audiol, 2008; 47: 607-14.

Geal-Dor M, Freeman S, Li G, Sohmer H. Development of hearing in neonatal rats: air and bone conducted ABR thresholds. Hearing research, 1993; 69: 236-42.

Gengel RW. Temporal effects in frequency discrimination by hearing-impaired listeners. J Acoust Soc Am, 1973; 54: 11-5.

Ghosh A, Antonini A, McConnell SK, Shatz CJ. Requirement for subplate neurons in the formation of thalamocortical connections. Nature, 1990; 347: 179-81.

Gillespie DC, Kim G, Kandler K. Inhibitory synapses in the developing auditory system are glutamatergic. Nature neuroscience, 2005; 8: 332-8.

Glantz SA. Primer of biostatistics, Fifth ed. McGraw-Hill, Medical Pub. Div., 2002.

Glendenning KK, Baker BN, Hutson KA, Masterton RB. Acoustic chiasm V: inhibition and excitation in the ipsilateral and contralateral projections of LSO. The Journal of comparative neurology, 1992; 319: 100-22.

Glendenning KK, Masterton RB. Acoustic chiasm: efferent projections of the lateral superior olive. J Neurosci, 1983; 3: 1521-37.

Glowatzki E, Fuchs PA. Cholinergic synaptic inhibition of inner hair cells in the neonatal mammalian cochlea. Science, 2000; 288: 2366-8.

Goodman CS, Shatz CJ. Developmental mechanisms that generate precise patterns of neuronal connectivity. Cell, 1993; 72 Suppl: 77-98.

Goutman JD, Fuchs PA, Glowatzki E. Facilitating efferent inhibition of inner hair cells in the cochlea of the neonatal rat. J Physiol, 2005; 566: 49-59.

Guinan JJ, Jr. Effect of efferent neural activity on cochlear mechanics. Scand Audiol Suppl, 1986; 25: 53-62.

Halliday LF, Bishop DV. Frequency discrimination and literacy skills in children with mild to moderate sensorineural hearing loss. J Speech Lang Hear Res, 2005; 48: 1187-203.

Hanson MG, Landmesser LT. Increasing the frequency of spontaneous rhythmic activity disrupts pool-specific axon fasciculation and pathfinding of embryonic spinal motoneurons. J Neurosci, 2006; 26: 12769-80.

Hanson MG, Milner LD, Landmesser LT. Spontaneous rhythmic activity in early chick spinal cord influences distinct motor axon pathfinding decisions. Brain Res Rev, 2008; 57: 77-85.

Hashimoto K, Kano M. Functional differentiation of multiple climbing fiber inputs during synapse elimination in the developing cerebellum. Neuron, 2003; 38: 785-96.

Hashimoto K, Kano M. Postnatal development and synapse elimination of climbing fiber to Purkinje cell projection in the cerebellum. Neurosci Res, 2005; 53: 221-8.

Hata Y, Stryker MP. Control of thalamocortical afferent rearrangement by postsynaptic activity in developing visual cortex. Science, 1994; 265: 1732-5.

He DZ, Cheatham MA, Pearce M, Vetter DE. Mouse outer hair cells lacking the alpha9 ACh receptor are motile. Brain research, 2004; 148: 19-25.

Hoffman HS, Ison JR. Reflex modification in the domain of startle: I. Some empirical findings and their implications for how the nervous system processes sensory input. Psychological review, 1980; 87: 175-89.

Hoffpauir BK, Marrs GS, Mathers PH, Spirou GA. Does the brain connect before the periphery can direct? A comparison of three sensory systems in mice. Brain Res, 2009; 1277: 115-29.

Housley GD, Ashmore JF. Direct measurement of the action of acetylcholine on isolated outer hair cells of the guinea pig cochlea. Proc Biol Sci, 1991; 244: 161-7.

Huberman AD. Mechanisms of eye-specific visual circuit development. Curr Opin Neurobiol, 2007; 17: 73-80.

Huberman AD, Feller MB, Chapman B. Mechanisms underlying development of visual maps and receptive fields. Annu Rev Neurosci, 2008; 31: 479-509.

Huffman KJ, Cramer KS. EphA4 misexpression alters tonotopic projections in the auditory brainstem. Developmental neurobiology, 2007; 67: 1655-68.

Igarashi M, Cranford JL, Allen EA, Alford BR. Behavioral auditory function after transection of crossed olivo-cochlear bundle in the cat. V. Pure-tone intensity discrimination. Acta Otolaryngol, 1979a; 87: 429-33.

Igarashi M, Cranford JL, Nakai Y, Alford BR. Behavioral auditory function after transection of crossed olivo-cochlear bundle in the cat. IV. Study on pure-tone frequency discrimination. Acta Otolaryngol, 1979b; 87: 79-83.

Ison J. The acoustic startle response: reflex elicitation and reflex modification by preliminary stimuli. In Willott JF, editor. The Handbook of Mouse Auditory Research. CRC Press, 2001.

Ison JR, Bowen P, Pak J, Gutierrez E. Changes in the strength of prepulse inhibition with variation in the startle baseline associated with individual differences and with old age in rats and mice. Psychobiology, 1997; 25: 266-74.

Ison JR, Hoffman HS. Reflex modification in the domain of startle: II. The anomalous history of a robust and ubiquitous phenomenon. Psychol Bull, 1983; 94: 3-17.

Ison JR, McAdam DW, Hammond GR. Latency and amplitude changes in the acoustic startle reflex of the rat produced by variation in auditory prestimulation. Physiology & behavior, 1973; 10: 1035-9.

Ison JR, Pinckney LA. Reflex inhibition in humans: sensitivity to brief silent periods in white noise. Percept Psychophys, 1983; 34: 84-8.

Jackson H, Parks TN. Functional synapse elimination in the developing avian cochlear nucleus with simultaneous reduction in cochlear nerve axon branching. J Neurosci, 1982; 2: 1736-43.

Jhaveri S, Morest DK. Sequential alterations of neuronal architecture in nucleus magnocellularis of the developing chicken: an electron microscope study. Neuroscience, 1982; 7: 855-70.

Johnsrude IS, Penhune VB, Zatorre RJ. Functional specificity in the right human auditory cortex for perceiving pitch direction. Brain, 2000; 123 (Pt 1): 155-63.

Jonas P, Bischofberger J, Sandkuhler J. Corelease of two fast neurotransmitters at a central synapse. Science, 1998; 281: 419-24.

Jones TA, Jones SM, Paggett KC. Emergence of hearing in the chicken embryo. Journal of neurophysiology, 2006; 96: 128-41.

Jones TA, Jones SM, Paggett KC. Primordial rhythmic bursting in embryonic cochlear ganglion cells. J Neurosci, 2001; 21: 8129-35.

Jones TA, Leake PA, Snyder RL, Stakhovskaya O, Bonham B. Spontaneous discharge patterns in cochlear spiral ganglion cells before the onset of hearing in cats. Journal of neurophysiology, 2007; 98: 1898-908.

Kakazu Y, Akaike N, Komiyama S, Nabekura J. Regulation of intracellular chloride by cotransporters in developing lateral superior olive neurons. J Neurosci, 1999; 19: 2843-51.

Kalamida D, Poulas K, Avramopoulou V, Fostieri E, Lagoumintzis G, Lazaridis K, Sideri A, Zouridakis M, Tzartos SJ. Muscle and neuronal nicotinic acetylcholine receptors. Structure, function and pathogenicity. FEBS J, 2007; 274: 3799-845.

Kamke MR, Brown M, Irvine DR. Plasticity in the tonotopic organization of the medial geniculate body in adult cats following restricted unilateral cochlear lesions. J Comp Neurol, 2003; 459: 355-67.

Kandler K, Clause A, Noh J. Tonotopic reorganization of developing auditory brainstem circuits. Nature neuroscience, 2009; 12: 711-7.

Kandler K, Friauf E. Development of glycinergic and glutamatergic synaptic transmission in the auditory brainstem of perinatal rats. J Neurosci, 1995; 15: 6890-904.

Kandler K, Friauf E. Pre- and postnatal development of efferent connections of the cochlear nucleus in the rat. The Journal of comparative neurology, 1993; 328: 161-84.

Kano M, Hashimoto K. Synapse elimination in the central nervous system. Curr Opin Neurobiol, 2009; 19: 154-61.

Kapfer C, Seidl AH, Schweizer H, Grothe B. Experience-dependent refinement of inhibitory inputs to auditory coincidence-detector neurons. Nature neuroscience, 2002; 5: 247-53.

Kasthuri N, Lichtman JW. The role of neuronal identity in synaptic competition. Nature, 2003; 424: 426-30.

Katz E, Elgoyhen AB, Gomez-Casati ME, Knipper M, Vetter DE, Fuchs PA, Glowatzki E. Developmental regulation of nicotinic synapses on cochlear inner hair cells. J Neurosci, 2004; 24: 7814-20.

Katz LC, Shatz CJ. Synaptic activity and the construction of cortical circuits. Science, 1996; 274: 1133-8.

Katz LC, Weliky M, Dalva M. Relationships between local synaptic connections and orientation domains in primary visual cortex. Neuron, 1998; 20: following 819.

Kavanagh GL, Kelly JB. Midline and lateral field sound localization in the ferret (Mustela putorius): contribution of the superior olivary complex. Journal of neurophysiology, 1992; 67: 1643-58.

Kawase T, Liberman MC. Antimasking effects of the olivocochlear reflex. I. Enhancement of compound action potentials to masked tones. Journal of neurophysiology, 1993; 70: 2519-32.

Keller AF, Coull JA, Chery N, Poisbeau P, De Koninck Y. Region-specific developmental specialization of GABA-glycine cosynapses in laminas I-II of the rat spinal dorsal horn. J Neurosci, 2001; 21: 7871-80.

Khazipov R, Sirota A, Leinekugel X, Holmes GL, Ben-Ari Y, Buzsaki G. Early motor activity drives spindle bursts in the developing somatosensory cortex. Nature, 2004; 432: 758-61.

Kil J, Kageyama GH, Semple MN, Kitzes LM. Development of ventral cochlear nucleus projections to the superior olivary complex in gerbil. The Journal of comparative neurology, 1995; 353: 317-40.

Kilman V, van Rossum MC, Turrigiano GG. Activity deprivation reduces miniature IPSC amplitude by decreasing the number of postsynaptic GABA(A) receptors clustered at neocortical synapses. J Neurosci, 2002; 22: 1328-37.

Kim DO. Active and nonlinear cochlear biomechanics and the role of outer-hair-cell subsystem in the mammalian auditory system. Hear Res, 1986; 22: 105-14.

Kim G. Refinement of Inhibitory Circuits During Development of the Mammalian Auditory Brainstem. Department of Neurobiology. University of Pittsburgh, 2004.

Kim G, Kandler K. Elimination and strengthening of glycinergic/GABAergic connections during tonotopic map formation. Nature neuroscience, 2003; 6: 282-90.

Kim G, Kandler K. Synaptic changes underlying the strengthening of GABA/glycinergic connections in the developing lateral superior olive. Neuroscience, 2010; 171: 924-33.

Knudsen EI, Zheng W, DeBello WM. Traces of learning in the auditory localization pathway. Proceedings of the National Academy of Sciences of the United States of America, 2000; 97: 11815-20.

Koch M. The neurobiology of startle. Prog Neurobiol, 1999; 59: 107-28.

Koch M, Kungel M, Herbert H. Cholinergic neurons in the pedunculopontine tegmental nucleus are involved in the mediation of prepulse inhibition of the acoustic startle response in the rat. Experimental brain research. Experimentelle Hirnforschung, 1993; 97: 71-82.

Koch M, Schnitzler HU. The acoustic startle response in rats--circuits mediating evocation, inhibition and potentiation. Behav Brain Res, 1997; 89: 35-49.

Kotak VC, Korada S, Schwartz IR, Sanes DH. A developmental shift from GABAergic to glycinergic transmission in the central auditory system. J Neurosci, 1998; 18: 4646-55.

Kotak VC, Sanes DH. Gain adjustment of inhibitory synapses in the auditory system. Biol Cybern, 2003; 89: 363-70.

Kotak VC, Sanes DH. Long-lasting inhibitory synaptic depression is age- and calcium-dependent. J Neurosci, 2000; 20: 5820-6.

Kotak VC, Sanes DH. Postsynaptic kinase signaling underlies inhibitory synaptic plasticity in the lateral superior olive. Journal of neurobiology, 2002; 53: 36-43.

Kotak VC, Sanes DH. Synaptically evoked prolonged depolarizations in the developing auditory system. Journal of neurophysiology, 1995; 74: 1611-20.

Koundakjian EJ, Appler JL, Goodrich LV. Auditory neurons make stereotyped wiring decisions before maturation of their targets. J Neurosci, 2007; 27: 14078-88.

Kulesza RJ, Jr., Berrebi AS. Superior paraolivary nucleus of the rat is a GABAergic nucleus. J Assoc Res Otolaryngol, 2000; 1: 255-69.

Kulesza RJ, Jr., Spirou GA, Berrebi AS. Physiological response properties of neurons in the superior paraolivary nucleus of the rat. J Neurophysiol, 2003; 89: 2299-312.

Kullmann PH, Ene FA, Kandler K. Glycinergic and GABAergic calcium responses in the developing lateral superior olive. The European journal of neuroscience, 2002; 15: 1093-104.

Kullmann PH, Kandler K. Dendritic Ca2+ responses in neonatal lateral superior olive neurons elicited by glycinergic/GABAergic synapses and action potentials. Neuroscience, 2008; 154: 338-45.

Kullmann PH, Kandler K. Glycinergic/GABAergic synapses in the lateral superior olive are excitatory in neonatal C57Bl/6J mice. Brain research, 2001; 131: 143-7.

Kurt S, Ehret G. Auditory discrimination learning and knowledge transfer in mice depends on task difficulty. Proc Natl Acad Sci U S A, 2010; 107: 8481-5.

Kushmerick C, Price GD, Taschenberger H, Puente N, Renden R, Wadiche JI, Duvoisin RM, Grandes P, von Gersdorff H. Retroinhibition of presynaptic Ca2+ currents by endocannabinoids released via postsynaptic mGluR activation at a calyx synapse. J Neurosci, 2004; 24: 5955-65.

Kuwabara N, Zook JM. Classification of the principal cells of the medial nucleus of the trapezoid body. J Comp Neurol, 1991; 314: 707-20.

Larson J, Lynch G. Induction of synaptic potentiation in hippocampus by patterned stimulation involves two events. Science, 1986; 232: 985-8.

Larson J, Wong D, Lynch G. Patterned stimulation at the theta frequency is optimal for the induction of hippocampal long-term potentiation. Brain Res, 1986; 368: 347-50.

Leake PA, Snyder RL, Hradek GT. Postnatal refinement of auditory nerve projections to the cochlear nucleus in cats. The Journal of comparative neurology, 2002; 448: 6-27.

Leao RN, Sun H, Svahn K, Berntson A, Youssoufian M, Paolini AG, Fyffe RE, Walmsley B. Topographic organization in the auditory brainstem of juvenile mice is disrupted in congenital deafness. The Journal of physiology, 2006; 571: 563-78.

Leitner DS, Cohen ME. Role of the inferior colliculus in the inhibition of acoustic startle in the rat. Physiology & behavior, 1985; 34: 65-70.

Leitner DS, Hammond GR, Springer CP, Ingham KM, Mekilo AM, Bodison PR, Aranda MT, Shawaryn MA. Parameters affecting gap detection in the rat. Percept Psychophys, 1993; 54: 395-405.

LeVay S, Wiesel TN, Hubel DH. The development of ocular dominance columns in normal and visually deprived monkeys. The Journal of comparative neurology, 1980; 191: 1-51.

Li L, Priebe RP, Yeomans JS. Prepulse inhibition of acoustic or trigeminal startle of rats by unilateral electrical stimulation of the inferior colliculus. Behav Neurosci, 1998; 112: 1187-98.

Liberman MC. Effects of chronic cochlear de-efferentation on auditory-nerve response. Hear Res, 1990; 49: 209-23.

Liberman MC. Response properties of cochlear efferent neurons: monaural vs. binaural stimulation and the effects of noise. Journal of neurophysiology, 1988; 60: 1779-98.

Liberman MC, Brown MC. Physiology and anatomy of single olivocochlear neurons in the cat. Hearing research, 1986; 24: 17-36.

Liberman MC, O'Grady DF, Dodds LW, McGee J, Walsh EJ. Afferent innervation of outer and inner hair cells is normal in neonatally de-efferented cats. The Journal of comparative neurology, 2000; 423: 132-9.

Lichtman JW, Wilkinson RS, Rich MM. Multiple innervation of tonic endplates revealed by activity-dependent uptake of fluorescent probes. Nature, 1985; 314: 357-9.

Lippe WR. Rhythmic spontaneous activity in the developing avian auditory system. J Neurosci, 1994; 14: 1486-95.

Lohof AM, Delhaye-Bouchaud N, Mariani J. Synapse elimination in the central nervous system: functional significance and cellular mechanisms. Rev Neurosci, 1996; 7: 85-101.

Lowel S, Singer W. Selection of intrinsic horizontal connections in the visual cortex by correlated neuronal activity. Science, 1992; 255: 209-12.

Lu T, Trussell LO. Development and elimination of endbulb synapses in the chick cochlear nucleus. J Neurosci, 2007; 27: 808-17.

Lujan R, Shigemoto R, Lopez-Bendito G. Glutamate and GABA receptor signalling in the developing brain. Neuroscience, 2005; 130: 567-80.

Luo L, Bennett T, Jung HH, Ryan AF. Developmental expression of alpha 9 acetylcholine receptor mRNA in the rat cochlea and vestibular inner ear. The Journal of comparative neurology, 1998; 393: 320-31.

Luscher B, Keller CA. Regulation of GABAA receptor trafficking, channel activity, and functional plasticity of inhibitory synapses. Pharmacol Ther, 2004; 102: 195-221.

Magnusson AK, Park TJ, Pecka M, Grothe B, Koch U. Retrograde GABA signaling adjusts sound localization by balancing excitation and inhibition in the brainstem. Neuron, 2008; 59: 125-37.

Malenka RC, Bear MF. LTP and LTD: an embarrassment of riches. Neuron, 2004; 44: 5-21.

Masterton B, Jane JA, Diamond IT. Role of brainstem auditory structures in sound localization. I. Trapezoid body, superior olive, and lateral lemniscus. Journal of neurophysiology, 1967; 30: 341-59.

May BJ, Budelis J, Niparko JK. Behavioral studies of the olivocochlear efferent system: learning to listen in noise. Arch Otolaryngol Head Neck Surg, 2004; 130: 660-4.

May BJ, Prosen CA, Weiss D, Vetter D. Behavioral investigation of some possible effects of the central olivocochlear pathways in transgenic mice. Hearing research, 2002; 171: 142-57.

McBain CJ, Fisahn A. Interneurons unbound. Nat Rev Neurosci, 2001; 2: 11-23.

McDermott HJ, Lech M, Kornblum MS, Irvine DR. Loudness perception and frequency discrimination in subjects with steeply sloping hearing loss: possible correlates of neural plasticity. J Acoust Soc Am, 1998; 104: 2314-25.

Meister M, Wong RO, Baylor DA, Shatz CJ. Synchronous bursts of action potentials in ganglion cells of the developing mammalian retina. Science, 1991; 252: 939-43.

Micheva KD, Beaulieu C. An anatomical substrate for experience-dependent plasticity of the rat barrel field cortex. Proceedings of the National Academy of Sciences of the United States of America, 1995; 92: 11834-8.

Micheyl C, Collet L. Involvement of the olivocochlear bundle in the detection of tones in noise. J Acoust Soc Am, 1996; 99: 1604-10.

Morales B, Choi SY, Kirkwood A. Dark rearing alters the development of GABAergic transmission in visual cortex. J Neurosci, 2002; 22: 8084-90.

Muchnik C, Ari-Even Roth D, Othman-Jebara R, Putter-Katz H, Shabtai EL, Hildesheimer M. Reduced medial olivocochlear bundle system function in children with auditory processing disorders. Audiol Neurootol, 2004; 9: 107-14.

Nabekura J, Katsurabayashi S, Kakazu Y, Shibata S, Matsubara A, Jinno S, Mizoguchi Y, Sasaki A, Ishibashi H. Developmental switch from GABA to glycine release in single central synaptic terminals. Nature neuroscience, 2004; 7: 17-23.

Nelson DA, Freyman RL. Psychometric functions for frequency discrimination from listeners with sensorineural hearing loss. J Acoust Soc Am, 1986; 79: 799-805.

Noh J, Seal RP, Garver JA, Edwards RH, Kandler K. Glutamate co-release at GABA/glycinergic synapses is crucial for the refinement of an inhibitory map. Nature neuroscience, 2010; 13: 232-8.

O'Brien JA, Berger AJ. Cotransmission of GABA and glycine to brain stem motoneurons. Journal of neurophysiology, 1999; 82: 1638-41.

O'Donovan MJ. The origin of spontaneous activity in developing networks of the vertebrate nervous system. Curr Opin Neurobiol, 1999; 9: 94-104.

Ono K, Kudoh M, Shibuki K. Roles of the auditory cortex in discrimination learning by rats. Eur J Neurosci, 2006; 23: 1623-32.

Owens DF, Kriegstein AR. Is there more to GABA than synaptic inhibition? Nat Rev Neurosci, 2002; 3: 715-27.

Palombi PS, Caspary DM. GABA inputs control discharge rate primarily within frequency receptive fields of inferior colliculus neurons. J Neurophysiol, 1996; 75: 2211-9.

Parisi T, Ison JR. Development of the acoustic startle response in the rat: ontogenetic changes in the magnitude of inhibition by prepulse stimulation. Dev Psychobiol, 1979; 12: 219-30.

Park TJ, Pollak GD. GABA shapes a topographic organization of response latency in the mustache bat's inferior colliculus. J Neurosci, 1993; 13: 5172-87.

Penn AA, Riquelme PA, Feller MB, Shatz CJ. Competition in retinogeniculate patterning driven by spontaneous activity. Science, 1998; 279: 2108-12.

Penzo MA, Pena JL. Endocannabinoid-mediated long-term depression in the avian midbrain expressed presynaptically and postsynaptically. J Neurosci, 2009; 29: 4131-9.

Pierce JP, Mendell LM. Quantitative ultrastructure of Ia boutons in the ventral horn: scaling and positional relationships. J Neurosci, 1993; 13: 4748-63.

Pilz PK, Schnitzler HU, Menne D. Acoustic startle threshold of the albino rat (Rattus norvegicus). J Comp Psychol, 1987; 101: 67-72.

Pollak GD, Gittelman JX, Li N, Xie R. Inhibitory projections from the ventral nucleus of the lateral lemniscus and superior paraolivary nucleus create directional selectivity of frequency modulations in the inferior colliculus: A comparison of bats with other mammals. Hear Res, 2010.

Rajan R, Irvine DR, Wise LZ, Heil P. Effect of unilateral partial cochlear lesions in adult cats on the representation of lesioned and unlesioned cochleas in primary auditory cortex. J Comp Neurol, 1993; 338: 17-49.

Ramakrishnan NA, Drescher MJ, Drescher DG. Direct interaction of otoferlin with syntaxin 1A, SNAP-25, and the L-type voltage-gated calcium channel Cav1.3. J Biol Chem, 2009; 284: 1364-72.

Rietzel HJ, Friauf E. Neuron types in the rat lateral superior olive and developmental changes in the complexity of their dendritic arbors. The Journal of comparative neurology, 1998; 390: 20-40.

Robertson D, Irvine DR. Plasticity of frequency organization in auditory cortex of guinea pigs with partial unilateral deafness. J Comp Neurol, 1989; 282: 456-71.

Roux I, Safieddine S, Nouvian R, Grati M, Simmler MC, Bahloul A, Perfettini I, Le Gall M, Rostaing P, Hamard G, Triller A, Avan P, Moser T, Petit C. Otoferlin, defective in a human deafness form, is essential for exocytosis at the auditory ribbon synapse. Cell, 2006; 127: 277-89.

Rubel EW, Cramer KS. Choosing axonal real estate: location, location, location. The Journal of comparative neurology, 2002; 448: 1-5.

Russier M, Kopysova IL, Ankri N, Ferrand N, Debanne D. GABA and glycine co-release optimizes functional inhibition in rat brainstem motoneurons in vitro. The Journal of physiology, 2002; 541: 123-37.

Saldana E, Aparicio MA, Fuentes-Santamaria V, Berrebi AS. Connections of the superior paraolivary nucleus of the rat: projections to the inferior colliculus. Neuroscience, 2009; 163: 372-87.

Sanes DH, Chokshi P. Glycinergic transmission influences the development of dendrite shape. Neuroreport, 1992; 3: 323-6.

Sanes DH, Constantine-Paton M. Altered activity patterns during development reduce neural tuning. Science, 1983; 221: 1183-5.

Sanes DH, Constantine-Paton M. The development of stimulus following in the cochlear nerve and inferior colliculus of the mouse. Brain Res, 1985a; 354: 255-67.

Sanes DH, Constantine-Paton M. The sharpening of frequency tuning curves requires patterned activity during development in the mouse, Mus musculus. J Neurosci, 1985b; 5: 1152-66.

Sanes DH, Friauf E. Development and influence of inhibition in the lateral superior olivary nucleus. Hearing research, 2000; 147: 46-58.

Sanes DH, Markowitz S, Bernstein J, Wardlow J. The influence of inhibitory afferents on the development of postsynaptic dendritic arbors. The Journal of comparative neurology, 1992a; 321: 637-44.

Sanes DH, Merickel M, Rubel EW. Evidence for an alteration of the tonotopic map in the gerbil cochlea during development. The Journal of comparative neurology, 1989; 279: 436-44.

Sanes DH, Rubel EW. The ontogeny of inhibition and excitation in the gerbil lateral superior olive. J Neurosci, 1988; 8: 682-700.

Sanes DH, Siverls V. Development and specificity of inhibitory terminal arborizations in the central nervous system. Journal of neurobiology, 1991; 22: 837-54.

Sanes DH, Song J, Tyson J. Refinement of dendritic arbors along the tonotopic axis of the gerbil lateral superior olive. Brain research, 1992b; 67: 47-55.

Sanes DH, Takacs C. Activity-dependent refinement of inhibitory connections. The European journal of neuroscience, 1993; 5: 570-4.

Schmidt JT, Eisele LE. Stroboscopic illumination and dark rearing block the sharpening of the regenerated retinotectal map in goldfish. Neuroscience, 1985; 14: 535-46.

Schofield BR, Cant NB. Descending auditory pathways: projections from the inferior colliculus contact superior olivary cells that project bilaterally to the cochlear nuclei. The Journal of comparative neurology, 1999; 409: 210-23.

Schofield BR, Coomes DL. Pathways from auditory cortex to the cochlear nucleus in guinea pigs. Hearing research, 2006; 216-217: 81-9.

Schwaber MK, Garraghty PE, Kaas JH. Neuroplasticity of the adult primate auditory cortex following cochlear hearing loss. Am J Otol, 1993; 14: 252-8.

Simmons DD. Development of the inner ear efferent system across vertebrate species. Journal of neurobiology, 2002; 53: 228-50.

Simmons DD, Mansdorf NB, Kim JH. Olivocochlear innervation of inner and outer hair cells during postnatal maturation: evidence for a waiting period. The Journal of comparative neurology, 1996; 370: 551-62.

Simmons DD, Morley BJ. Differential expression of the alpha 9 nicotinic acetylcholine receptor subunit in neonatal and adult cochlear hair cells. Brain Res Mol Brain Res, 1998; 56: 287-92.

Snyder RL, Leake PA. Topography of spiral ganglion projections to cochlear nucleus during postnatal development in cats. The Journal of comparative neurology, 1997; 384: 293-311.

Snyder RL, Leake PA, Hradek GT. Quantitative analysis of spiral ganglion projections to the cat cochlear nucleus. The Journal of comparative neurology, 1997; 379: 133-49.

Sommer I, Lingenhohl K, Friauf E. Principal cells of the rat medial nucleus of the trapezoid body: an intracellular in vivo study of their physiology and morphology. Experimental brain research. Experimentelle Hirnforschung, 1993; 95: 223-39.

Sonntag M, Englitz B, Kopp-Scheinpflug C, Rubsamen R. Early postnatal development of spontaneous and acoustically evoked discharge activity of principal cells of the medial nucleus of the trapezoid body: an in vivo study in mice. J Neurosci, 2009; 29: 9510-20.

Spangler KM, Warr WB, Henkel CK. The projections of principal cells of the medial nucleus of the trapezoid body in the cat. The Journal of comparative neurology, 1985; 238: 249-62.

Sretavan D, Shatz CJ. Prenatal development of individual retinogeniculate axons during the period of segregation. Nature, 1984; 308: 845-8.

Steininger TL, Rye DB, Wainer BH. Afferent projections to the cholinergic pedunculopontine tegmental nucleus and adjacent midbrain extrapyramidal area in the albino rat. I. Retrograde tracing studies. The Journal of comparative neurology, 1992; 321: 515-43.

Stellwagen D, Shatz CJ. An instructive role for retinal waves in the development of retinogeniculate connectivity. Neuron, 2002; 33: 357-67.

Stitt CL, Hoffman HS, Marsh R, Boskoff KJ. Modification of the rat's startle reaction by an antecedent change in the acoustic environment. J Comp Physiol Psychol, 1974; 86: 826-36.

Swerdlow NR, Geyer MA, Braff DL. Neural circuit regulation of prepulse inhibition of startle in the rat: current knowledge and future challenges. Psychopharmacology (Berl), 2001; 156: 194-215.

Tessier-Lavigne M, Goodman CS. The molecular biology of axon guidance. Science, 1996; 274: 1123-33.

Thai-Van H, Micheyl C, Moore BC, Collet L. Enhanced frequency discrimination near the hearing loss cut-off: a consequence of central auditory plasticity induced by cochlear damage? Brain, 2003; 126: 2235-45.

Thai-Van H, Micheyl C, Norena A, Collet L. Local improvement in auditory frequency discrimination is associated with hearing-loss slope in subjects with cochlear damage. Brain, 2002; 125: 524-37.

Thompson AM, Schofield BR. Afferent projections of the superior olivary complex. Microsc Res Tech, 2000; 51: 330-54.

Thompson AM, Thompson GC. Projections from the posteroventral cochlear nucleus to the superior olivary complex in guinea pig: light and EM observations with the PHA-L method. J Comp Neurol, 1991; 311: 495-508.

Tollin DJ. The lateral superior olive: a functional role in sound source localization. Neuroscientist, 2003; 9: 127-43.

Tollin DJ, Koka K, Tsai JJ. Interaural level difference discrimination thresholds for single neurons in the lateral superior olive. J Neurosci, 2008; 28: 4848-60.

Torborg CL, Feller MB. Spontaneous patterned retinal activity and the refinement of retinal projections. Prog Neurobiol, 2005; 76: 213-35.

Torborg CL, Hansen KA, Feller MB. High frequency, synchronized bursting drives eye-specific segregation of retinogeniculate projections. Nature neuroscience, 2005; 8: 72-8.

Trahiotis C, Elliott DN. Behavioral investigation of some possible effects of sectioning the crossed olivocochlear bundle. J Acoust Soc Am, 1970; 47: 592-6.

Tramo MJ, Cariani PA, Koh CK, Makris N, Braida LD. Neurophysiology and neuroanatomy of pitch perception: auditory cortex. Ann N Y Acad Sci, 2005; 1060: 148-74.

Tramo MJ, Shah GD, Braida LD. Functional role of auditory cortex in frequency processing and pitch perception. J Neurophysiol, 2002; 87: 122-39.

Tritsch NX, Bergles DE. Developmental regulation of spontaneous activity in the Mammalian cochlea. J Neurosci, 2010; 30: 1539-50.

Tritsch NX, Rodriguez-Contreras A, Crins TT, Wang HC, Borst JG, Bergles DE. Calcium action potentials in hair cells pattern auditory neuron activity before hearing onset. Nature neuroscience, 2010; 13: 1050-2.

Tritsch NX, Yi E, Gale JE, Glowatzki E, Bergles DE. The origin of spontaneous activity in the developing auditory system. Nature, 2007; 450: 50-5.

Tsuchitani C. Functional organization of lateral cell groups of cat superior olivary complex. Journal of neurophysiology, 1977; 40: 296-318.

Turner JG, Brozoski TJ, Bauer CA, Parrish JL, Myers K, Hughes LF, Caspary DM. Gap detection deficits in rats with tinnitus: a potential novel screening tool. Behav Neurosci, 2006; 120: 188-95.

Turrigiano GG. The self-tuning neuron: synaptic scaling of excitatory synapses. Cell, 2008; 135: 422-35.

Turrigiano GG, Nelson SB. Homeostatic plasticity in the developing nervous system. Nat Rev Neurosci, 2004; 5: 97-107.

Tzounopoulos T, Rubio ME, Keen JE, Trussell LO. Coactivation of pre- and postsynaptic signaling mechanisms determines cell-specific spike-timing-dependent plasticity. Neuron, 2007; 54: 291-301.

Vetter DE, Liberman MC, Mann J, Barhanin J, Boulter J, Brown MC, Saffiote-Kolman J, Heinemann SF, Elgoyhen AB. Role of alpha9 nicotinic ACh receptor subunits in the development and function of cochlear efferent innervation. Neuron, 1999; 23: 93-103.

Walsh EJ, McGee J. Rhythmic discharge properties of caudal cochlear nucleus neurons during postnatal development in cats. Hearing research, 1988; 36: 233-47.

Walsh EJ, McGee J, McFadden SL, Liberman MC. Long-term effects of sectioning the olivocochlear bundle in neonatal cats. J Neurosci, 1998; 18: 3859-69.

Warr WB. Fiber degeneration following lesions in the multipolar and globular cell areas in the ventral cochlear nucleus of the cat. Brain Res, 1972; 40: 247-70.

Warr WB. Olivocochlear efferent systems in mammals. In Webster; DB, Popper; AN, Fay RR, editors. The mammalian auditory pathway: neuroanatomy, 1992: 410-48.

Warren EH, 3rd, Liberman MC. Effects of contralateral sound on auditory-nerve responses. I. Contributions of cochlear efferents. Hearing research, 1989; 37: 89-104.

Weliky M. Correlated neuronal activity and visual cortical development. Neuron, 2000; 27: 427-30.

Werthat F, Alexandrova O, Grothe B, Koch U. Experience-dependent refinement of the inhibitory axons projecting to the medial superior olive. Developmental neurobiology, 2008; 68: 1454-62.

Willott JF. The Auditory psychobiology of the mouse. C.C. Thomas: Springfield, Ill., 1983.

Willott JF. Handbook of mouse auditory research : From behavior to molecular biology. CRC Press, 2001.

Winslow RL, Sachs MB. Single-tone intensity discrimination based on auditory-nerve rate responses in backgrounds of quiet, noise, and with stimulation of the crossed olivocochlear bundle. Hearing research, 1988; 35: 165-89.

Withington-Wray DJ, Binns KE, Dhanjal SS, Brickley SG, Keating MJ. The Maturation of the Superior Collicular Map of Auditory Space in the Guinea Pig is Disrupted by Developmental Auditory Deprivation. The European journal of neuroscience, 1990; 2: 693-703.

Wong RO. Retinal waves and visual system development. Annu Rev Neurosci, 1999; 22: 29-47.

Wu SH, Oertel D. Maturation of synapses and electrical properties of cells in the cochlear nuclei. Hearing research, 1987; 30: 99-110.

Wyatt RM, Balice-Gordon RJ. Activity-dependent elimination of neuromuscular synapses. J Neurocytol, 2003; 32: 777-94.

Yang L, Pollak GD, Resler C. GABAergic circuits sharpen tuning curves and modify response properties in the mustache bat inferior colliculus. J Neurophysiol, 1992; 68: 1760-74.

Youssoufian M, Oleskevich S, Walmsley B. Development of a robust central auditory synapse in congenital deafness. Journal of neurophysiology, 2005; 94: 3168-80.

Zhang LI, Bao S, Merzenich MM. Disruption of primary auditory cortex by synchronous auditory inputs during a critical period. Proceedings of the National Academy of Sciences of the United States of America, 2002; 99: 2309-14.

Zhang LI, Bao S, Merzenich MM. Persistent and specific influences of early acoustic environments on primary auditory cortex. Nature neuroscience, 2001; 4: 1123-30.

Zhang LI, Poo MM. Electrical activity and development of neural circuits. Nature neuroscience, 2001; 4 Suppl: 1207-14.

Zhao Y, Rubio ME, Tzounopoulos T. Distinct functional and anatomical architecture of the endocannabinoid system in the auditory brainstem. Journal of neurophysiology, 2009; 101: 2434-46.

Zhou X, Merzenich MM. Enduring effects of early structured noise exposure on temporal modulation in the primary auditory cortex. Proceedings of the National Academy of Sciences of the United States of America, 2008; 105: 4423-8.

Zook JM, DiCaprio RA. Intracellular labeling of afferents to the lateral superior olive in the bat, Eptesicus fuscus. Hearing research, 1988; 34: 141-7.